Quantitative Analysis of Cytokine-Induced Hepatocellular Death in the Context of Hepatotoxic Therapeutics

by

Benjamin D. Cosgrove

B.Bm.E., Biomedical Engineering
University of Minnesota, 2003

Submitted to the Department of Biological Engineering
in partial fulfillment of the requirements for the degree of

Doctor of Philosophy in Bioengineering

at the

Massachusetts Institute of Technology

February 2009

Signature of Author: _____
Department of Biological Engineering
December 15, 2008

Certified by: _____
Linda G. Griffith
Professor of Biological and Mechanical Engineering
Thesis Supervisor

Certified by: _____
Douglas A. Lauffenburger
Professor of Biological Engineering, Biology, and Chemical Engineering
Thesis Supervisor

Accepted by: _____
Alan J. Grodzinsky
Professor of Electrical, Mechanical, and Biological Engineering
Graduate Program Committee Chairperson

THESIS COMMITTEE

Forest M. White
Associate Professor, Department of Biological Engineering
Massachusetts Institute of Technology
Thesis Committee Chair

Linda G. Griffith
Professor, Departments of Biological and Mechanical Engineering
Massachusetts Institute of Technology
Thesis Supervisor

Douglas A. Lauffenburger
Professor, Departments of Biological Engineering, Biology, and Chemical Engineering
Massachusetts Institute of Technology
Thesis Supervisor

Donna B. Stolz
Associate Professor, Department of Cell Biology and Physiology
University of Pittsburgh Medical School

Quantitative Analysis of Cytokine-Induced Hepatocellular Death in the Context of Hepatotoxic Therapeutics

by

Benjamin D. Cosgrove

Submitted to the Department of Biological Engineering on December 15, 2008,
in partial fulfillment of the requirements for the degree of
Doctor of Philosophy in Bioengineering

ABSTRACT

Numerous therapeutics, such as viral gene therapy vectors, have unintended toxicity in part due to interactions with inflammatory cytokine signaling to elicit hepatocyte death, thus limiting their clinical use. Although much is known about how cytokines and certain therapeutics individually induce hepatotoxicity, there is little understanding of how they jointly regulate the complex cellular signaling network governing hepatocellular death. In this thesis, we explored the signaling mechanisms governing the cytokine-induced hepatocellular death in the context of adenoviral vector (Adv) infection and pharmaceutical compounds with idiosyncratic hepatotoxicity.

Initially, we examined the role of autocrine and intracellular signaling pathways in governing the synergistic induction of hepatocyte apoptosis by the cytokine tumor necrosis factor-α (TNF) in the presence of Adv infection in a primary rat hepatocyte cell culture model. We demonstrated that Adv/TNF-induced hepatocyte apoptosis is regulated by a coupled and self-antagonizing autocrine signaling cascade involving the sequential release of anti-apoptotic transforming growth factor-α (TGF-α), pro-apoptotic interleukin-1α/β (IL-1α/β), and anti-apoptotic IL-1 receptor antagonist (IL-1ra). This three-part autocrine cascade regulates multiple intracellular signal pathways, including ERK and JNK, that serve to integrate TNF- and Adv-induced signals and govern the resultant hepatocellular death response.

Following this, we demonstrated that numerous idiosyncratic hepatotoxins, whose hepatotoxicities are not evident in standard cell preclinical screening models, elicit synergistic induction of hepatocellular death upon multi-cytokine co-stimulation in primary rat and human hepatocyte cell culture models. We showed that this drug-cytokine co-treatment model could be usefully scaled to the high-throughput demands of pharmaceutical screening while maintaining idiosyncratic hepatotoxicity prediction accuracy. To identify the signaling mechanisms regulating these drug/cytokine hepatocellular death synergies, we collected multi-pathway signal-response data compendia from two human hepatocyte donors. Through the use of partial least-squares regression modeling, we showed that hepatocytes integrate signals from four pathways -- ERK, Akt, mTOR, and p38 -- to specify their cell death responses to toxic drug/cytokine conditions and that accurate prediction of hepatocellular death responses can be made across human hepatocyte donors.

Together, these findings demonstrate that cytokine-induced hepatocellular death in the context of hepatotoxic therapeutics is governed by integrated network activity of multiple autocrine and intracellular signaling pathways.

Thesis Supervisor: Linda G. Griffith
Title: School of Engineering Professor of Biological and Mechanical Engineering

Thesis Supervisor: Douglas A. Lauffenburger
Title: Whitaker Professor of Biological Engineering, Biology, and Chemical Engineering

BIOGRAPHICAL NOTE

Ben Cosgrove received a Bachelor of Biomedical Engineering degree, with *summa cum laude* honors, from the University of Minnesota in May 2003. While at the University of Minnesota, Ben studied in the research laboratory of Dave Odde, where he developed laser-guided direct-writing systems for cell patterning in tissue engineering and computational models of actin filament protrusion and branching.

In September 2003, Ben started his graduate work in the Department of Biological Engineering at the Massachusetts Institute of Technology. Under the joint supervision of Linda Griffith and Doug Lauffenburger, he conducted a Ph.D. thesis entitled "Quantitative Analysis of Cytokine-Induced Hepatocellular Death in the Context of Hepatotoxic Therapeutics", which was completed in December 2008. For the first three years of his Ph.D. thesis, Ben was supported by a biomedical engineering research fellowship from the Whitaker Foundation. In 2008, Ben was honored with the Benjamin Trump Award at the Aspen Cancer Conference and the BMES Graduate Research Award for his Ph.D. thesis research.

In January 2009, Ben will start a postdoctoral fellowship in Stanford University's Molecular Imaging Scholars program. His postdoctoral research will be supervised by Sanjiv Sam Gambhir and Helen Blau and will be focused on noninvasive molecular imaging of signal transduction governing *in vivo* stem cell differentiation.

ACKNOWLEDGMENTS

Foremost, I would like to thank my thesis advisors, Linda Griffith and Doug Lauffenburger, who were both instrumental in every aspect of this work. Linda and Doug maintain a wonderfully collaborative joint research laboratory, and have impressed upon me an appreciation for rigorously quantitative cell biology. Linda is a uniquely creative scientist and engineer, and I thank her for inspiring -- and allowing -- me to take risks in my thesis work. Doug demonstrates unparalleled scientific judgment and vision, and I thank him for guiding my work to fruitful ends. I have been extremely fortunate to have been advised by Linda and Doug, and to be involved in the nascent biological engineering community at M.I.T. that they are so instrumental in fostering.

I would also like to thank a number of professors that helped shape my appreciation for biomedical engineering as an undergraduate at the University of Minnesota. Notably, I extremely grateful to my undergraduate research advisor David Odde and his student Koby Nahmias, who together taught me how to be a scientist. I am also grateful to Victor Barocas and Bob Tranquillo not only for their inspirational teaching, but also for persuading me to attend graduate school at M.I.T.

I am indebted to the careful advice of my thesis committee members Donna Stolz and Forest White, who both also spent time with me in their own research laboratories showing me techniques that ultimately did not get included in my final thesis work. I am grateful for invaluable conversations with Pete Dedon and Steve Tannenbaum on many aspects of toxicology.

This work would not have been possible without the efforts of a number of exceptional collaborators at M.I.T. and elsewhere. I would like to thank Connie Cheng, a Harvard University undergraduate, who diligently and methodically contributed to the work in Chapter 2. I am very proud of Connie's scientific efforts and am glad to see her proceed as a graduate student at the University of Washington. I am appreciative of the work by Bracken King and Bruce Tidor on information theory analysis related to the material presented in Chapter 3. I am greatly indebted to the efforts of Leo Alexopoulos, Julio Saez-Rodriguez, and Peter Sorger at Harvard Medical School for the development and analysis of the drug-cytokine hepatotoxicity synergy model in Chapters 3 and 4. Similarly, I would like to thank Jim Xu, Arthur Smith, Margaret Dunn, David de Graaf, Bart Hendriks, Chris Espelin, and Fei Hua at Pfizer Research Technology Center for their helpful discussions and assistance with the hepatotoxicity work in Chapters 3 and 4. Additionally, I am grateful of Pfizer's generous donation of many compounds and reagents used in this work and H. Steven Wiley of the Pacific Northwest National Laboratory for the generous donation of the c225 monoclonal antibody. I also would like to respectfully acknowledge the anonymous human liver tissue donors from whom I used primary human hepatocytes.

I am extremely thankful of the advice, support, and general camaraderie of everyone in the Griffith and Lauffenburger laboratories and M.I.T. Cell Decision Process Center. I would like to especially thank Evi Farazi, Maya Hasan, Justin Pritchard, and Ta-Chun Hang for their help with much of the experimental work in this thesis. Evi helped develop the drug-cytokine hepatotoxicity synergy approach in Chapter 3. Maya was instrumental in collecting and analyzing data to perform the factorial analyses in Chapter 3. Justin and Ta-Chun assisted in data collection for numerous aspects of

Chapter 2 and 4, respectively. I am also grateful of discussions with John Albeck, Bree Aldridge, John Burke, Ajit Dash, Eileen Dimalanta, Suzanne Gaudet, Nancy Guillen, Albert Hwa, Walker Inman, Lisa Joslin, Brian Joughlin, Melissa Kemp, Pam Kreeger, Matt Lazzara, Kevin Leach, Jose Ricardo Llamas Vidales, Nick Marcantonio, Corey Moore, Joe Moritz, Ericka Noonan, Megan Palmer, Manu Platt, Alexandria Sams, Alejandro Wolf-Yadlin, and Andrea Tentner. I would like to thank Nate Tedford, Anand Sivaraman, Kevin Janes, and Kathryn Miller-Jensen for all serving as scientific role models and for their thoughtful advice and instruction at the beginning of my project. Also, I would like to thank Neil Kumar and Arthur Goldsipe for teaching me the partial least-squares regression approaches used in Chapter 4. Finally, I am grateful for the kind friendship and support of my housemate, labmate, and scientific sounding board, Hyung-Do Kim.

This work would not have been possible without the under-recognized efforts of the following laboratory managers and technicians: Stacey Pawson, Megan Whittemore, Emily Larson, Laura Vineyard, Romie Littrell, and Rachel Pothier. Similarly, I would like to thank the following office and research staff for their tremendous work: Dan Darling, Cathy Greene, Aran Parillo, Michelle Berry, JoAnn Sorrento, and Glenn Paradis.

I am extremely appreciative to the wonderful friends I have made in Boston. In particular, I am grateful for my classmates in Course 20, especially my humorous and joyful housemates Brian Cook and Dave Appleyard.

I could not have completed this work without the constant support of my family. My parents Dave and Joanne, brother Andy, and grandparents all helped instill in me an appreciation for learning and teaching, and it is with their examples that I set off for a life in science and education.

Lastly, I am forever grateful for the love, guidance, and patience of my wife Elissa. She brings me more joy than I deserve. Elissa and I are proud of and overwhelmed by our new son, Ansel. I am thankful to him for his happy disposition and good health, which has afforded me time to finish my thesis over the past six months.

TABLE OF CONTENTS

LIST OF FIGURES AND TABLES

CHAPTER 1

Introduction

This thesis investigates the cellular signaling mechanisms governing the relationship between inflammatory cytokine signaling and therapeutics with inflammation-associated hepatotoxicities, such as adenoviral vectors and idiosyncratic hepatotoxic drugs through the use of quantitative experimental and computational cell biology approaches. This chapter contains background and motivating information pertaining to liver biology, hepatocyte culture methods, inflammatory cytokine signaling, drug hepatotoxicity, and systems biology methods and models fundamental to this thesis.

1.1. Liver organization, function, and cell types

The liver is a vascularized organ composed of multiple cell types in a highly ordered three-dimensional structure. Important liver functions include xenobiotic, protein, steroid, and fat metabolism; blood detoxification; secretion of blood and bile components such as albumin, bile salts, and cholesterol; and storage of vitamins and sugars [1]. Hepatocytes, or parenchymal cells, form single-layer cell plates of the liver lobule and are the key function cell of the liver. Hepatic plates extend from the portal vein to the central vein and are separated by capillary-like sinusoidal spaces [2]. Tissue organization and extra-cellular matrix (ECM) molecules maintain hepatocyte polarity, as defined by three functionally different cellular domains. The hepatic sinusoidal domain contacts ECM molecules and sinusoidal endothelial cells in the Space of Disse that lines the liver sinusoid. The Space of Disse contains the primary hepatic ECM molecules types I-IV collagen, tenascin, laminin, fibronectin, and proteoglycans (heparan sulfate, heparin, chondroitin sulfate, dermatan sulfate). The hepatic lateral domain consists of cell-cell adhesions that are mediated by homotypic E-cadherin associations and are important for cell-cell communication via desmosomes and gap junctions. The hepatic canalicular domain contains bile canaliculi, which serve as functional conduits for bile secretion.

The maintenance of hepatocyte polarity is essential for biliary excretion and xenobiotic elimination.

The non-parenchymal liver cells (NPC's) are comprised of bile duct epithelial cells, sinusoidal endothelial cells (SEC's), Kupffer cells, and stellate cells. Sinusoidal endothelial cells line the sinusoidal space and contain fenestrations, which allow for the transfer of solutes between the hepatic blood and the Space of Disse [2]. Kupffer cells, the resident liver macrophages, are attached to the sinusoidal wall, have phagocytotic activity, and, upon activation, secrete proteases and cytokines. Hepatic stellate cells reside in the Space of Disse and synthesize and secrete ECM components (and their proteases) and the growth factors epidermal growth factor (EGF), hepatocyte growth factor (HGF), and transforming growth factor beta-1 (TGF-β1). Aberrant ECM regulation by stellate cells can lead to liver fibrosis or cirrhosis [2].

1.2. Hepatocyte differentiation

Differentiated hepatocytes are characterized by many specific functions including, but not limited to, urea and albumin synthesis; xenobiotic metabolizing activity via phase I and II enzymes, especially the family of inducible cytochrome P450 enzymes; bile acid transport and secretion via canalicular networks; and morphological hepatic polarity [1]. This functional specialization is a consequence of precise transcriptional regulation of a cohort of liver-specific genes through the cooperation of multiple families of hepatocyte-enriched DNA-binding proteins, promoters, and enhancers [3]. These hepatocyte-enriched regulatory proteins include the hepatocyte nuclear factor (HNF) family consisting of HNF1α/β, HNF3α/β/γ, HNF4α, and HNF6; the CAAAT/enhancer binding protein (C/EBP) family. Differentiated hepatocyte function and gene transcription is regulated by a combination of soluble (hormones, growth factors, cytokines) and insoluble (ECM adhesion, heterotypic and homotypic cell-cell contacts) factors (which are regulated, in part, by non-parenchymal cells), cellular morphology, and biophysical stimuli [1].

1.3. Hepatocyte culture systems

1.3.1. Two-dimensional culture systems

Long-term primary hepatocyte cultures on two-dimensional (2D) surfaces have limited ability to retain liver-specific function and have albumin secretion and cytochrome P450 expression levels below those of isolated hepatocytes [1]. The nature of hepatocyte-ECM interactions are thought to determine both cell shape, cytoarchitecture, and expression of liver-specific families of transcription factors [4, 5]. Many approaches have been studied for the culture of primary hepatocytes on 2D surfaces modified with ECM components. Typical approaches use either coated or gelled type I collagen and/or Matrigel, either in a monolayer or a "gel sandwich" configuration [5]. Matrigel (BD Biosciences) is reconstituted basement membrane from an acid-urea extract from Engelbreth-Holm-Swarm tumor tissue consisting of ~60% laminin, ~30% type IV collagen, and ~3% heparin sulfate proteoglycan and trace other ECM components.

On collagen-coated tissue culture polystyrene (TCPS) surfaces, primary hepatocytes exhibit a rapid loss of albumin section and cytochrome P450 expression and rapid increase on non-specific genes such as actin and tubulin, leading to a flattened, stretched cellular morphology that displays focal adhesion and actin stress fibers [6]. Primary hepatocytes cultured on monolayer gels of type I collagen maintain a cuboidal shape and a cortical distribution of actin filaments and have better retention of liver-specific gene expression [6]. Primary hepatocytes cultured on Matrigel monolayer gels form aggregated clusters, while retaining albumin secretion rates, cytochrome P450 expression and inducibility levels, and C/EBP, HNF1, and HNF4 expression levels near to those in isolated hepatocytes [4, 5]. Primary hepatocytes cultured in between two layers of gelled type I collagen show enhanced cuboidal morphology and the formation of gap junctions and functional bile canalucilar networks and have improved bile acid transport and cytochrome P450 inducibility compared with monolayer collagen gel cultures. Similarly, Matrigel overlay aids in the restoration and maintenance of long-term function of primary hepatocytes in regards to inducibility of cytochrome P450 enzymes, albumin secretion, and cellular morphology [7]. Matrigel and type I collagen gel overlay cultures exhibit no substantial differences in cytochrome P450 inducibility in long-term cultures [1]. Currently, type I collagen gel sandwich cultures serve as the standard long-

term primary hepatocyte culture system for study of xenobiotic metabolism and toxicity, even considering their inability to retain *in vivo* expression levels of liver-specific transcriptional factor and cytochrome P450 enzymes [8].

1.3.2. Three-dimensional culture systems

Scaffold- and capillary-based three-dimensional (3D) bioreactor culture systems have been developed to better retain the tissue structure and function of primary hepatocytes in long-term cultures [9]. The retention of *in vivo*-like hepatic function in long-term hepatocytes cultures is important for the development of high throughput tools for accurate prediction of xenobiotic metabolism and toxicity and other liver-specific functions [8]. Three-dimensional hepatocyte culture systems are proposed to enable primary hepatocytes to form hierarchical tissue structures and cell-cell interactions more closely resembling *in vivo* hepatic tissue than 2D culture systems. In addition, these systems are capable of media perfusion similar to *in vivo* sinusoidal blood flow. Long-term culture (>7 days after cell isolation) of primary hepatocytes in this 3D perfused liver bioreactor has been shown to maintain constant albumin and urea secretion rates and to retain expression levels of HNF and C/EBP families of liver-specific transcription factors and cytochrome P450 enzymes at levels closer to those of freshly isolated hepatocytes than standard 2D collagen gel sandwiches [8-10]. It is hypothesized that the retention of more *in vivo*-like regulation of liver-specific gene expression in this 3D culture system compared to 2D collagen gel sandwich cultures is caused by differences in signaling pathways mediated by soluble paracrine signals, cell-ECM interactions, cell-cell interactions, and biophysical stresses.

1.4. Inflammatory cytokine signaling in hepatocytes

In the liver, inflammatory cytokines are primarily released by the resident liver macrophages, or Kupffer cells, following viral infection and/or injury. These inflammatory cytokines include tumor necrosis factor-α (TNF), interleukin-1α/β (IL-1α/β), interferon-γ (IFN-γ), and interleukin-6 (IL-6). These cytokine binds to their cognate receptors on hepatocytes, activating a diversity of intracellular survival, stress,

and apoptosis pathways (see Figure 1-1). The following section summarizes key features of their intracellular signaling pathways.

1.4.1. Caspase cascade and NF-κB signaling

TNF is a proinflammatory cytokine secreted macrophages that binds to two different transmembrane receptors, TNFR1 and TNFR2. TNFR1 trimerization leads to the recruitment of TRADD (TNFR1 associated death domain protein) which further recruits FADD (Fas-associated death domain protein) and TRAF-2 (TNFR-associated factor-2) through binding with their death domains [11]. FADD binding leads to cleavage and activation of caspase 8, triggering both intrinsic and extrinsic apoptosis cascades. Caspase 8, through BID, induces a mitochondria membrane permeability changes leading to cytochrome c release and subsequent activation of caspase 9 and, finally, the effector caspase 3. Caspase 8 can also directly activate caspase 3. Activated caspase 3 cleaves many intracellular protein targets including cytokeratins and PARP. TRAF-2 binding leads to the activation IKK proteins. IKK-α phosphorylates IκB-α, targeting it for ubiquination and degradation by proteosomes, disassociating it from the transcription factor NF-κB thus allowing NF-κB to translocate to the nucleus [12]. Once translocated, NF-κB promotes the transcription of various anti-apoptotic (*e.g.* Bcl-2 and XIAP) genes. TRAF-2 also mediates c-Jun N-terminal kinase (JNK) activity leading to AP-1 promotion of the cell cycle.

1.4.2. STAT3 and Akt signaling

The pleotropic cytokine IL-6 (interleukin-6) binds to a complex of the transmembrane receptor gp130 (glycoprotein 130) and IL-6R (IL-6 receptor) to activate a variety of proinflammatory, pro- and anti-apoptotic, and acute-phase immune response pathways [13]. IL-6-bound gp-130 activates Janus kinase (JAK) via tyrosine phosphorylation. Phosphorylated JAK and gp-130 subsequently phosphorylates both STAT3 (signal transducer and activator of transcription-3) and SHP2 (SH2-domain-containing protein tyrosine phosphatase-2). Phosphorylated STAT3 (at Y705) dimerizes and translocates to the nucleus, where it activates many "immediate-early" genes associated with liver regeneration, acute-phase response, and hepato-protection. Activated SHP2 interacts

with Grb2 (growth factor receptor-bound protein-2) leading to downstream activation of the Ras–Raf–MEK–ERK pathway. Also, activated gp130 is thought to lead to PI3K (phosphatidylinositol 3-kinase) activation via lipid phosphorylation [13]. This results in recruitment of PDK1 and Akt/protein kinase B (Akt), a serine/threonine kinase, via their Pleckstrin homology (PH) domains, to the plasma membrane, where PDK1 (phosphoinositide-dependent kinase-1) phosphorylates Akt on T308 and Akt S473 is auto-phosphorylated [14]. Active Akt dimerizes and phosphorylates intracellular targets regulating pro-survival (Bad, caspase 9) and transcription (Forkhead transcription factor) regulators. It has also been suggested that active PI3K can also lead to activation of JNK and p38 and their downstream stress/apoptotic pathways [15]. IL-6R/gp130 signaling is inhibited by SOCS3 (suppressor of cytokine signaling-3), which is expressed following STAT3 dimer translocation, forming a negative feedback loop [13]. JNK-mediated activation of AP-1 also contributes to the expression of "immediate-early" genes, including the c-Fos, c-Jos, and c-Myc [16].

1.4.3. p38 and JNK signaling

The p38 mitogen-activated protein kinase (p38) and JNK pathways are activated by proinflammatory cytokines (TNF, IL-1) and cellular stresses (UV radiation, hyperosmolarity) [17]. Both pathways are controlled by multiple upstream MAP3K's including MEKK1 and ASK1. JNK phosphorylates the proto-oncogene c-Jun, a component of the transcription factor AP-1, which binds and activates transcription. JNK mediates apoptosis through the phosphorylation of Bcl-2 family proteins. p38 affects downstream effectors such as transcription factors MK2, ATF-2 and HSP27 and ultimately activates the caspase cascade [17].

1.4.4. Apoptosis: programmed cell death

Apoptosis is a form of programmed cell death characterized by nuclear and cellular fragmentation and loss of plasma membrane polarity. Apoptosis is an important physiological process in maintaining epithelial cell biology and is implicated in liver disease, response to injury, and fibrosis [18]; dysregulation of hepatocyte apoptosis occurs in hepatocellularcarcinoma. Apoptosis occurs via two distinct pathways that

converge to activate the effector cysteine protease caspase 3: (1) the extrinsic pathway, extracellular ligands bind to death receptors (*e.g.* TNF/TNFR1) and activate a cascade of intracellular signals, leading to the activation of the initiator caspase 8; and (2) the intrinsic pathway, in which dysfunction of intracellular organelles (*e.g.* mitochondrial cytochrome c release) due to various cellular stresses leads to activation of the initiator caspase 9 [19].

1.5. Inflammation-related hepatotoxicity of therapeutics

1.5.1. Adenoviral vectors

Recombinant adenovirus vectors (Adv) are widely used as transfection tools for gene therapy and cell biology. The liver is an important organ for Adv-based gene therapy due to the fact that a variety of human disorders originate from genetic defects in hepatocytes and that liver cells are exposed to systematically delivered viral vectors due to portal circulation. In the liver, Kupffer cells readily uptake Adv via phagocytosis and, through an innate immune response, release the proinflammatory cytokines TNF, IL-1α/β and IL-6 into the surrounding liver [20, 21]. Consequently, Adv administration as liver-directed gene therapy is confounded by hepatotoxicity through programmed cell death.

Using a replication-deficient E1/E3-deleted adenovirus vector serotype 5, Miller *et al* demonstrated that Adv sensitizes multiple human epithelial cell lines (including the C3A hepatoblastoma cell line) to TNF-mediated apoptosis [22]. Adv and TNF both upregulate pro-survival (PI3K–Akt) and stress (p38–HSP27) signaling pathways [22, 23]. Adv infection of epithelial cells is mediated by viral entry dependent of coxsackie- and adenovirus-receptor (CAR) and integrin docking and endocytosis [24]. Adv infection renders epithelial cells unable to generate sufficient survival signals (Akt activity becomes saturated) to overcome to TNF-mediated apoptosis [22]. Demonstrating another mechanism of virus-sensitization to TNF-mediated cell death, Wang *et al* have shown that hepatitis B virus X protein activates p38 kinase/JNK stress pathways leading to the upregulation of the death receptors TNFR1 and FasL and increased sensitivity to TNF-mediated apoptosis [25]. These results have significant implications for our understanding of viral vector-induced hepatotoxicity and demonstrate that viral gene therapy vectors sensitize cells to cytokine-induced cell death.

1.5.2. Inflammation-associated idiosyncratic drug hepatotoxicity

Idiosyncratic drug hepatotoxicity is defined as drug-induced liver injury that occurs in a very small fraction of human patients, is unrelated to the pharmacologic target of the drug, and exhibits no apparent relationship to dose or duration of drug exposure [26-28]. Multiple hypotheses have been suggested to explain the mechanisms underlying idiosyncratic drug hepatotoxicity. These include (i) variations in drug metabolism, particularly associated with alterations in the expression and/or activities of the cytochrome P450 family enzymes, due to variable environmental conditions and/or genetic polymorphisms in the human population [29]; and (ii) a relationship with concomitant liver inflammation associated with viral or bacterial infection or liver or inflammatory disease [26].

A number of preclinical models have been developed in attempts to predict idiosyncratic drug hepatotoxicity, including the assessment of reactive metabolites through glutathione (GSH) conjugation assays and the evaluation of animals models by toxicogenomic and metabolonomic approaches to identify common idiosyncratic hepatotoxicity-associated biomarkers, with little overall predictive success [27, 30, 31]. Rodent models administered with bacterial lipopolysaccharide (LPS) have been recently developed to assess inflammation-associated idiosyncratic drug hepatotoxicity. In these rodent models, LPS exposure induces a mild inflammatory response that has been demonstrated to synergistically induce hepatotoxicity in the presence of a number of idiosyncratic hepatotoxic drugs, including diclonfenac, sulindac, trovafloxacin, ranitidine, chlorpromazine, but not non- or less-toxic control drugs [32-35]. In rats, LPS administration upregulates plasma concentrations of the cytokines tumor necrosis factor-α (TNF), interferon-γ (IFNγ), interleukin-1α and -1β (IL-1α/β), interleukin-6 (IL-6), and the chemokine interleukin-10 (IL-10) [36]. Of these, TNF, IFNγ, IL-1α/β, IL-6, and LPS itself all stimulate hepatocyte signaling responses. In LPS-administered rat models, synergistic induction of hepatocellular death in the presence of the idiosyncratic hepatotoxins ranitidine and trovafloxacin has been reported to be dependent on TNF signaling [35, 37].

The observations in LPS-administered rodent models suggest that idiosyncratic drug hepatotoxicity can arise when mild drug-induced hepatocellular stress synergizes

with LPS-induced inflammatory cytokine signaling to elicit acute hepatocellular death [27, 38]. These stresses may be idiosyncratic in nature in human patients due variations in drug metabolism, exposure, and/or clearance. The sensitizing role of hepatocellular stress is supported by the fact that drug-induced depletion of glutathione is known to sensitize hepatocytes to TNF-induced apoptosis [39]. Furthermore, both LPS and inflammatory cytokine signaling can alter hepatocyte expression of cytochrome P450 enzymes and thus lead to dysregulated drug metabolism and clearance in conditions of LPS-induced liver inflammation [40, 41].

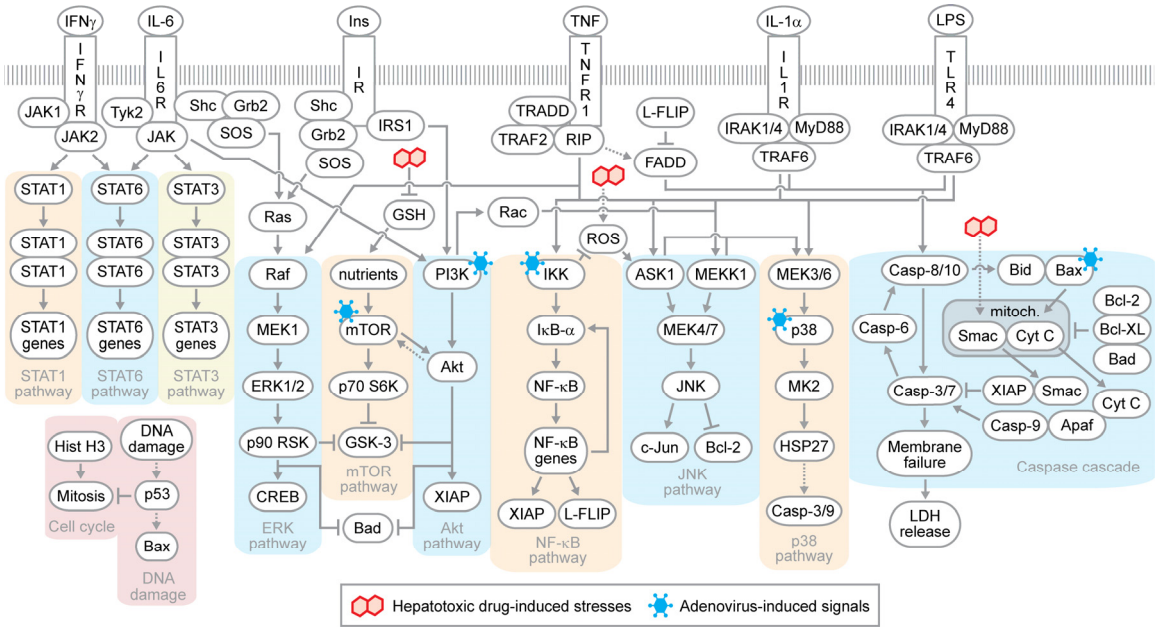

Figure 1-1. A schematic hepatocyte signaling network demonstrating the intersection of inflammatory cytokine signaling and hepatotoxic therapeutics, such as replication-deficient adenovirus and idiosyncratic hepatotoxic drugs.

1.6. Systems biology models of cell behaviors

Systems biology seeks a deep quantitative understanding of complex biological processes through the integration of multivariate molecular-level measurement and modeling approaches, and thus differs from proteomic and genomic efforts that aim to catalogue a broad listing of biological components and their functions [42, 43]. Advances in high-throughput and multiplex techniques for quantifying the abundances and activities of the molecular components involved in gene expression [44], metabolism [45], and signal transduction [42] make it feasible to collect large data sets of diverse cellular processes.

Large-scale quantitative studies of complex biomolecular processes are difficult to interpret by inspection and intuition alone. Computational modeling allows simplification of large-scale biological data sets and can suggest mechanistic insights and enable quantitative predictions of cellular processes [43, 46].

1.6.1. System-level measurement of cell signaling and behavioral phenotypes

In systems biology, the collection of experimental data sets is organized and conducted with regard to intended modeling efforts and practical limitations. Systems models largely require dynamic, highly multivariate, and quantitative data of protein activities and cell behavioral phenotypes collected in specific cell types subjected to defined, and often diverse, stimuli. A wide variety of high-throughput and multiplex experimental techniques are utilized to collect data sets for systems models. These include mass spectrometry [47], kinase activity assays [48, 49], immunoblotting [50], "in-cell westerns" [51], bead-based protein arrays [52], protein microarrays [53, 54], and multicolor flow [55, 56] and image [57, 58] cytometry.

In selecting appropriate measurement techniques, one often considers the identity and number of simultaneously measureable signals (whether assays can be "multiplexed"), the amount of sample required per assay, and whether single-cell or population-level behavior is measured [42]. Mass spectrometry can be used to quantify the relative abundance of hundreds of regulatory protein phosphorylation sites across multiple biological samples, but requires 10^5-10^7 cells per sample due to the fractionation required to detect low abundance peptides in a complex cellular lysate [59]. Kinase activity assays directly measure the enzymatic activity of kinases to phosphorylate substrates via radiochemical [48] or fluorescence [49] readouts and are multiplexible but require ~10^5 cells per kinase assayed. In-cell westerns are a form of immuno-fluorescence microscopy that measures protein levels or states in fixed cells still adherent to culture surfaces [51]; this method is not currently multiplexible but requires only 10^4-10^5 cells per protein assayed. Bead-based arrays utilize flow cytometric quantification of bead-conjugated, fluorescently-labeled antibody sandwich assays [52]. A number of commercial vendors provide well-validated, highly multiplexible reagents for phosphoprotein quantification in a cell lysate using the Luminex platform. In practical

applications, ~10-20 phosphoproteins can be quantified in a lysate from 10^4-10^5 cells. Protein microarrays allow detection of binding avidities of cellular proteins to hundreds of printed protein and/or substrate features and can be conducted with a lysate from 10^4-10^5 cells [54]. Multicolor flow and image cytometry can assess phosphoprotein levels and cellular phenotypes (such as proliferation, apoptosis, and migration) at a single-cell level. Using well-validated antibodies and stains, multiplexing ~10 and ~4 parallel measurements are typical current practical upper limits for flow [55] and image [58] cytometry, respectively, but informative data sets can be collected in as few as 10^2-10^3 cells per condition.

As no individual measurement technique can capture the full diversity of protein signals important to the operation of cell signaling networks, systems biology models of cell signaling and responses are increasingly relying on data compendia assembled from heterogeneous assay types [50]. Assembly of such data compendia requires careful consideration to data fusion, normalization, and scaling when applied to quantitative models (see [42, 50]).

1.6.2. Data-driven modeling of cell signaling and behavioral phenotypes

A wide spectrum of computational modeling approaches for studying cell signaling and its regulation of behavioral phenotypes is available [60]. Because the mechanisms connecting disparate cell signaling pathways to each other and to integrated cell behaviors are largely unknown, approaches such as differential equation-based physicochemical models [61] that require substantial mechanistic knowledge are currently limited in their practical applicability for analyzing relationships between regulatory network activities and downstream cell phenotypic behavior. Accordingly, this discussion focuses on a set of more abstract modeling approaches more suitable for characterizing the operational relationships, influences, and logic of cell signaling networks as they relate to cell functions: partial least-squares regression, decision trees, and Bayesian network inference.

1.6.3. Partial least-squares regression

Partial least-squares regression (PLSR) models are based on the hypothesis that, across multiple treatment conditions, cell behavioral phenotypes ("responses") are inherently dependent on quantitative combinations of a subset of measureable activities or states of key signaling molecules ("signals") [46, 62]. Measured signaling variables (including both protein activities at multiple time points and extracted time-dependent metrics) and measured cell behaviors are cast into two separate data matrices: an independent block of signaling variables (X) and a dependent block of response variables (Y), both arrayed across multiple cellular conditions. Since the number of cellular conditions measured often is exceeded by the number of signaling variables, PLSR is necessary to calculate a unique regression solution to the hypothesized relationship $Y = f(X)$. PLSR identifies a linear solution to the signaling-response relationship within a reduced-dimensionality data space defined by a set of orthogonal principal components [63]. (It should be noted that nonlinear relationships can be readily modeled through inclusion of nonlinear combinations of variables and/or nonlinear variable transformations.) The calculation of principal components-based regression weights is biased towards those signaling variables that most strongly correlate with the responses and to optimize prediction accuracy of the responses in cross-validation.

PLSR models can be used to elucidate an integrative model of network operation that can identify key combinations of signaling activities governing measured cell behaviors. Moreover, they can be used to quantitatively and accurately predict responses of cells to additional treatments, such as pharmacologic perturbations, *a priori* using newly measured and/or estimated signaling data. To generate a model capable of accurate *a priori* predictions, the conditions used to train a PLSR model need to strongly and differently activate the breadth of measured cell signaling activities and behaviors [50, 64]. PLSR models have been generated using cell signaling and response data from a number of the aforementioned measurement techniques, and have been successful at interpreting and predicting cell signaling-response relationships in varied contexts such as ECM-regulated embryonic stem cell self-renewal and differentiation [65], cytokine- and pathogen-induced epithelial cell apoptosis-survival [50, 62, 64], receptor agonist-induced

T-cell and B-cell cytokine release [66, 67], and growth factor-induced mammary epithelial cell proliferation and migration [68].

1.6.4. Decision trees

Decision tree (DT) models can be useful as network-function models to interpret and predict cell signal-response relationships in terms of logical combinations of multiple signal activity levels. Decision tree models are generated from a learning algorithm that approximates a cellular output by constructing a "tree" where the "branches" classify logical combinations of signals based on their measured or estimated levels, and the "leaves" at the end of the branches predict the cellular output. The idea behind DT modeling is to recursively split signal-response data into successively smaller branches in order to end up with a tree in which signal combination branches are obtained that can classify response behavior as correctly as possible. A decision tree model is usually obtained via a two-step process [69, 70]. The first step, tree growing, is done until all response observations are classified correctly. The second step, tree pruning, is done in order to avoid over-fitting. In generally, decision tree models have several properties that are appealing in biological research [69]: (a) they can be effectively applied to broad classes of data, in particular to discrete, continuous or mixed data; (b) they are capable of good prediction accuracy for highly nonlinear prediction problems; (c) their prediction rules are easy to visualize and interpret; and (d) they are very robust against outliers. Additionally, a DT model provides quantitative predictions to guide interventions, such as using pharmacologic inhibitors, even when such interventions only partially diminish the signal. Moreover, the DT approach facilitates incorporation of nonlinear behavior more readily through its alternative inclusions of qualitatively diverse model branches characterizing different logical relationships among the signaling nodes. Successful decision tree models have been developed for growth factor- and ECM-induced fibroblast migration [70, 71] and Fas-mediated T lymphoma apoptosis [72].

1.6.5. Bayesian networks

Bayesian networks offer a modeling technique for identifying causal relationships among multiple signals as well as from signals to responses. Bayesian network models illustrate

the interactions of pathway components in the form of influence diagrams that can contain both direct molecular interactions (*e.g.* kinase-substrate phosphorylation) and indirect influences that proceed through unobserved intermediates [56]. Models are inferred through probabilistic calculations of covariations in activities of multiple signaling species, usually sparsely distributed across different signaling pathways, collected from single cells [56] or populations of cells [73] exposed to diverse combinations of extracellular stimuli and genetic and/or pharmacologic pathway interventions, with effective inference requiring many observations. As such, flow cytometry data containing simultaneous measurement of multiple phosphoproteins of thousands of individual cells under a variety of treatment conditions are well-suited for Bayesian inference and have resulted in accurately inferred influence networks [56]. In comparison, Bayesian models based on population-based multivariate signaling data [56, 73] require more diverse treatments and have reduced network inference accuracy, in part due to the obfuscation of informative heterogeneity at the single-cell level. Inferred influence networks can suggest novel signal transduction hypotheses [56] but also could be useful in identifying context-specific signaling network structures. This kind of model can also be used to make predictions about how interventions in the network influence downstream cell phenotypic behaviors, as demonstrated for the example of embryonic stem cell self-renewal and differentiation responses to combinations of cytokine and extracellular matrix cues [56]. Bayesian network modeling efforts to date have been restricted to static models, but the feedback loops inherent in cell signaling networks will likely often require dynamic Bayesian network models adapted to handle cyclic connectivities [74].

1.7. Thesis overview

This work utilizes quantitative experimental and computational cell biology approaches to explore the relationship between inflammatory cytokine signaling and therapeutics with inflammation-associated hepatotoxicities, such as adenoviral vectors and idiosyncratic hepatotoxic drugs. Initially, the role of autocrine signaling in governing the synergistic induction of rat hepatocyte cell death following adenoviral vector infection and TNF signaling is examined. Subsequently, a multi-cytokine *in vitro* model of

inflammatory cytokine-associated idiosyncratic drug hepatotoxicity is developed and analyzed in primary rat and human hepatocytes and HepG2 cells. Through the use of data-driven modeling, it is demonstrated that the synergistic induction of hepatocellular death by idiosyncratic hepatotoxins and inflammatory cytokines is governed through the network-level interaction of four key phosphoprotein signaling pathways.

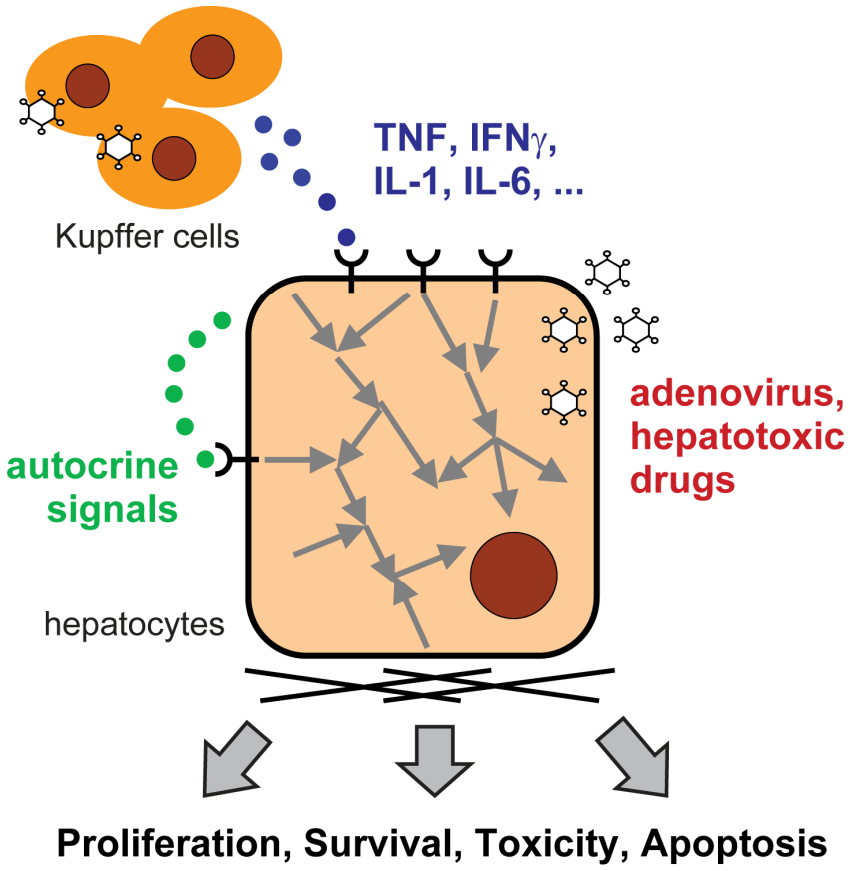

Figure 1-2. A schematic overview of the biological questions investigated in this thesis. In general, this work applies quantitative experimental and computational cell biology approaches to study hepatocyte responses to diverse inflammatory cytokine stimuli in the context of hepatotoxic therapeutics, such as replication-deficient adenovirus and idiosyncratic hepatotoxic drugs.

CHAPTER 2

Autocrine signaling control of hepatocyte proliferation and apoptosis responses to tumor necrosis factor-α

Note: The content of this chapter is based on the published article: Cosgrove BD, Cheng C, Pritchard JR, Stolz DB, Lauffenburger DA, Griffith LG. *Hepatology* 2008, 48(1):276-288.

2.1. Introduction

2.1.1. TNF-mediated hepatocyte signaling and responses

Tumor necrosis factor-α (TNF) can stimulate multiple disparate hepatocyte responses – proliferation, survival, or apoptosis – depending on the cellular context. In the liver, TNF is secreted by Kupffer cells, the resident macrophages, following partial hepatectomy (PHx) and during inflammatory responses [75, 76]. Secreted TNF binds to and activates its receptor TNFR1, leading to downstream activation of the NF-κB, JNK, and p38 MAPK signaling pathways and the cascade of caspase proteases [76] (see also Figure 1-1). The modulation of these and other intracellular signaling pathways by concomitant synergistic and antagonistic cytokine stimuli, viruses, and/or pharmacological treatments determine specific cell responses to TNF [11, 22, 77].

In the PHx model of liver regeneration, normally quiescent hepatocytes are stimulated to proliferate in a process regulated by multiple redundant signaling pathways and molecules [75]. Following PHx, Kupffer cells are activated and secrete TNF and IL-6. These cytokines stimulate the transcription of a set of "immediate early" genes and a G_0–G_1 cell cycle progression in hepatocytes [78, 79]. TNF signaling primes hepatocytes for DNA replication through subsequent stimulation by hepatocyte growth factor (HGF) and epidermal growth factor receptor (EGFR) ligands [75, 79-81]. In primary hepatocyte cultures, TNF not only potentiates growth factor-stimulated proliferation, but acts as a

mitogen itself [78, 82] through the induced release of autocrine transforming growth factor-α (TGF-α) and its activation of Akt and ERK signaling [83, 84]. The functionally similar interleukin-1 receptor (IL-1R) agonists IL-1α and IL-1β antagonize, through iNOS activation and nitric oxide production, hepatocyte proliferation when produced by non-parenchymal cells *in vivo* during liver regeneration and when added exogenously to mitogenic factors *in vitro* [85-87].

Hepatocytes are resistant to apoptosis stimulated by TNF alone as it activates both pro- and anti-apoptotic signaling pathways [11, 76]. Consequently, pharmacologic or genetic interference with anti-apoptotic signaling is commonly used to examine TNF-induced hepatocyte apoptosis [11]. In diseased and/or virus-infected hepatocytes, TNF signaling contributes to apoptotic and necrotic cell death [11, 25]. Recently, we have shown that infection with a replication-deficient adenoviral vector (Adv) potently sensitizes human epithelial cell lines, including the C3A hepatocarcinoma cell line, to TNF-induced apoptosis [22]. In these human epithelial cell lines, Adv infection potentiates TNF-induced apoptosis through the activation of both pro-apoptotic p38 MAPK signaling and anti-apoptotic NF-κB and Akt signaling [22]. Further, Adv infection saturates pro-survival signaling effectors downstream of Akt and thus limits insulin-mediated rescue of TNF-induced apoptosis [22]. Adenoviral gene therapy vectors targeting the liver and other organs are often compromised due to hepatocyte death induced by both the viral vector itself and cytokines of the innate immune response such as TNF and IL-1β [20]. Therefore, Adv infection might provide a physiologically relevant environment to potentiate TNF-induced apoptosis in primary hepatocytes and could lead to insights in liver adenoviral gene therapy.

Hepatocyte death responses to TNF and other inflammatory cytokines can be antagonized by many of the same growth factors that stimulate hepatocyte proliferation [81, 88] or by naturally occurring inhibitors of cytokine signaling such as IL-1 receptor antagonist (IL-1ra) [89]. While many of the factors, such as TNF, that affect hepatocytes during injury or stress arise primarily from exogenous sources, hepatocytes themselves secrete numerous growth factors and cytokines that act in autocrine fashion to enhance or oppose exogenous stimuli [80, 81, 83, 84, 88, 90]. Recently, we have demonstrated that the response of IFN-γ-sensitized human epithelial cell lines to TNF involves release of

TGF-α, IL-1α, and IL-1ra, which provide conflicting and interlinked autocrine feedback signals governing apoptotic responses to TNF [62, 77]. Furthermore, this multi-ligand autocrine circuit can self-limit apoptosis when anti-apoptotic autocrine TGF-α and IL-1ra signaling outweigh pro-apoptotic signaling by exogenous TNF and autocrine IL-1α [77]. Whether a similar multi-ligand autocrine circuit influences the disparate possible hepatocyte responses to TNF stimulation is unknown. However, hepatocytes express TGF-α, IL-1α, IL-1β, and IL-1ra and their receptors but it is unknown whether these ligands operate via interlinked autocrine circuits to modulate hepatocyte proliferation and apoptosis responses to TNF [82, 83, 90-92].

2.1.2. Chapter overview

Here we show that rat hepatocyte proliferation and apoptosis responses to TNF are both mediated by an inducible, coupled, and self-antagonizing TGF-α–IL-1α/β–IL-1ra autocrine cascade. The net effect of this coupled autocrine cascade is pro-proliferative as induced by TNF alone but pro-apoptotic when induced by TNF in Adv-infected hepatocytes. Moreover, elucidation of this self-antagonizing autocrine cascade is a useful paradigm that helps rationalize the diverse landscape of hepatocyte phenotypic responses to TNF and TGF-α co-stimulation and their induction of autocrine IL-1α/β signaling.

2.2. Experimental procedures

2.2.1. Primary rat liver cell isolation

Primary hepatocytes were isolated from 150-230 g male Fisher rats using a modified two-step collagenase perfusion using Blendzyme 3 (Roche, Indianapolis, IN), essentially as described previously [8, 93, 94]. Following isolation, cells were suspended in Dulbecco's Modified Eagle's Medium (DMEM; Invitrogen, Carlsbad, CA) supplemented with 2 mg/ml bovine serum albumin (BSA) and 50 μg/ml gentamicin and centrifuged at 50*g* for 2 minutes twice. All non-sedimented cells from the 50*g* centrifugation were combined as the non-parenchymal cell (NPC)-enriched isolate, which was subsequently resuspended in red blood cell lysing buffer (NH_4Cl 150 mM, $KHCO_3$ 1 mM, Na_2EDTA 0.1 mM, pH ~7.4) to remove red blood cells. The remaining hepatocyte-enriched cell

pellet was resuspended to a concentration of 5×10^6 cells/ml in supplemented DMEM and then mixed with Percoll (45% final) and 10× Hank's Balanced Salt Solution (HBSS; 5% final) and centrifuged at 50*g* for 10 minutes. Final cell viability of the hepatocyte-enriched isolates was assessed by trypan blue exclusion using a Vi-Cell instrument (Beckman-Coulter, Fullerton, CA) and was routinely 90-95%. Flow cytometric analysis of immunostained cells (see below) showed that purified hepatocyte isolates comprised ~97% hepatocytes (albumin$^+$-cytokeratin-18$^+$ cells), ~0.4% Kupffer cells (ED2$^+$), ~0.4% stellate cells (GFAP$^+$), and ~0.2% sinusoidal endothelial cells (SE-1$^+$) (see Chapter 2.2.5, Figure 2-1, Table 2-1). Unless noted, all products were obtained from Sigma (St. Louis, MO).

2.2.2. Adenoviral vector

A replication-deficient recombinant adenovirus type 5 vector with E1 and E3 regions deleted and expressing *Escherichia coli* β-galactosidase under a cytomegalovirus enhancer/promoter was obtained from Puresyn, Inc. (Malvern, PA). This Adv vector has a ratio of 1 infectious viral particle (v.p.) per 6.6 total v.p. as determined by the manufacturer in a fluorescent focus assay. The multiplicity of infection (MOI) is defined as the number of infectious Adv particles per seeded hepatocyte. Storage buffer (10% glycerol in PBS) was used for mock infection controls.

2.2.3. Rat hepatocyte cell culture and stimulation

For all studies, rat hepatocyte isolates from after the Percoll purification step were cultured on single-layer collagen type I (BD Biosciences, Franklin Lakes, NJ) gels in HGM at 37°C and 5% CO_2. Collagen gels were made in 6-well tissue culture-treated polystyrene plates (BD Biosciences) by adding 600 µl/well of collagen type I (BD Biosciences) diluted to 1.6 mg/ml in PBS containing 2 mg/ml glucose and 3.7 mg/ml sodium bicarbonate (pH ~7.8) for 2 hours at 37°C [1, 8]. Collagen gels were blocked with 1% bovine serum album (BSA) in PBS for 2 hours at 37°C to inhibit cytokine binding. Hepatocytes were maintained in a modified, serum-free hepatocyte growth medium (HGM; [95]) comprising DMEM supplemented with 2 mg/ml BSA, 100 nM dexamethasone, 2.25 mg/ml glucose, 2 mg/ml galactose, 110 µg/ml sodium pyruvate, 30

mg/ml L-proline, 100 μg/ml L-ornithine, 305 μg/ml niacinamide, 1 mM L-glutamine (Invitrogen), 5 μg/ml sodium selenite, 5 μg/ml transferrin (Roche), 54.4 ng/ml $ZnCl_2$, 75 ng/ml $ZnSO_4$, 20 ng/ml $CuSO_4$, 25 ng/ml $MnSO_4$, 50 μg/ml gentamicin, and 5 μg/ml insulin.

For proliferation studies, hepatocytes were seeded at 40,000 cells/cm^2 and media were changed 4 hours post-seeding. Twenty four hours after seeding, hepatocytes were stimulated with 0 or 100 ng/ml TNF (recombinant rat TNF; R&D Systems, Minneapolis, MN) and 0, 1, 10, or 100 ng/ml TGF-α (recombinant human TGF-α; R&D Systems) as a 40× stock solutions in HGM. After 24 hours of cytokine stimulation, 10 μM 5-bromo-2'-deoxyuridine (BrdU; Invitrogen) was added as a 40× stock solution in HGM to label S-phase cells. After 24 hours of BrdU incubation, hepatocytes were harvested and fixed for flow cytometry. Conditioned medium samples were collected at 0, 12, 24, 36, and 48 hours following cytokine stimulation to assay cytokine release. Lysates were collected at 0, 0.25, 2, 12, and 24 hours following cytokine stimulation to assay phosphoprotein signaling.

For apoptosis studies, hepatocytes were seeded at 50,000 cells/cm^2 and media were changed 4 hours post-seeding. Twenty four hours after seeding, hepatocytes were infected with 0, 12.5, 25, 50, or 100 MOI (0, 1.1, 2.2, 4.3, or 8.7×10^7 infectious v.p./ml) Adv in fresh media. To remove non-infectious particles, Adv infection medium was removed after 6 hours and was replaced with fresh medium following a PBS wash. Twenty four hours after the start of Adv infection, hepatocytes were stimulated with 0, 1, 5, 20, 100, or 200 ng/ml TNF and 0, 1, 5, 20, or 100 ng/ml TGF-α as a 40× stock solutions in HGM. After 24 hours of cytokine stimulation, hepatocytes were harvested and fixed for flow cytometry. Conditioned medium samples were collected at 0, 6, 12, 18, and 24 hours following cytokine stimulation to assay cytokine and lactate dehydrogenase (LDH) release. Lysates were collected at 0, 0.25, 2, 6, 12, and 24 hours following cytokine stimulation to assay phosphoprotein signaling.

For both proliferation and apoptosis studies, 10 μg/ml anti-TGF-α neutralizing antibody (R&D Systems), 10 μM CI1033 (a pan-EGFR/ErbB receptor tyrosine kinase inhibitor; Pfizer, New York, NY), 10 μg/ml IL-1ra (recombinant rat IL-1ra; R&D Systems), 10 μg/ml anti-IL-1α neutralizing antibody (R&D Systems), or 10 μg/ml anti-

IL-1β neutralizing antibody (R&D Systems) were added as 40× stock solutions one hour before cytokine stimulation to perturb autocrine ligand activity. For analysis of cell types in hepatocyte cultures, hepatocyte-enriched isolates from both before and after the Percoll purification step were seeded and treated as described above for apoptosis studies with the treatments indicated in Table 2-1.

2.2.4. Flow cytometry analysis of proliferation and apoptosis

After 24 (apoptosis studies) or 48 hours (proliferation studies) of cytokine treatment, culture medium was collected and 0.12 mg/ml Blendzyme 3 in PBS was added to the culture wells to partially digest the collagen gel for ~6 minutes at 25°C. Hepatocytes were then removed by adding PBS with 0.1% Tween-20 (PBS-T) and pipetting vigorously and then were combined with the culture media to ensure collection of both floating and adherent cells from each well. Collected cells were centrifuged, fixed in 2% paraformaldehyde (PFA) for 20 minutes, washed in PBS-T, and then fixed in 100% methanol at -20°C for up to 1 week. After centrifugation to remove excess methanol, cells were washed once in PBS-T. For proliferation staining, cells were then incubated for 20 minutes in 2 M HCl to denature DNA and expose the BrdU epitope. After centrifugation to remove excess HCl, cells were washed three times in PBS-T and then stained with anti-albumin (rat-specific polyclonal; MP Biomedicals, Solon, OH) and anti-BrdU (clone PRB-1; Invitrogen) antibodies in PBS-T with 1% BSA (PBS-TB) for 1 hour. Cells were washed twice with PBS-TB and stained with AlexaFluor 488-conjugated goat anti-rabbit and AlexaFluor 647-conjugated goat anti-mouse secondary antibodies (Invitrogen) in PBS-TB for 1 hour. Cells were then washed once with PBS-T, resuspended in PBS, and 30,000 cells from each biological replicate were analyzed by flow cytometry using a FACS-Calibur instrument (BD Biosciences) and FlowJo software (Tree Star, Ashland, OR). Proliferating hepatocytes were reported as $BrdU^+$ cells within the $albumin^+$ population. For apoptosis studies, cells were stained and analyzed as described for proliferation studies with the omission of the DNA denaturation step and were stained with an anti-cleaved caspase 3 primary antibody (clone C92-605; BD Biosciences) and an AlexaFluor 488-conjugated goat anti-rabbit secondary antibody (Invitrogen). Apoptotic hepatocytes were reported as cleaved $caspase\ 3^+$ cells.

2.2.5. Flow cytometry analysis of cell type markers

Cell type markers were analyzed in freshly isolated NPC and hepatocyte fractions (from both immediately before and after the Percoll step) and in cultured hepatocytes (harvested as described above). For both perfusion isolates and cultured hepatocytes, collected cells were centrifuged, fixed in 2% PFA for 20 minutes, washed in PBS-T, and then fixed in 100% methanol at -20°C for up to 1 week. After centrifugation to remove excess methanol, cells were washed once in PBS-T. Cells were immunostained with anti-albumin (rat-specific polyclonal; MP Biomedicals, Solon, OH), anti-cytokeratin-18 (clone CY-90; Sigma), anti-CD163/ED2 (clone ED2; Serotec, Raleigh, NC), anti-GFAP (clone 4A11; BD Biosciences), and/or anti-SE-1 (clone SE-1; IBL America, Minneapolis, MN) primary antibodies in PBS-T with 1% BSA (PBS-TB) for 1 hour. Cells were washed twice with PBS-TB and stained with AlexaFluor 488-conjugated goat anti-rabbit and AlexaFluor 647-conjugated goat anti-mouse secondary antibodies (Invitrogen) in PBS-TB for 1 hour. Cells were then washed once with PBS-T, resuspended in PBS, and 30,000 cells from each biological replicate were analyzed by flow cytometry using a FACS-Calibur instrument (BD Biosciences) and FlowJo software (Tree Star, Ashland, OR). Cell populations were reported as follows: hepatocytes, albumin$^+$-cytokeratin-18$^+$ cells [95, 96]; Kupffer cells, ED2$^+$ cells [97]; stellate cells, GFAP$^+$ cells [98]; and sinusoidal endothelial cells, SE-1$^+$ cells [94, 99].

2.2.6. Enzyme-linked immunoabsorbant assays

Cytokines in culture supernatants were quantified using human TGF-α, rat IL-1α, rat IL-1β, and mouse IL-1ra ELISA kits according to manufacturer's recommendations (R&D Systems). The human TGF-α ELISA kit was validated with a recombinant rat TGF-α standard (Phoenix Pharmaceuticals, Burlingame, CA), which showed a 26% cross-reactivity relative to recombinant human TGF-α and linearity from 5-500 pg/ml (R^2 = 0.99; data not shown). The mouse IL-1ra ELISA kit was validated with a recombinant rat IL-1ra standard (R&D Systems), which showed a 65% cross-reactivity relative to recombinant mouse IL-1ra and linearity from 100-1500 pg/ml (R^2 = 0.97; data not shown).

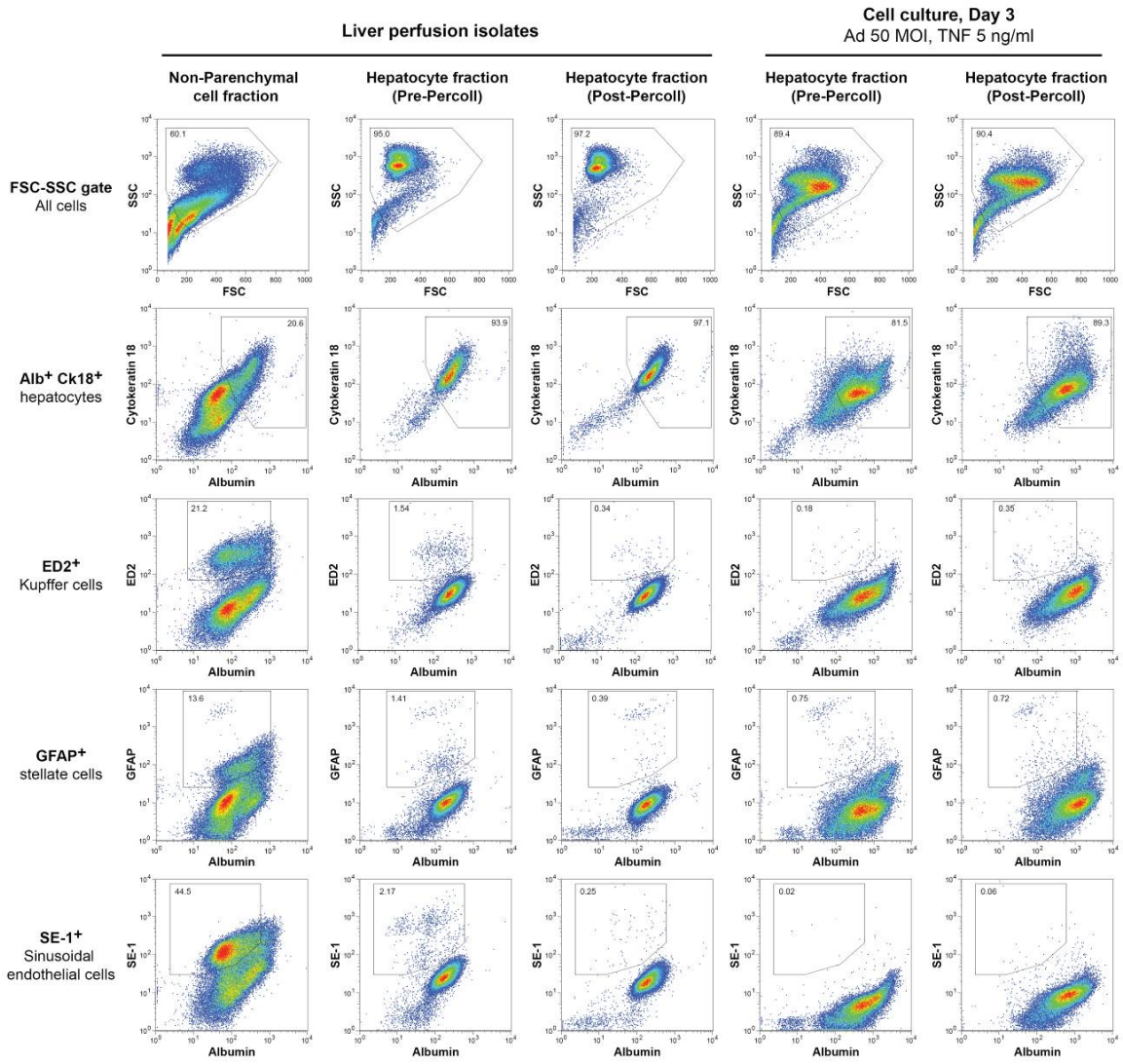

Figure 2-1. Representative flow cytometry scatter plots of cell population analysis of liver perfusion isolates and cultured hepatocytes. See Table 2-1 for a summary of cell type fractions in each perfusion isolate and in multiple cell culture conditions relevant to this study.

Table 2-1. Flow cytometry analysis of liver cell populations in perfusion isolates and cell culture conditions related to TNF-induced hepatocyte proliferation and apoptosis studies.

Cell isolate[1]		Cell culture treatment[2]			Flow cytometry analysis of cell population[3]			
Isolate fraction	**Percoll**	**Adv MOI**	**TNF (ng/ml)**	**TGF-α (ng/ml)**	**% Alb^+-$Ck\text{-}18^+$ cells**	**% $ED2^+$ cells**	**% $GFAP^+$ cells**	**% $SE\text{-}1^+$ cells**
NPC	n/a	*perfusion isolate*[4]			22.3	20.4	16.0	44.8
Hepatocyte	Pre	*perfusion isolate*			94.9	1.49	1.40	1.85
Hepatocyte	Post	*perfusion isolate*			96.5	0.41	0.39	0.24
Hepatocyte	Pre	0	0	0	86.0	0.27	2.25	0.05
Hepatocyte	Pre	0	0	20	86.4	0.68	2.62	0.04
Hepatocyte	Pre	0	5	0	80.7	0.40	1.24	0.05
Hepatocyte	Pre	0	5	20	79.4	0.28	1.18	0.02
Hepatocyte	Pre	50	0	0	79.0	0.21	0.89	0.03
Hepatocyte	Pre	50	0	20	76.4	0.17	0.96	0.01
Hepatocyte	Pre	50	5	0	78.3	0.16	0.67	0.02
Hepatocyte	Pre	50	5	20	73.7	0.14	0.63	0.02
Hepatocyte	Post	0	0	0	88.9	0.64	2.28	0.07
Hepatocyte	Post	0	0	20	81.1	0.47	1.80	0.07
Hepatocyte	Post	0	5	0	79.0	1.06	2.41	0.16
Hepatocyte	Post	0	5	20	82.9	0.44	2.23	0.11
Hepatocyte	Post	50	0	0	72.0	0.42	1.15	0.09
Hepatocyte	Post	50	0	20	87.4	0.32	1.09	0.06
Hepatocyte	Post	50	5	0	89.2	0.27	0.63	0.06
Hepatocyte	Post	50	5	20	88.9	0.24	0.80	0.09

[1]Cell fractions from liver perfusions were isolated as described in Chapter 2.2.1. Non-parenchymal cell (NPC)-enriched and hepatocyte-enriched isolates (before and after the Percoll isolation step) were analyzed for cell type population distribution by flow cytometry.

[2]Hepatocyte-enriched perfusion isolates from both pre- and post-Percoll isolation steps were cultured as described in Chapter 2.2.3. Briefly, cells were seeded on collagen gel monolayers for 24 hours, infected with either 0 or 50 MOI Adv for 24 hours, and then stimulated with combinations of 0 or 5 ng/ml TNF and 0 or 20 ng/ml TGF-α for 24 hours.

[3]Cell type markers were analyzed by flow cytometry (see Chapter 2.2.5) using the gating presented in Figure 1-1. Hepatocytes are reported as $albumin^+$-$cytokeratin\text{-}18^+$ cells, Kupffer cells are reported as $ED2^+$ cells, stellate cells are reported as $GFAP^+$ cells, and sinusoidal endothelial cells are reported as $SE\text{-}1^+$ cells. Mean values of duplicate biological samples are reported. Median SEM values were 4.4% for $albumin^+$-$cytokeratin\text{-}18^+$, 0.18% for $ED2^+$, 0.70% for $GFAP^+$, and 0.03% for $SE\text{-}1^+$.

[4]Cell fractions from a Seglen 2-step collagenase isolation have previously been reported to be comprised of ~98% hepatocytes and ~2% non-parenchymal cells including bile duct epithelial cells [93]. Bile duct epithelial cells, which immunostain positive for cytokeratin-19, were not quantified in this study.

2.2.7. Multiplexed phosphoprotein assays

Phosphoprotein signaling was quantified using multiplexed bead-based Luminex assays. Cells were plated and treated as described above and lysates were collected at 0, 0.25, 2, 6, 12, and 24 hours following cytokine stimulation. Cells were placed on ice and culture medium was removed and centrifuged at 1000*g* for 4 minutes at 4°C to pellet non-adherent cells. Adherent cells and pelleted non-adherent cells were lysed with Phosphoprotein Lysis Buffer (Bio-Rad, Hercules, CA) for 20 minutes at 4°C. Lysates were clarified by centrifugation at 16,000*g* for 15 minutes at 4°C. Clarified lysates were analyzed using a bicinchonicic assay (Pierce, Rockford, IL) to determine the total protein concentration. In each culture plate, a well without cells was maintained, lysed, and analyzed to calculate the protein contribution from the collagen gel alone and estimate the cellular protein concentration. Bio-Plex assays (Bio-Rad) were used to quantify the following phosphoproteins: p-Akt (Ser^{473}), p-c-Jun (Ser^{63}), p-GSK-3α/β (Ser^{21}/Ser^{9}), p-IκB-α (Ser^{32}/Ser^{36}), p-ERK1/2 (Thr^{202}/Tyr^{204}, Thr^{185}/Tyr^{187}), p-HSP27 (Ser^{78}), p-JNK (Thr^{183}/Tyr^{185}), p-MEK1 (Ser^{217}/Ser^{221}), and p-p38 (Thr^{180}/Tyr^{182}). Each phosphoprotein assay was individually validated using multiple positive control treatments over a range of cellular protein loading concentrations. Optimal protein loading concentrations that maintained robust fold-change consistency across the positive control treatments were selected as follows: 5 μg/well for multiplexing p-Akt, p-c-Jun, and p-ERK1/2, and 10 μg/well for multiplexing p-GSK-3α/β, p-IκB-α, p-HSP27, p-JNK, p-MEK1, and p-p38. Bio-Plex multiplexed phosphoprotein assays were conducted per manufacturer's recommendations on a Luminex 200 instrument (Luminex, Austin, TX). Multiple positive control treatments were loaded on each assay plate to scale raw fluorescence data to self-consistent relative values. For each phosphoprotein assay, relative fluorescence data were then normalized to the minimum and maximum value observed across all conditions and time points. See Appendix B for additional details.

2.2.8. Lactate dehydrogenase assay

Lactate dehydrogenase (LDH) activity in culture supernatants was quantified using the CytoTox-ONE Homogeneous Membrane Integrity Assay according to manufacturer's recommendations (Promega, Madison, WI). All LDH measurements were fold-change

normalized to the mock infection/mock treatment control at 24 hours post-cytokine stimulus.

2.2.9. Statistical analysis

For comparing two individual means, a Student's *t* test was used. For comparing two time courses or two dose-response curves, two-way analysis of variance (ANOVA) was used. All tests were performed at a significance level of $\alpha = 0.05$ with a false discovery rate correction for multiple comparisons of cytokine release and phosphoprotein signaling time courses. False discovery rate-corrected *P*-values were calculated as:
$P = \alpha \cdot (N+1)/(2N)$, where N is the number of comparisons.

2.3. Results

2.3.1. TNF-induced hepatocyte proliferation is regulated by a set of coupled, self-antagonizing autocrine circuits involving TGF-α, IL-1α/β, and IL-1ra

Rat hepatocytes were cultured on a collagen gel monolayer for 24 hours then stimulated with TNF and other co-treatments for 48 hours, with BrdU added from 24 to 48 hours to capture maximal cytokine-induced hepatocyte DNA synthesis [78, 82, 84]. Cells were harvested and analyzed by flow cytometry for intracellular albumin and BrdU to quantify the fraction of proliferating hepatocytes (Figure 2-1A). Proliferation of non-parenchymal cells (NPC's) was negligible across all treatments as measured by $BrdU^{+}$-$albumin^{-}$ cells (Figure 2-1A and data not shown) and by assaying changes in abundance of NPC's by flow cytometry (Table 2-1).

TNF modestly stimulated hepatocyte proliferation compared to basal media alone (Figure 2-1B). Pretreatment with an antibody neutralizing TGF-α activity (Figure 2-1B-C) or the EGFR kinase inhibitor CI1033 (Figure 2-1C) reduced hepatocyte proliferation stimulated by TNF to basal levels, demonstrating that autocrine TGF-α is necessary for TNF-induced hepatocyte proliferation in accordance with previous reports [83, 84]. Pretreatment with IL-1ra, an inhibitor of IL-1α/β binding to IL-1R, slightly increased hepatocyte proliferation stimulated by TNF (Figure 2-1B), showing that autocrine IL-1α/β inhibits TNF-induced hepatocyte proliferation. Pretreatment with isoform-specific neutralizing antibodies for IL-1α and IL-1β showed that IL-1β contributes a larger anti-

proliferative autocrine effect (Figure 2-1C). Moreover, the increased proliferation observed under IL-1α/β inhibition was not evident when TGF-α was also inhibited (Figure 2-1B), indicating that the anti-proliferative effects of autocrine IL-1α/β are contingent on autocrine TGF-α activity. TNF stimulated a slight increase in TGF-α release (Figure 2-1C) and more substantial increases in IL-1α (Figure 2-1E), IL-1β (Figure 2-1F), and IL-1ra (Figure 2-1G) release over 48 hours of treatment compared to untreated controls. TNF-induced autocrine IL-1α and IL-1β release, at 24 hours post-stimulus, were both completely inhibited by neutralizing autocrine TGF-α activity (Figure 2-1H-I), in accordance with previous reports in mammary and colonic epithelial cells [77]. TNF-induced IL-1ra release was not dependent on autocrine TGF-α or IL-1α/β activity (data not shown). Thus, TNF-induced hepatocyte proliferation is regulated by a set of coupled and self-antagonizing autocrine circuits involving pro-proliferative TGF-α, anti-proliferative IL-1α/β, and IL-1ra, with the release and anti-proliferative effects of autocrine IL-1α/β contingent on TNF-induced autocrine TGF-α signaling (Figure 2-4G).

2.3.2. Autocrine TGF-α and IL-1α/β contribute to multiple signaling pathways related to TNF-induced hepatocyte proliferation

To investigate how autocrine TGF-α and IL-1α/β signaling contributes to TNF-induced

Figure 2-2. (Following page) Coupled and self-antagonizing autocrine TGF-α, IL-1α/β, and IL-1ra circuits regulate TNF-induced hepatocyte proliferation. Primary rat hepatocytes were isolated, treated, and assayed as described in Chapter 2.2 for proliferation studies. (A) Representative scatter plots of $BrdU^+$ flow cytometry assays for cells stimulated with carrier only (left) or 100 ng/ml TNF (right). The proliferative fraction of cultured hepatocytes is reported as percentage of $BrdU^+$ cells within the $albumin^+$ (hepatocyte) population. (B-C) Regulation of TNF-induced hepatocyte proliferation by autocrine TGF-α and IL-1α/β. Autocrine ligand inhibitors were added 1 hour before mock or 100 ng/ml TNF treatment. Autocrine TGF-α ligand activity was perturbed with 10 μg/ml anti-TGF-α or 10 μM CI1033 (a pan-EGFR/ErbB receptor tyrosine kinase inhibitor) pretreatment. Autocrine IL-1 activity was perturbed with 10 μg/ml IL-1ra, 10 μg/ml anti-IL-1α, or 10 μg/ml IL-1β pretreatment. In panel (C), dashed red line indicates proliferation induced by 100 ng/ml TNF alone. (D-G) Conditioned media samples were collected from 0-48 hours following mock or 100 ng/ml TNF treatment and were assayed for autocrine TGF-α (D), IL-1α (E), IL-1β (F), and IL-1ra (G) release by quantitative ELISA. Differences between each pair of ligand release time courses were assessed using two-way ANOVA (TGF-α: $P < 0.022$; IL-1α: $P < 0.032$; IL-1β: $P < 10^{-4}$; IL-1ra: $P < 0.005$). (H-I) Perturbation of TNF-induced IL-1α and IL-1β release at 24 hours post-stimulus in the presence of 10 μg/ml anti-TGF-α. In panels (B), (C), (H), and (I), differences between mock and TNF treatments are labeled as significant (*) if $P < 0.05$. Differences between pairs of uninhibited and inhibitor treatments are labeled as significant (‡) if $P < 0.05$. In panel (C), the difference between TNF and TNF + IL-1ra is slightly less than significant (‡‡; $P = 0.06$). Data are presented as the mean ± SEM of three biological samples in panels (B), (C), (H), and (I) and six biological samples in (D) to (G).

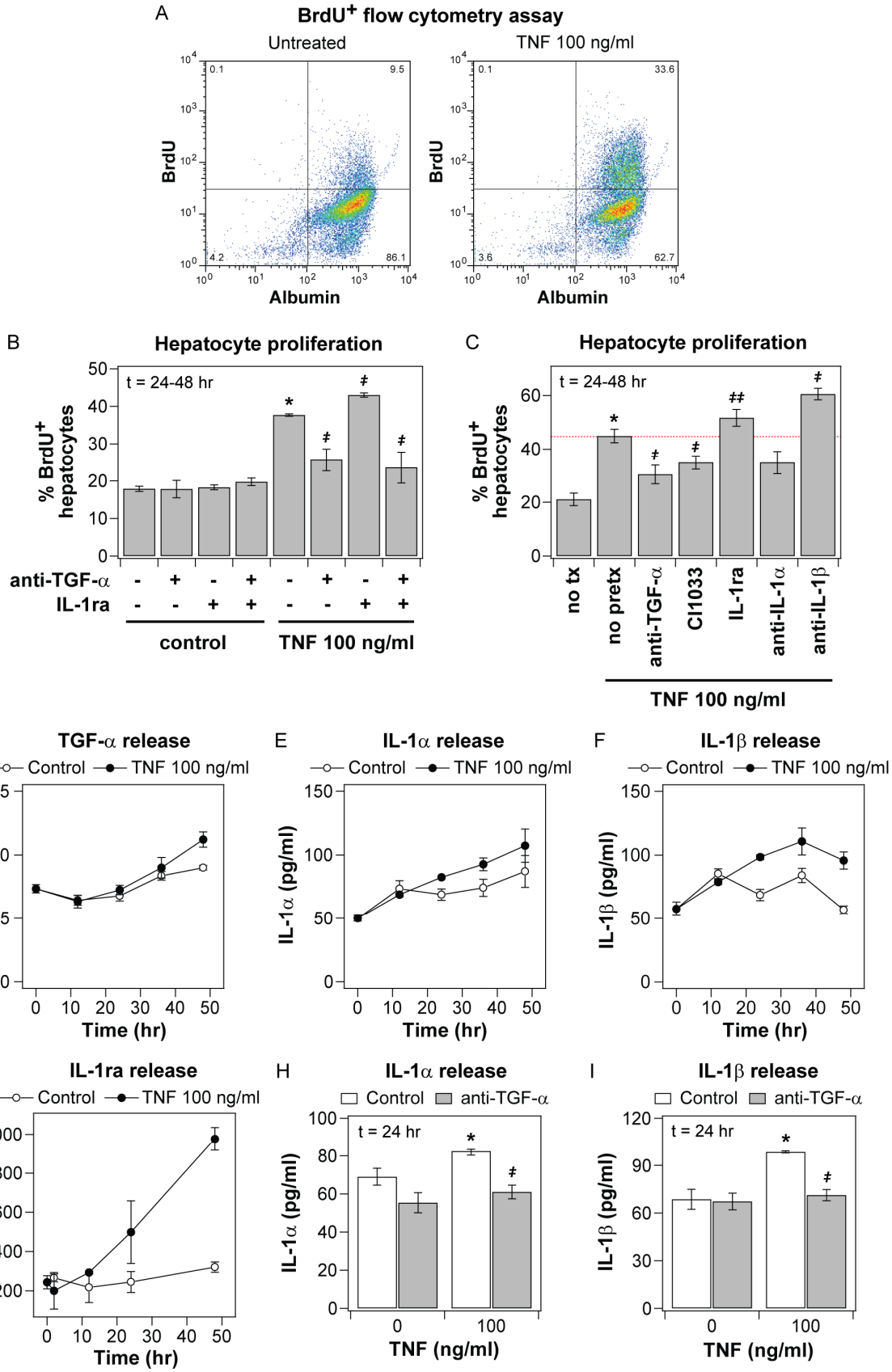
A
BrdU+ flow cytometry assay
Untreated
TNF 100 ng/ml
BrdU
Albumin
0.1
9.5
4.2
86.1
0.1
33.6
3.6
62.7
B
Hepatocyte proliferation
t = 24-48 hr
% BrdU+ hepatocytes
anti-TGF-α
IL-1ra
control
TNF 100 ng/ml
C
Hepatocyte proliferation
t = 24-48 hr
% BrdU+ hepatocytes
no tx
no pretx
anti-TGF-α
Cl1033
IL-1ra
anti-IL-1α
anti-IL-1β
TNF 100 ng/ml
D
TGF-α release
Control
TNF 100 ng/ml
TGF-α (pg/ml)
Time (hr)
E
IL-1α release
Control
TNF 100 ng/ml
IL-1α (pg/ml)
Time (hr)
F
IL-1β release
Control
TNF 100 ng/ml
IL-1β (pg/ml)
Time (hr)
G
IL-1ra release
Control
TNF 100 ng/ml
IL-1ra (pg/ml)
Time (hr)
H
IL-1α release
Control
anti-TGF-α
t = 24 hr
IL-1α (pg/ml)
TNF (ng/ml)
I
IL-1β release
Control
anti-TGF-α
t = 24 hr
IL-1β (pg/ml)
TNF (ng/ml)

hepatocyte proliferation, we quantified phosphoprotein signaling in multiple pathways associated with TNF signaling and hepatocyte proliferation. TNF-induced hepatocyte proliferation *in vitro* is dependent on autocrine TGF-α and its activation of EGFR and downstream signaling through the pro-proliferative Akt and ERK pathways [83, 84]. Here, TNF-induced activation of the Akt–GSK-3α/β and MEK–ERK signaling, on both transient and sustained time scales, was dependent on autocrine TGF-α (Figure 2-3A-D). IL-1 ligands activate multiple pathways downstream of IL-1R that are shared by TNF signaling, including JNK, IKK–NF-κB, and p38, but it is uncertain how these pathways contribute to IL-1's antagonism of hepatocyte proliferation, which is largely attributed to nitric oxide (NO) signaling [87, 100]. TNF-induced activation of JNK–c-Jun and IKK–NF-κB (as measured by p-IκB-α) signaling at 2-12 hours post-stimulus were partially dependent on autocrine IL-1α/β signaling (Figure 2-3E-G). These signaling pathways were similarly perturbed upon inhibition of autocrine TGF-α, again demonstrating that autocrine IL-1α/β signaling is contingent on autocrine TGF-α activity. While both JNK and IKK–NF-κB signaling are activated by TNF immediately following partial hepatectomy and are associated with pro-proliferative functions, these pathways are not absolutely necessary for hepatocyte proliferation [11, 75, 76, 78, 101]. Sustained signaling via autocrine stimulation can govern cellular behaviors in counterintuitive manners, as has been observed in mammary epithelial cells in which TNF-induced autocrine IL-1α signaling contributes to sustained activation of IKK–NF-κB signaling, which is associated with a pro-apoptotic function rather than its canonical anti-apoptotic role [62, 77]. Similarly, the JNK and IKK–NF-κB pathways could function, through their sustained activation, to antagonize hepatocyte proliferation through mechanisms such as accumulation of reactive oxygen species (ROS), which is associated with JNK signaling [76] and inhibits hepatocyte proliferation [102].

Phosphoprotein signaling data can provide evidence of autocrine ligand activities with greater temporal resolution than can be inferred from their accumulation in culture media alone (Figure 2-2D-G). The transient (15 minutes post-stimulus) activation of the MEK–ERK pathway (Figure 2-3C-D) depends on autocrine TGF-α, indicating that TGF-α release and activity immediately follows TNF stimulation. Similarly, the prolonged (2 hours post-stimulus) activation of the JNK–c-Jun (Figure 2-3E-F) and IKK–NF-κB

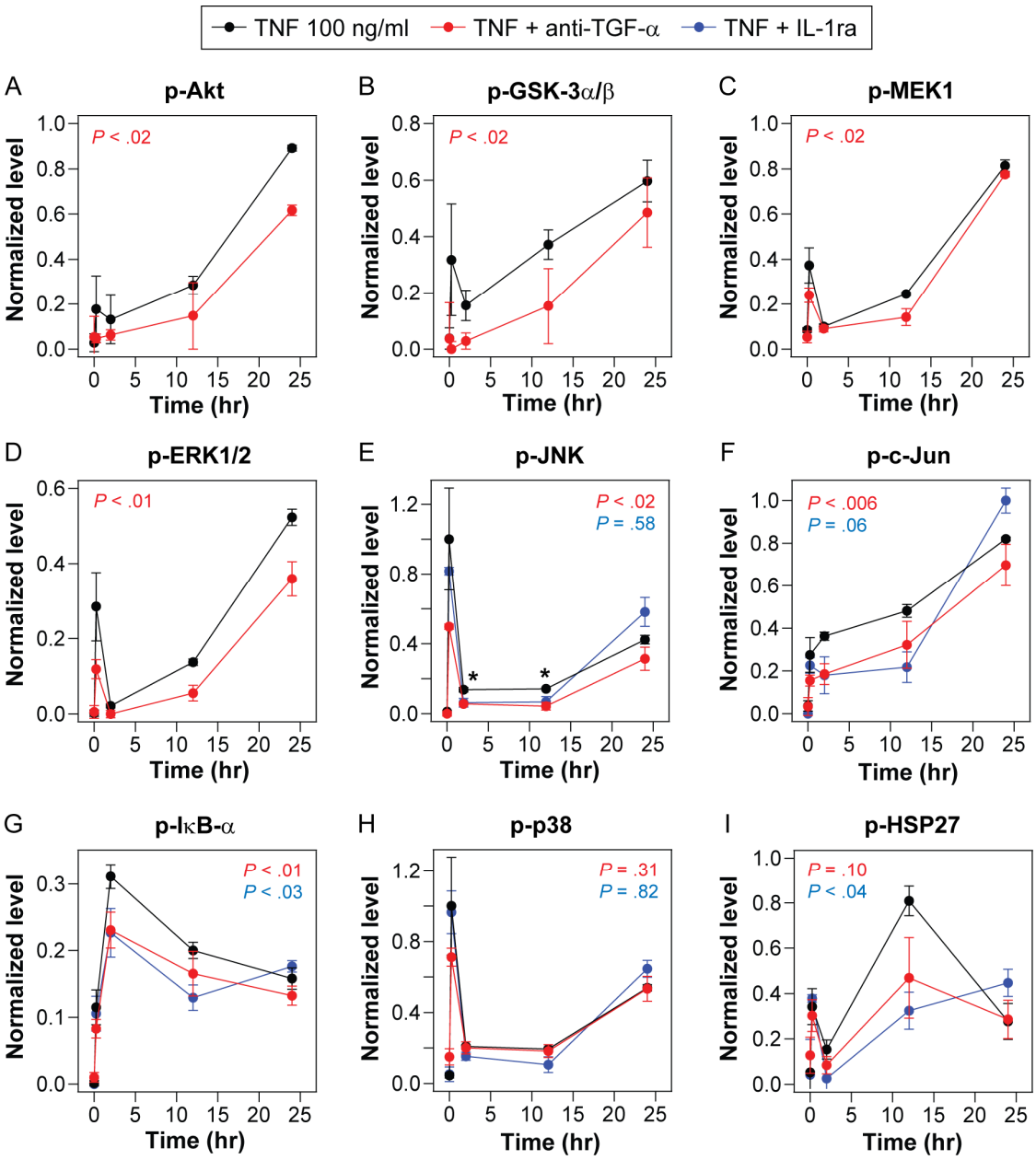

Figure 2-3. Autocrine TGF-α and IL-1α/β contribute to TNF-induced phosphoprotein signaling regulating hepatocyte proliferation. Primary rat hepatocytes were isolated, treated, and assayed as described in Chapter 2.2 for proliferation studies. Lysates were collected from 0, 0.25, 2, 12, and 24 hours following 100 ng/ml TNF treatment with mock, 10 μg/ml anti-TGF-α, or 10 μg/ml IL-1ra pretreatments to perturb autocrine ligand activity. Lysates were analyzed using multiplexed phosphoprotein assays for p-Akt (A), p-GSK-3α/β (B), p-MEK1 (C), p-ERK1/2 (D), p-JNK (E), p-c-Jun (F), p-IκB-α (G), p-p38 (H), and p-HSP27 (I). In (A) to (D), IL-1ra inhibition treatments were unchanged from uninhibited treatments and thus not shown. Differences between uninhibited and inhibited phosphoprotein signaling time courses were assessed using two-way ANOVA and *P* values are shown in each panel for anti-TGF-α (red) and IL-1ra (blue) pretreatments. For phosphoproteins that did not demonstrate significant differences by ANOVA between uninhibited and inhibition treatment time courses for both autocrine ligands, individual time points that did demonstrate significant differences in both comparisons are labeled (*) if $P < 0.05$. Data are presented as the mean ± SEM of three biological samples.

(Figure 2-3G) pathways depends on autocrine IL-1α/β, indicating the early release and activity of IL-1α/β. Lastly, the inability of exogenously added IL-1ra to perturb late-phase JNK and IKK–NF-κB signaling (at ~24 hours) indicates the on-set of detectable autocrine IL-1ra activity. Together, these data suggest that TGF-α, IL-1α/β, and IL-1ra operate in a coupled and time-varying autocrine "cascade"; TNF stimulates the immediate release of TGF-α and its activation of Akt and ERK signaling, the slightly delayed release of IL-1α/β and its activation of JNK and IKK–NF-κB signaling, and the late-phase release of IL-1ra, which antagonizes IL-1 signaling (Figure 2-9).

2.3.3. TNF-TGF-α cooperation in inducing hepatocyte proliferation is self-limited by release of autocrine IL-1α/β

Exogenous TGF-α stimulated a dose-dependent increase in hepatocyte proliferation in the absence of TNF and co-treatment with TNF did not elicit additional hepatocyte proliferation (Figure 2-4A) in discordance with previous reports demonstrating cooperation between TNF and EGFR ligands in stimulating hepatocyte proliferation *in vitro* under some media formulations [78, 82, 103]. We note that exogenous TNF and TGF-α exhibited slightly cooperative stimulation of hepatocyte proliferation when insulin was removed from the culture media (Figure 2-4B). We were motivated to ask whether cooperation between exogenous TNF and TGF-α in the presence of insulin could be limited by anti-proliferative autocrine IL-1α/β.

Figure 2-4. (Following page) Exogenous TGF-α has limited effect in synergizing with TNF-induced hepatocyte proliferation due to an anti-proliferative IL-1α/β autocrine circuit. Primary rat hepatocytes were isolated, treated, and assayed as described in Chapter 2.2 for proliferation studies. (A) Hepatocyte proliferation induced by 0, 1, 10, or 100 ng/ml exogenous TGF-α with either mock or 100 ng/ml TNF co-treatment. (B) TNF and TGF-α stimulate cooperative induction of hepatocyte proliferation in the absence, but not presence, of insulin. Rat hepatocytes were isolated, treated and assayed as referenced above, except 5 μg/ml insulin was either excluded from or included in the culture and stimulation medium for all steps after the 4 hours post-seeding medium change. In medium containing either 0 or 5 μg/ml insulin, cells were stimulated with 0 or 100 ng/ml TNF and 0 or 10 ng/ml TGF-α. (C) "Cue-response landscape" plot of hepatocyte proliferation and autocrine IL-1α/β release induced by multiple combinations of TNF and TGF-α stimuli. Mean values of three biological samples are plotted for $BrdU^+$ hepatocytes (lines and vertices; z-axis) and total autocrine IL-1α/β concentration at 24 hours post-stimulus (interpolated surface colormap) for multiple concentrations of exogenous TNF and either inhibited, autocrine (uninhibited), or exogenous TGF-α. See Table 2-2 for details of treatment conditions and measured values plotted. (D-E) IL-1α (D) and IL-1β (E) release at 24 hours post-stimulus induced by 0, 1, 10, or 100 ng/ml exogenous TGF-α with either mock or 100 ng/ml TNF co-treatment. Dashed red lines indicate ligand release level in the absence of exogenous TGF-α stimulus for clarity. (F) Hepatocyte proliferation induced by 100 ng/ml TNF, 1 ng/ml TGF-α, or TNF + TGF-α in the absence or presence of 10 μg/ml IL-1ra. (G) A molecular "logic" model of

the effects of autocrine TGF-α, IL-1α/β, and IL-1ra ligands in regulating TNF-induced hepatocyte proliferation. Exogenous TNF stimulates the release of anti-proliferative autocrine IL-1α and IL-1β ligands contingent of the activity of autocrine TGF-α, a pro-proliferative ligand itself, and the release of IL-1ra independent of activity of other autocrine ligands. Thus, this coupled autocrine circuit is self-antagonizing in its control of hepatocyte proliferation. In panels (A), (B), and (D) to (F), differences between pairs of treatments connected by brackets are labeled as significant (*) if $P < 0.05$. Data are presented as the mean ± SEM of three biological samples in panels (A), (B), and (D) to (F).

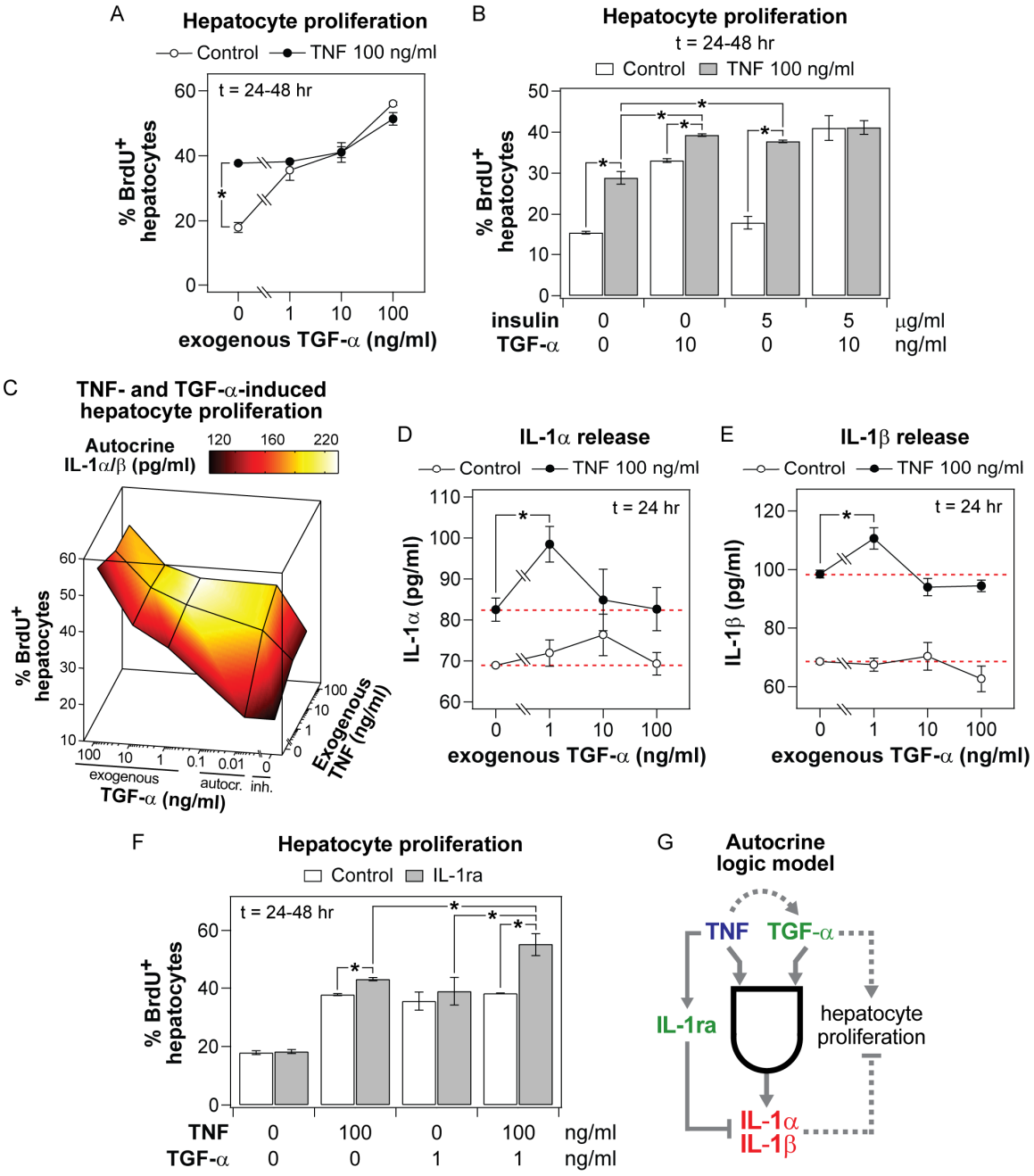

Table 2-2. Measured values of proliferation and autocrine IL-1α/β release in TNF- and TGF-α-treated hepatocytes[1].

Exogenous TNF conc. (ng/ml)	TGF-α conc. (ng/ml)	TGF-α category	% BrdU$^+$ hepatocytes	Autocrine IL-1α conc. (pg/ml)	Autocrine IL-1β conc. (pg/ml)	Total autocrine IL-1α/β conc. (pg/ml)[2]
0	0	Inhibited[3]	17.8	55.4	67.2	122.6
0	0.0068	Autocrine[4]	17.9	68.9	68.6	137.5
0	1	Exogenous[5]	35.6	71.9	67.6	139.5
0	10	Exogenous	41.0	76.4	70.4	146.7
0	100	Exogenous	56.0	69.3	62.7	132.0
5	0	Inhibited	24.7	61.0	71.2	132.2
5	0.0071	Autocrine	32.5	86.4	96.3	182.7
5	1	Exogenous	38.0	95.5	107.8	203.3
5	10	Exogenous	42.1	88.4	94.1	182.5
5	100	Exogenous	51.5	81.1	86.0	167.0
100	0	Inhibited	25.6	61.0	71.2	132.2
100	0.0072	Autocrine	37.7	82.5	98.4	180.9
100	1	Exogenous	38.2	98.5	110.6	209.1
100	10	Exogenous	41.1	84.9	94.0	178.8
100	100	Exogenous	51.3	82.7	94.4	177.0

[1]See Figure 2-4C for a surface plot of hepatocyte proliferation and autocrine IL-1α/β release induced by these combinations of TNF and TGF-α stimuli.
[2]Total autocrine IL-1α/β concentration was calculated by adding the measured IL-1α and IL-1β concentrations and is an estimate of their net activity.
[3]Endogenous TGF-α activity inhibited by 10 μg/ml anti-TGF-α and, accordingly, TGF-α is plotted as having an effective concentration of zero.
[4]Autocrine TGF-α concentration measured by ELISA (in the absence of TGF-α neutralizing antibody).
[5]Exogenous TGF-α concentration set by the addition of recombinant TGF-α.

To examine whether autocrine IL-1α/β could affect TNF-TGF-α cooperativity in inducing hepatocyte proliferation, hepatocyte IL-1α/β release and proliferation were assayed under multiple combinations of exogenous TNF and autocrine/exogenous TGF-α stimuli and were plotted in a multivariate "cue-response landscape" (Figure 2-4C). In this perspective, the two hepatocyte responses (IL-1α/β release and proliferation) show disparate dependences on the two stimulatory cues (TNF and TGF-α). That is, the conditions that lead to maximal IL-1α/β release (100 ng/ml TNF + 1 ng/ml TGF-α; Figure 2-4C-E) are different than those associated with maximal proliferation (100 ng/ml TNF + 100 ng/ml TGF-α; Figure 2-4A,C). This suggested that autocrine IL-1α/β could

serve as a negative regulator of hepatocyte proliferation under certain exogenous TNF-TGF-α co-stimuli conditions – in particular, those with intermediate exogenous TGF-α concentrations. Following this, IL-1ra pretreatment elicited a slight increase in proliferation stimulated by 100 ng/ml TNF and a more substantial increase upon 100 ng/ml TNF + 1 ng/ml TGF-α co-stimulation, but not a significant increase in proliferation stimulated by 1 ng/ml TGF-α only (Figure 2-4F). Moreover, TNF + TGF-α + IL-1ra treatment significantly increased hepatocyte proliferation compared to both TNF + IL-1ra and TGF-α + IL-1ra treatments (Figure 2-4F), demonstrating TNF and TGF-α can stimulate additive induction of hepatocyte proliferation, even in the presence of insulin, but this cooperation is inhibited by their induction of anti-proliferative autocrine IL-1α/β release. Thus, induced autocrine IL-1α/β release not only antagonizes hepatocyte proliferation stimulated by exogenous TNF, contingent on its induced autocrine release of TGF-α, but also potently self-limits hepatocyte proliferation induced by exogenous TNF-TGF-α co-stimulation (Figure 2-4G).

2.3.4. Adenoviral vector infection synergistically sensitizes hepatocytes to TNF-induced apoptosis

Common models of TNF-induced hepatocyte apoptosis require non-physiological interference with anti-apoptotic signaling pathways [11, 76]. Here, we examined TNF-induced hepatocyte apoptosis in the context of adenoviral infection because of the relevance of this condition to physiological and therapeutic applications and because we have found it to be an important modulator of TNF-induced apoptosis in other epithelial cell types [22, 64]. Rat hepatocytes were cultured on collagen gel for 24 hours, then infected with a replication-deficient adenovirus expressing a β-gal transgene at 0-100 MOI. Twenty four hours post-Adv infection, hepatocytes were stimulated with TNF and other co-treatments for 24 hours. Cells were harvested and analyzed by flow cytometry for the cleaved form of the effector caspase 3 (Figure 2-5A) and LDH release (an indicator of loss of plasma membrane integrity in necrotic and apoptotic cell death) was measured in culture supernatants. Over a range of infection levels, Adv potently sensitized TNF-induced apoptosis as measured by both LDH release (Figure 2-5B) and cleaved caspase 3^+ cells (Figure 2-5C) with the sensitization effect plateauing at ~50 MOI

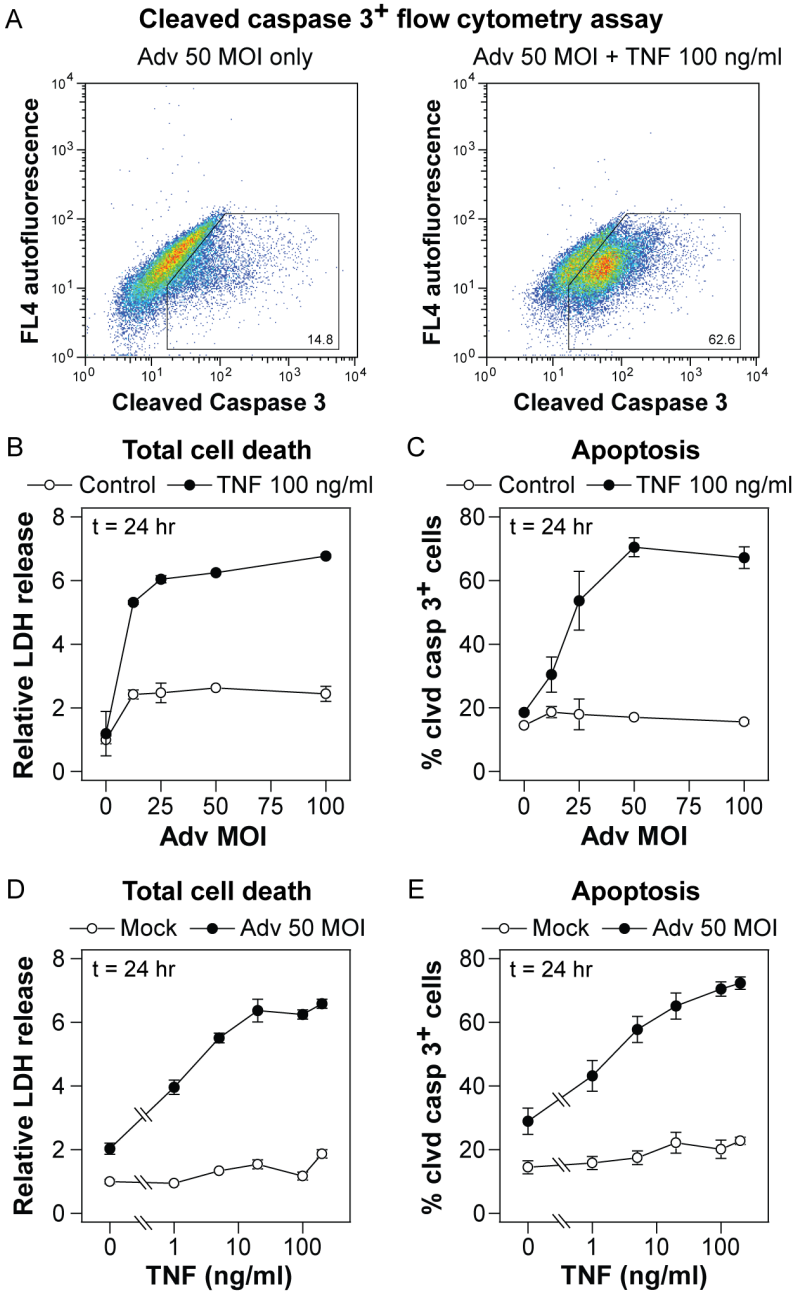

Figure 2-5. Replication-deficient adenoviral vector infection synergistically sensitizes hepatocytes to TNF-induced apoptosis. Primary rat hepatocytes were isolated, treated, and assayed as described in Chapter 2.2 for apoptosis studies. (A) Representative scatter plots of a cleaved caspase 3^+ flow cytometry assay for cells infected with 50 MOI Adv and stimulated with carrier only (left) or 100 ng/ml TNF (right). (B-C) Effect of Adv infection level on TNF-induced (B) total cell death as assayed by relative LDH release and (C) apoptosis as assayed by the cleaved caspase 3^+ cells. Cells were infected with storage buffer only or 12.5, 25, 50, or 100 MOI Adv and then stimulated with mock or 100 ng/ml TNF for 24 hours. LDH release values were normalized to mock treatment condition at 24 hours post-stimulus and in (B) and (D). (D-E) Effect of TNF concentration on Adv infection-sensitized (D) total cell death and (E) apoptosis. Cells were infected with storage buffer only or 50 MOI Adv and then stimulated with 0, 1, 5, 20, 100, or 200 ng/ml TNF for 24 hours. Differences between all pairs of cell death and apoptosis dose-response curves in (B) to (E) were assessed using two-way ANOVA and were all statistically significant ($P < 10^{-4}$). Data are presented as the mean ± SEM of three biological samples in panels (B) to (E).

Adv, which was used for all subsequent Adv infections. At time points later than 24 hours post-cytokine stimulation, hepatocyte death induced by Adv infection alone increased significantly, reducing the level of observed synergy between Adv and TNF in inducing hepatocyte death (data not shown). In hepatocytes infected with 50 MOI Adv, TNF induced apoptosis as measured by both LDH release (Figure 2-5D) and cleaved caspase 3^+ cells (Figure 2-5E), with half-maximal and maximal responses induced at ~5 ng/ml and ~100 ng/ml TNF, respectively. Thus, Adv infection potently sensitizes hepatocytes to TNF-induced apoptosis and provides a physiologically relevant model to examine the role of autocrine ligands in regulating TNF-induced apoptosis.

2.3.5. TNF-induced apoptosis in Adv-infected hepatocytes is regulated by a coupled, pro-apoptotic TGF-α–IL-1α/β–IL-1ra autocrine cascade

Because we found that a coupled TGF-α–IL-1α/β–IL-1ra autocrine cascade regulates hepatocyte proliferation induced by TNF, and a similar autocrine mechanism operates in determining apoptotic responses of colonic epithelial cells [62, 77], we investigated whether this autocrine cascade regulates TNF-induced apoptosis in Adv-infected hepatocytes. In hepatocytes infected with 50 MOI Adv, TNF treatment significantly upregulated the release of autocrine TGF-α, IL-1α, IL-1β, and IL-1ra as measured over 24 hours (Figure 2-6A-D). Adv infection alone induced an increased release of TGF-α but not IL-1α, IL-1β, or IL-1ra compared to uninfected control cells (Figure 2-6E-G and data not shown). Inhibition of autocrine TGF-α reduced the release of IL-1α induced by both Adv infection alone and Adv infection followed by 5 or 100 ng/ml TNF treatment (Figure2-6H) but only reduced the release of IL-1β upon Adv + 5 ng/ml TNF treatment (Figure 2-6I) and did not perturb the release of autocrine IL-1ra (data not shown). Pretreatment with anti-TGF-α, IL-1ra, or both inhibitors significantly reduced TNF-induced apoptosis in Adv-infected hepatocytes treated with 5 ng/ml TNF, but did not perturb apoptosis in a statistically significant manner under 0 or 100 ng/ml TNF treatments (Figure 2-6J). In Adv-infected hepatocytes, pretreatment with CI1033 and anti-IL-1β also reduced apoptosis induced by 5 ng/ml TNF (Figure 2-6K).

Thus, in Adv-infected hepatocytes, TNF-induced apoptosis is regulated by the coupled activity of autocrine TGF-α and IL-1α/β. At sub-saturating TNF concentrations

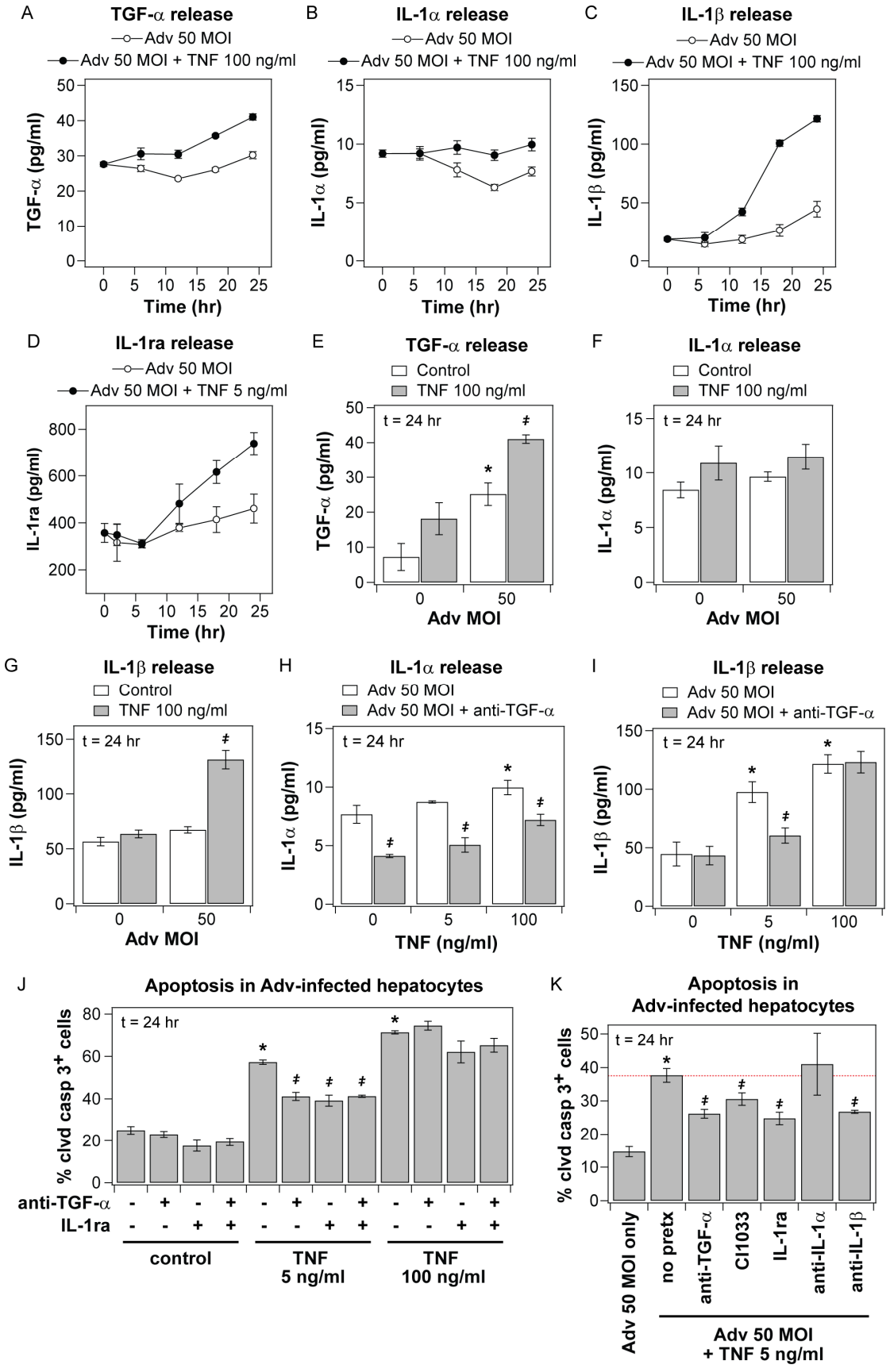
A
TGF-α release
Adv 50 MOI
Adv 50 MOI + TNF 100 ng/ml
TGF-α (pg/ml)
Time (hr)
B
IL-1α release
Adv 50 MOI
Adv 50 MOI + TNF 100 ng/ml
IL-1α (pg/ml)
Time (hr)
C
IL-1β release
Adv 50 MOI
Adv 50 MOI + TNF 100 ng/ml
IL-1β (pg/ml)
Time (hr)
D
IL-1ra release
Adv 50 MOI
Adv 50 MOI + TNF 5 ng/ml
IL-1ra (pg/ml)
Time (hr)
E
TGF-α release
Control
TNF 100 ng/ml
t = 24 hr
TGF-α (pg/ml)
Adv MOI
F
IL-1α release
Control
TNF 100 ng/ml
t = 24 hr
IL-1α (pg/ml)
Adv MOI
G
IL-1β release
Control
TNF 100 ng/ml
t = 24 hr
IL-1β (pg/ml)
Adv MOI
H
IL-1α release
Adv 50 MOI
Adv 50 MOI + anti-TGF-α
t = 24 hr
IL-1α (pg/ml)
TNF (ng/ml)
I
IL-1β release
Adv 50 MOI
Adv 50 MOI + anti-TGF-α
t = 24 hr
IL-1β (pg/ml)
TNF (ng/ml)
J
Apoptosis in Adv-infected hepatocytes
t = 24 hr
% clvd casp 3+ cells
anti-TGF-α
IL-1ra
control
TNF 5 ng/ml
TNF 100 ng/ml
K
Apoptosis in Adv-infected hepatocytes
t = 24 hr
% clvd casp 3+ cells
Adv 50 MOI only
no pretx
anti-TGF-α
CI1033
IL-1ra
anti-IL-1α
anti-IL-1β
Adv 50 MOI + TNF 5 ng/ml

Figure 2-6. (Previous page) Autocrine TGF-α, IL-1α/β, and IL-1ra regulate TNF-induced apoptosis in Adv-infected hepatocytes in a coupled autocrine circuit. Primary rat hepatocytes were isolated, treated, and assayed as described in Chapter 2.2 for apoptosis studies. (A-D) Conditioned media samples were collected from 0-24 hours following mock, 5 ng/ml (D) or 100 ng/ml (A-C) TNF treatment in hepatocytes infected with 50 MOI Adv and were assayed for autocrine TGF-α (A), IL-1α (B), IL-1β (C), and IL-1ra (D) release by quantitative ELISA. Differences between each pair of ligand release time courses were assessed using two-way ANOVA and were all statistically significant ($P < 10^{-3}$). (E-G) Effect of both Adv infection and TNF treatment on hepatocyte autocrine TGF-α and IL-1α/β release. Rat hepatocytes were infected with storage buffer only (uninfected) or 50 MOI Adv and then stimulated with mock or 100 ng/ml TNF treatment. Conditioned media samples were collected at 24 hours following TNF stimulus and were assayed for autocrine TGF-α (E), IL-1α (F), and IL-1β (G) release by quantitative ELISA. (H-I) Perturbation of IL-1α (H) and IL-1β (I) release induced by 0, 5, or 100 ng/ml TNF treatment at 24 hours post-stimulus in 50 MOI Adv-infected hepatocytes in the presence of 10 μg/ml anti-TGF-α. (J-K) Regulation of TNF-induced apoptosis in Adv-infected hepatocytes by autocrine TGF-α and IL-1α/β. Autocrine ligand inhibitors were added 1 hour before 0, 5, or 100 ng/ml TNF treatment in 50 MOI Adv-infected hepatocytes. Autocrine TGF-α ligand activity was perturbed with 10 μg/ml anti-TGF-α or 10 μM CI1033 pretreatment. Autocrine IL-1 activity was perturbed with 10 μg/ml IL-1ra, 10 μg/ml anti-IL-1α, or 10 μg/ml IL-1β pretreatment. In panel (K), the dashed red line indicates apoptosis induced by Adv + 5 ng/ml TNF alone. In panels (E) to (G), differences between uninfected and 50 MOI Adv infection treatments are labeled as significant (*) if $P < 0.05$. Differences between mock and 100 ng/ml TNF treatments are labeled as significant (ǂ) if $P < 0.05$. In panels (H) to (K), differences between mock and TNF treatments are labeled as significant (*) if $P < 0.05$ and differences between pairs of uninhibited and inhibitor treatments are labeled as significant (ǂ) if $P < 0.05$. Data are presented as the mean ± SEM of six biological samples in (A) to (D) and three biological samples (E) to (K).

(5 ng/ml), the induced release of IL-1α and IL-1β is contingent on autocrine TGF-α, the induced release of IL-1ra is independent of autocrine TGF-α or IL-1α/β, and the net effect of the coupled TGF-α–IL-1α/β autocrine circuit in Adv-infected hepatocytes is pro-apoptotic. At saturating concentrations (100 ng/ml), TNF induces TGF-α and IL-1α/β release in Adv-infected hepatocytes, but these mediators only provide a negligible contribution to apoptosis and the requirement of autocrine TGF-α activity for IL-1β release is not apparent. Taken together, the observations across all treatment conditions imply that autocrine TGF-α can act paradoxically as a pro-apoptotic signal in Adv-infected hepatocytes by coupling TNF treatment to release of pro-apoptotic autocrine IL-1α/β (Figure 2-8G).

2.3.6. Autocrine TGF-α and IL-1α/β contribute to multiple signaling pathways related to TNF-induced apoptosis in Adv-infected hepatocytes

To investigate how autocrine TGF-α and IL-1α/β signaling contributes to TNF-induced hepatocyte apoptosis, we quantified phosphoprotein signaling in hepatocytes infected with 50 MOI Adv and stimulated with TNF at 5 ng/ml, a sub-saturating concentration

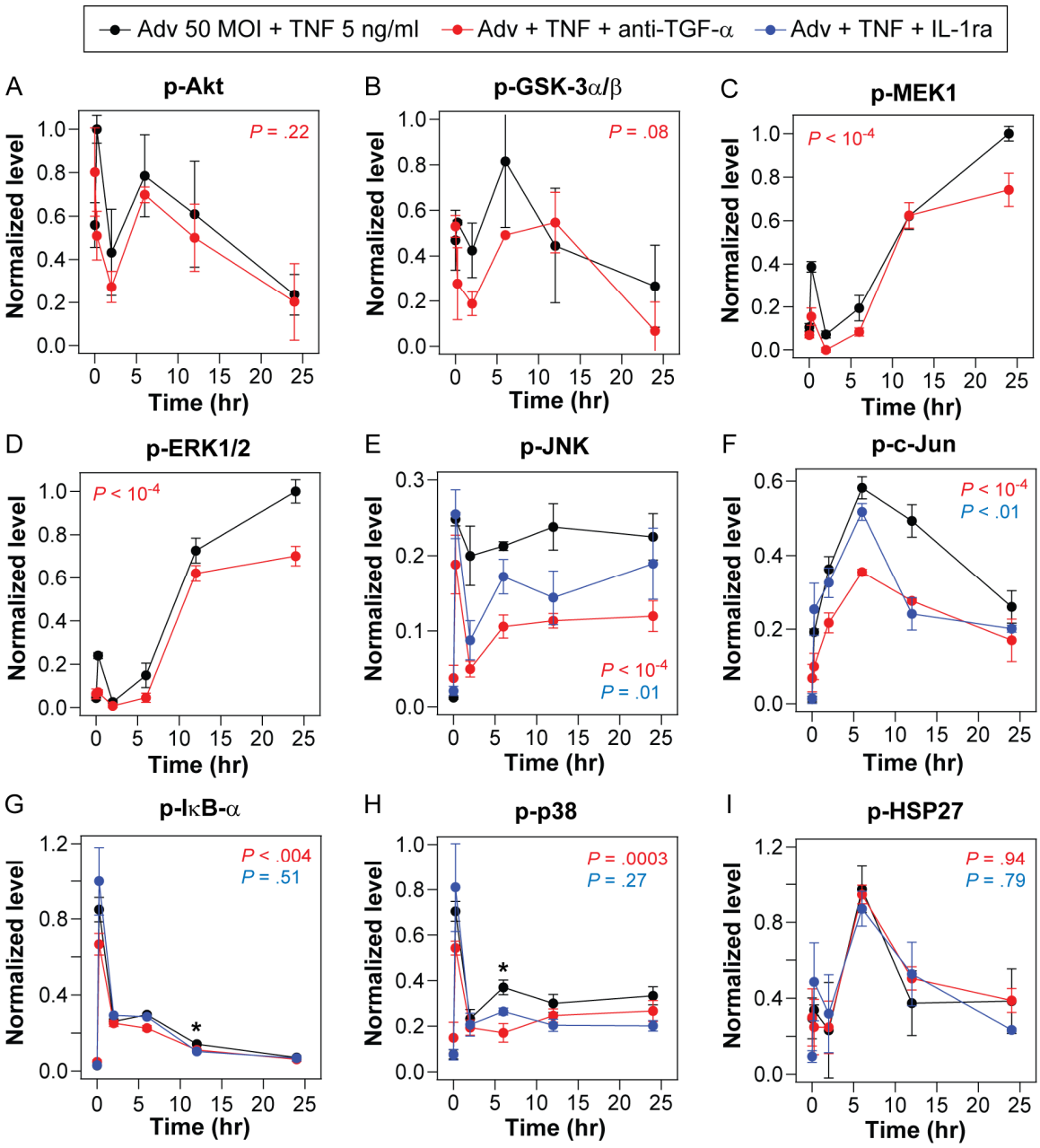

Figure 2-7. Autocrine TGF-α and IL-1α/β contribute to TNF-induced phosphoprotein signaling regulating hepatocyte apoptosis. Primary rat hepatocytes were isolated, treated, and assayed as described in Chapter 2.2 for apoptosis studies. Lysates were collected 0, 0.25, 2, 6, 12, and 24 hours following 5 ng/ml TNF treatment of 50 MOI Adv-infected hepatocytes with mock, 10 μg/ml anti-TGF-α, or 10 μg/ml IL-1ra pretreatments to perturb autocrine ligand activity. Lysates were analyzed using multiplexed phosphoprotein assays for p-Akt (A), p-GSK-3α/β (B), p-MEK1 (C), p-ERK1/2 (D), p-JNK (E), p-c-Jun (F), p-IκB-α (G), p-p38 (H), and p-HSP27 (I). In panels (A) to (D), IL-1ra inhibition treatments were unchanged from uninhibited treatments and thus not shown. Differences between uninhibited and inhibited phosphoprotein signaling time courses were assessed using two-way ANOVA and *P* values are shown in each graph for anti-TGF-α (red) and IL-1ra (blue) pretreatments. For phosphoproteins that did not demonstrate significant differences by ANOVA between uninhibited and inhibition treatment time courses for both autocrine ligands, individual time points that did demonstrate significant differences in both comparisons are labeled (*) if $P < 0.05$. Data are presented as the mean ± SEM of three biological samples.

that showed dependence on autocrine signaling in its induction of apoptosis. In Adv-infected hepatocytes, TNF activated anti-apoptotic MEK–ERK signaling, dependent on autocrine TGF-α, but did not significantly activate Akt–GSK-3α/β signaling (Figure 2-7A-D). Adv infection itself strongly activates Akt signaling [22, 23], which can be observed by comparing basal Akt activation in uninfected (Figure 2-3A) and Adv-infected (Figure 2-7A) cells. TNF-induced activation of pro-apoptotic JNK–c-Jun and p38–HSP27 signaling (at ~6-12 hours post-stimulus) were both dependent on autocrine IL-1α/β signaling, as observed by direct inhibition with IL-1ra or through the inhibition of autocrine TGF-α (Figure 2-7E-F,H-I). In contrast to uninfected hepatocytes (Figure 2-3G), TNF-induced IKK–NF-κB signaling in Adv-infected hepatocytes was only marginally dependent on autocrine signaling (Figure 2-7G). As observed in uninfected hepatocytes, TGF-α, IL-1α/β, and IL-1ra operate in an autocrine cascade that contributes to multiple signaling pathways related to TNF-induced apoptosis signaling in Adv-infected hepatocytes (Figure 2-9).

2.3.7. TGF-α biphasically regulates apoptosis/survival in Adv-infected, TNF-treated hepatocytes mediated by autocrine IL-1α/β

To further investigate the paradoxical roles of TGF-α in regulating TNF-induced apoptosis in Adv-infected hepatocytes, we treated Adv-infected hepatocytes with multiple combinations of exogenous TNF and autocrine/exogenous TGF-α stimuli and assayed IL-1α/β release and apoptosis. In examining the "cue-response landscape" of autocrine IL-1α/β release and apoptosis induced by these TNF-TGF-α co-stimuli in Adv-infected hepatocytes, we observed that both IL-1α/β release and apoptosis responses were maximally stimulated at intermediate concentrations of exogenous TGF-α for both 5 and 100 ng/ml TNF treatments (Figure 2-8A). This indicated that exogenous TGF-α could induce increased apoptosis in Adv-infected, TNF-treated hepatocytes through the correlated release of additional autocrine IL-1α/β. In Adv-infected hepatocytes treated with 100 ng/ml TNF, exogenous TGF-α co-treatment increased apoptosis at 1 and 5 ng/ml TGF-α and a decreased apoptosis at 20 and 100 ng/ml TGF-α (Figure 2-8B). In comparison, release of autocrine IL-1α (Figure 2-8C) and IL-1β (Figure 2-8D) was

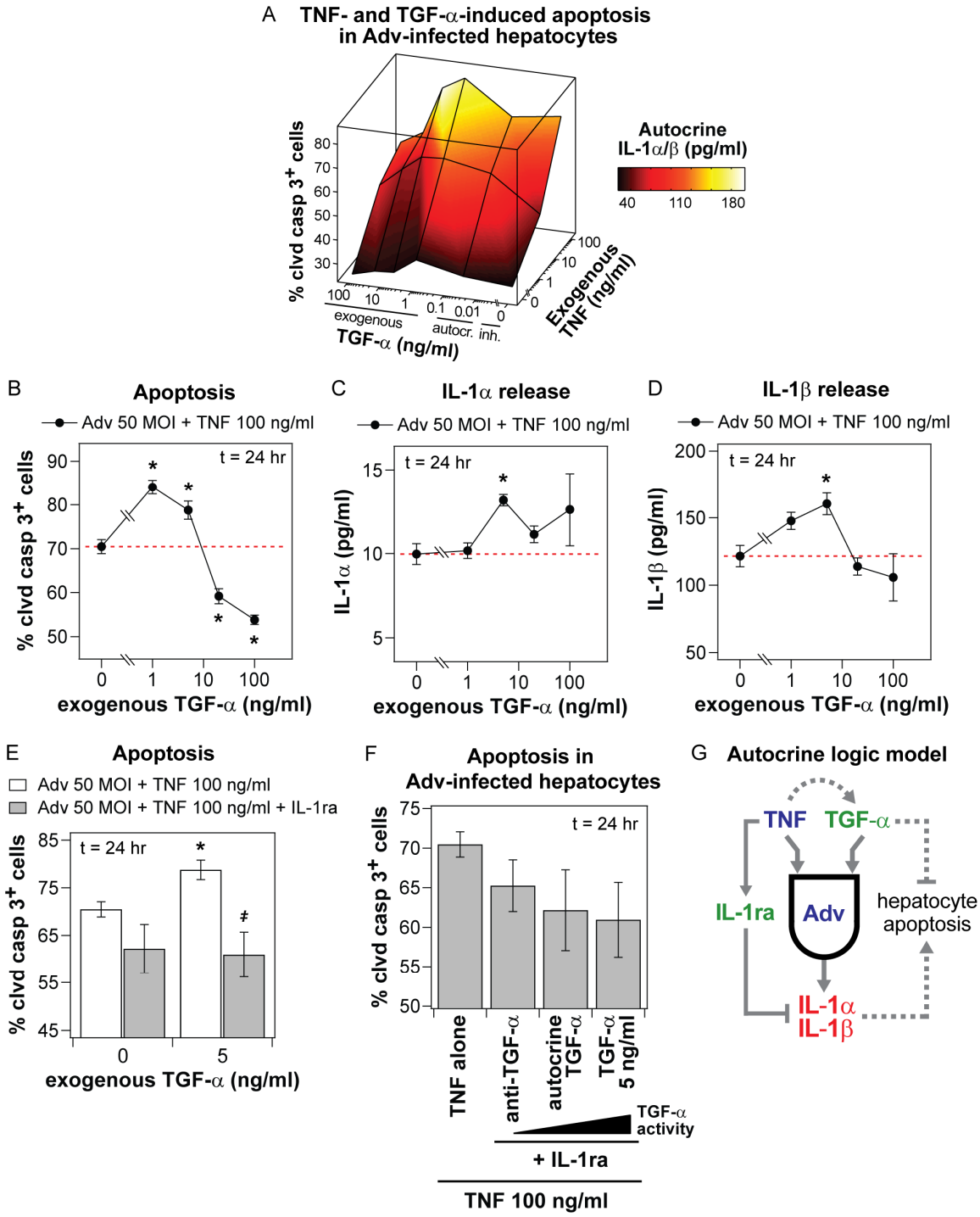

Figure 2-8. Exogenous TGF-α biphasically regulates apoptosis/survival in Adv-infected, TNF-treated hepatocytes through an autocrine IL-1α/β circuit. Primary rat hepatocytes were isolated, treated, and assayed as described in Chapter 2.2 for apoptosis studies. (A) "Cue-response landscape" plot of apoptosis and autocrine IL-1α/β release induced by multiple combinations of TNF and TGF-α stimuli in 50 MOI Adv-infected hepatocytes. Mean values of three biological samples are plotted for cleaved caspase 3^+ cells (lines and vertices; z-axis) and total autocrine IL-1α/β concentration (interpolated surface colormap) at 24 hours post-stimulus for multiple concentrations of exogenous TNF and either inhibited, autocrine (uninhibited), or exogenous TGF-α. See Table 2-3 for details of treatment conditions and measured values

plotted. (B) Apoptosis induced by 0, 1, 5, 20, or 100 ng/ml exogenous TGF-α with 100 ng/ml TNF co-treatment in 50 MOI Adv-infected hepatocytes. Dashed red lines indicate apoptosis level in the absence of exogenous TGF-α stimulus for clarity. (C-D) IL-1α (C) and IL-1β (D) release at 24 hours post-stimulus induced by 0, 1, 5, 20, or 100 ng/ml exogenous TGF-α with 100 ng/ml TNF co-treatment in 50 MOI Adv-infected hepatocytes. Dashed red lines indicate ligand release level in the absence of exogenous TGF-α stimulus for clarity. (E) Apoptosis induced by 100 ng/ml TNF only treatment or 100 ng/ml TNF + 5 ng/ml TGF-α co-treatment in the absence or presence of 10 μg/ml IL-1ra in 50 MOI Adv-infected hepatocytes. (F) Autocrine and sub-saturating exogenous levels of TGF-α both have a negligible anti-apoptotic effect in regulating TNF-induced apoptosis in Adv-infected hepatocytes. Apoptosis was measured by the fraction of cleaved caspase 3^+ cells for Adv-infected hepatocytes treated with TNF alone; TNF + 10 μg/ml IL-1ra + 10 μg/ml anti-TGF-α; TNF + IL-1ra; or TNF + IL-1ra + 5 ng/ml exogenous TGF-α. (G) A molecular "logic" model of the effects of autocrine TGF-α, IL-1α/β, and IL-1ra ligands in regulating TNF-induced apoptosis in Adv-infected hepatocytes. Exogenous TNF stimulates the release of pro-apoptotic autocrine IL-1α and IL-1β contingent of the activity of autocrine TGF-α, which is an anti-apoptotic ligand at saturating exogenous concentrations but not at autocrine concentrations, and the release of IL-1ra independent of activity of other autocrine ligands. In panels (B) to (E), differences between control treatments and treatments with exogenous TGF-α are labeled as significant (*) if $P < 0.05$. In panel (E), differences between pairs of control treatments and IL-1ra treatments are labeled as significant (‡) if $P < 0.05$. In panel (F), no differences were statistically significant. Data are presented as the mean ± SEM of three biological samples in panels (B) to (F).

upregulated for TNF co-treated with TGF-α at 5 ng/ml but not other concentrations. Therefore, at high concentrations, exogenous TGF-α rescued TNF-induced apoptosis, in agreement with the recognized anti-apoptotic role of EGFR ligands [81, 88], but, at intermediate concentrations, exogenous TGF-α contributed to TNF-induced apoptosis, mirroring its role as a pro-apoptotic autocrine mediator in Adv-infected, TNF-treated hepatocytes. A similar biphasic TGF-α synergism and antagonism in regulating apoptosis has been observed in interferon-γ-sensitized, TNF-treated human colonic epithelial cells [77]. Furthermore, the upregulation of apoptosis in Adv-infected, TNF-treated hepatocytes by 5 ng/ml exogenous TGF-α, which coincided with increased IL-1α/β release, was completely attenuated in the presence of IL-1α/β inhibition, confirming that autocrine IL-1α/β act as signaling mediators of the increased apoptosis stimulated by exogenous TGF-α (Figure 2-8E).

Given that exogenous TGF-α at saturating concentrations acted as anti-apoptotic stimulus, we asked if autocrine or sub-saturating exogenous TGF-α could be serve as an anti-apoptotic stimulus when de-coupled from its induction pro-apoptotic IL-1α/β release. In Adv-infected hepatocytes pretreated with IL-1ra, then stimulated with 100 ng/ml TNF, TGF-α at autocrine or sub-saturating exogenous (5 ng/ml) concentrations induced a slight, but not statistically significant, reduction in apoptosis compared to treatment with anti-TGF-α (Figure 2-8F). The negligible anti-apoptotic effect of autocrine and sub-

Table 2-3. Measured values of apoptosis and autocrine IL-1α/β release in TNF- and TGF-α-treated, Adv-infected hepatocytes[1].

Adv MOI	Exogenous TNF conc. (ng/ml)	TGF-α conc. (ng/ml)	TGF-α category	% cleaved caspase 3^+ cells	Autocrine IL-1α conc. (pg/ml)	Autocrine IL-1β conc. (pg/ml)	Total autocrine IL-1α/β conc. (pg/ml)[2]
50	0	0	Inhibited[3]	27.3	4.1	43.4	47.5
50	0	0.030	Autocrine[4]	28.9	7.7	44.7	52.3
50	0	1	Exogenous[5]	33.2	6.9	43.1	50.1
50	0	5	Exogenous	26.8	7.1	43.1	50.2
50	0	20	Exogenous	26.3	8.9	43.4	52.3
50	0	100	Exogenous	23.9	7.0	40.7	47.7
50	5	0	Inhibited	43.4	5.1	60.4	65.5
50	5	0.032	Autocrine	57.7	8.7	97.5	106.2
50	5	1	Exogenous	61.4	6.8	114.0	120.8
50	5	5	Exogenous	60.7	6.0	66.1	72.0
50	5	20	Exogenous	54.6	5.1	64.3	69.4
50	5	100	Exogenous	46.8	7.8	72.3	80.1
50	100	0	Inhibited	73.3	7.2	123.0	130.2
50	100	0.041	Autocrine	70.5	10.0	121.5	131.4
50	100	1	Exogenous	84.0	10.2	147.7	157.9
50	100	5	Exogenous	78.8	13.2	160.4	173.5
50	100	20	Exogenous	59.2	11.1	113.8	124.9
50	100	100	Exogenous	53.8	12.6	105.8	118.5

[1]See Figure 2-8A for a surface plot of apoptosis and autocrine IL-1α/β release induced by these combinations of TNF and TGF-α stimuli in Adv-infected hepatocytes.
[2]Total autocrine IL-1α/β concentration was calculated by adding the measured IL-1α and IL-1β concentrations and is an estimate of their net activity.
[3]Endogenous TGF-α activity inhibited by 10 μg/ml anti-TGF-α and, accordingly, TGF-α is plotted as having an effective concentration of zero.
[4]Autocrine TGF-α concentration measured by ELISA and in the absence of TGF-α neutralizing antibody.
[5]Exogenous TGF-α concentration set by the addition of recombinant TGF-α.

saturating exogenous TGF-α are likely due to its limited ability to further supplement anti-apoptotic Akt signaling in the presence of Adv infection and insulin (Figure 2-7A); and, instead, saturating concentrations of TGF-α are required to exert a substantial anti-apoptotic effect. Thus, an integrated balance of signaling by exogenous TNF, autocrine and exogenous TGF-α, and autocrine IL-1α/β determines hepatocyte apoptosis responses in the presence of Adv infection. At autocrine and sub-saturating exogenous

concentrations, TGF-α exerts a negligible anti-apoptotic stimulus that is overwhelmed by pro-apoptotic signaling from exogenous TNF and induced autocrine IL-1α/β, which are antagonized by released IL-1ra. But, at saturating exogenous concentrations, TGF-α effectively antagonizes pro-apoptotic signaling by these factors (Figure 2-8G).

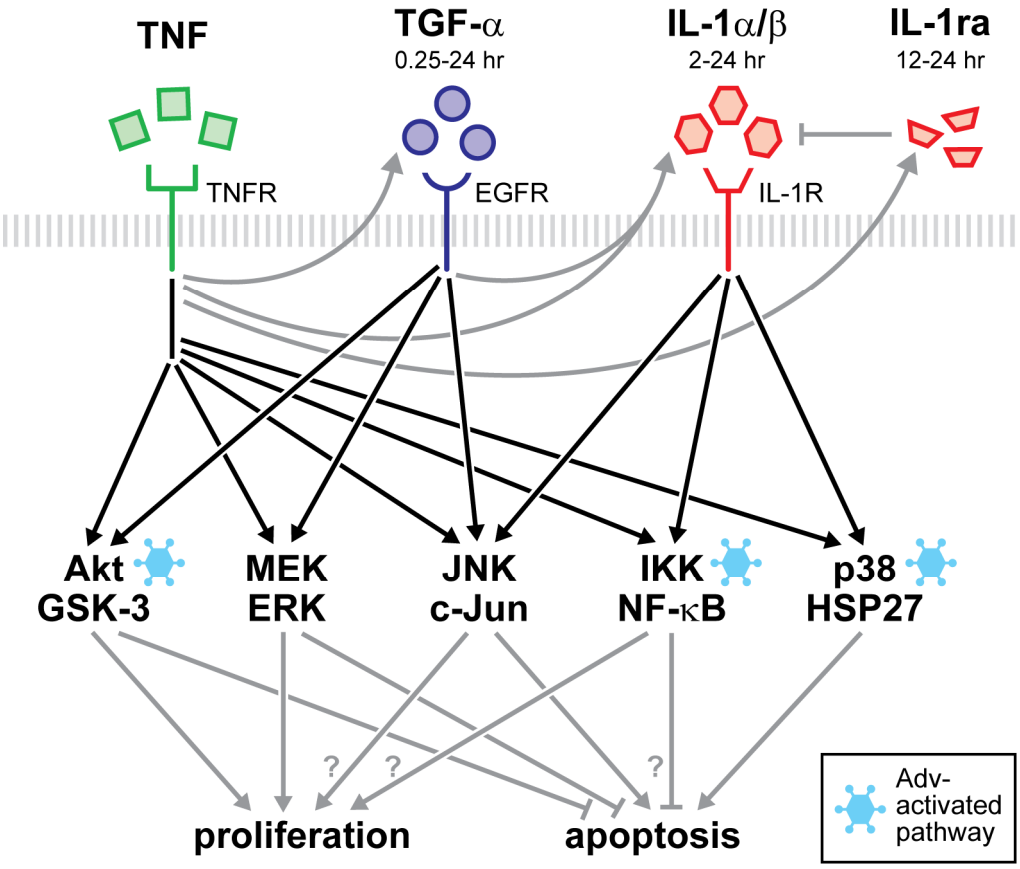

Figure 2-9. A TGF-α–IL-1α/β–IL-1ra autocrine cascade contributes to TNF-induced hepatocyte proliferation and Adv-infection sensitized apoptosis through the regulation of multiple shared signaling pathways. TNF activates the Akt, ERK, JNK, IKK–NF-κB, and p38 signaling pathways both directly downstream of TNFR [11, 76] and indirectly through this autocrine cascade. Replication-deficient Adv infection can activate Akt, NF-κB, and p38 pathway signaling [22, 23]. TNF induces TGF-α release, which activates Akt, ERK, and JNK signaling over a time scale of 0.25-24 hours. Induced IL-1α/β release is contingent on both TNF and autocrine TGF-α. Autocrine IL-1α/β activates JNK, IKK–NF-κB, and p38 signaling over a time scale of 2-24 hours. Independent of autocrine TGF-α or IL-1α/β, TNF also induces the release of IL-1ra, which antagonizes IL-1α/β ligand activity and accumulates over a time scale of 12-24 hours. These signaling pathways have diverse function in regulating hepatocyte proliferation and apoptosis [11, 75, 76, 84].

2.4. Discussion

We have demonstrated that hepatocyte responses to TNF are regulated by an inducible, coupled, and self-antagonizing TGF-α–IL-1α/β–IL-1ra autocrine cascade. This autocrine cascade promotes both TNF-induced apoptosis in hepatocytes infected with Adv -- a therapeutically and physiologically relevant sensitization for hepatocyte apoptosis induced by TNF developed herein -- and TNF-induced proliferation in the absence of viral infection.

2.4.1. Autocrine signaling control of adenovirus- and TNF-induced intracellular signaling pathways

TNF-induced autocrine TGF-α and IL-1α/β contribute to multiple intracellular signaling pathways that govern both hepatocyte proliferation and apoptosis (Figure 2-9). Autocrine TGF-α regulates pro-proliferative/anti-apoptotic signaling through the ERK and, in the absence of Adv infection, Akt pathways [83, 84]. Autocrine IL-1α/β regulates pro-apoptotic signaling through JNK and p38 pathways. From our results, it is unclear how autocrine IL-1α/β signaling antagonizes hepatocyte proliferation, but one possibility is through the sustained activation of JNK signaling and its association with anti-proliferative ROS accumulation [102]. When added exogenously, IL-1 antagonizes hepatocyte proliferation through its induction of NO signaling [87], which was not assayed in our study. NO has been shown to impair DNA synthesis through its activation of ribonucleotide reductase [87], but could also inhibit DNA synthesis, and effector caspase activation, through its S-nitrosylation and deactivation of initiator caspases [104], whose cleavage and activation is necessary for both DNA synthesis [38] and apoptosis. Thus, autocrine-dependent signaling modulates diverse signaling pathways and further investigation is necessary to identify how the pathways assayed herein and other signaling mechanisms interact to govern hepatocyte responses to TNF.

2.4.2. Regulation of autocrine ligand expression and release

Although not mechanistically investigated here, the expression and/or post-translational processing and shedding of TGF-α, IL-1α/β, and IL-1ra ligands are regulated by a number of signaling pathways activated by TNF and Adv infection, including JNK, IKK–

NF-κB, and p38 [84, 90, 105-107]. TGF-α expression is regulated by ERK-, NF-κB-, and JNK–AP-1-related transcription factor activity [90, 108]. Post-translational processing, mediated by the protease ADAM17 (as known as TACE), is required for mature TGF-α release. ADAM17 is activated by ERK and p38 signaling in mammary epithelial cells [107] and downstream of TNF stimulation in the AML-12 hepatocyte cell line [84]. Moreover, ADAM17 processes the EGFR ligands HB-EGF and amphiregulin and TNF itself, which were not examined in this study but are produced by hepatocytes under certain conditions [81, 109] and could provide additional autocrine feedback signals to exogenous TNF treatment. Thus, NF-κB, JNK, and p38 signaling could mediate TNF-stimulated TGF-α transcription and processing in hepatocytes, with release of TGF-α leading to transactivation of ERK signaling and its further stimulation of TGF-α release. IL-1α and IL-1β maturation and release are also controlled by both transcriptional and post-translational mechanisms. Although less is known about these mechanisms, both IL-1 transcription and processing, involving the proteases caspase-1 and MMP-3, can be activated by signaling mediators downstream of toll-like receptors and TNFR1 [106].

The time courses of TGF-α, IL-1α, and IL-1β ligand accumulation reported here indicate that, in the absence of Adv infection, TNF-induced hepatocyte shedding of these ligands requires transcriptional activation, which could be further modified by post-translational processing (Figure 2-2D-F). In Adv-infected hepatocytes, TNF-induced release of TGF-α was upregulated earlier (by 4 hours post-TNF treatment; Figure 2-6A) and release of IL-1β was dramatically increased at later times (12-24 hours after TNF treatment; Figure 2-6C). This suggests that Adv infection sensitizes TNF-treated hepatocytes to release TGF-α on time scales consistent with post-translational rather than transcriptional regulation. The earlier and more pronounced IL-1β release suggests that Adv similarly potentiates TNF-induced IL-1β transcription and/or processing possibly due to shared activation of the NF-κB signaling by Adv and TNF (see Figures 2-3G and 2-7G to compare TNF-induced NF-κB signaling in uninfected and Adv-infected hepatocytes). Moreover, these results suggest that signaling activation via autocrine TGF-α is necessary for TNF-stimulated IL-1α/β release in hepatocytes in the presence (Figure 2-2H-I) or absence of Adv (Figure 2-6H-I).

During liver regeneration following PHx, both TNF and IL-1α/β levels in the liver peak within 24 hr post-PHx with IL-1α/β levels rising again at 48-96 hr post-PHx, coinciding with cessation of growth factor-stimulated hepatocyte proliferation [86, 110]. Following this, the initial phase of IL-1α/β-mediated growth inhibition following PHx could be contributed by TNF-stimulated autocrine release and the later phase could be due to through Kupffer cell paracrine release.

2.4.3. Interpretation of autocrine signaling mechanisms is context-dependent

Our results also underscore the challenges in unraveling the complexities of context-dependent cues such as TNF, and we note several factors that should be considered in interpretation of these results. In this study, we inferred the activity of autocrine factors by assaying their accumulation in culture medium and their control of multiple phosphoprotein signaling pathways and resultant cellular responses. The rate of ligand accumulation in culture medium does not, however, completely reflect activity of autocrine factors, especially when receptor-mediated ligand consumption is significant compared to production [111]. The outcome of autocrine effects can be influenced by cell density, which differed in the proliferation and apoptosis studies here, through the modulation of local ligand concentrations achieved by the net effects of ligand production and uptake [112]. Cell density could similarly influence hepatocyte autocrine signaling in physiological processes such as liver regeneration, in which hepatocyte cell density varies in different microenvironments and time points following PHx [75]. Further, ligand-dependent receptor degradation, prolonged culture duration, and viral infection can all modulate receptor expression levels in hepatocytes [25, 113], which in turn could lead to amplification and/or attenuation of the exogenous and autocrine ligand activities observed here. Finally, autocrine factors not examined in this study might also be involved in hepatocyte responses to TNF. These could include other ligands that are processed by ADAM17 in hepatocytes such as the EGFR ligands HB-EGF and amphiregulin and even TNF itself [81, 109].

2.4.4. Importance of autocrine signaling in hepatocyte biology

Results herein, and those previously reported, collectively illustrate the integral role of autocrine factors in hepatocyte proliferation, apoptosis, survival [114], and transformation [88] responses to exogenous cytokine stimuli and implicate diverse autocrine signaling connections between cytotoxic, inflammatory, and mitogenic ligands in hepatocytes. Integration of opposing positive and negative feedback mechanisms, such as those observed here, has previously been proposed to confer robustness in the control of cell phenotypic responses [115]. The disruption of self-limiting control mechanisms present in the TNF-induced TGF-α–IL-1α/β–IL-1ra autocrine cascade could provide means by which hepatocyte pathophysiological responses to inflammatory cytokine stimuli arise and lead to oncogenic transformation and hepatocellular carcinoma [100, 116]. Our results also suggest ways that manipulation of autocrine loops may influence therapeutic interventions in liver disease. For example, targeted interference with IL-1 signaling has been shown to reduce hepatotoxicity and improve efficacy of Adv gene therapy *in vivo* [20], positive effects that may arise in part by disruption of autocrine IL-1 signaling. Our findings that TGF-α is pro-apoptotic at, and slightly above, concentrations associated with autocrine secretion imply that adenoviral gene therapies might be especially hepatotoxic under conditions in which both TNF and TGF-α (or other EGFR ligands) are mildly upregulated, as is observed following PHx [75].

Clearly, the delicate balance between opposing signals requires careful examination using quantitative experimental models in order to achieve desired outcomes. Moreover, further development of animal models will be critical to parse the complex autocrine and paracrine signaling mechanisms regulating TNF signaling in hepatocytes and other liver cell types *in vivo* and to validate any therapeutic interventions directed towards the autocrine control mechanisms identified in this study.

CHAPTER 3

Development and analysis of an *in vitro* drug-cytokine hepatocellular death synergy model for the study of inflammation-associated idiosyncratic drug hepatotoxicity

3.1. Introduction

3.1.1. Idiosyncratic drug hepatotoxicity

Idiosyncratic drug hepatotoxicity is defined as drug-induced liver injury that occurs in a very small fraction of human patients, is unrelated to the pharmacologic target of the drug, and exhibits no apparent relationship to dose or duration of drug exposure [26-28]. Idiosyncratic drug hepatotoxicity is poorly predicted by standard preclinical cell culture and animal models as well as in clinical trials, and, consequently, most idiosyncratic drug hepatotoxicities are not evident until after approval for human use. Due to the inability to predict idiosyncratic hepatotoxicities in the drug development process, idiosyncratic drug hepatotoxicity frequently leads to drug withdrawal or "black box" warnings and accounts for more than 10% of acute liver failure cases [27, 117]. Multiple hypotheses have been suggested to explain the mechanisms underlying idiosyncratic drug hepatotoxicity. These include (i) variations in drug metabolism, particularly associated with alterations in the expression and/or activities of the cytochrome P450 family enzymes, due to variable environmental conditions and/or genetic polymorphisms in the human population [29]; and (ii) a relationship with concomitant liver inflammation associated with viral or bacterial infection or liver or inflammatory disease [26]. Moreover, it is likely that multiple factors -- both genetic and environmental -- contribute, at relative degrees which are not predictable at the present time, to a drug's hepatotoxicity idiosyncrasies [31].

3.1.2. *In vitro* and *in vivo* models of idiosyncratic drug hepatotoxicity

A number of preclinical models have been developed in attempts to predict idiosyncratic drug hepatotoxicity, including the assessment of reactive metabolites through glutathione (GSH) conjugation assays and the evaluation of animals models by toxicogenomic and

metabolonomic approaches to identify common idiosyncratic hepatotoxicity-associated biomarkers, with little overall predictive success [27, 30, 31]. Rodent models administered with bacterial lipopolysaccharide (LPS) have been recently developed to assess inflammation-associated idiosyncratic drug hepatotoxicity. In these rodent models, LPS exposure induces a mild inflammatory response that has been demonstrated to synergistically induce hepatotoxicity in the presence of a number of idiosyncratic hepatotoxic drugs, including diclonfenac, sulindac, trovafloxacin, ranitidine, chlorpromazine, but not non- or less-toxic control drugs [32-35]. In rats, LPS administration upregulates plasma concentrations of the cytokines tumor necrosis factor-α (TNF), interferon-γ (IFNγ), interleukin-1α and -1β (IL-1α/β), interleukin-6 (IL-6), and the chemokine interleukin-10 (IL-10) [36]. Of these, TNF, IFNγ, IL-1α/β, IL-6, and LPS itself all stimulate hepatocyte signaling responses through the activation of a diversity of intracellular signal transduction pathways, including the IKK–NF-κB, p38, and JNK pathways (associated with TNF, IL-1α/β, and LPS signaling) and the STAT1 and STAT3 pathways (associated with IFNγ and IL-6 signaling, respectively), which all are implicated in hepatocellular death in liver diseases and injuries (reviewed in [76, 118-120]). In LPS-administered rat models, synergistic induction of hepatocellular death in the presence of the idiosyncratic hepatotoxins ranitidine and trovafloxacin has been reported to be dependent on TNF signaling [35, 37].

The observations in LPS-administered rodent models suggest that idiosyncratic drug hepatotoxicity can arise when mild drug-induced hepatocellular stress synergizes with LPS-induced inflammatory cytokine signaling to elicit acute hepatocellular death [27, 38]. These stresses may be idiosyncratic in nature in human patients due variations in drug metabolism, exposure, and/or clearance. The sensitizing role of hepatocellular stress is supported by the fact that drug-induced depletion of glutathione is known to sensitize hepatocytes to TNF-induced apoptosis [39]. Furthermore, both LPS and inflammatory cytokine signaling can alter hepatocyte expression of cytochrome P450 enzymes and thus lead to dysregulated drug metabolism and clearance in conditions of LPS-induced liver inflammation [40, 41]. Although they offer promise for improved predictability of idiosyncratic hepatotoxicity in preclinical screening, LPS-administered rodent models lack sufficient throughput for preclinical screening of candidate

pharmaceuticals. Moreover, it has been shown that animal models are in general not highly predictive of human drug hepatotoxicity, as combined preclinical testing in rodents, dogs, and monkeys can only identify ~50% of known human hepatotoxins [121].

Recent advances in the maintenance and characterization of *in vitro* hepatocyte culture systems offer substantial promise for their more wide-spread utilization in high-throughput preclinical screening approaches for the prediction of both non-idiosyncratic and idiosyncratic drug hepatotoxicity in humans. Amongst hepatocyte culture systems that are commonly employed for high-throughput preclinical studies, primary human hepatocytes are considered the "gold standard" for evaluating drug metabolism, transport, and toxicity [122, 123]. In comparison, primary rat hepatocytes, while more readily available and similarly capable of maintaining differentiated hepatic function in time-scales of a few days *in vitro*, do not reproduce some aspects of human drug metabolism [8, 124]. Immortalized and transformed human cell lines (*e.g.* HepG2 cells) are also frequently employed but have poor maintenance of liver-specific functions and are relatively insensitive to human hepatotoxins in simple cytotoxicity assays [124, 125]. A small number of hepatocyte cell culture models have been recently developed to assess idiosyncratic drug hepatotoxicity. Of note, Xu *et al* utilized human hepatocyte cell culture models to assay four sub-lethal hepatotoxicity injuries with high-throughput live-cell microscopy for over 300 drugs, including many that cause idiosyncratic liver toxicity in humans [126]. Using a well-calibrated random forest prediction model of the imaging data, they were able to predict drug hepatotoxicity with a ~50% true-positive rate and ~5% false-positive rate. A rat hepatocyte-Kupffer cell co-culture model has been developed and shown to successfully predict chlorpromazine idiosyncratic hepatotoxicity through its synergistic induction of hepatocellular death following LPS treatment [127]. The further development and validation of hepatocyte cell culture models would provide much-needed tools for the preclinical evaluation of idiosyncratic drug hepatotoxicity and could offer greater predictive ability and higher throughput than LPS-administered animal models.

3.1.3. Chapter overview

Here, we describe a model of inflammatory cytokine-associated idiosyncratic drug hepatotoxicity in three standard hepatocyte cell culture systems amenable to high-throughput preclinical screening -- primary rat and human hepatocytes and the HepG2 human hepatoblastoma cell line. We initially validate this model to demonstrate that a number of idiosyncratic hepatotoxic drugs (ranitidine, trovafloxacin, nefazodone, nimesulide, clarithromycin) synergistically induce hepatocellular death *in vitro* when co-administered with a cytokine mix containing the LPS-upregulated cytokines TNF, IFNγ, and IL-1α, and LPS itself. We then collect a hepatotoxicity data compendium comprised of combinations of drug and cytokine mix co-treatments covering ~1500 experimental conditions and analyze it to identify informative cytokine mix treatments and hepatocyte cell systems for predicting inflammation-associated idiosyncratic drug hepatotoxicity. Using this data compendium, we show that *in vitro* drug-cytokine synergies are predominantly potentiated by TNF, IL-1α, and LPS within the context of multi-cytokine mixes and that patterns of drug-cytokine mix synergies across a landscape of multi-cytokine environments can be shown to correlate to drug-induced sub-lethal hepatocyte injuries. Lastly, we demonstrate the predictive utility of this drug-cytokine mix co-treatment model by screening a set of 90 drugs in human hepatocytes and show that a significantly larger fraction of idiosyncratic hepatotoxins synergize with a single cytokine mix at physiologically relevant dosing concentrations than do non-toxic drugs. Our results indicate promise for employing our approach for efficient *in vitro* investigation of inflammation-associated idiosyncratic drug hepatotoxicity.

3.2. Experimental procedures

3.2.1. Drugs and cytokines

Most drugs were obtained from Sigma (St. Louis, MO) or Sequoia Research Products (Pangbourne, UK). Trovafloxacin was obtained from Pfizer's chemical sample bank (Groton, CT). Unless otherwise noted, the following drug concentrations were used: 450 μM ranitidine, 450 μM trovafloxacin, 70 μM nefazodone, 450 μM nimesulide, 175 μM clarithromycin, and 175 μM telithromycin. TPCA-1, an IKK-2 inhibitor, was obtained from Tocris Bioscience (Ellisville, MS). All drugs were suspended in 0.25% final

DMSO. Recombinant rat or human cytokines were obtained from R&D Systems (Minneapolis, MN) and were used at the following concentrations: 100 ng/ml tumor necrosis factor-α (TNF), 100 ng/ml interferon-γ (IFNγ), 20 ng/ml interleukin-1α (IL-1α), and 20 ng/ml interleukin-6 (IL-6). Lipopolysaccharides (LPS) serotype 1 from *E. coli* 0111:B4 was used at 10 μg/ml. Unless noted, all reagents were obtained from Sigma.

Table 3-1. Drug-induced liver injury (DILI) categories.

DILI categories (sorted by hepatotoxicity level)		
Group	Category	Description
hepatotoxic	P1	associated with drug-induced liver injury, type 1: hepatotoxic in animals and/or humans in a dose-dependent manner
	O1	hepatotoxic in animals, untested in humans
	P2	associated with drug-induced liver injury, type 2: hepatotoxic in animals and/or humans in a dose-independent manner, generally regarded as idiosyncratic hepatotoxicity
minimally or not hepatotoxic	O2	elevated liver enzymes in humans, but generally regarded as safe
	N3	sporadic cases of liver injury in humans, but generally safe
	N2	not known to cause liver injury, but known to cause other organ injury
	N1	not known to cause liver injury

3.2.2. Drug hepatotoxicity classifications and pharmacokinetic properties

Drug hepatotoxicity classifications were made according to a drug-induced liver injury (DILI) scale (see Table 3-1) based on clinical data collected from PubMed searches, as in [126]. For select drugs, idiosyncratic hepatotoxicity classifications were assigned according to literature references (see Table 3-2). Therapeutically appropriate drug exposure levels were defined by average plasma maximum concentration (C_{max}) values observed in humans upon single- or multi-dose administration at commonly recommended therapeutic doses. C_{max} values were obtained from a combination of literature searches and available databases, as in [126], and are reported in Table 3-3. Unless noted otherwise, a concentration of 100-fold C_{max}, encompassing a scaling factor to account for human population pharmacokinetic and toxicodynamic variabilities, was

considered as a therapeutically relevant dosing limit for each drug, as previously discussed [126].

3.2.3. Hepatocyte cell isolation, culture, and stimulation

Primary rat hepatocytes were isolated from male Fisher rats using a modified collagenase perfusion and Percoll isolation, routinely yielding >90% viability and >97% purity, as in Chapter 2.2.1. Rat hepatocytes were seeded on collagen type I-coated 96-well plates (BD Biosciences, Franklin Lakes, NJ) at 1×10^5 cells/cm^2 in insulin-containing, serum-free hepatocyte growth medium (HGM; as in Chapter 2.2.3, but supplemented with 1 μM trichostatin A). One day post-seeding, rat hepatocytes were overlayed with 0.25 mg/ml Matrigel (growth factor-reduced; BD Biosciences) in fresh HGM. One day following Matrigel overlay, primary rat hepatocytes were stimulated with drugs and/or cytokines in fresh HGM. For rat and human hepatocyte studies, multiple donors were used throughout this work, with a single donor used for each self-consistent data set.

Primary human hepatocytes were obtained in suspension from CellzDirect (Durham, NC). Human hepatocytes were seeded on collagen type I-coated 96-well plates at 1.5×10^5 cells/cm^2 in "plating medium" consisting of Dulbecco's modified Eagle's medium (DMEM) supplemented with 5% fetal bovine serum (FBS; Hyclone, Logan, UT), 100 U/ml penicillin, 100 μg/ml streptomycin, 0.58 mg/ml L-glutamine, 1 μM trichostatin A, 0.5 μM dexamethasone, and 5 μg/ml insulin. One day post-seeding, human hepatocytes were overlayed with 0.25 mg/ml Matrigel in "culturing medium" consisting of William's E medium (WEM) supplemented with 15 mM HEPES, 100 U/ml penicillin, 100 μg/ml streptomycin, 0.29 mg/ml L-glutamine, 1 μM trichostatin A, 0.1 μM dexamethasone, 5 μg/ml insulin, 5 μg/ml transferrin, and 5 ng/ml sodium selenite. One day following Matrigel overlay, human hepatocytes were stimulated with drugs and/or cytokines in "dosing medium" (consisting of "culturing medium" but without transferrin and sodium selenite).

HepG2 cells were obtained from ATCC (Manassas, VA) and were maintained per ATCC recommendations. HepG2 cells were seeded on collagen type I-coated 96-well plates at 1×10^5 cells/cm^2 in Eagle's minimum essential medium (EMEM; ATCC) supplemented with 10% FBS, 100 U/ml penicillin, and 100 μg/ml streptomycin. One day

after seeding, medium was changed to fresh EMEM without FBS. One day after medium change, HepG2 cells were stimulated with drugs and/or cytokines in fresh EMEM without FBS. All cells were maintained at 37°C and 5% CO_2.

3.2.4. Quantitative cell death assays

At 12, 24, or 48 hours post-drug and/or cytokine treatment, conditioned medium samples were collected to assay lactate dehydrogenase (LDH) release (indicator of necrotic and apoptotic cell death) and cells were assayed for caspase 3/7 activity (indicator of apoptotic cell death). LDH activity in culture supernatants was quantified using a CytoTox-ONE Homogeneous Membrane Integrity Assay (Promega, Madison, WI) according to manufacturer's recommendations. Cellular caspase 3/7 activity was quantified using a Caspase-Glo 3/7 Assay (Promega) according to manufacturer's recommendations. For each cell system and time-point, LDH and caspase 3/7 activity assay results were fold-change normalized to the average DMSO control/no cytokine treatment value from four or more biological samples from the same 96-well culture plate.

3.2.5. Quantitative sub-lethal hepatotoxicity imaging assays

Drug-induced sub-lethal hepatotoxicity phenotypes were quantitatively imaged in human hepatocytes in the absence of cytokine co-treatment, essentially as described previously [126]. Briefly, human hepatocytes at 24 or 48 hours post-treatment were stained with four fluorescent probes: DRAQ5 (Biostatus, Shapshed, UK) to stain nuclei and lipids, CM-H_2DCFDA (Invitrogen, Carlsbad, CA) to stain reactive oxygen species (ROS), TMRM (Invitrogen) to stain mitochondrial membrane potential (MtMP), and mBCl (Invitrogen) to stain glutathione (GSH). Automated live-cell, multi-color image acquisition was performed on a Kinetic Scan Reader (Cellomics, Pittsburgh, PA) using a 20× objective and a XP93 filter set (Omega Optical, Brattleboro, VT). Quantitative image analysis was performed using ImagePro Plus software (Media Cybermetrics, Bethesada, MD). In each image, five features were quantified: nuclei count and intracellular lipid (non-nuclear DRAQ5 stain), ROS, MtMP, and GSH contents. For each feature, the summed intensity value from each well was normalized by the total nuclei

count (~500 imaged per well), and then the intensity-per-cell values were fold-change normalized to the average DMSO control value from eight or more biological samples from the same 96-well culture plate.

3.2.6. Factorial analysis

The drug-cytokine mix hepatotoxicity compendium was collected such that a full factorial design of the five cytokine or LPS treatments ($2^5 = 32$ mixes) was included for each drug co-treatment in each cell system. For each drug/cell system, the fold-change normalized toxicity assay values were subjected to factorial analysis. One-, two-, three-, four-, and five-factor effects and their associated errors were calculated according to standard factorial analysis formulae [128].

3.2.7. Hierarchical clustering

The drug-cytokine mix combinatorial hepatotoxicity compendium was fused across all cell systems and assay types to generate a hepatotoxicity matrix spanning 192 "experimental conditions" (*i.e.*, combinations of cell type, assay readout, and cytokine treatment) and 8 drug treatments. For each combination of cell system and assay type, the fold-change normalization values were linearly mapped to a scale from the minimum observed value (set to 0) and the maximum observed value (set to 1). The fused data compendium was subjected to two-way clustering using the unweighted pair group method with arithmetic mean and a Pearson distance metric.

3.2.8. Statistical analysis

To identify drug-cytokine mix co-treatment conditions that elicited supra-additive hepatotoxicity synergies, additive projections of drug-cytokine mix co-treatments were estimated by adding mean values of drug-only and cytokine mix-only toxicities and propagating their associated variances. Supra-additive synergies were identified for conditions in which the observed drug-cytokine mix co-treatment results exceeded the additive projections as assessed by two-sample, one-tailed (Student's) *t* test with a false discovery rate correction for multiple comparison testing for multiple drug doses or multiple cytokine mixes. The statistical significance of each factorial effect and its

associated error was assessed using one-sample, two-tailed *t* test with a false discovery rate correction for multiple cytokine mixes. Statistical significance of drug-induced sub-lethal hepatotoxicities was assessed by a Student's *t* test. In the 90-drug study, a threshold two-fold above the additive projection was used instead of a Student's *t* test to identify supra-additive drug-cytokine mix synergy due to the limited number of replicate samples. The statistical significance of the observed number of synergistic drugs in the each hepatotoxic group was assessed using a hypergeometric test (see Table 3-4 for details). All tests were performed at a significance level of $\alpha = 0.05$. False discovery rate-corrected *P*-values were calculated as: $P = \alpha \cdot (N+1)/(2N)$, where N is the number of comparisons.

3.3. Results

3.3.1. Several idiosyncratic hepatotoxic drugs, but not their control-paired compounds, exhibit drug-cytokine mix hepatotoxicity synergies *in vitro*

We developed an *in vitro* model of inflammation-associated idiosyncratic drug hepatotoxicity by co-administering drug compounds with known idiosyncratic hepatotoxicities in humans with a variety of inflammatory cytokines mixtures (comprised of the cytokines TNF, IFNγ, IL-1α, and IL-6, along with LPS) in multiple hepatocellular cell culture systems (primary human and rat hepatocytes and HepG2 human hepatoblastoma cells). For each drug compound associated with idiosyncratic hepatotoxicity, a less- or non-hepatotoxic "comparison" control compound was used. In this study, the term "comparison" compound was applied to drugs with similar molecular target and clinical indication and, were possible, similar chemical structure. Initially, this *in vitro* drug-cytokine mix co-treatment model was applied to primary rat hepatocytes and HepG2 cells treated with five pairs of drug compounds in the presence or absence of a single cytokine mix containing TNF, IFNγ, IL-1α, and LPS and assayed for LDH release as a marker of both apoptotic and necrotic cell death (Figure 3-1). In developing this model, we investigated drug-cytokine mix hepatotoxicity synergies for the following idiosyncratic hepatotoxic drugs (in conjunction with corresponding control compounds): ranitidine and its control compounds cimetidine and famotidine (histamine H2-receptor antagonists); trovafloxacin and its non-toxic control levofloxacin (fluoroquinolone

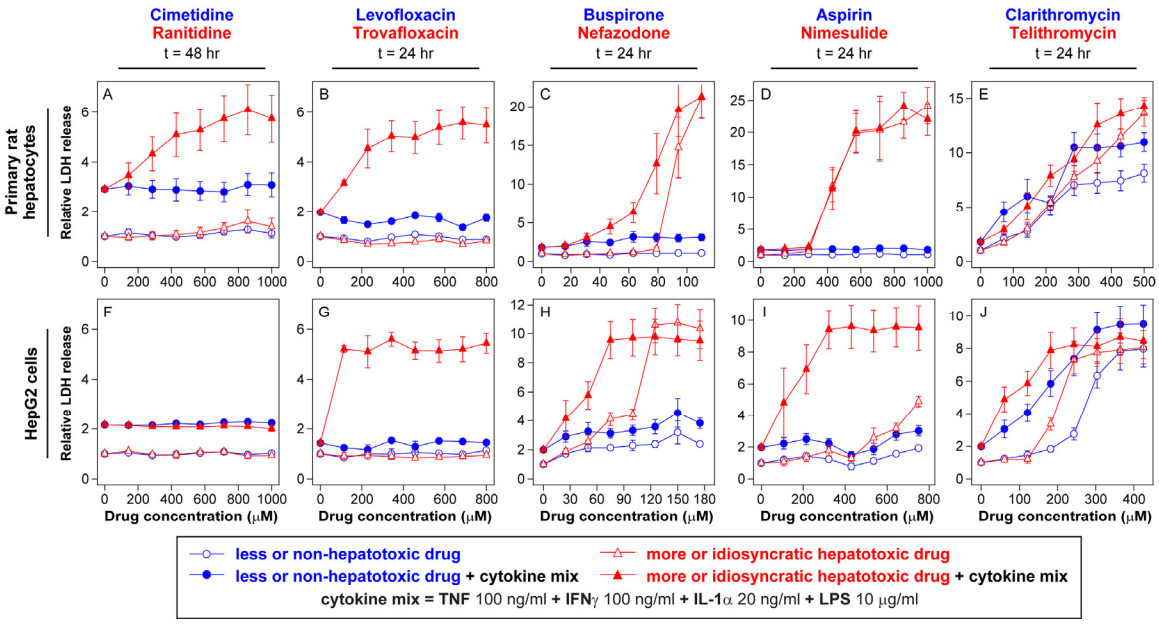

Figure 3-1. Identification of drug dose-dependent hepatotoxicity synergies between a cytokine mix and multiple idiosyncratic hepatotoxic drugs in primary rat hepatocytes (A-E) and HepG2 cells (F-J). Primary rat hepatocytes and HepG2 cells were cultured, treated, and assayed for LDH (at 24 or 48 hours post-treatment) as described in Chapter 3.2. Drugs were dosed at varying concentrations in the presence or absence of a cytokine mix containing 100 ng/ml TNF, 100 ng/ml IFNγ, 20 ng/ml IL-1α, and 10 μg/ml LPS. LDH release values were fold-change normalized to DMSO/no cytokine control samples from the same cell system. (Note that LDH release axes are separately scaled for each plot.) Drugs from similar chemical class and/or molecular target are plotted together, with the less or non-hepatotoxic drug in blue and the more idiosyncratic hepatotoxic drug in red. Data are presented as mean ± SEM of four biological samples. For results from additional time points, with drug doses plotted with respect to both molecular concentrations and drug C_{max} values, see [129].

antibiotics); nefazodone and its non-toxic control buspirone (serotonin receptor inhibitors); nimesulide and its non-toxic control aspirin (non-steroidal anti-inflammatory drugs); and telithromycin and the less idiosyncratic control compound clarithromycin (ketolide and macrolide antibiotics, respectively, binding to bacterial ribosomal subunit 50S). For additional information on these drugs, see Table 3-2 and [27, 31, 130, 131]. Synergistic induction of hepatocellular death was assessed by a supra-additive synergy criterion that compares the experimentally observed cell death induced by drug and cytokine co-treatment to the additive projection of cell death observed for drug-only and cytokine mix-only treatments (Figure 3-2).

In this co-treatment model, we observed drug-cytokine mix synergies for ranitidine but not cimetidine or famotidine (data not shown) in rat hepatocytes (but not HepG2 cells), matching similar observations in a LPS-administered rat model [34]. We

observed drug-cytokine mix synergies for trovafloxacin but not levofloxacin in both rat hepatocytes and HepG2 cells, again matching similar observation in a LPS-administered mouse model [35]. For drugs not previously examined in LPS-administered animal models, we observed drug-cytokine mix synergies for nefazodone (but not buspirone) and clarithromycin in both rat hepatocytes and HepG2 cells, and nimesulide (but not aspirin) and telithromycin in only HepG2 cells. In this initial study, drug-cytokine mix synergies were only observed for the more idiosyncratic hepatotoxic drugs, except for clarithromycin and telithromycin, which both have associated idiosyncratic hepatotoxicity with telithromycin having a greater incidence (see Table 3-2 and [31, 132]). Drug-cytokine mix hepatotoxicity synergies were observed within 24 hr following co-treatment except for ranitidine in rat hepatocytes, which required 48 hr of co-treatment to elicit hepatotoxicity synergy, demonstrating that, at the drug and cytokine treatment concentrations used, this *in vitro* model captures acute, rather than chronic, hepatotoxicity responses. The delay in ranitidine-cytokine mix synergy compared to other compounds, in concert with the observation that it only occurs in rat hepatocytes and not HepG2 cells, indicates that a more prolonged mechanism (*e.g.* requiring significant accumulation of ranitidine metabolites) may be required to potentiate ranitidine-cytokine hepatotoxicity synergy.

Specific concentrations and time-points for each drug were selected for further investigation (see summary in Table 3-2) based on the criteria that the concentration induce robust supra-additive hepatotoxicity synergy with this representative cytokine mix (see Figure 3-2) and elicit minimal drug-only hepatotoxicity. This selection criteria allowed for identification of drug concentrations within a physiologically relevant dosing limit of 100-fold its C_{max} value (see Chapter 3.2.2 for additional explanation) for all cytokine-synergizing drugs except ranitidine, for which a dose of 450 μM or 317*C_{max} was used.

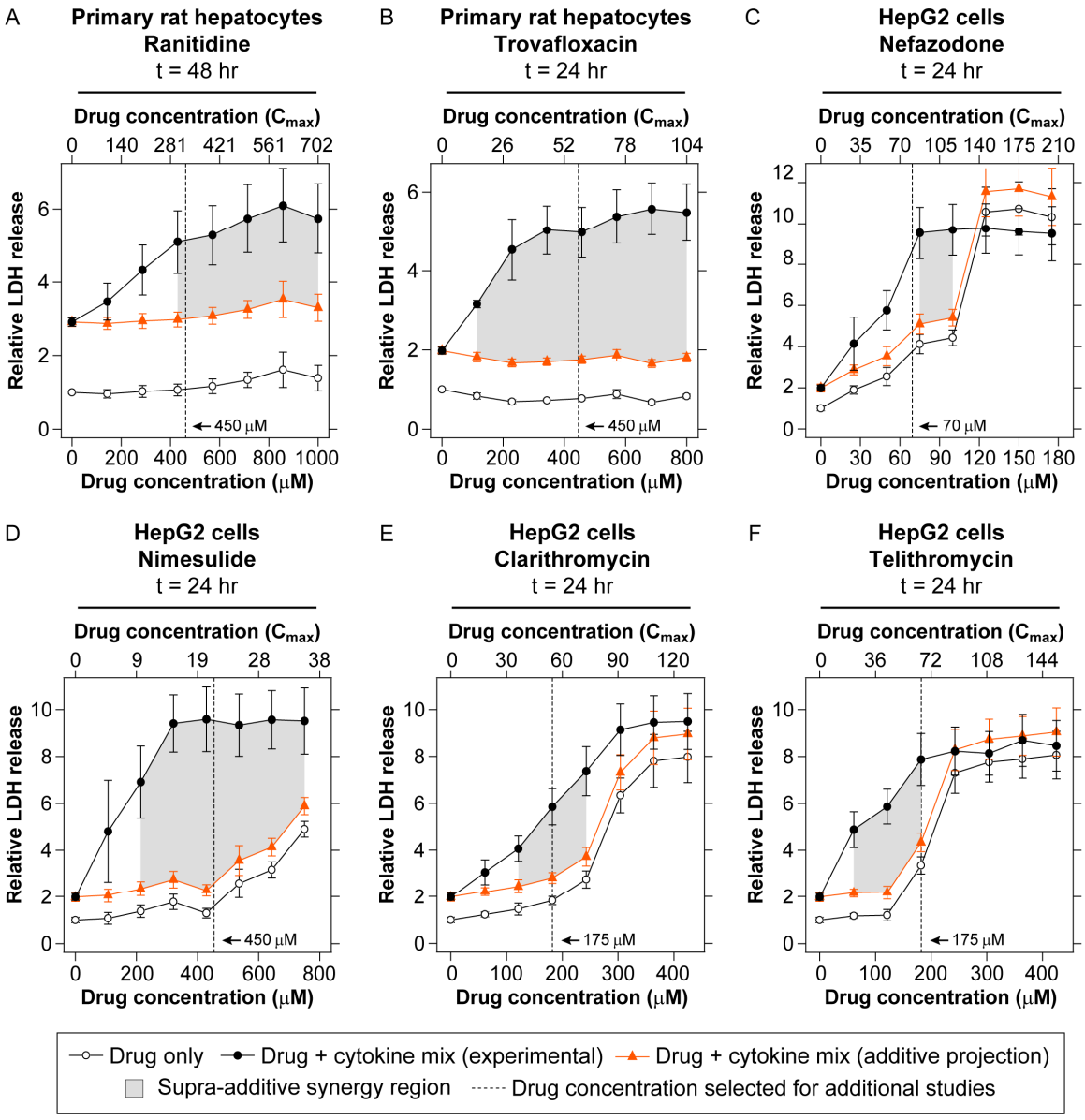

Figure 3-2. Identification of drug dosing concentration ranges that elicit supra-additive drug-cytokine hepatotoxicity synergies. Primary rat hepatocytes and HepG2 cells were cultured, treated, and assayed for LDH release (24 or 48 hours post-treatment) as described in Chapter 3.2. LDH release values were fold-change normalized to DMSO/no cytokine control samples. Drug concentrations are plotted with respect to molar concentration (μM) on the bottom axis and each drug's C_{max} value on the top axis. Optimal drug dosing concentrations for combinatorial studies were selected by identifying drug concentrations that elicited supra-additive drug-cytokine hepatotoxicity synergies for a single cytokine mix (TNF, IFNγ, IL-1α, and LPS). Projections of drug-cytokine mix co-treatments were estimated by adding mean values of drug-only and cytokine mix-only toxicities and propagating their associated variances. Observed drug and cytokine mix co-treatment toxicity results that exceeded the additive projections in a statistically significant manner ($P < 0.029$, as assessed by a false discovery rate-corrected Student's t test) are overlayed with a gray coloring. Drug concentrations that demonstrated robust supra-additive drug-cytokine mix hepatotoxicity synergy and minimal drug-only hepatotoxicity were selected by inspection for additional combinatorial cytokine mix studies and are indicated on each graph and in Table 3-2. Data are presented as the mean ± SEM of four biological samples.

Table 3-2. Drugs examined in initial drug-cytokine mix co-treatment model studies.

Drug	DILI category	Drug class	Idiosyncratic hepatotoxin[1]	Synergy with LPS in animal models[2]	Synergy with cytokine mix cell culture model[3]		Conditions selected for combinatorial cytokine experiments[4]	
					Primary rat hepatocytes	Hep G2 cells	Conc. (μM, C_{max})	End point
Famotidine	N3	histamine H2-receptor antagonist	-	-	-	-	*n.s.*	*n.s.*
Cimetidine	N3		-	*n.r.*	-	-	*n.s.*	*n.s.*
Ranitidine	N3		++	+	+	-	450 μM 317*C_{max}	48 hr
Levofloxacin	N3	fluoroquinolone antibiotic	-	-	-	-	*n.s.*	*n.s.*
Trovafloxacin	P2		++	+	+	+	450 μM 59*C_{max}	24 hr
Buspirone	N1	serotonin receptor inhibitor	-	*n.r.*	-	-	*n.s.*	*n.s.*
Nefazodone	P2		++	*n.r.*	+	+	70 μM 73*C_{max}	24 hr
Aspirin	O2	NSAID	-	*n.r.*	-	-	*n.s.*	*n.s.*
Nimesulide	P2		++	*n.r.*	-	+	450 μM 21*C_{max}	24 hr
Clarithromycin	N1	macrolide and ketolide antibiotic	+	*n.r.*	+	+	175 μM 52*C_{max}	24 hr
Telithromycin	P2		++	*n.r.*	-	+	175 μM 63*C_{max}	24 hr

[1]Idiosyncratic hepatotoxin classification based on published reports and reviews [27, 31, 130-132].
[2]Drug hepatotoxicity synergy with LPS administration in rodent models ranitidine but not famotidine has been reported in [34] and trovafloxacin but not levofloxacin has been reported in [35].
[3]Observed drug-cytokine supra-additive hepatotoxicity synergy using a cytokine mix containing TNF, IFNγ, IL-1α, and LPS in primary rat hepatocytes and/or HepG2 cells (see Figures 3-1 and 3-2).
[4]The listed conditions were selected, as shown in Figure 3-2, for further investigation in combinatorial cytokine co-treatment experiments. Abbreviations: DILI, drug-induced liver injury; C_{max}, average plasma maximum drug concentration in human use; *n.r.*, not reported in the literature; *n.s.*, not selected; NSAID, non-steroidal anti-inflammatory drug.

3.3.2. Collection of a combinatorial drug- and cytokine mix-induced hepatotoxicity compendium from multiple hepatocyte cell systems

To characterize drug-cytokine mix synergies in a more diverse set of cytokine environments and to make comparisons across hepatocyte cell culture systems, we collected a multi-cue data compendium from all combinations of six idiosyncratic hepatotoxic drugs from the initial study, each at one concentration and time-point, and a DMSO control, and the 32 combinatorial mixtures of TNF, IFNγ, IL-1α, IL-6, and LPS. (Note that IL-6, not included in the initial study due to its presumed pro-survival effects [133], was included in this combinatorial study.) Experiments were performed in rat hepatocytes, human hepatocytes, and HepG2 cells and then assayed for both LDH release and caspase 3/7 activity, a marker specific to apoptotic cell death (Figure 3-3). For rat and human hepatocyte studies, multiple donors were used throughout this work, with a single donor used for each self-consistent data set (*i.e.* each cell system's data compendium in Figure 3-3 represents a single donor). For rat hepatocytes, donor-to-donor variability was assessed by comparing two drug- and cytokine mix-induced hepatotoxicity data compendia (each consisting of the same 256 treatment conditions) collected from two separate primary rat hepatocyte isolations. The two separate data compendia showed a high degree of reproducibility ($R = 0.98$; see Figure 3-4).

The hepatotoxicity data compendium, comprised of ~1500 combinations of cell system, assay type, and drug-cytokine treatment, was observed to contain a diverse array of drug-cytokine synergy patterns not clearly interpretable by inspection alone, so we subjected it to three analytical approaches. (i) We discretized the hepatotoxicity data compendium into conditions that did or did not elicit supra-additive drug-cytokine mix synergy (Figure 3-5). (ii) We subjected the hepatotoxicity data compendium to factorial analysis to identify which underlying cytokine treatment factors potentiate cell death across the entire combinatorial landscape of cytokine environments (Figure 3-6). (iii) We employed hierarchical clustering of the hepatotoxicity data compendium with respect to both drug treatments and "experimental" conditions (*i.e.*, combinations of cell type, assay readout, and cytokine treatment; Figure 3-8).

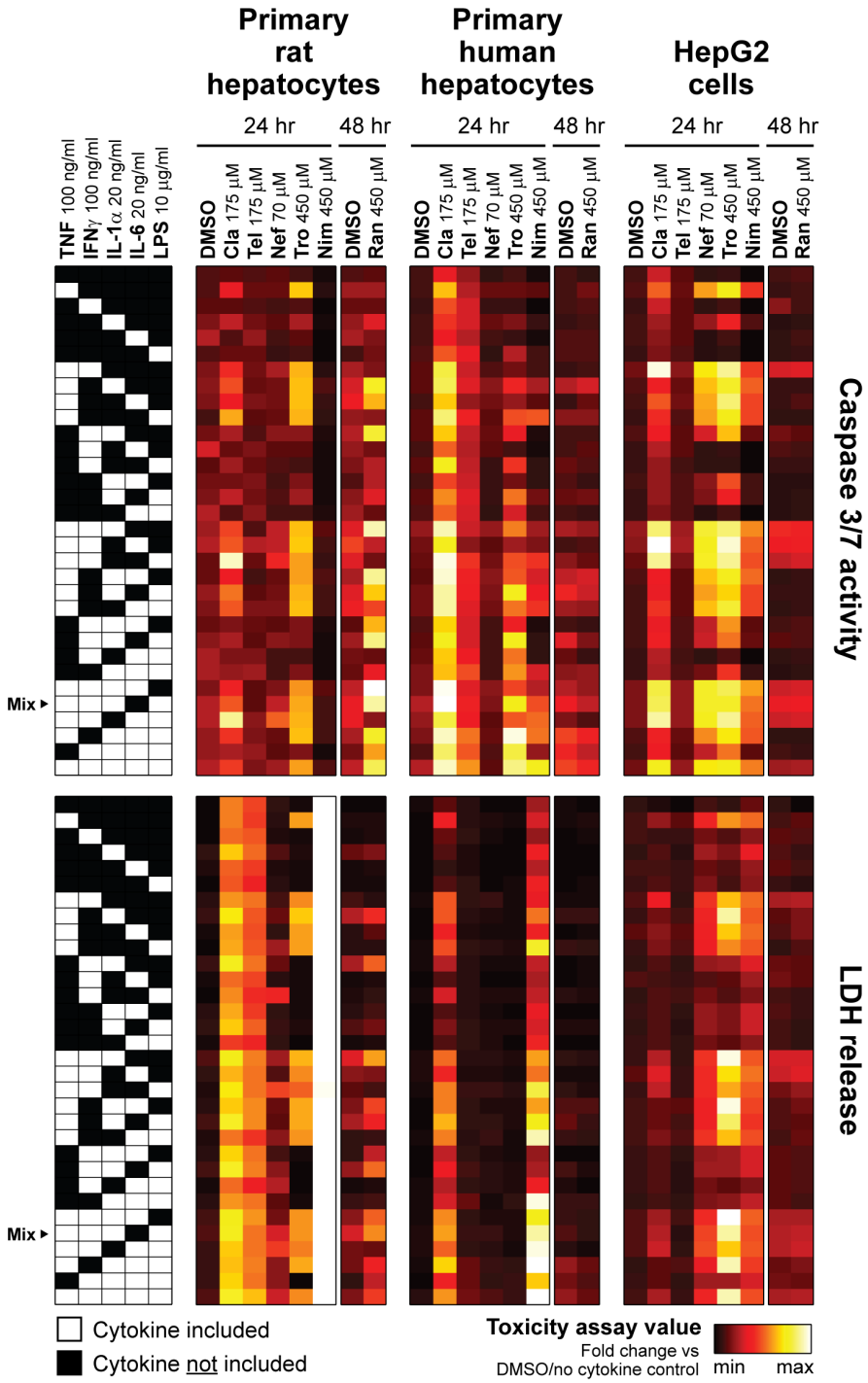

Figure 3-3. A drug- and cytokine mix-induced hepatotoxicity data compendium. Primary rat hepatocytes (left), primary human hepatocytes (center), and HepG2 cells (right) were cultured, treated, and assayed for caspase 3/7 activity (top) or LDH release (bottom) at 24 or 48 hours post-treatment as described in Chapter 3.2. Caspase 3/7 activity and LDH release values were both fold-change normalized to DMSO/no cytokine samples from the same cell system. Mean toxicity assay values of three to six biological samples are plotted in the heatmaps using linear color-scales indexed separately to the minimum and maximum observed value for each combination of cell system and assay type. The cytokine mix (TNF, IFNγ, IL-1α, and LPS) used in Figure 3-1 is noted as "Mix". Abbreviations: Cla, clarithromycin; Tel, telithromycin; Nef, nefazodone; Tro, trovafloxacin; Nim, nimesulide; Ran, ranitidine.

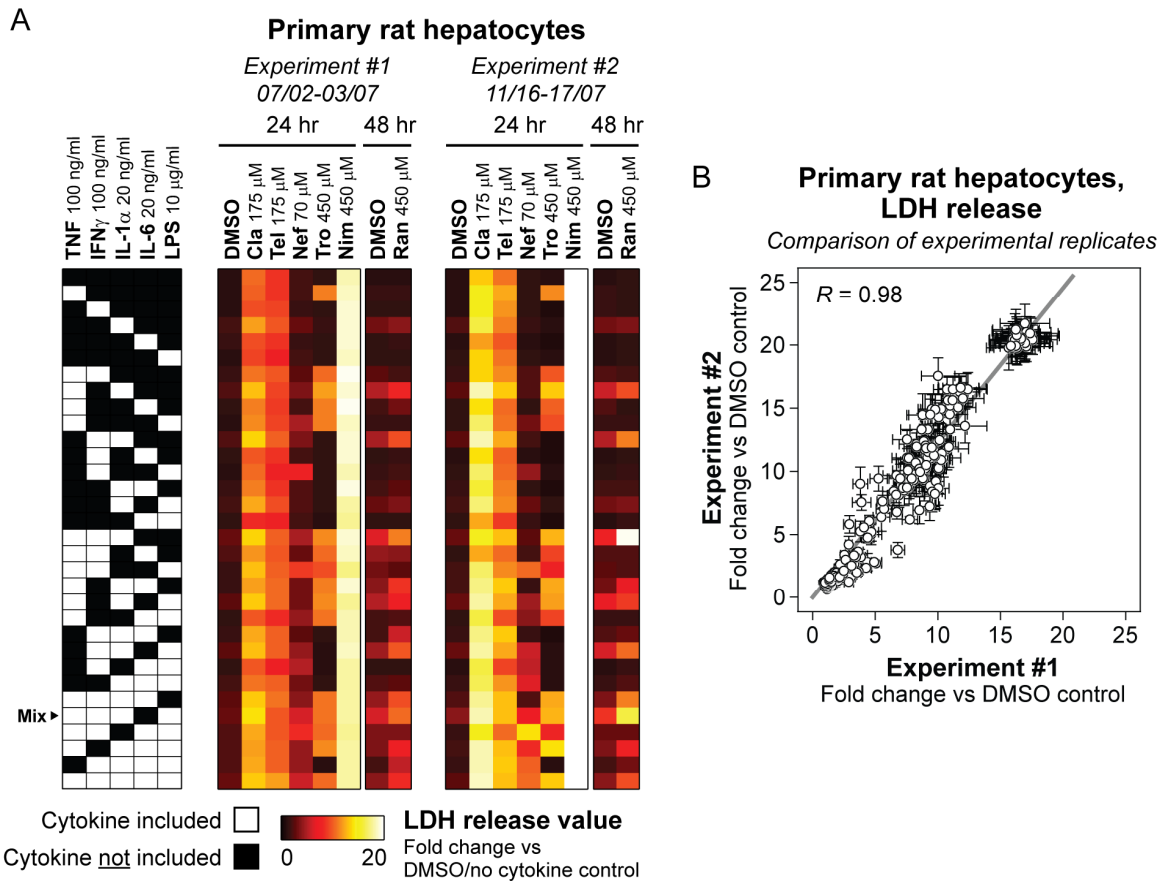

Figure 3-4. Evaluation of reproducibility in collection of drug-cytokine mix hepatotoxicity data compendium in primary rat hepatocytes. From two separate rat liver cell isolations conducted on different days, primary rat hepatocytes were cultured, treated with multiple drug and cytokine co-treatments, and assayed for LDH release (24 or 48 hours post-treatment) as described in Chapter 3.2. LDH release values were fold-change normalized to DMSO/no cytokine samples at the same time-point from the same isolation. (A) Mean LDH release assay values, of three to six biological samples per condition, from each individual drug-cytokine data compendium experiment are plotted in heatmaps. (B) LDH release assay values from the two compendium collections are plotted as mean ± SEM. Across all conditions, these two experiments had a Pearson correlation coefficient (*R*) of 0.98. Abbreviations: Cla, clarithromycin; Tel, telithromycin; Nef, nefazodone; Tro, trovafloxacin; Nim, nimesulide; Ran, ranitidine.

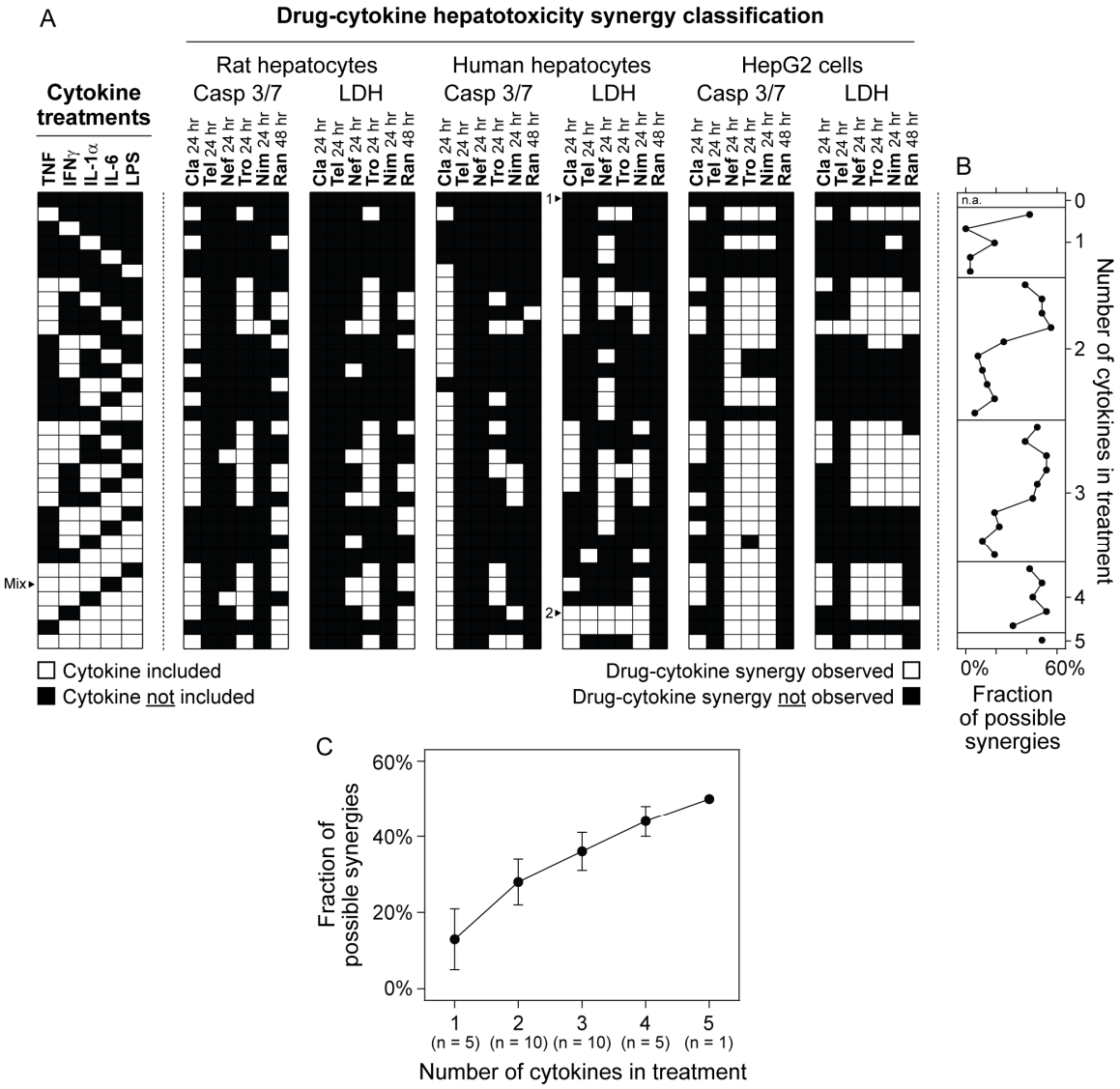

Figure 3-5. Drug-cytokine mix supra-additive synergy classifications in combinatorial treatment compendium. The drug-cytokine mix hepatotoxicity compendium (see Figure 3-3 for experimental details) was analyzed to identify cytokine mix co-treatment conditions that demonstrated supra-additive hepatotoxicity synergy for each drug in each combination of cell system (primary rat hepatocytes, primary human hepatocytes, and HepG2 cells) and toxicity assay (caspase 3/7 activity and LDH release). Drug-cytokine mix supra-additive synergy was assessed by comparing the observed drug-cytokine mix co-treatment result and an additive projection of the drug-only and cytokine mix-only results. (A) Discretized synergy classifications. All conditions which demonstrated supra-additive synergy with a statistical significance of $P < 0.026$ in a false discovery rate-corrected Student's t test are presented in white. The cytokine mix (TNF, IFNγ, IL-1α, and LPS) used in Figure 3-1 is noted as "Mix". Conditions used for the large-scale primary human hepatocyte toxicity study (assayed by LDH release; see Figure 3-9) are noted: (1) no cytokines and (2) TNF, IL-1α, IL-6, and LPS. (B-C) Cytokine treatment synergy efficacy. (B) The fraction of observed synergies from possible synergies across all 32 combinations of cell system, toxicity assay, and drug co-treatment for each cytokine mix are presented. (C) The fraction of possible synergies are presented (mean ± SEM) grouped by number of cytokines in the treatment. Abbreviations: Cla, clarithromycin; Tel, telithromycin; Nef, nefazodone; Tro, trovafloxacin; Nim, nimesulide; Ran, ranitidine; n.a., not applicable.

3.3.3. Discretization of the drug-cytokine mix data compendium into synergistic toxicity conditions

From the first analysis approach, examining discretized drug-cytokine synergy classification (Figure 3-5), it is evident that higher-order (four- or five-factor) cytokine environments were more efficient at identifying possible drug synergies (~50% of possible synergies across combination of all cell systems and drugs) than were lower-order (one-, two-, or three-factor) environments (~15-35% of possible synergies). Of note, there are higher-order cytokine mixes other than the mix of TNF, IFNγ, IL-1α, and LPS (which was used in the initial study) that are more efficient at synergizing with these idiosyncratic drugs in human hepatocytes. This is in part due to the fact that the initial cytokine mix is mildly toxic by itself for human primary hepatocytes, limiting its ability to synergize with drug co-treatments in a supra-additive manner. Instead, slightly less-toxic five-factor mixes (in particular, the five-factor mixes that instead do not contain either TNF or IFNγ [the latter noted as "2" in Figure 3-5A]) are far more efficient at eliciting supra-additive hepatotoxicity synergies with these six idiosyncratic drugs in human hepatocytes, and therefore would likely serve as a more predictive cytokine environment for assessing drug-cytokine synergies in human hepatocytes.

3.3.4. Factorial analysis of drug-cytokine mix hepatotoxicity identifies TNF and IL-1α as key cytokine factors potentiating inflammation-associated idiosyncratic drug hepatotoxicity

We applied factorial analysis to the hepatotoxicity data compendium (which contained a full factorial design of $2^5 = 32$ cytokine combinations) to identify underlying cytokine effects potentiating drug-cytokine hepatotoxicity synergies across the entire landscape of cytokine environments. As applied here, factorial analysis calculates the effect of the addition or removal of component treatment "variables", each containing one-to-four cytokines and/or LPS, from all treatment conditions in which they are present or absent, and, as such, summarizes the average effect of each cytokine treatment "variable" within each data set in which it is applied [128]. Factorial analysis was applied separately to each combination of hepatocyte cell system, hepatotoxicity assay,

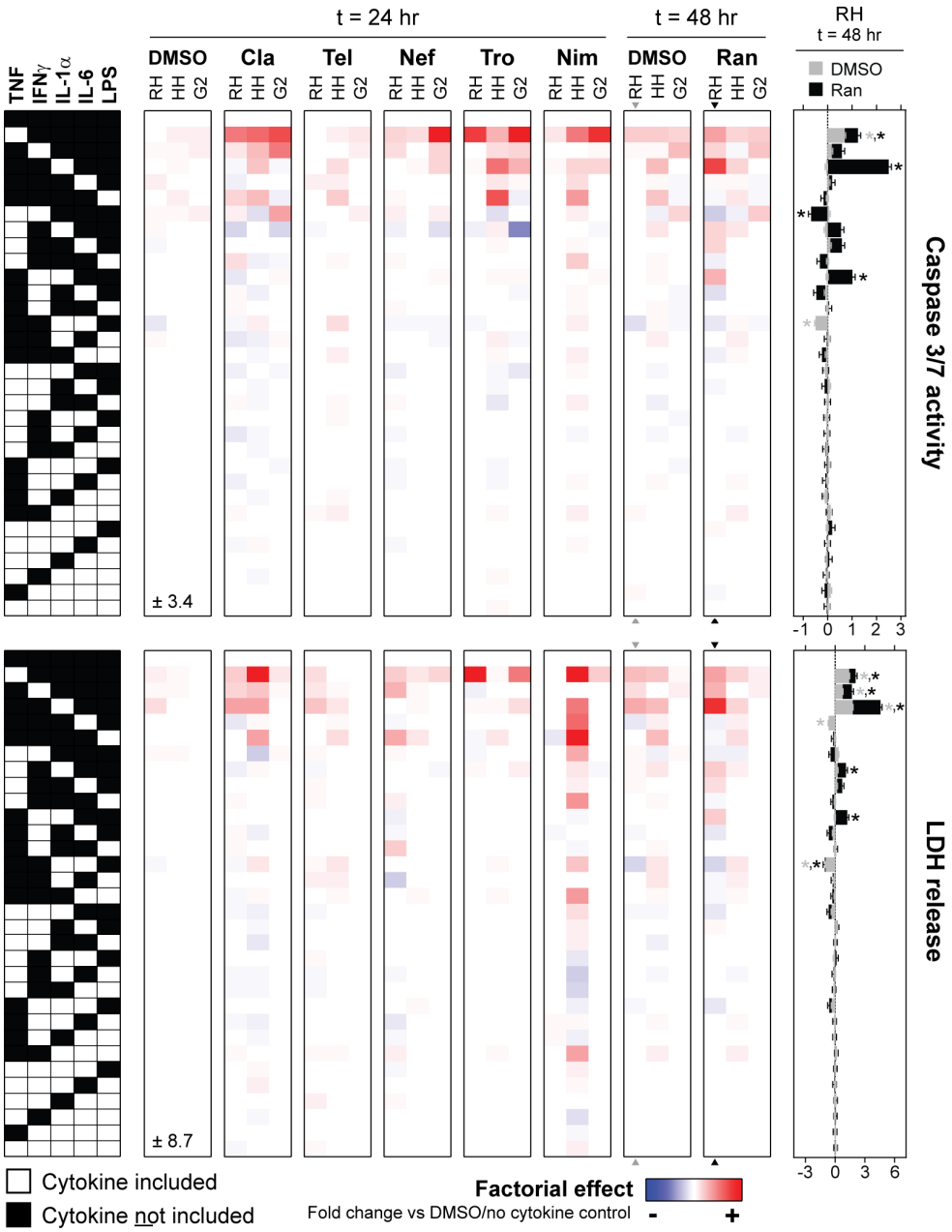

Figure 3-6. Factorial analysis of the drug-cytokine mix hepatotoxicity compendium. Each combination of cell system, toxicity assay type, and drug treatment from the drug-cytokine mix hepatotoxicity compendium (see Figure 3-3) was subjected to factorial analysis (see Chapter 3.2.6 for details). Factorial effects are plotted as heatmaps organized by assay type (top, caspase 3/7 activity; bottom, LDH release) and drug co-treatment to compare effects across cell systems (left) and as bar plots (with ± factorial error) for only DMSO control and ranitidine treatments in primary rat hepatocytes at 48 hours post-treatment (right). The factorial effect color-scales used in these heatmaps are indexed separately for each toxicity assay type to capture the full range of factorial effects in each assay type (±3.4 fold-change for the caspase v3/7 activity assay effects and ±8.7 fold-change for the LDH release assay effects). Statistical significance of each effect was assessed by a false discovery rate-corrected one-sample, two-tailed *t* test. In the bar plots, factorial effects are labeled as significant (*) if $P < 0.026$. Abbreviations: Cla, clarithromycin; Tel, telithromycin; Nef, nefazodone; Tro, trovafloxacin; Nim, nimesulide; Ran, ranitidine; RH, primary rat hepatocytes; HH, primary human hepatocytes; G2, HepG2 cells.

and idiosyncratic drug co-treatment, and factorial effects were interpreted by comparing the calculated effects between drug and DMSO control treatments for each combination of cell system and assay type (Figure 3-6).

Across all three hepatocytic cell types, higher-order factorial effects (those containing more than two cytokine variables) are generally modest, indicating that there is minimal cytokine-cytokine synergy in these multi-cytokine treatment environments. Instead, one- and two-cytokine factorial effects dominate the observed drug- and cytokine mix-induced hepatotoxicities, with the most significant effects arising from the single-cytokine treatment variables of TNF and, to a lesser extent, IL-1α and LPS. LPS yielded significant factorial effects predominantly in human hepatocytes. Some drugs appear to potentiate hepatotoxicity synergy with cytokines by amplifying the effects of the cytokines alone, and thus magnifying but not altering the pattern of the factorial effects (compare DMSO control to clarithromycin in human hepatocytes). By contrast, other drugs dramatically altered the pattern of cytokine synergies and their calculated factorial effects (compare DMSO control to telithromycin in human hepatocytes). Whereas some drugs (*e.g.* clarithromycin) had very similar patterns of factorial effects across all three cell types, drugs such as trovafloxacin had dramatically altered patterns of factorial effects among them, indicating a significant degree of cell type-specificity in certain drug-cytokine hepatotoxicity responses. This high degree of cell type-specificity to particular cytokine effects is in agreement our recent findings that primary human hepatocytes and HepG2 cells, in response to numerous inflammatory cytokine treatments, utilize dramatically different intracellular signaling mechanisms and secrete different patterns of cytokines and chemokines [134].

In LPS-administered rodent models, the induction of hepatotoxicity upon both ranitidine and trovafloxacin treatment has been shown to be partially dependent on TNF [35, 37]. In concordance with those reports, we observed that TNF contributed a significant factorial effect in potentiating the toxicity of both ranitidine and trovafloxacin in rat hepatocytes (Figure 3-6). It should be noted that the treatment of TNF alone did result in the induction of supra-additive hepatotoxicity synergy in trovafloxacin- but not ranitidine-treated rat hepatocytes (Figure 3-5), indicating that higher-order combinations of TNF with other cytokine co-treatments were necessary to potentiate TNF's

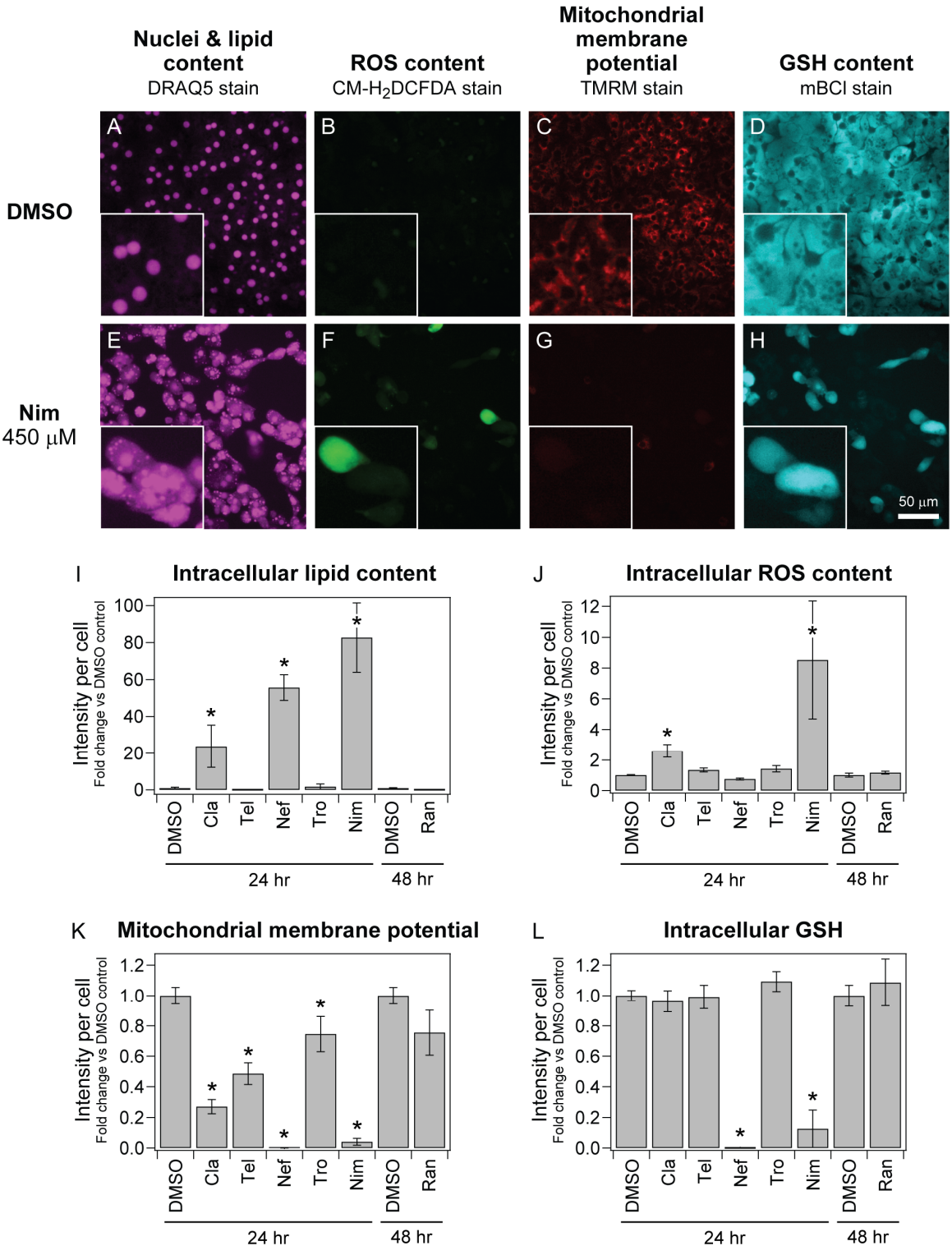

Figure 3-7. Quantitative imaging assays of drug-induced sub-lethal hepatotoxicities. Primary human hepatocytes were cultured and treated with drugs (but no cytokines) as described in Chapter 3.2. The following drug doses were used: 175 μM Cla, 175 μM Tel, 70 μM Nef, 175 μM Tro, 450 μM Nim, and 450 μM Ran. At 24 or 48 hours post-treatment, cells were stained with multiple fluorescence probes and imaged on a four-color, live-cell Cellomics instrument (see Chapter 3.2.5 for additional details). Representative

images from DMSO control wells (A-D) and nimesulide treatment (E-H) are shown for: DRAQ5 stain (nuclei and lipid content; A,E), CM-H_2DCFDA probe (ROS content; B,F), TMRM stain (mitochondrial membrane potential; C,G), and mBCl stain (GSH content; D,H). Image insets are 2.5× magnified from the remainder of the image. Quantitative image analysis was performed as described in Chapter 3.2.5. Intensity of each stain was normalized to the number of nuclei counted in each sample then fold-change normalized to the DMSO/no cytokine control samples at 24 hr post-treatment. Increases in intracellular lipid (I) and ROS (J) content and decreases in mitochondrial membrane potential (K) and intracellular GSH (L) are indicative of sub-lethal hepatotoxicity. In panels (I) to (L), data are presented as mean ± SEM of five biological samples. Treatments significantly different from the DMSO control at the same time point are labeled as significant (*) if $P < 0.05$ by a Student's t test. Abbreviations: Cla, clarithromycin; Tel, telithromycin; Nef, nefazodone; Tro, trovafloxacin; Nim, nimesulide; Ran, ranitidine; ROS, reactive oxygen species; GSH, glutathione.

synergizing effect, as elucidated by factorial analysis, with ranitidine in rat hepatocytes.

3.3.5. Clustering of the drug-cytokine mix hepatotoxicity compendium identifies correlations between drug-cytokine mix hepatocellular death synergies and drug-induced sub-lethal hepatocyte injuries

Factorial analysis of the hepatotoxicity data compendium suggested a significant degree of variability in cytokine factors potentiating idiosyncratic drug hepatotoxicity synergies in different drug backgrounds and cell systems. To further assess these differences, we fused the hepatotoxicity data compendium into a single data matrix of 192 "experimental" conditions (comprised of all combinations of three cell systems, two assay types, and five cytokine/LPS treatment variables) by eight "drug" conditions (six idiosyncratic drugs and two DMSO controls). This hepatotoxicity data matrix was subjected to two-way hierarchical clustering using a Pearson correlation metric to group similar patterns of drug-cytokine synergies across both the 192 experimental conditions and the 8 drug or DMSO backgrounds (Figure 3-8).

Pearson clustering yielded the most distinct separation with respect to assay readouts due to the fact that they are poorly correlated ($R = 0.18$) across the entire data set. A second notable grouping was that of the different cell types, with large sections of each assay type cluster consisting solely of the conditions from each cell system, showing that there was little overlap between the three hepatocyte cell systems. Within the LDH data cluster, human hepatocytes clustered closer to rat hepatocytes, but within the caspase data cluster, human hepatocytes clustered closer to HepG2 cells, suggesting that neither rat hepatocytes nor HepG2 cells were distinctly better correlated with human hepatocytes

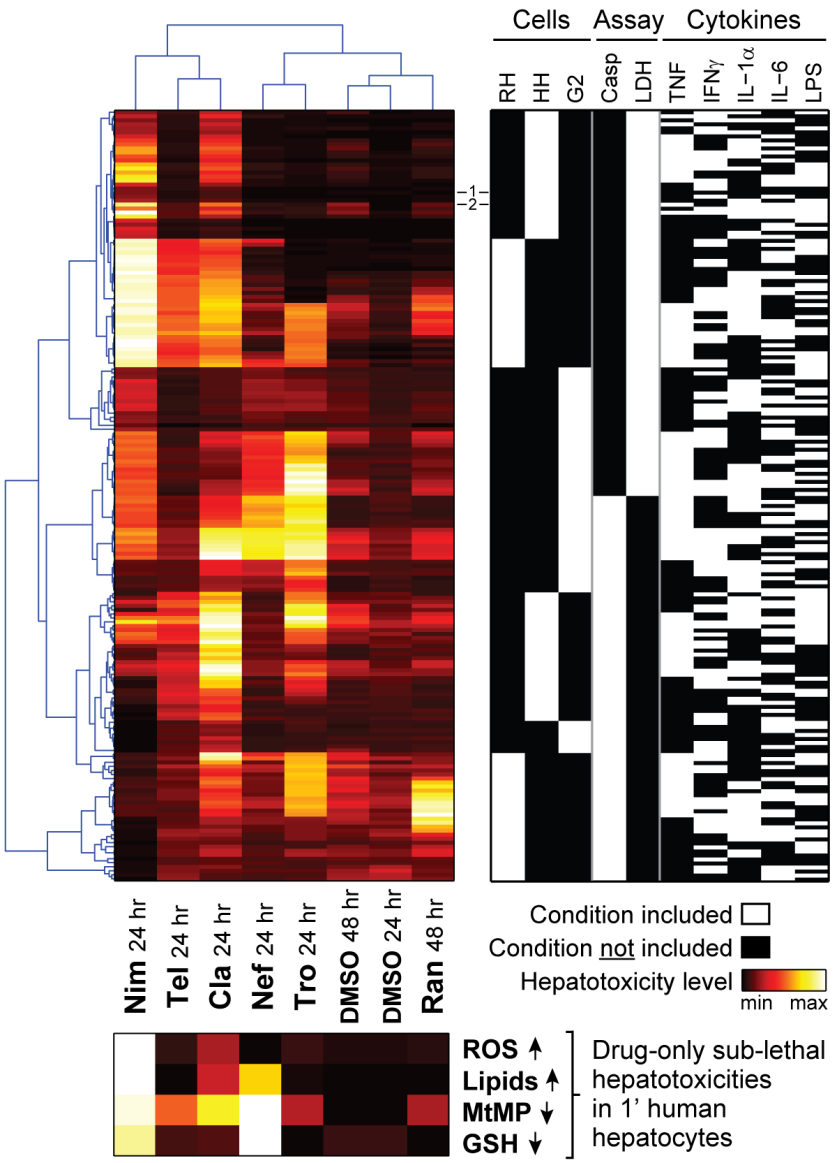

Figure 3-8. Hierarchical clustering of the drug-cytokine mix hepatotoxicity compendium allows comparison of drug- and cytokine-induced hepatotoxicities between different cell systems and with sub-lethal hepatotoxicities in human hepatocytes. The drug-cytokine mix combinatorial hepatotoxicity compendium was fused across all cell systems and assay types into a single data matrix, which was then subjected to two-way Pearson clustering (top left; see Chapter 3.2.7 for additional details). First, this clustering was used to re-sort a matrix of 192 "experimental" conditions, comprised of combinations of three cell systems, two assay types, and five cytokine treatment variables (top right). Second, this clustering was used re-sort to a sub-lethal hepatotoxicity data matrix of eight drug conditions and four drug (only)-induced sub-lethal hepatotoxicities (bottom). The sub-lethal hepatotoxicities (measured by quantitative imaging in primary human hepatocytes; see Figure 3-7) are plotted in the bottom heatmap using linear color-scales indexed separately to the minimum and maximum observed toxicity value for each assay type. (Note that the MtMP and GSH assay scales are inverted compared to Figures 3-7K-L.) Conditions used for the large-scale primary human hepatocyte toxicity study (assayed by LDH release; see Figure 3-9) are noted: (1) no cytokines and (2) TNF, IL-1α, IL-6, and LPS. Abbreviations: RH, primary rat hepatocytes; HH, primary human hepatocytes; G2, HepG2 cells; Cla, clarithromycin; Tel, telithromycin; Nef, nefazodone; Tro, trovafloxacin; Nim, nimesulide; Ran, ranitidine; ROS, reactive oxygen species; MtMP, mitochondrial membrane potential; GSH, glutathione.

in this drug-cytokine data compendium. This indicated it would be difficult to make accurate predictions of drug- and cytokine-induced hepatotoxicities in primary human hepatocytes (generally considered as the most predictive cell culture system for evaluating acute human hepatotoxicity [123, 135]) from primary rat hepatocyte and/or HepG2 data, especially when the comparison is dependent on only a few cytokine treatment conditions.

It has been hypothesized that a conserved mechanism of inflammation-associated idiosyncratic toxicity is that sub-lethal hepatocellular injuries (*e.g.* oxidative stress, GSH depletion) induced by idiosyncratic drugs and/or their metabolites sensitize hepatocytes to undergo cytokine-stimulated cell death [27]. To investigate this hypothesis for the six idiosyncratic drugs in this study, we examined the correlations between the patterns of drug-cytokine mix lethal hepatotoxicities across all cell systems and assay types and a set of four drug-induced sub-lethal hepatocyte injury measurements. Drug-induced sub-lethal hepatocyte injuries were measured in human hepatocytes, in the absence of any cytokines, using a high-throughput live-cell microscopy approach [126], which quantifies lipid content, reactive oxygen species (ROS), mitochondrial membrane potential (MtMP), and glutathione (GSH) depletion (see Figure 3-7). Nimesulide induced a substantial ROS and lipid accumulation and depletion of both MtMP and GSH, in concordance with previous reports that it can induce oxidative stress and mitochondrial injury in hepatocytes [136]. Clarithromycin induced mild ROS and lipid accumulation and mild MtMP depletion. Nefazodone induced mild lipid accumulation and substantial MtMP and GSH depletion, in concordance with previous reports that it depletes GSH and causes mitochondrial injury in hepatocytes [137, 138]. Telithromycin and trovafloxacin induced mild depletions of MtMP.

Pearson clustering with regards to the idiosyncratic drugs yielded three groups of drug/DMSO backgrounds. One group contained the DMSO controls and ranitidine, which induced only mild MtMP depletion in the sub-lethal assays. A second group contained nefazodone and trovafloxacin, and a third group contained nimesulide, telithromycin, and clarithromycin. The sub-lethal injuries induced by the second group of drugs are largely MtMP and GSH depletion and notably absent of ROS accumulation, whereas the third group of drugs similarly induced MtMP depletion but notably induced

ROS accumulation. While these correlations are not statistically verifiable due to the limited number of drugs and sub-lethal injuries assayed, these comparisons nonetheless strongly suggest that drugs that induce similar sub-lethal injuries also make hepatocytes susceptible to the induction of apoptosis by similar combinations of cytokine treatments.

3.3.6. Large-scale screen in primary human hepatocytes demonstrates predictive utility of cytokine co-treatment synergy model as a tool for identifying idiosyncratic hepatotoxic drugs

To test the drug-cytokine mix hepatotoxicity synergy model as a tool for predicting inflammation-associated idiosyncratic drug hepatotoxicity, we assayed drug-cytokine mix synergy for 90 drugs in human hepatocytes. This set of 90 drugs included 53 hepatotoxic drugs from DILI classes P1, O1, and P2 and 36 non-hepatotoxic drugs from DILI classes O2, N3, N2, and N1 (see Tables 3-1 and 3-3 for additional details). DILI class P2 is substantially comprised of drugs with idiosyncratic hepatotoxicities in humans and therefore assumed for analysis purposes here and previously [126] to represent idiosyncratic drugs. The non-hepatotoxic group (DILI O2, N3-N1) is used to provide corresponding non-toxic control compounds, although we note that the idiosyncratic drugs clarithromycin and ranitidine used in the initial study here are in DILI classes N1 and N3, respectively. In this ninety drug screen, comparisons were made by examining the differences between the idiosyncratic group (DILI P2) and the non-hepatotoxic group (DILI O2, N3-N1) as not all idiosyncratic drugs could be individually paired with "comparison" control drugs. This has the effect of neglecting the idiosyncratic hepatotoxicity signature of drugs such as ranitidine in order to provide a simplified comparison.

Due to practical limitations in conducting medium-to-high-throughput screens in primary human hepatocytes, we assessed drug-cytokine mix synergy only for a single cytokine mix (TNF, IL-1α, IL-6, and LPS), which was equally effective at inducing hepatotoxicity synergies across the six idiosyncratic drugs as the full set of cytokine mixes in the initial drug-cytokine mix data compendium (see Figure 3-5A, mix noted as "2"). Human hepatocytes were treated with one of 90 drugs, each dosed between 0 and 150 μM, in the presence or absence of TNF, IL-1α, IL-6, and LPS and assayed for LDH

Table 3-3. Drugs used in the large-scale human hepatocyte study.

Drug name	DILI category	C_{max} (μM)	Drug name	DILI category	C_{max} (μM)
Acetaminophen	P1	75.1	Nimodipine	P2	0.13
Benzbromarone	P1	5.79	Fluvoxamine	P2	0.12
Didanosine	P1	4.43	Bumetanide	P2	0.11
Demeclocycline HCl	P1	3.89	Nortriptyline HCl	P2	0.10
Azathioprine	P1	3.19	Mebendazole	P2	0.09
Amiodarone	P1	1.86	Busulphan	P2	0.07
Retinoic acid	P1	1.13	Estrone	P2	0.02
Albendazole	P1	0.91	Norgestrel	P2	0.01
Danazol	P1	0.03	Aspirin	O2	8.72
Menadione	O1	102	Tacrine	O2	0.04
Cyclophosphamide	P2	247	Levofloxacin	N3	12.9
Nimesulide	P2	20.5	Erythromycin	N3	8.84
Fluconazole	P2	17.7	Cimetidine	N3	6.03
Bromfenac	P2	16.4	Ranitidine	N3	4.00
Lomefloxacin	P2	12.1	Pioglitazone	N3	3.48
Trovafloxacin	P2	11.9	Rosiglitazone	N3	1.43
Trazodone HCl	P2	11.0	Glyburide	N3	0.94
Phenacetin	P2	9.83	Bupropion HCl	N3	0.79
Diclofenac	P2	9.77	Benazepril	N3	0.54
Erythromycin estolate	P2	9.49	Amoxapine	N3	0.20
Quinine	P2	9.26	Famotidine	N3	0.18
Telithromycin	P2	7.30	Maprotiline	N3	0.18
Troglitazone	P2	5.27	Amitriptyline HCl	N3	0.11
Chlorzoxazone	P2	2.77	Paroxetine	N3	0.07
Captopril	P2	2.62	Fluoxetine	N3	0.04
Labetalol	P2	2.49	Colchicine	N3	0.01
Bepridil HCl	P2	2.34	Moxifloxacin	N2	6.39
Pyrimethamine	P2	2.29	Citalopram	N2	0.16
Diethylcarbamazine	P2	2.12	Bupivacaine	N2	0.14
Methotrexate	P2	1.50	Memantine	N2	0.06
Quinapril	P2	1.39	Phenelzine	N2	0.05
Nefazodone	P2	1.34	Clarithromycin	N1	3.34
Chlorpromazine	P2	1.11	Dexamethasone	N1	0.37
Riluzole	P2	1.07	Nadolol	N1	0.28
Tamoxifen	P2	1.06	Pindolol	N1	0.25
Hydrochlorothiazide	P2	0.95	Pyridostigmine bromide	N1	0.25
Mexiletine HCl	P2	0.88	Propranolol	N1	0.23
Methimazole	P2	0.86	Clotrimazole	N1	0.10
Nifedipine	P2	0.76	Promethazine HCl	N1	0.06
Flutamide	P2	0.40	Brompheniramine maleate	N1	0.05
Progesterone	P2	0.23	Nalmefene	N1	0.04
Spironolactone	P2	0.19	Oxybutynin HCl	N1	0.03
Nomifensine	P2	0.19	Loperamide HCl	N1	0.01
Nicardipine HCl	P2	0.16	Buspirone	N1	0.01
Clomipramine	P2	0.13	TPCA-1 (IKK inhibitor)	*n.a.*	unknown

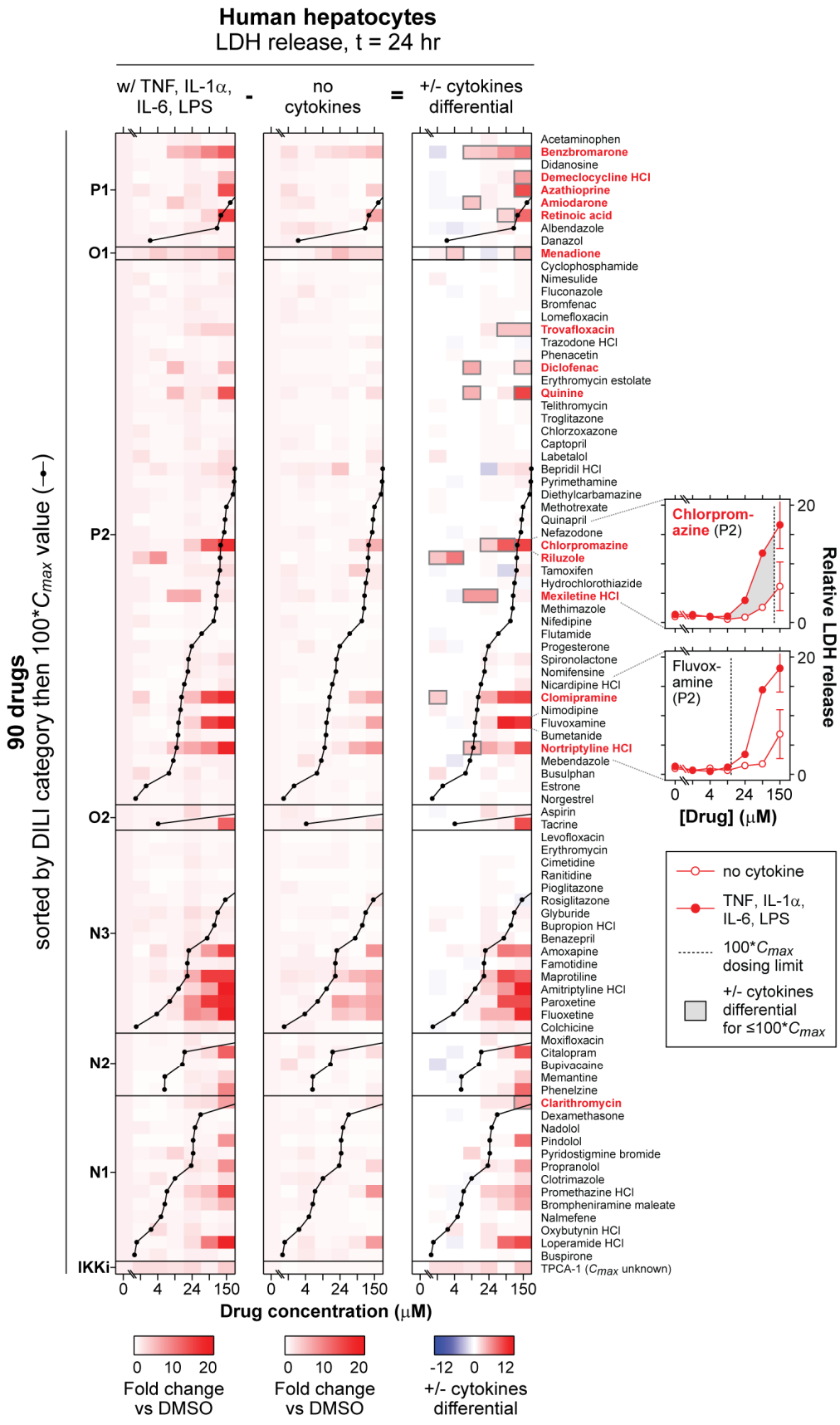
Human hepatocytes
LDH release, t = 24 hr
w/ TNF, IL-1α, IL-6, LPS
-
no cytokines
=
+/- cytokines differential
90 drugs
sorted by DILI category then 100*Cmax value (-•-)
P1
O1
P2
O2
N3
N2
N1
IKKi
Acetaminophen
Benzbromarone
Didanosine
Demeclocycline HCl
Azathioprine
Amiodarone
Retinoic acid
Albendazole
Danazol
Menadione
Cyclophosphamide
Nimesulide
Fluconazole
Bromfenac
Lomefloxacin
Trovafloxacin
Trazodone HCl
Phenacetin
Diclofenac
Erythromycin estolate
Quinine
Telithromycin
Troglitazone
Chlorzoxazone
Captopril
Labetalol
Bepridil HCl
Pyrimethamine
Diethylcarbamazine
Methotrexate
Quinapril
Nefazodone
Chlorpromazine
Riluzole
Tamoxifen
Hydrochlorothiazide
Mexiletine HCl
Methimazole
Nifedipine
Flutamide
Progesterone
Spironolactone
Nomifensine
Nicardipine HCl
Clomipramine
Nimodipine
Fluvoxamine
Bumetanide
Nortriptyline HCl
Mebendazole
Busulphan
Estrone
Norgestrel
Aspirin
Tacrine
Levofloxacin
Erythromycin
Cimetidine
Ranitidine
Pioglitazone
Rosiglitazone
Glyburide
Bupropion HCl
Benazepril
Amoxapine
Famotidine
Maprotiline
Amitriptyline HCl
Paroxetine
Fluoxetine
Colchicine
Moxifloxacin
Citalopram
Bupivacaine
Memantine
Phenelzine
Clarithromycin
Dexamethasone
Nadolol
Pindolol
Pyridostigmine bromide
Propranolol
Clotrimazole
Promethazine HCl
Brompheniramine maleate
Nalmefene
Oxybutynin HCl
Loperamide HCl
Buspirone
TPCA-1 (Cmax unknown)
0 4 24 150
Drug concentration (μM)
Chlorprom-azine (P2)
Fluvox-amine (P2)
20
0
Relative LDH release
0 4 24 150
[Drug] (μM)
no cytokine
TNF, IL-1α, IL-6, LPS
100*Cmax dosing limit
+/- cytokines differential for ≤100*Cmax
0 10 20
Fold change vs DMSO
0 10 20
Fold change vs DMSO
-12 0 12
+/- cytokines differential

Figure 3-9. (Previous page) Large-scale drug-cytokine mix hepatotoxicity study in primary human hepatocytes demonstrates utility of cytokine co-treatment approach for identifying idiosyncratic hepatotoxic drugs. Primary human hepatocytes were cultured, treated, and assayed for LDH release (at 24 hours post-treatment) as described in Chapter 3.2. Ninety drugs (see Table 3-3) were each dosed at seven non-zero concentrations (2.5× serial dilutions from a high concentration of 150 μM) in the presence (left) or absence (middle) of a cytokine mix containing TNF, IL-1α, IL-6, and LPS. The differential between + and - cytokine mix co-treatment for each drug dose was calculated and plotted (right). Note that DILI classes P1, O1, and P2 are hepatotoxic, with DILI class P2 is substantially comprised of drugs with idiosyncratic hepatotoxicities in humans, and DILI classes O2, N3, N2, and N1 are not or minimally hepatotoxic (see Table 3-1). Within each DILI class, drugs are sorted in order of 100*C_{max} value (a physiologically relevant dosing limit). Drug 100*C_{max} values are plotted in an overlayed line plot, with values exceeding 150 μM not shown. Individual drug doses that exhibited supra-additive drug-cytokine mix synergy (see Chapter 3.2.8 and Table 3-4) at concentrations less than their drug's 100*C_{max} limit are highlighted with gray boxes. Drugs with one or more dose exhibiting drug-cytokine mix supra-additive toxicity synergy at less than their 100*C_{max} concentration are listed in red font. A representative DILI P2 drug (chlorpromazine) displaying drug-cytokine mix synergy at dosing concentrations less than 100*C_{max} is shown in the expanded plot at the bottom right (data presented mean ± SEM of two biological samples). TPCA-1, a small molecule IKK inhibitor (IKKi), was used (at ten-fold lower concentrations than are noted by the axis labels for the other drugs) as a positive control for drug-cytokine mix synergy, as inhibition of pro-survival IKK–NF-κB signaling sensitizes hepatocytes to apoptosis induced by TNF [139], but is not labeled in red as its C_{max} is unknown.

release at 24 hr post-treatment (Figure 3-9). Supra-additive drug-cytokine synergy was assessed with regards to two different methods of defining a physiologically relevant dosing limit: (i) using each drug's own 100*C_{max} concentration, or (ii) using multiples (33× or 100×) of the median C_{max} concentration for all drugs in this study (0.91 μM) as an general estimate of physiological exposure limit, which may be a necessary approximation if clinical human pharmacokinetic data is unavailable. For doses less than each drug's own 100*C_{max} concentration, drug-cytokine mix synergy was observed for the P1 compounds benzbromarone, demeclocycline, azathioprine, amiodarone, retinoic acid; the O1 compound menadione; the P2 compounds trovafloxacin, diclofenac, quinine, chlorpromazine, riluzole, mexiletine, clomipramine, nortriptyline; and the N1 compound clarithromycin (which has reported idiosyncratic hepatotoxicity in humans [31, 132] and was used as a test idiosyncratic hepatotoxin in the initial study here). Among these cytokine mix synergy compounds, three of the six overtly hepatotoxic drugs (P1 compounds benzbromarone and azathioprine and the O1 compound menadione) and two of the eight idiosyncratic hepatotoxic drugs (P2 compounds quinine and chlorpromazine) also induced significant drug-only hepatotoxicity at doses less than each drug's own 100*C_{max} concentration (Figure 3-9). In this data set, drug-only hepatotoxicity was defined as greater than two-fold increase in LDH release. Using this approach to

Table 3-4. Drug-cytokine hepatotoxicity synergies in the large-scale human hepatocyte toxicity study evaluated by DILI class and physiological dosing limit.

Drug hepatotoxicity classification by DILI categories[1]	N	Drugs with one or more dose with cytokine synergy within the applied physiological dosing limit[2]			
		Using each drug's C_{max} value		Using the median C_{max} value	
		100*C_{max}	33*C_{max}	100*C_{max}	33*C_{max}
Idiosyncratic hepatotoxic (DILI P2)	43	8 (19%)	7 (16%)	9 (21%)	7 (16%)
Not or minimally hepatotoxic (DILI O2, N3-N1)	36	1 (3%)	0 (0%)	7 (19%)	0 (0%)
Hypergeometric test *P*-value[3]		0.028	0.011	0.55	0.011

[1]DILI categories are described in Table 3-1.
[2]Hepatotoxicity in this large-scale primary human hepatocyte study was assayed by LDH release (see Figure 3-9). Drug-cytokine synergies that were at least two-fold (with respect to the LDH release, reported as fold-change compared to the DMSO/no cytokine control condition) greater than the calculated supra-additive synergy threshold were characterized as synergistic. This "rule-of-thumb" threshold was used instead of a supra-additive Student's *t* test (see Chapter 3.2.8 and Figure 3-2) as two or three biological samples per condition were used due to the screening nature of this large-scale study, thus limiting the ability to satisfy statistical significance tests. Drug-cytokine synergy was assessed with regards to two different methods of defining a physiologically relevant dosing limit: (i) using each drug's own 33*C_{max} or 100*C_{max} concentration, or (ii) using the median 33*C_{max} (30 μM) or 100*C_{max} (91 μM) concentration for all drugs in this study (as an general estimate of physiological exposure limit). If a drug demonstrated cytokine synergy at one or more dosing concentration within the physiological dosing limit applied, it was included in the aggregate for its hepatotoxicity class. See Figure 3-9 for a list (those drugs in red font) of the drugs that satisfied synergy condition using each drug's 100*C_{max} concentration limit.
[3]The statistical significance of the observed number of synergistic drugs in the idiosyncratic hepatotoxic class was assessed using a hypergeometric test with a null hypothesis that synergistic drugs would not preferentially populate either of the hepatotoxicity groupings.

physiological concentration limit, a significantly larger fraction of the idiosyncratic hepatotoxic drugs (8 of 43 = 19%) demonstrated hepatotoxicity synergy with the cytokine mix than did the non-hepatotoxic drugs (1 of 36 = 3%; see Table 3-4). In contrast, using 100-fold the median C_{max} concentration (91 μM) as an general estimate of physiologically relevant dosing limit, the idiosyncratic hepatotoxic drugs (9 of 43 = 21%) did not elicit more frequent hepatotoxicity synergy then the non-hepatotoxic drugs (7 of 36 = 19%). But in using 33-fold the median C_{max} concentration (30 μM), the idiosyncratic hepatotoxic drugs (7 of 43 = 16%) did elicit more frequent hepatotoxicity synergy then the non-hepatotoxic drugs (0 of 36 = 0%).

This demonstrates that synergistic induction of hepatotoxicity with a cytokine mix, even when limited to a single hepatocyte cell system and cytokine mix, can be utilized as a predictive tool for evaluating inflammation-associated idiosyncratic drug hepatotoxicity. As implemented here, optimized prediction requires knowledge of the drug's C_{max} value, which necessitates human clinical pharmacokinetic data, but a reduced set of idiosyncrasies can be predicted with a more conservative estimate of liver exposure ($33*C_{max}$ rather than $100*C_{max}$) based on a generalized C_{max} estimate calculated from many drugs. Moreover, idiosyncratic hepatotoxic drugs (P2 compounds) largely induce drug-cytokine mix synergies in the absence of drug-only hepatotoxicities, which are more often evident for synergizing drugs that associated with overt hepatotoxicity (P1 and O1 compounds). This dependency on C_{max} to optimally calibrate the drug-cytokine mix synergy model to distinguish between drugs with idiosyncratic hepatotoxicity and those with either no or overt hepatotoxicity is in concert with Paracelsus' concept that "exposure makes a poison".

3.4. Discussion

3.4.1. *In vitro* drug-cytokine mix synergy as a model for inflammation-associated idiosyncratic drug hepatotoxicity

Hepatotoxicity is a major cause of failures in both the clinical and post-approval stages of drug development and thus represents a major challenge for the pharmaceutical industry [140, 141]. Furthermore, drug hepatotoxicity represents a serious public health problem, as it is the leading cause of acute liver failure in the United States [142]. Idiosyncratic drug hepatotoxicity -- a hepatotoxicity subset that occurs in a very small fraction of human patients (~1 in 10,000) and accounts for ~10% of acute liver failure cases -- is poorly predicted by standard preclinical models and in clinical trials and frequently leads to post-approval drug failure [27]. Thus, the development and validation of novel preclinical tools that demonstrate successful prediction of idiosyncratic drug hepatotoxicity is a paramount need for the pharmaceutical industry and the public health. Recent findings in LPS-administered rodent models suggest that idiosyncratic drug hepatotoxicity can arise when mild drug-induced hepatocellular stresses synergize with

inflammatory cytokine signaling to elicit hepatocellular death, but these models lack sufficient throughput for preclinical hepatotoxicity screening [26, 27].

In this work, we develop and evaluate *in vitro* hepatocyte cell culture models of idiosyncratic drug hepatotoxicity, which are more suitable to the high-throughput demands of preclinical pharmaceutical screening. We demonstrate that numerous idiosyncratic hepatotoxic drugs, but not comparison non-toxic control compounds, synergistically induce death in multiple hepatocyte cell systems when co-administered with multi-cytokine mixes associated with LPS-induced liver inflammation (Figure 3-1). These drug-cytokine synergies, depending upon the cell system, appear to be both drug dose-independent (above some dose threshold; Figures 3-1A,B,G,H,I), matching the characteristic that idiosyncratic drug hepatotoxicity is poorly correlated with dose [27], and drug-dose dependent (Figures 3-1C,J), agreeing with a recently published report that certain idiosyncratic hepatotoxins can exhibit dose-dependent toxicity [143]. In primary rat and human hepatocyte cultures in particular, drug-cytokine mix synergies were most frequently observed for higher-order (containing four or five cytokines or LPS) cytokine mixes (Figure 3-5), whose hepatotoxicity was potentiated in a drug- and cell system-specific manner by the additive combination of the single-factor effects of TNF, IL-1α, and/or LPS (Figure 3-6). Potentiation of drug-cytokine synergy by TNF, IL-1α, and LPS, more so than by IFNγ or IL-6, suggests that intracellular signal transduction pathways that are similarly activated by these factors, namely IKK–NF-κB, p38, and JNK, are likely critical components of hepatocellular toxicity responses to idiosyncratic drug-inflammatory cytokine co-exposure.

3.4.2. Drug-induced sub-lethal injury as a sensitizing stress for drug-cytokine hepatocellular death synergy

Idiosyncratic hepatotoxins are hypothesized to induce a diversity of sub-lethal injuries that sensitize hepatocytes to inflammatory cytokine-induced cell death [27]. This hypothesis is supported by the demonstration that acetaminophen (APAP), at high doses, can elicit an idiosyncratic-like hepatotoxicity that is dependent on cytokine signaling as part of the innate immune response [27]. At high doses, accumulation of a cytochrome

P450-dependent APAP metabolite leads to depletion of GSH in hepatocytes, which is known to sensitize hepatocytes to TNF-induced apoptosis [39].

Here, we implemented hierarchical clustering of a drug-cytokine hepatotoxicity data compendium to identify if particular drug-induced sub-lethal injuries sensitize hepatocytes to specific combinations of cytokine-induced death (Figure 3-8). It was difficult to discern clear correlations between sub-lethal injuries (measured in human hepatocytes) and cytokine synergy patterns (across all three hepatocyte systems) for nimesulide, clarithromycin, and nefazodone due to the numerous sub-lethal hepatotoxicities induced by these drugs, and thus synergy correlations possibly reflect the convolution of multiple sub-lethal injury-cytokine synergy mechanisms. In contrast, the only sub-lethal injury induced by both telithromycin and trovafloxacin that was statistically significant was MtMP depletion (Figure 3-7). In human hepatocytes, telithromycin and trovafloxacin elicited markedly similar patterns of cytokine synergy as assayed by caspase 3/7 activity and represented through factorial analysis (Figure 3-6). For both drugs, cytokine synergy effects were evident, in decreasing magnitude, for LPS and IL-1α but not other treatment variables. This pattern of cytokine synergy effects was not shared by any other drugs at 24 hours post-treatment in human hepatocytes. This unique and specific sub-lethal injury-cytokine synergy relationship suggests that drug-induced mitochondrial injury may sensitize hepatocytes to apoptosis induced by LPS and IL-1α, as has been similarly hypothesized for alcoholic hepatitis-induced mitochondrial injury in hepatocytes [144].

3.4.3. Cytokine mix-specific hepatotoxicity synergizes suggest personalized administration of idiosyncratic hepatotoxic drugs

The cytokine mix-specific responses evident in the hepatotoxicity data compendium collected here (Figures 3-3 and 3-5) suggest that inflammation-associated idiosyncratic drug hepatotoxicities might be avoided by limiting drug treatments to patients that do not have plasma cytokine signatures (due to pre-existing inflammatory episodes, for example) corresponding to known synergizing inflammatory environments. Further investigation of drug-cytokine mix synergies over across greater number of drug compounds and cytokine environments, beyond those associated with LPS-induced

inflammation, would have to be conducted to more thoroughly capture the diversity of patient-specific drug-cytokine interactions in humans. This suggestion of "personalized" or "stratified" drug treatment [145] to avoid toxicity would likely be necessitated only for drugs for which comparably efficacious compounds are not available and could be combined with pharmaco-metabolonomic phenotyping approaches [146] to avoid both inflammation- and metabolism-associated idiosyncratic hepatotoxicities in a patient-specific manner.

3.4.4. Applying drug-cytokine hepatotoxicity synergy model to high-throughput pharmaceutical screening

In a ninety-drug screen in human hepatocytes, ~20% of idiosyncratic hepatotoxins (those compounds associated with DILI category P2; see Table 3-1) elicited hepatocellular death synergy with a cytokine mix compared to only 3% of non-hepatotoxic drugs when using each drug's 100*C_{max} concentration as a physiological dosing limit (Figure 3-9, Table 3-4). Using a generalized physiological dosing limit of 30 μM (based on 33-times the median C_{max} concentration across all drugs in the study), ~15% of idiosyncratic hepatotoxins and none of non-hepatotoxic drugs elicited synergy. This demonstrates that, given drug pharmacokinetic parameters to define a physiologically relevant dosing window (ideally individually defined for each drug), *in vitro* drug-cytokine hepatocellular death synergy can be utilized as a much-needed preclinical tool for assessing inflammation-associated idiosyncratic drug hepatotoxicity in a high-throughput manner. As conducted here, successful prediction of inflammation-associated idiosyncratic drug hepatotoxicity based on *in vitro* hepatocellular models depends on human pharmacokinetic data and would be most reasonably used within an iterative preclinical-clinical toxicity assessment paradigm. Furthermore, this work demonstrates the utility of a physiologically relevant drug dosing limit of 100*C_{max} as many non-hepatotoxic drugs synergistically induced human hepatocyte death at concentrations exceeding 100*C_{max} (see Figure 3-9). Hence the application of a 100*C_{max} limit was critical to obtain a low false-positive rate.

At least for a subset of six drugs, this study demonstrates that, in addition to human hepatocytes, both rat hepatocytes and HepG2 cells can be useful hepatocellular

systems for identifying idiosyncratic drug hepatotoxicities in humans. This unexpected success in using hepatocellular systems more amenable to high-throughput screening suggests that cytokine mix synergy screens may be implementable to the demands of preclinical drug evaluation. The utility of rat hepatocytes and HepG2 cells for screening inflammation-associated idiosyncratic drug hepatotoxicity will need to be evaluated for a greater diversity drug compounds to generate more confidence in their predictive ability. We also employed an information theoretic technique to identify a subset of ~15 cytokine co-treatment conditions that maintains the "information" contained in the full set of 32 cytokine conditions across the three hepatocytic cell types (B.D.C., B. M. King, B. Tidor, unpublished observations). Further, we showed that these "informative" condition sets can act as better training sets for predicting drug- and cytokine-induced hepatotoxicities in primary human hepatocytes from observations in primary rat hepatocytes and HepG2 cells (B.D.C., B.M.K., B.T., unpublished observations).

The *in vitro* cytokine synergy model developed herein and other complementary cell culture [126] and animal models [32, 34, 35] offer much-needed preclinical tools for the assessment and prediction of idiosyncratic drug hepatotoxicity. This cytokine synergy model would be most useful simply for its ability to identify likely idiosyncratic hepatotoxicity phenomenologies, although particular trends in cytokine mix synergy and identification of important cytokine factor effects can suggest the underlying mechanistic relationships between the drug-induced hepatocellular injuries and possible points of signal transduction convergence with inflammatory cytokine signaling. As such, screening drug-cytokine mix hepatotoxicity synergies in cell culture may allow for suggestion of more detailed follow-up experiments to parse the mechanisms of particular candidate idiosyncratic hepatotoxins to help guide drug compound development.

This work suggests numerous improvements in the further development of high-throughput cell culture models used to predict inflammation-associated idiosyncratic drug hepatotoxicity. In the large-scale screen conducted here (Figure 3-9), the limited number of cytokine synergies with idiosyncratic hepatotoxins (8 of 43 = 19%) was likely due to the use of only one cytokine environment and one hepatocyte cell system and the fact that not all DILI P2 drugs have idiosyncratic hepatotoxicities associated with inflammation. More accurate prediction of idiosyncratic drug hepatotoxicity could be obtained using a

multi-variate predictive model [126] calibrated from expanded measurements of drug-cytokine synergies at multiple doses (up to the 100*C_{max} limit) across multiple hepatocyte cell systems, additional cytokine environments, and/or toxicity assays. Additionally, hepatocyte cell culture models, such as three-dimensional microreactor cultures using primary rat hepatocytes, that better maintain hepatic drug metabolism and biliary transport characteristics over a chronic time-scale (more than 7 days) and are scalable to medium-throughput screening demands [8, 10] could be utilized to develop more physiologically relevant models of inflammation-associated idiosyncratic drug hepatotoxicity. These systems could better capture the mix of chronic and acute hepatocyte responses to drugs and inflammatory cytokines [26]. This is particularly motivated by the observation that ranitidine-cytokine mix synergy was delayed compared to other compounds and was only observed with high frequency in rat hepatocytes and not human hepatocytes or HepG2 cells (Figures 3-1 and 3-3). These observations suggest that a more prolonged mechanism, perhaps requiring significant accumulation of ranitidine metabolites that only occurs in the rat hepatocyte cultures, is necessary to potentiate ranitidine-cytokine hepatotoxicity synergy and therefore future screening would benefit from a hepatocyte cell culture system that maintains *in vivo*-like metabolism over a chronic time-scale.

Nonetheless, the work presented here validates the use of synergistic induction of hepatocellular death by idiosyncratic hepatotoxins and an inflammatory cytokine environment as a much-needed *in vitro* tool for predicting inflammation-associated idiosyncratic drug hepatotoxicity and provides a framework for further development of such *in vitro* models to capture a greater complexity of and to elucidate the mechanistic basis of inflammation-associated idiosyncratic drug hepatotoxicity.

CHAPTER 4

Signaling network modeling of drug- and cytokine-induced hepatotoxicity

4.1. Introduction

4.1.1. Signaling control of inflammatory cytokine-induced idiosyncratic drug hepatotoxicity.

Recent findings in animal [26, 27, 35, 37] and cell culture models (see Chapter 3 and [127]) suggest that a subset of idiosyncratic drug hepatotoxicities are caused by synergistic interactions with inflammatory cytokine signaling. These findings have led to the proposal of model that suggests idiosyncratic hepatotoxins induce mild hepatocellular stresses that synergize with cytokine signaling to elicit hepatocellular death in a context-specific manner [27], but there is little experimental evidence demonstrating the hepatocellular signaling mechanisms underlying this drug-cytokine synergy model.

Supporting this model is the example of acetaminophen (APAP), which, at high doses, can elicit an idiosyncratic-like hepatotoxicity that is dependent on cytokine signaling as part of the innate immune response [27]. At high doses, accumulation of a cytochrome P450-dependent APAP metabolite leads to depletion of glutathione (GSH) in hepatocytes, which is known to sensitize hepatocytes to TNF-induced apoptosis [39]. Recent findings suggest that APAP toxicity is controlled by JNK pathway signaling [147], but it is unclear how the hepatocyte signaling network integrates multiple survival, stress, and apoptosis signaling pathways to elicit a death response even for the well-studied case of APAP toxicity. Further complicating this model, most idiosyncratic hepatotoxins induce a diversity of hepatocellular stresses, ranging from GSH depletion to reactive oxygen species (ROS) accumulation to mitochondrial injury, with individual compounds inducing unique spectrums of these and other cellular stresses [126].

The inflammatory cytokines identified as potentiating inflammation-associated idiosyncratic drug hepatotoxicity (TNF, IL-1α, IFN-γ, IL-6, and LPS; see Chapter 3.1) stimulate a diversity of intracellular signaling pathways related to cell survival,

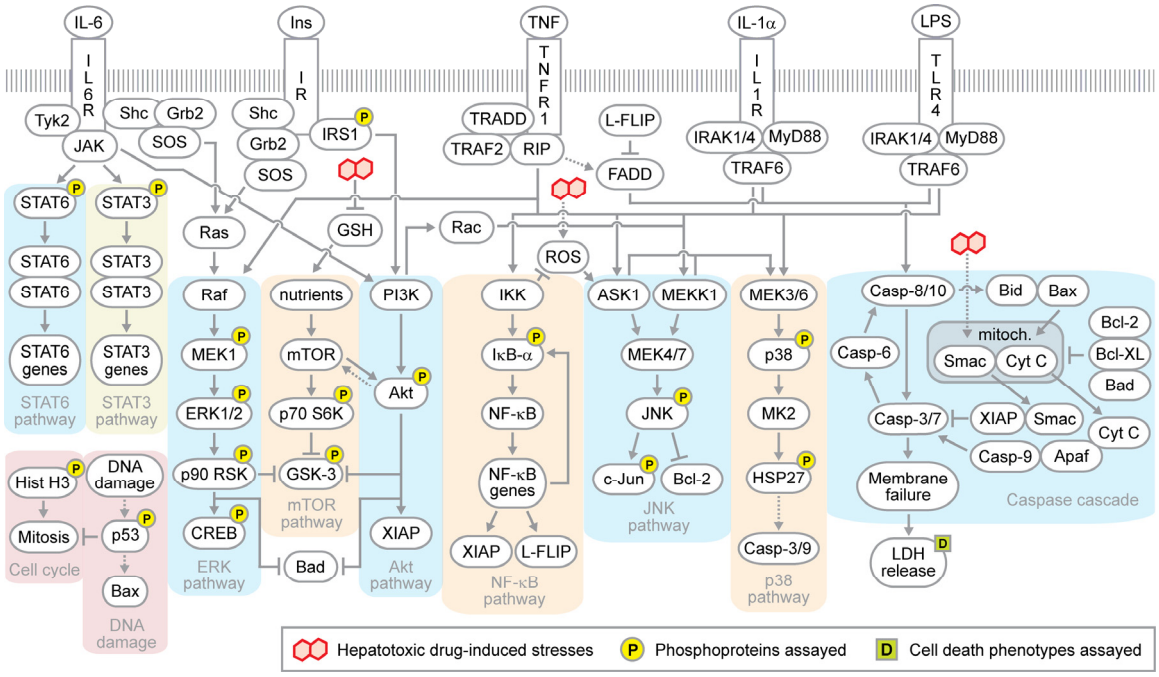

Figure 4-1. A schematic of the drug- and cytokine-induced hepatocellular death signaling network. Cytokines bind to their cognate receptors and activate shared downstream phosphoprotein signaling pathways regulating cell death. Drugs lead to various cellular stresses (*e.g.* ROS accumulation) that are integrated into stress-related phosphoprotein signaling (such as the JNK pathway) and mitochondrial control of apoptosis. Experimentally measured phosphoproteins and cell death phenotypes are indicated.

survival, stress, and apoptosis (reviewed in [35, 37, 76, 118-120]; see also Chapter 1-4 and Figure 4-1). Many of the complex signaling mechanisms activated by these individual cytokines are well-studied. For example, TNF activates numerous signaling pathways in hepatocytes including the MEK–ERK, IKK–NF-κB, JNK, and p38–HSP27 pathways and the caspase cascade (reviewed in [76, 148]), whose integrated activities specificity hepatocyte responses to TNF in a context-sensitive manner. Moreover, physiologically relevant growth factor co-stimuli such as insulin can provide activation of survival signaling pathways that antagonize cytokine-induced apoptosis [62, 77]. Similarly, drug-induced hepatocellular stresses can induce activation of many of the signaling pathways stimulated by inflammatory cytokine and/or growth factors. GSH depletion can perturb cellular nutrient levels, possibly leading to attenuation of mTOR signaling [149, 150], and can alter mitochondrial redox potentials, increasing susceptibility to mitochondria-mediated apoptosis [151]. ROS accumulation can activate the JNK and p38–HSP27 stress-response signaling pathways [76]. Clearly, investigation of the signaling mechanisms governing hepatocyte cell death responses to idiosyncratic

hepatotoxins and inflammatory cytokines requires a broad, network-level examination of multiple intracellular signaling pathways in a physiologically complex context.

4.1.2. Chapter overview

To gain greater mechanistic understanding of the signaling mechanisms regulating inflammatory cytokine-associated idiosyncratic drug hepatotoxicity, we collected a "cue-signal-response" (CSR) drug- and cytokine-induced hepatotoxicity data compendium in primary human hepatocytes. In this data compendium, human hepatocytes were treated with 66 different combinations of 11 "drug" conditions (six idiosyncratic hepatotoxins, four corresponding control-paired [or "comparison"] compounds, and a DMSO control condition) and six "cytokine" conditions (no cytokine, IL-1α, LPS, TNF, IL-6, and a mix containing all three cytokines plus LPS) in the presence of insulin to capture a diverse physiological complexity. This multi-cytokine mix was selected based on previous observations that it serves as a highly efficient inflammatory environment for the potentiation of idiosyncratic drug hepatotoxicities in human hepatocytes (see Figure 3-5A). We quantitatively assayed the dynamic activation of 17 phosphoproteins mechanistically connected to eight key signaling pathways (including the MEK–ERK, mTOR–p70 S6K, Akt, IKK–NF-κB, JNK, p38–HSP27, STAT3, and STAT6 pathways), cell cycle regulatory pathways, and DNA damage pathways that are plausibly induced by these combinations of drug-cytokine co-stimuli (see Figure 4-1). Inspection of this multivariate data set identified multiple signaling network features that were reasonably correlated with, but poorly predictive of, the measured hepatotoxicities. So, we subjected the CSR data compendium to orthogonal partial-least squares regression (OPLSR), a data-driven modeling approach useful for suggesting relationships between intracellular signals and cell phenotypes without requiring *a priori* mechanistic knowledge [46, 62, 64, 66, 68]. An OPLSR model suggested that hepatocytes integrate signals from four key pathways -- Akt and mTOR–p70 S6K signaling, associated with pro-survival function by the model, and MEK–ERK and p38–HSP27 signaling, associated with pro-death function by the model -- to specify their cell death responses to toxic drug/cytokine conditions. The model-suggested pro-death signaling contributions from MEK–ERK and p38–HSP27 signaling were

confirmed using small molecule kinase inhibitors. Furthermore, an OPLSR model focused on the four informative signaling pathways (together, comprising a useful and simplified signaling network "gauge") demonstrated quantitatively accurate predictions of drug- and cytokine-induced hepatotoxicities in a second human hepatocyte donors and qualitatively accurate predictions of the effects of MEK and p38 inhibitor treatments in a third human hepatocyte donor. This signaling network approach suggests that inflammatory cytokine-associated idiosyncratic drug hepatotoxicity is governed at the hepatocellular level through the integration of four key signaling pathways -- MEK–ERK, Akt, mTOR–p70 S6K, and p38–HSP27 -- and allows for accurate prediction of hepatocellular death responses across human hepatocyte donors and drug/cytokine treatment conditions.

4.2. Experimental procedures

4.2.1. Human hepatocyte cell culture and stimulation

Primary human hepatocytes were obtained in suspension from CellzDirect (Durham, NC). Human hepatocytes from multiple donors were used in this study, and donor identification is noted for each data set. Detailed donor information is provided in Appendix C. Human hepatocytes were seeded on collagen type I-coated 12- or 96-well plates (BD Biosciences) at 1.5×10^5 cells/cm^2 in medium containing 5% FBS (Hyclone) and 5 μg/ml insulin (Sigma), as described in Chapter 3.2.3. One day post-seeding, human hepatocytes were overlayed with 0.25 mg/ml Matrigel (BD Biosciences) in medium containing insulin but not FBS, as described in Chapter 3.2.3. One day following Matrigel overlay, fresh culture medium containing insulin but not FBS was added. For kinase and autocrine ligand inhibition studies, this medium contained inhibitors at 2× final concentration. One hour later, an equal volume of medium containing drugs and/or cytokines at 2× final concentration was added.

4.2.2. Drug, cytokines, and inhibitors

Hepatotoxic and corresponding "comparison" drugs were obtained from Sigma (cimetidine, ranitidine, levofloxacin, buspirone, nefazodone, aspirin, nimesulide, chlorpromazine, nortriptyline, clomipramine, mexiletine, and riluzole), Sequoia Research

Products (clarithromycin and telithromycin), or Pfizer's chemical sample bank (trovafloxacin). All drugs were dosed at 100*C_{max} concentrations, corresponding to the following molecular concentrations: 1.5 mM cimetidine, 142 μM ranitidine, 1.6 mM levofloxacin, 770 μM trovafloxacin, 0.46 μM buspirone, 86 μM nefazodone, 552 μM aspirin, 2.1 mM nimesulide, 334 μM clarithromycin, 277 μM telithromycin, 111 μM chlorpromazine, 10 μM nortriptyline, 13 μM clomipramine, 88 μM mexiletine, and 107 μM riluzole. Additional information on the relevance of 100*C_{max} dosing concentrations and the drug-induced liver injury classifications of these drugs can be found in Chapter 3.2.2 and Table 3-3, respectively. All drugs were suspended in 0.25% final DMSO.

Recombinant human cytokines were obtained from R&D Systems and were used at the following concentrations: 100 ng/ml tumor necrosis factor-α (TNF), 20 ng/ml interleukin-1α (IL-1α), and 20 ng/ml interleukin-6 (IL-6). Lipopolysaccharides (LPS) serotype 1 from *E. coli* 0111:B4 (Sigma) was used at 10 μg/ml.

The MEK kinase inhibitors PD98059, U0126, and MEK inhibitor I were obtained from EMD Biosciences (San Diego, CA). The p38 kinase inhibitors SB202474 (inactive control), SB202190 and SB203580 were obtained from EMD Biosciences. The MEK kinase inhibitor PD325901 and p38 kinase inhibitors PHA-460448 (inactive control), SC-80036A, PF-04334950-00, PHA-666859, and PHA-818637 were obtained from Pfizer's chemical sample bank. All inhibitors were suspended in 0.1% final DMSO. To perturb autocrine EGFR ligand activity, 5 μg/ml anti-TGF-α neutralizing antibody (R&D Systems) or 10 μg/ml c225 monoclonal antibody (a generous gift of H. S. Wiley) were used. To perturb autocrine IL-1 activity, 10 μg/ml recombinant human IL-1ra (R&D Systems) was used.

4.2.3. Multiplexed phosphoprotein assays

Phosphoprotein signaling was quantified using multiplexed bead-based Luminex assays. Cells were plated and treated as described above. Cell lysates were collected at 0 and 20 minutes and 4, 24, and 48 hours following drug and/or cytokine stimulation. At the desired time point, cells were placed on ice and culture medium was removed. Matrigel overlays were partially dissolved by adding ice cold PBS for 15 minutes at 4°C. PBS was removed and cells were lysed with Phosphoprotein Lysis Buffer (Bio-Rad) for 20

minutes at 4°C. Lysates were collected by scrapping and vigorous pipetting. Lysates were clarified by centrifugation at 16,000*g* for 15 minutes at 4°C. Clarified lysates were analyzed using a bicinchonicic assay (Pierce) to determine the total protein concentration. In each culture plate, a well without cells was maintained, lysed, and analyzed to calculate the protein contribution from the Matrigel overlay alone and estimate the cellular protein concentration in the other wells. Bio-Plex bead-based assays (Bio-Rad) were used to quantify the following 17 phosphoproteins: p-Akt (Ser^{473}), p-CREB (Ser^{133}), p-c-Jun (Ser^{63}), p-GSK-3α/β (Ser^{21}/Ser^{9}), p-IκB-α (Ser^{32}/Ser^{36}), p-IRS-1 (Ser^{636}/Ser^{639}), p-ERK1/2 (Thr^{202}/Tyr^{204}, Thr^{185}/Tyr^{187}), p-Histone H3 (Ser^{10}), p-HSP27 (Ser^{78}), p-JNK (Thr^{183}/Tyr^{185}), p-MEK1 (Ser^{217}/Ser^{221}), p-STAT3 (Ser^{727}), p-STAT6 (Tyr^{641}), p-p38 (Thr^{180}/Tyr^{182}), p-p53 (Ser^{15}), p-p70 S6 kinase (Thr^{421}/Ser^{424}), and p-p90 RSK (Thr^{359}/Ser^{363}). Bio-Plex assays were conducted per manufacturer's recommendations on a Luminex 200 instrument (Luminex) with protein lysates loaded at 10 μg/well in technical duplicate. Multiple positive control treatments were loaded on each assay plate to scale raw fluorescence data to self-consistent relative values. See Appendix B for more details.

4.2.4. Lactate dehydrogenase cell death assay

At 20 minutes and 4, 24, and 48 hours post-drug and/or cytokine treatment, conditioned medium samples were collected to assay lactate dehydrogenase (LDH) release (indicator of necrotic and apoptotic cell death) using a CytoTox-ONE Homogeneous Membrane Integrity Assay (Promega) according to manufacturer's recommendations.

4.2.5. Collection and normalization of signal-response data compendia

We collected a cue-signal-response (CSR) data compendia in human hepatocytes from two separate donors. In the initial data compendium (donor #1), human hepatocytes were treated with 66 different combinations of 11 "drug" conditions (six idiosyncratic hepatotoxins, four "comparison" compounds, and a DMSO control condition) and six "cytokine" conditions (no cytokine, IL-1α, LPS, TNF, IL-6, and a mix containing all three cytokines plus LPS). To broadly measure a diverse set of key phosphoprotein activities mechanistically connected to numerous drug- and/or cytokine-induced signaling

pathways, we quantitatively assayed the aforementioned 17 phosphoproteins at both early (0 and 20 minutes) and delayed time-points (4, 24, and 48 hours) following drug and/or cytokine stimulation. In this initial data compendium, single biological replicates were used for both phosphoprotein and LDH assays. The total number of individual phosphoprotein signaling measurements in the initial compendium was 4488 (= 66 conditions × 17 phosphoproteins × 4 time-points × 1 biological replicate).

In the second data compendium (donor #2), human hepatocytes were treated with 18 different combinations of nine "drug" conditions (three idiosyncratic hepatotoxins used in initial compendium, five idiosyncratic hepatotoxins not used in the initial compendium, and a DMSO control condition) and two "cytokine" conditions (no cytokine and the 3-cytokine/LPS mix). In this second compendium, quantitative phosphoprotein assays were focused on a reduced set of six highly informative signals (p-MEK1, p-ERK1/2, p-Akt, p-70 S6K, p-p38, p-HSP27). These phosphoproteins were assayed at the same time-points as in the CSR from donor #1, but with some drug/cytokine co-treatment conditions (all those containing the DMSO control, trovafloxacin, nefazodone, or clarithromycin) also assayed at 1 and 12 hours post-stimulation. Biological triplicates were used for both phosphoprotein and LDH assays. The total number of individual phosphoprotein signaling measurements in the second compendium was 1296 (= 18 conditions × 6 phosphoproteins × 4 time-points × 3 biological replicates).

Phosphoprotein data was fold-change normalized to untreated samples (at 0 minutes) for each phosphoprotein assay and separately for each hepatocyte donor. LDH release data was fold-change normalized to untreated samples at 48 hours post-drug and/or cytokine stimulation separately for each hepatocyte donor.

4.2.6. Metric extraction and scaling

For each phosphoprotein signaling time-course, two time-dependent signaling "metrics" were extracted: (i) the integral, or area-under-the-curve, for the entire time-course, and (ii) the average of the late time-points (4-48 hr), reflecting the steady-state signaling level [62]. These were added to the four time-points (20 minutes and 4, 24, and 48 hours) to yield six signaling metrics for each assayed phosphoprotein. For each compendia, the

signaling metrics from all measured phosphoproteins were then fused into a signaling network data matrix (X). Separately, the toxicity response data were cast into a vector (Y), with both X and Y arrayed across all treatment conditions. In the compendium from donor #1, X was a matrix of 66 rows of treatments and 102 columns (= 17 phospho-proteins × 6 metrics) of signaling metrics, and Y was a vector of 66 rows of treatments and single column (LDH release measured at 48 hours). Before modeling, all columns in the signaling data matrix and response vector were separately mean-centered and scaled to unit variance to non-dimensionalize different assay measurement dynamic ranges [50]. In modeling test data sets not present in model training, scaling parameters from the training data set were used to scale the test data.

4.2.7. Signal-response modeling through orthogonal partial-least squares regression

To relate the measured signaling and cell death response data, we assumed a linear relationship between the two data sets, such that:

$$Y = f(X) = X \cdot B,$$

where X is the signaling network data matrix, Y is the cell death response vector, and B is a vector of regression coefficients that reflect how each phosphoprotein signaling metric contributes to cell death. Framed as such, the signaling matrix X is a block of independent variables and the response vector Y is a block of dependent variables. Since the number of signaling metrics (columns of X) exceeds the number of treatment conditions (rows of X), an unique solution to this linear regression problem cannot be identified. Thus, we implemented partial least-squares regression (PLSR) to solve this regression problem. Instead of performing the linear regression in the original multi-dimensional data space, PLSR casts the problem in a principal-component space and regresses principal components-based coefficients associated with independent and dependent variables [63]. The calculation of principal components-based regression coefficients (or, "loadings") is biased towards those signaling variables that are most covariant with the response data and to optimize prediction accuracy of the response data in cross-validation.

We implemented PLSR using the NIPALS algorithm in SIMCA-P software (Umetrics, Inc., Kinnelon, NJ) following standard methods [62-64, 152, 153]. All PLSR

models were generated using four principal components under standard optimization criteria [63]. All calibrated PLSR models were subjected to a principal-component space linear transformation by rotating the projection of the single cell death response variable completely into the first principal-component, thus yielding an "orthogonal" PLSR (OPLSR) model (see Appendix D and [154]), to allow for simplified interpretation of model loadings and scores. Signaling metric model loadings were calculated using the mean-centered regression coefficients $w_a * c_a$ from the *a*-th OPLSR principal-component [62]. Model calibration was conducted using leave-one-out cross-validation, and model uncertainties were calculated by jack-knifing [155]. The accuracy of model predictions for both training and test data were assessed using the model fitness parameter R^2 [50]:

$$R^2 = 1 - \left[\frac{\sum_{i=1}^{n} \left(\text{Predicted}_i - \text{Observed}_i \right)^2}{\sum_{i=1}^{n} \left(\text{Predicted}_i \right)^2 - \frac{\left(\sum_{i=1}^{n} \text{Predicted}_i \right)^2}{n}} \right],$$

where Predicted_i is the predicted cell death value of the *i*-th treatment condition, Observed_i is the experimentally observed cell death value of the *i*-th treatment condition, and n is the total number of treatment conditions. This assessment of model fitness postulates a one-to-one equivalence between observed and predicted response values, and is more stringent than a simple correlation assessment that does not penalize for quantitatively inaccurate predictions that are nonetheless qualitatively correlative [153]. An R^2 value of 1 corresponds to a perfect fit between observed and predicted responses. An R^2 value of 0 corresponds a model break-point [153]. Negative R^2 values imply highly inaccurate model predictions.

To interpret the contributions of various signaling pathways to drug- and/or cytokine-induced hepatotoxicity, an initial OPLSR model was trained on the 17-phospho-protein, 66-condition CSR data compendium from human hepatocyte donor #1, and demonstrated good model fitness ($R^2 = 0.92$) of cross-validated predictions. All models were regressed against the LDH release data measured at t = 48 hours, as models of the LDH release response at earlier time-points were poorly fit (data not shown).

4.2.8. Model reduction

To identify the relative importance of individual phosphoprotein signaling metrics, the information content of each signaling metric was assessed by its variable importance of projection (VIP) score [156]:

$$VIP_k = \left(\frac{K \sum_{a=1}^{A} w_{a,k}^2 SS_a}{\sum_{a=1}^{A} SS_a} \right)^{1/2},$$

where K is the total number of signaling metrics, $w_{a,k}$ is the weight of the *k*-th metric for principal component a, A is the total number of principal components, and SS_a is the sum of squares explained by principal component a. Signaling metrics with a VIP > 1 have significant importance in the model and metrics with a VIP << 1 significantly lack unique information in the model [50, 156].

To reduce the initial 17-phosphoprotein model, phosphoproteins and all six of their associated signaling metrics were removed from the model step-wise in order of the lowest average VIP score across all six metrics. This model reduction approach yielded a set of 4-to-6-phosphoprotein models (R^2 = 0.87-0.91) that retained the model fitness of the full 17-phosphoprotein model (R^2 = 0.92; see Figure 4-5). The robustness of this model reduction approach was examined by testing the ability of a reduced 6-phospho-protein model, trained on CSR data from human hepatocyte donor #1, to accurately predict signal-response relationships in a 18-condition, 6-phosphoprotein CSR data compendium collected from human hepatocyte donor #2.

4.2.9. Kinase inhibitor evaluation and selection

Kinase inhibitors were evaluated for efficacy and toxicity in human hepatocytes (from donor #3) over a range of concentrations at seven 8× serial dilution concentrations from 20 μM (20 μM, 2.5 μM, 0.31 μM, 39 nM, 4.9 nM, 0.61 nM, 76 pM). To evaluate MEK kinase inhibitor efficacy, human hepatocytes were pretreated with inhibitor for one hour before treatment with 100 ng/ml TGF-α for 15 minutes and then were assayed for p-ERK1/2 activation. To evaluate p38 kinase inhibitor efficacy, human hepatocytes were pretreated with inhibitor for one hour before treatment with 100 ng/ml TNF for 15

minutes and then were assayed for p-HSP27 activation. To evaluate MEK and p38 kinase inhibitor toxicity, inhibitors were added at 1× final concentrations in fresh medium for 48 hours, then medium samples were assayed for LDH release. LDH results were normalized to wells from the same culture plate lysed in 1% Triton X for 10 minutes, and values were reported as % cell death (with the lysed samples assumed to represent 100% cell death). The following kinase inhibitors/concentrations were selected for their potent signaling inhibition and minimal toxicity and were used to perturb kinase activities in drug- and cytokine co-treatment experiments: 10 μM U0126, 1 μM PD325901, 1 μM PHA-666859, and 1 nM PHA-818637.

4.2.10. Model predictions of kinase inhibitor effects on drug- and cytokine-induced hepatotoxicity

To make *a priori* predictions of kinase inhibitor perturbation of drug- and/or cytokine-induced hepatocellular death responses, a set of "computationally inhibited" signaling time-courses was generated by reducing the activation levels of the specific phosphoprotein signaling molecules targeted by the kinase inhibitor of interest. These time courses were generated for the treatment conditions of DMSO ± cytokine mix and nortriptyline ± cytokine mix, in the presence or absence of 10 μM U0126, 1 μM PD325901, 1 μM PHA-666859, and 1 nM PHA-818637. To generate the uninhibited time-courses, mean values across donor #1 and #2 (DMSO ± cytokine mix) or from donor #2 only (nortriptyline ± cytokine mix) were used. For a phosphoprotein signals targeted by an inhibitor, the mean observed level at each time-point was reduced by a fraction equivalent to the percent signal reduction observed for that inhibitor in the signaling inhibition studies in donor #3 (as in [64, 66]; see Chapter 4.2.9). For MEK inhibitors, the phosphoprotein levels of both MEK and ERK at all time-points were reduced by 70% (U0126) and 99% (PD325901), but all other signaling proteins were not changed. For p38 inhibitors, the phosphoprotein levels of both p38 and HSP27 at all time-points were reduced by 93% (PHA-666859) and 99.5% (PHA-818637), but all other signaling proteins were not changed. After computationally inhibiting the time-point data, the integral and late average metrics were re-calculated. Predictions of kinase inhibitor effects based on these "computationally inhibited" signaling metric sets were

generated from two different 6-phosphoprotein OPLSR models (featuring either non- or *log*-scaled LDH release response data) trained on a fused CSR data compendium from both donors #1 and #2. Logarithmic transformation of response data can provide a more accurate OPLSR model prediction of low response level observations, especially for non-uniformly distributed response data sets (B.D.C., unpublished observations). Prediction accuracy was assessed by comparing to experimental observations collected in human hepatocytes from donor #4 using the model fitness metric.

4.2.11. Statistical analysis

Supra-additive drug-cytokine synergy was assessed as described in Chapter 3.2.8. For comparing two individual means, a Student's *t* test was used. All tests were performed at a significance level of $\alpha = 0.05$.

4.3. Results

4.3.1. Drug and cytokine co-treatments elicit shared regulation of multiple phosphoprotein signaling pathways

We collected a cue-signal-response (CSR) drug- and cytokine-induced hepatotoxicity data compendium in primary human hepatocytes to examine the signaling mechanisms regulating inflammatory cytokine-associated idiosyncratic drug hepatotoxicity (Figure 4-2). Human hepatocytes (donor #1) were treated with 66 different combinations of 11 "drug" conditions (six idiosyncratic hepatotoxins, four corresponding "comparison" compounds, and a DMSO control condition) and six "cytokine" conditions. Rigorously quantitative bead-based phosphoprotein (see Appendix B) and cell death assays were utilized to allow for investigation of the quantitative relationships between signaling pathway activation and cell death measurements. Seventeen phosphoproteins, mechanistically associated with the MEK–ERK, mTOR–p70 S6K, Akt, IKK–NF-κB, JNK, p38–HSP27, STAT3, STAT6, cell cycle regulatory, and DNA damage signaling pathways, were measured at both early (0 and 20 minutes) and delayed time-points (4, 24, and 48 hours) following drug and/or cytokine stimulation to capture a diversity of intracellular signaling pathways and dynamics.

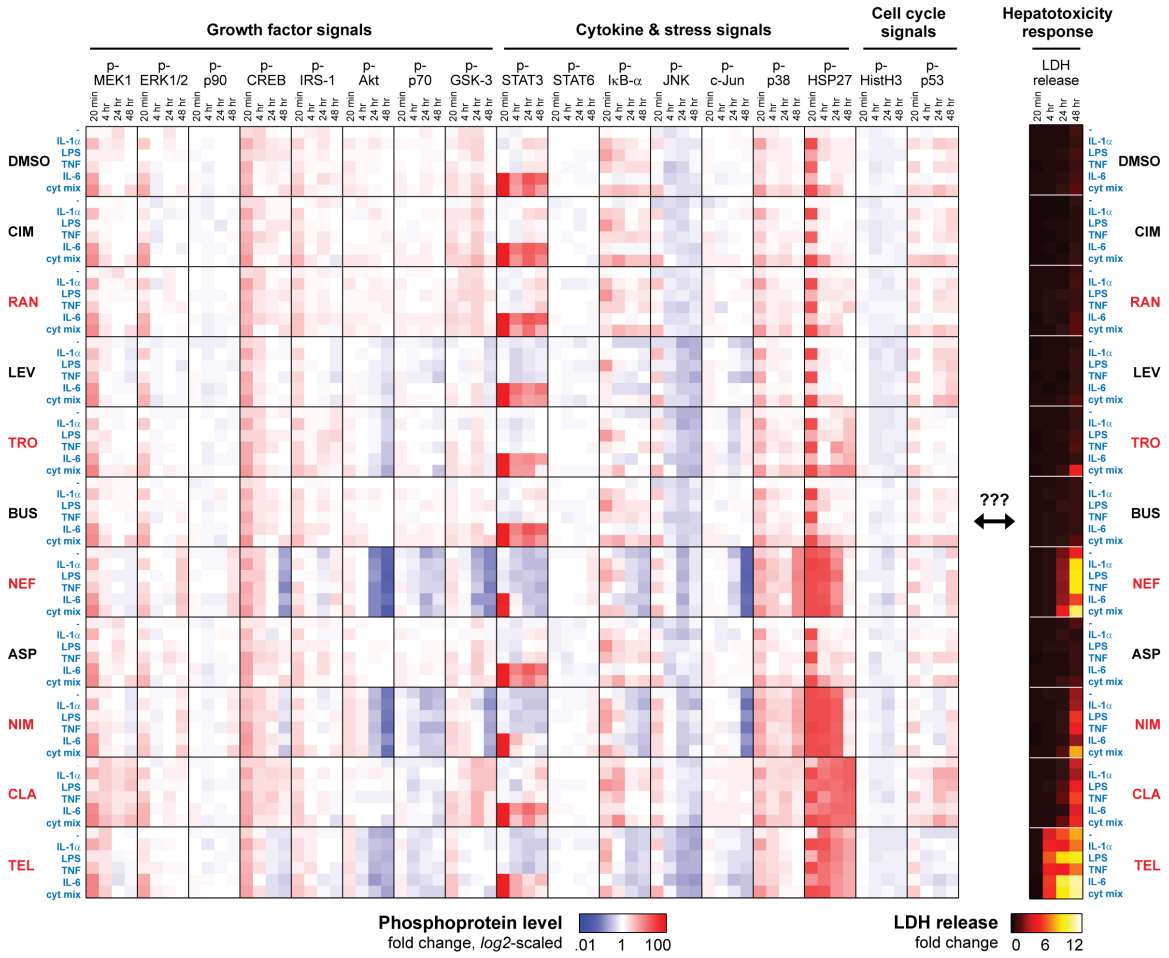

Figure 4-2. A cue-signal-response (CSR) drug- and cytokine-induced hepatotoxicity data compendium for model training. Primary human hepatocytes (from donor #1) were cultured, treated, lysed, and assayed for phosphoproteins and LDH release as described in Chapter 4.2. Human hepatocytes were treated with 66 different combinations of 11 "drug" conditions (six idiosyncratic hepatotoxins, four corresponding "comparison" compounds, and a DMSO control condition) and six "cytokine" conditions (no cytokine, 20 ng/ml IL-1α, 10 µg/ml LPS, 100 ng/ml TNF, 20 ng/ml IL-6, and a mix containing all three cytokines plus LPS). All drugs were dosed at 100*C_{max} concentrations, corresponding to the following molecular concentrations: 1.5 mM cimetidine (CIM), 142 µM ranitidine (RAN), 1.6 mM levofloxacin (LEV), 770 µM trovafloxacin (TRO), 0.46 µM buspirone (BUS), 86 µM nefazodone (NEF), 552 µM aspirin (ASP), 2.1 mM nimesulide (NIM), 334 µM clarithromycin (CLA), and 277 µM telithromycin (TEL). Idiosyncratic hepatotoxins (listed in red font) and corresponding "comparison" compounds are placed in vertical juxtaposition in the ordering of treatment conditions. (Note: clarithromycin serves as a less, but still idiosyncratic hepatotoxic, "comparison" compound to telithromycin.) To broadly measure a diverse set of key phosphoproteins mechanistically connected to numerous drug- and/or cytokine-induced signaling pathways, we quantitatively assayed the 17 phosphoprotein levels (and LDH release levels) at both early (0 and 20 minutes) and delayed time-points (4, 24, and 48 hours) following drug and/or cytokine stimulation. Single biological replicates were used for both phosphoprotein and LDH assays. The total number of individual phosphoprotein signaling measurements in this CSR compendium is 4488 (= 66 conditions × 17 phosphoproteins × 4 time-points × 1 biological replicate). Phosphoprotein levels were fold-change normalized to untreated samples at 0 minutes and are plotted on a log_2-scaled colormap to capture both up- and down-regulated signaling levels. LDH release data were fold-change normalized to untreated samples at 48 hours post-stimulation and are plotted on a linearly-scaled colormap.

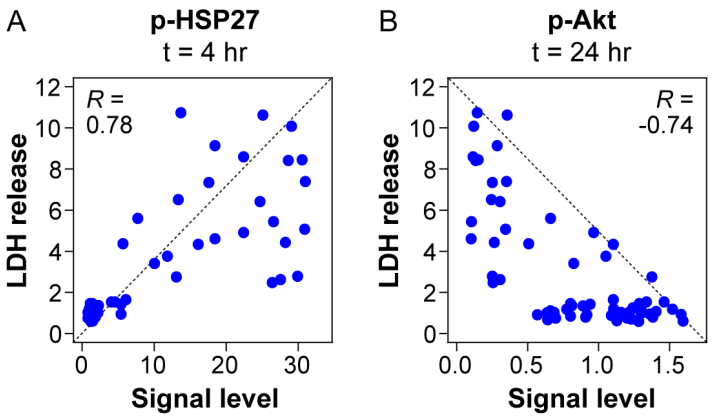

Figure 4-3. The most correlative signaling metrics are poorly predictive of the observed hepatotoxicity response. In the CSR compendium from donor #1, the single signaling metrics most positively (p-HSP27 at t = 4 hr; A) and negatively (p-Akt at t = 24 hr; B) correlated with the observed cell death response (LDH release at t = 48 hr) are plotted. One-to-one correlation lines shown for clarity. Pearson correlation coefficients (*R*) are shown in the insets.

Across this CSR compendium (Figure 4-2), it was evident that cytokine-only treatments induced early activation of multiple signals, including p-MEK1, p-STAT3, p-IκB-α, and p-p38, and many toxic drug-only treatments induced a late-phase down-regulation of certain pro-survival signals (*e.g.* p-Akt) and sustained activation of some stress signals (*e.g.* p-HSP27). Moreover, multiple drug-cytokine co-treatments elicited synergistic induction of sustained p38–HSP27 signaling. For the treatment conditions of trovafloxacin ± the 3-cytokine/LPS mix, this synergistic induction of sustained p38–HSP27 pathway signaling was correlated with synergistic induction of cell death, as measured by LDH release (Figures 4-2 [donor #1], 4-6B-C [donor #2]). This paired synergy suggested that perhaps a single phosphoprotein signal could be well-correlated with the observed cell death responses and yield a highly predictive readout of cell death across the entire data compendium. We then calculated Pearson correlation coefficients for the relationship between the observed cell death at 48 hours post-drug/cytokine treatment and all 17 phosphoprotein signal levels at each of the four time-points. Even the most positively (p-HSP27 at t = 4 hr, R = 0.78) and negatively (p-Akt at t = 24 hr, R = -0.74) correlated single phosphoprotein signaling features were poorly predictive of the measured cell death (Figure 4-3). These poorly predictive individual signaling relationships to the measured cell death responses suggested the need for a multivariate modeling approach to interpret the signal-response relationships present in this drug- and cytokine-induced hepatotoxicity data compendium.

4.3.2. Multipathway OPLSR modeling of a cue-signal-response data compendium identifies key molecular signals regulating drug- and cytokine-induced hepatotoxicity

To generate a multipathway model relating the observed signaling activities and cell death responses, we subjected the initial CSR data compendium to orthogonal partial-least squares regression (OPLSR), a data-driven modeling approach useful for suggesting relationships between intracellular signals and cell phenotypes without requiring *a priori* mechanistic knowledge (see Chapter 4.2.7 and [46, 62, 64, 66, 68]). The 102-signaling metric (17 phosphoproteins × 6 time-dependent metrics) OPLSR model demonstrated good model fitness ($R^2 = 0.92$) for cross-validated predictions of the observed cell death responses for all 66 drug/cytokine coo-treatment conditions (Figure 4-4A). An examination of the OPLSR model scores projections (Figure 4-4B) demonstrated the model's ability to distinguish between toxic and non-toxic treatment conditions by their scores in the first principal component (PC), which represents pro-death model contributions. The second PC of this OPLSR model captures remaining, orthogonal variation in the CSR data compendium, but is not used for prediction of the LDH release response.

An examination of OPLSR model loadings (w_1*c_1; Figures 4-4C, 4-5A) and variable importance of projection (VIP) scores (Figures 4-4C, 4-5B) identified four signaling pathways (MEK–ERK, Akt, mTOR–p70 S6K, and p38–HSP27) with phosphoproteins having informative model contributions at multiple time-points. Positive model loadings imply signaling metrics with pro-death contributions, and negative model loadings imply pro-survival contributions. p-ERK1/2, p-p38, and p-HSP27 were all identified as having significant pro-death contributions from multiple metrics, and p-Akt and p-p70 S6K were identified as having significant pro-survival contributions from multiple metrics. For all 17 phosphoprotein signals, the early time-point (20 min) metrics were uniformly uninformative (as assessed by VIP scores), likely due to these signaling activities being similarly activated by cytokines in the both the presence and absence of drug co-stimuli causing them to be minimally covariant with the measured cell death responses.

The distinct importance of these four signaling pathways suggested that many of the phosphoproteins in the full CSR data compendium were unnecessary for the model predictions and consequently the model could be reduced to a more interpretable set of protein signals. To reduce the complexity of the original 17-phosphoprotein model,

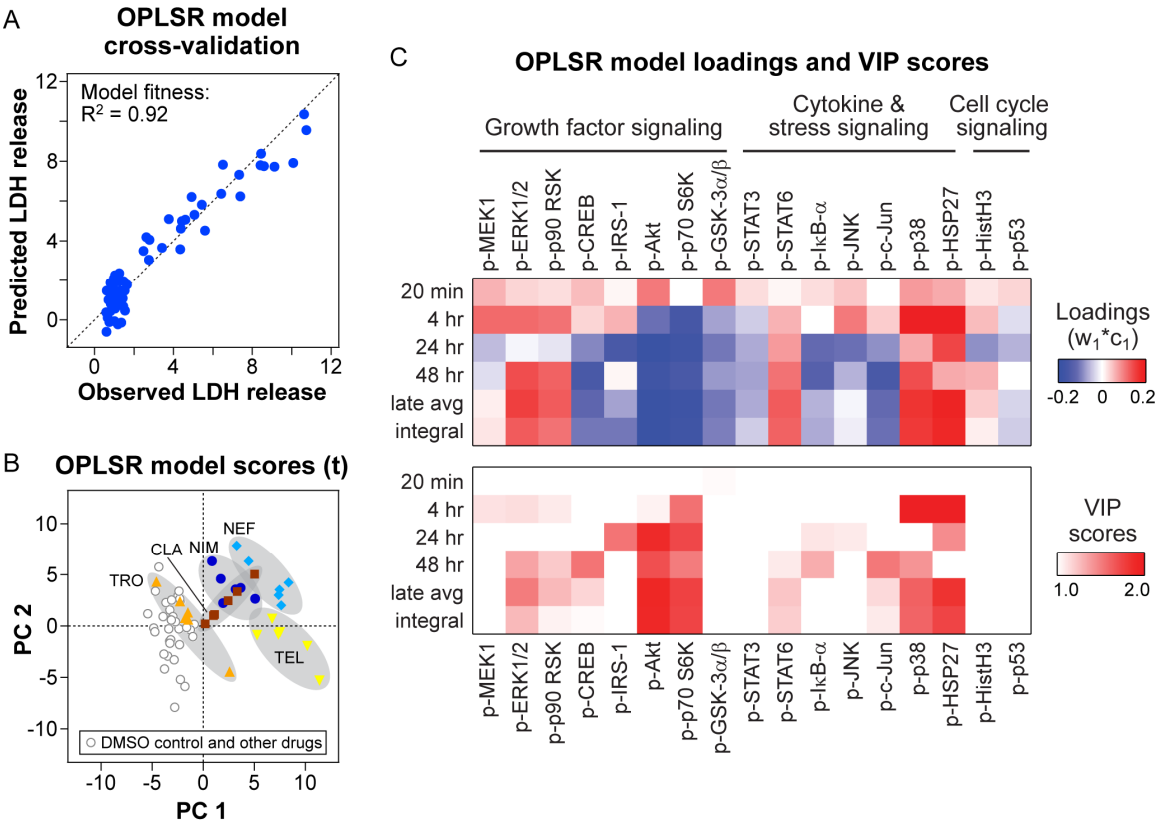

Figure 4-4. An OPLSR model trained on the CSR data compendium from human hepatocyte donor #1 identifies key molecular signals regulating drug- and/or cytokine-induced hepatotoxicity. An OPLSR model was trained on the 66-condition CSR data compendium from human hepatocyte donor #1 to relate the activities of 102 time-dependent phosphoprotein signaling metrics (17 phosphoproteins × 6 metrics) to the observed cell death response (LDH release at t = 48 hr), as described in Chapter 4.2. (A) A correlation plot relating the observed and model-predicted LDH release responses for all 66 drug/cytokine co-treatment conditions shows good model fitness (R^2 = 0.92) [50, 153]. A one-to-one correlation line demonstrating perfect model fitness (R^2 = 1) is shown for clarity. (B) A scores plot of the OPLSR model demonstrates the model's ability to distinguish between toxic and non-toxic treatment conditions by their scores in the first principal component (PC). The second PC of this OPLSR model captures remaining, orthogonal variation in the CSR data compendium, but is not used for prediction of the LDH release response. Conditions containing idiosyncratic hepatotoxins are highlighted. (C) Examination of OPLSR model loadings and variable importance of projection (VIP) scores identifies MEK–ERK, Akt, p70 S6K, and p38–HSP27 as key signaling pathways regulating drug/cytokine-induced hepatotoxicity. Positive model loadings (w_1*c_1) contribute to the predicted cell death, whereas negative loadings antagonize the cell death prediction. VIP scores identify the relative importance of individual phosphoprotein signaling metrics. Signaling metrics with a VIP > 1 have significant importance in the model and metrics with a VIP << 1 significantly lack unique information in the model [50, 156]. Note that VIP scores from the early time-point metric (20 min) are uniformly uninformative.

phosphoproteins (and all six of their associated signaling metrics) were removed from the model step-wise in order of the lowest average VIP score across all six metrics (Figure 4-5B-C). Model fitness was maintained until the top ~4-5 phosphoproteins remained (R^2 = ~0.87-0.91). Further removal of phosphoproteins resulted in the significant losses in model fitness (Figure 4-5C). This emphasized that an equivalently predictive multipathway network model could be generated by focusing on representative phosphoproteins from four pathways -- MEK–ERK, Akt, mTOR–p70 S6K, and p38–HSP27 -- and that these representative phosphoproteins (*e.g.* p-ERK1/2, p-Akt, p-p70 S6K, and p-HSP27) could serve as a useful signaling network "gauge" [68], whose integrated activities accurately specify hepatocellular death responses to drug and/or cytokine stimulation (Figure 4-5E).

4.3.3. A multipathway OPLSR model accurately predicts hepatotoxicity signal-response relationships across human hepatocyte donors

To test the utility of this reduced multipathway OPLSR model, we collected a second drug- and cytokine-induced CSR hepatotoxicity data compendium containing just six phosphoprotein signals (p-MEK1, p-ERK1/2, p-Akt, p-p70 S6K, p-p38, and p-HSP27) from the four "network gauge" pathways (Figure 4-6A). p-MEK1 and p-p38 are likely redundant measurements to p-ERK1/2 and p-HSP27, respectively, but were necessary to test subsequent model predictions pertaining to the effects of MEK and p38 inhibitors. In this second CSR data compendium, human hepatocytes (donor #2) were treated with 18 different combinations of nine "drug" conditions (three idiosyncratic hepatotoxins used in initial compendium, five idiosyncratic hepatotoxins not used in the initial compendium, and a DMSO control condition) and two "cytokine" conditions (no cytokine and the 3-cytokine/LPS mix).

An OPLSR model trained on the CSR data compendium from donor #1 but limited to signaling metrics from these six "network gauge" phosphoproteins was used to predict LDH release responses from signaling data collected in a human hepatocytes from donor #2 (Figure 4-7A). Model predictions of cell death responses from donor #2 were inaccurate for both the eight drug/cytokine co-treatment conditions present in the training

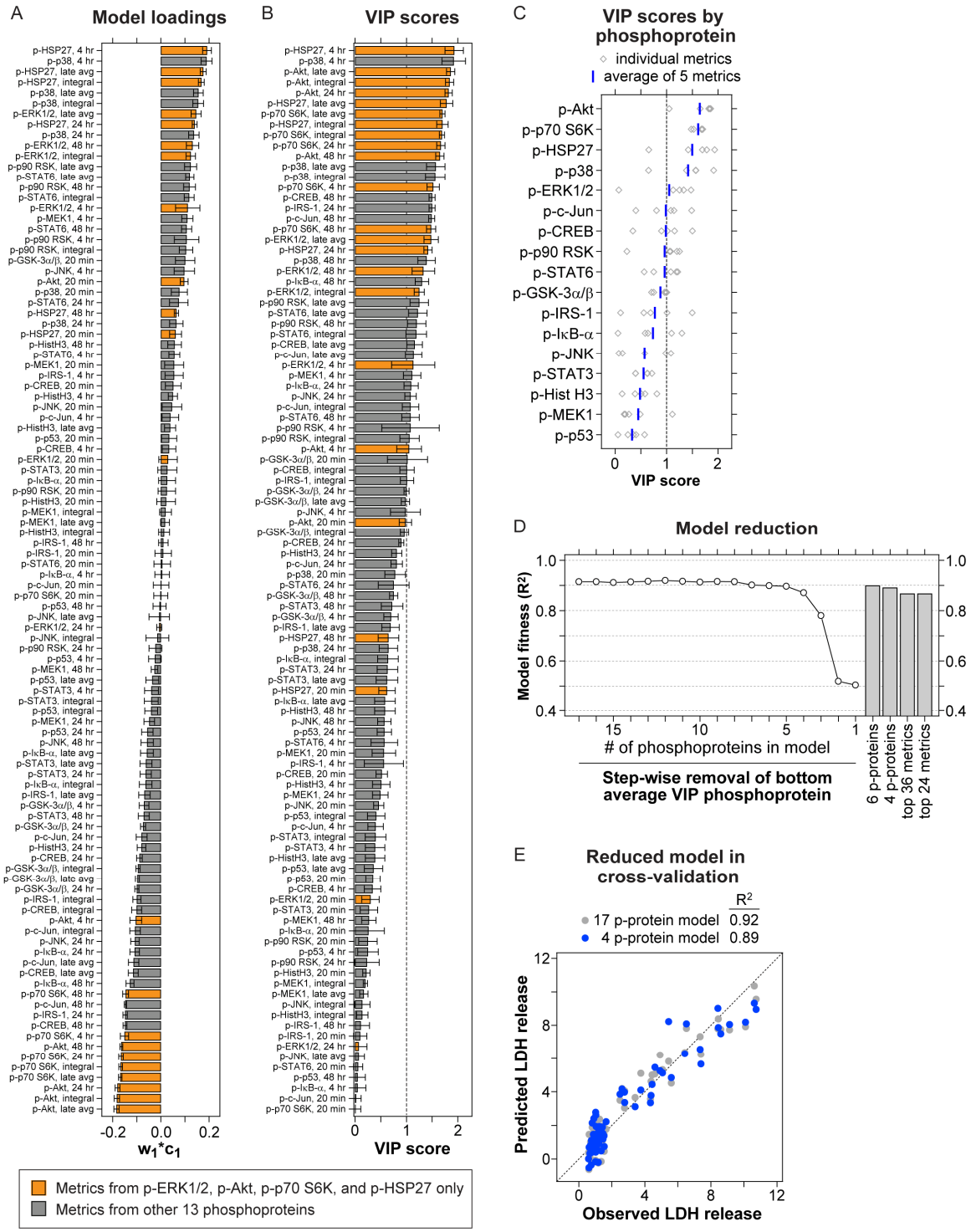

Figure 4-5. Reduction of the 17-phosphoprotein OPLSR model identifies equivalently predictive 4-to-6-phosphoprotein models. (A-B) Model loadings (A) and VIP scores (B) are plotted for all 102 phosphoprotein signaling metrics, with metrics from p-ERK1/2, p-Akt, p-p70 S6K, and p-HSP27 noted. Model loadings and VIP scores are presented as the mean values ± cross-validation standard error, calculated by jack-knifing [155]. (C) VIP scores for each phosphoprotein signal are shown, with the phosphoproteins ordered by the average VIP scores. VIP scores for the 20-minute signaling metrics were omitted from the plot and the calculated average as they were uniformly uninformative (<< 1). In (B) and

(C), a line indicating the threshold value of 1 for informative VIP scores is shown for clarity. (D) Model fitness sensitivity to the removal of phosphoprotein signaling metrics. Model complexity was reduced by either (i) step-wise removal of the bottom average VIP phosphoprotein; (ii) from selection of four (p-ERK1/2, p-Akt, p-p70 S6K, and p-HSP27) or six (those four plus p-MEK1 and p-p38) specific phosphoproteins from the highly informative MEK–ERK, Akt, p70 S6K, and p38–HSP27 signaling pathways; or (iii) using an equivalent number of signaling metrics as the four- and six-phosphoprotein models (24 and 36 metrics, respectively) but selected as the top VIP score metrics across all 17 phosphoproteins. Model fitness is maintained under phosphoprotein removal until ~4 phosphoproteins remain. (E) A comparison of the cross-validated prediction from a full 17-phosphoprotein model and a reduced 4-phosphoprotein (p-ERK1/2, p-Akt, p-p70 S6K, and p-HSP27) model. Both models demonstrate good model fitness across all 66 conditions (R^2 = 0.92 and 0.89 for 17- and 4-phosphoprotein models, respectively). A one-to-one correlation line demonstrating perfect model fitness (R^2 = 1) is shown for clarity.

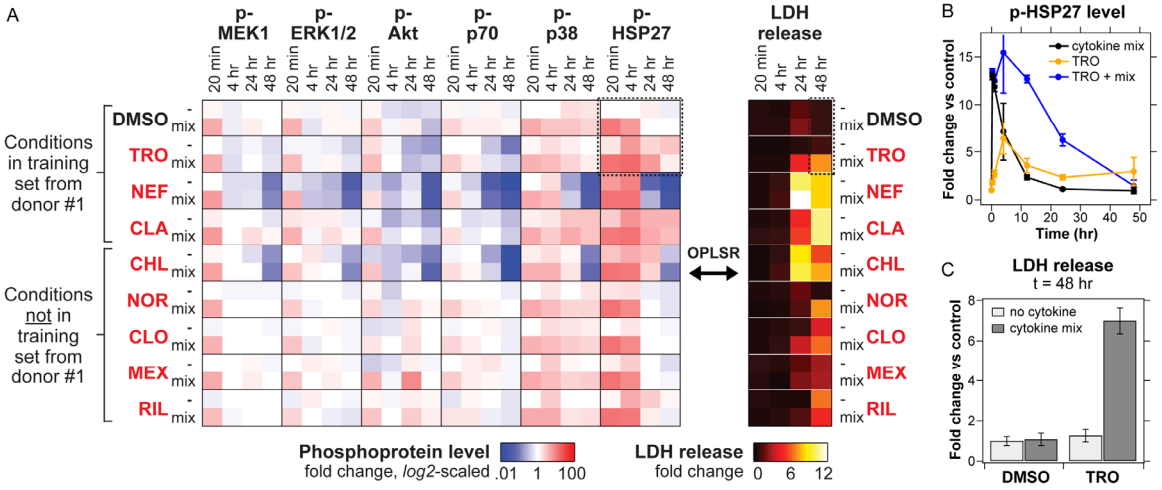

Figure 4-6. A cue-signal-response (CSR) drug- and cytokine-induced hepatotoxicity data compendium for model testing. Primary human hepatocytes (from donor #2) were cultured, treated, lysed, and assayed as described in Chapter 4.2. (A) Human hepatocytes were treated with 18 different combinations of nine "drug" conditions (three idiosyncratic hepatotoxins used in initial compendium, five idiosyncratic hepatotoxins not used in the initial compendium, and a DMSO control condition) and two "cytokine" conditions (no cytokine and the 3-cytokine/LPS mix) and were assayed for phosphoprotein signaling and LDH release. Idiosyncratic hepatotoxic drugs (listed in red font) were dosed at 100*C_{max} concentrations, corresponding to the following molecular concentrations: 770 µM trovafloxacin (TRO), , 86 µM nefazodone (NEF), 334 µM clarithromycin (CLA), 111 µM chlorpromazine (CHL), 10 µM nortriptyline (NOR), 13 µM clomipramine (CLO), 88 µM mexiletine (MEX), and 107 µM riluzole (RIL). Phosphoproteins assays were focused on a reduced set of six highly informative signals (p-MEK1, p-ERK1/2, p-Akt, p-70 S6K, p-p38, p-HSP27). These phosphoproteins and LDH release were assayed at both early (0 and 20 minutes) and delayed time-points (4, 24, and 48 hours) following drug and/or cytokine stimulation. A subset of drug/cytokine treatment conditions (all those containing the DMSO control, TRO, NEF, or CLA) were also assayed at 1 and 12 hours post-stimulation (see panel (B) and data not shown). Biological triplicates were used for both phosphoprotein and LDH assays. The total number of individual phosphoprotein signaling measurements in this CSR data compendium was 1296 (= 18 conditions × 6 phosphoproteins × 4 time-points × 3 biological replicates). Phosphoprotein levels were fold-change normalized to untreated samples at 0 minutes and are plotted on a log_2-scaled colormap to capture both up- and down-regulated signaling levels. LDH release data were fold-change normalized to untreated samples at 48 hours post-stimulation and are plotted on a linearly-scaled colormap. Note that the colormap scales are the same as in Figure 4-2. (B-C) Demonstration of drug-cytokine synergy in the sustained activation of p-HSP27 (B) and the induction of cell death (C) under conditions of trovafloxacin ± cytokine mix. Data are presented as the mean ± SEM of three biological replicates.

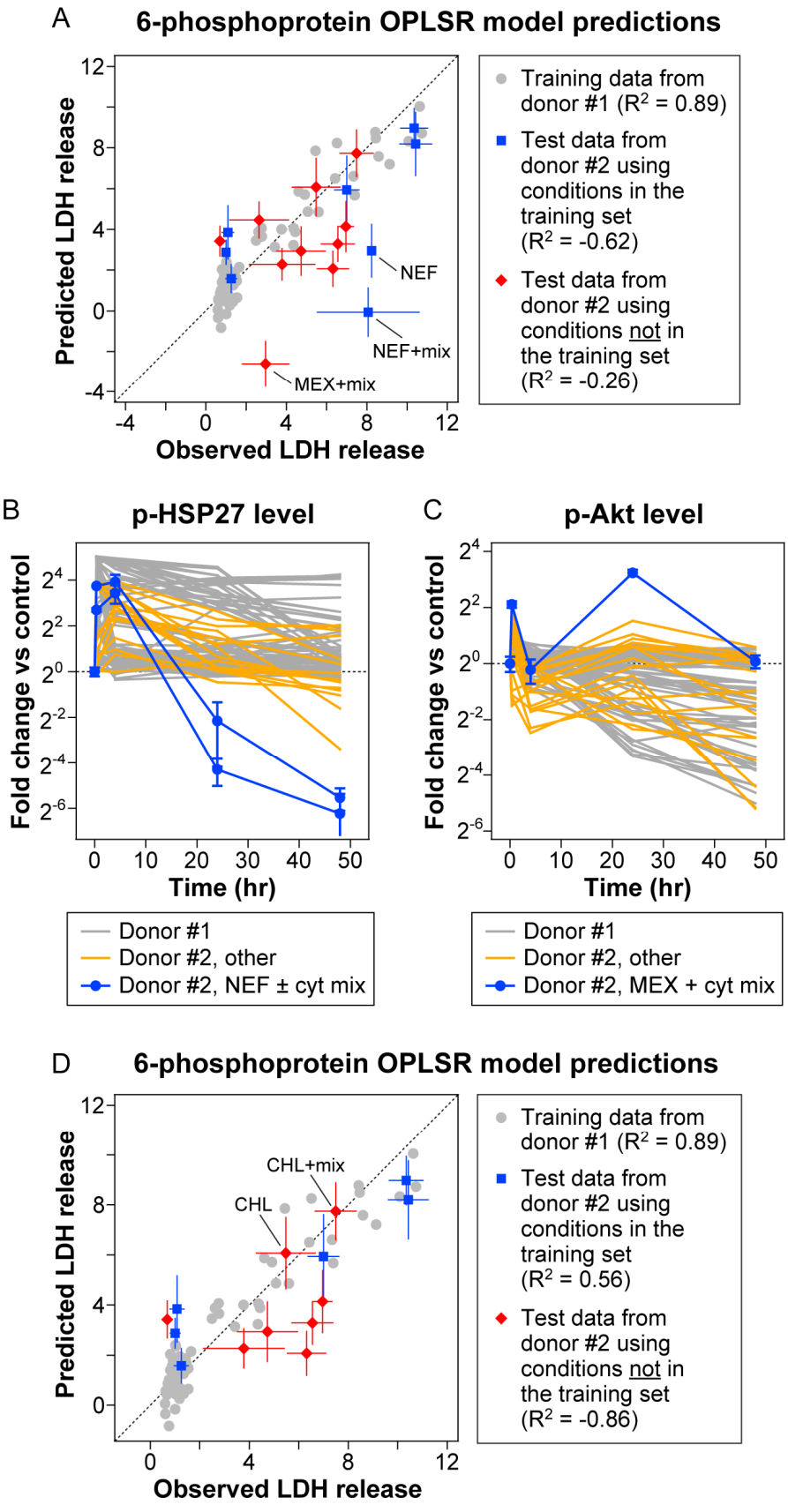
A
6-phosphoprotein OPLSR model predictions
Predicted LDH release
Observed LDH release
NEF
NEF+mix
MEX+mix
Training data from donor #1 (R^2 = 0.89)
Test data from donor #2 using conditions in the training set (R^2 = -0.62)
Test data from donor #2 using conditions not in the training set (R^2 = -0.26)
B
p-HSP27 level
Fold change vs control
Time (hr)
Donor #1
Donor #2, other
Donor #2, NEF ± cyt mix
C
p-Akt level
Fold change vs control
Time (hr)
Donor #1
Donor #2, other
Donor #2, MEX + cyt mix
D
6-phosphoprotein OPLSR model predictions
Predicted LDH release
Observed LDH release
CHL+mix
CHL
Training data from donor #1 (R^2 = 0.89)
Test data from donor #2 using conditions in the training set (R^2 = 0.56)
Test data from donor #2 using conditions not in the training set (R^2 = -0.86)

Figure 4-7. (Previous page) A 6-phosphoprotein OPLSR model accurately predicts drug/cytokine responses across human hepatocyte donors, but only for drug/cytokine treatments present in the training data compendium. An OPLSR model of LDH release (t = 48 hr) was trained on the time-dependent signaling metrics from six phosphoproteins (p-MEK1, p-ERK1/2, p-Akt, p-70 S6K, p-p38, p-HSP27) using the drug/cytokine-induced hepatotoxicity data compendium from donor #1. This trained model was used to predict LDH release responses from the same six phosphoprotein signals collected in human hepatocytes from donor #2. The CSR data compendium from donor #2 contained 18 different combinations of nine "drug" conditions (three idiosyncratic hepatotoxins used in training compendium, five idiosyncratic hepatotoxins not used in the training compendium, and a DMSO control condition) and two "cytokine" conditions (no cytokine and the 3-cytokine/LPS mix). (A) A correlation plot relating the observed and predicted LDH release responses for all 66 drug/cytokine treatment conditions in the training (donor #1) CSR compendium (grey, R^2 = 0.89), 8 drug/cytokine treatment conditions from the test (donor #2) CSR compendium that were also present in the training data (blue, R^2 = -0.62), and 10 drug/cytokine treatment conditions from the test (donor #2) CSR compendium that were not present in the training data (red, R^2 = -0.26). Quantitatively accurate model predictions have positive R^2 values, negative R^2 values imply highly inaccurate model predictions, and an R^2 value of 0 corresponds a model break-point [153]. A one-to-one correlation line demonstrating perfect model fitness (R^2 = 1) is shown for clarity. Conditions (nefazodone [NEF] ± cytokine mix and mexiletine [MEX] + cytokine mix) with highly inaccurate predictions are noted. In (A) and (D), experimental data is presented as mean ± SEM of three biological replicates and the model-predicted responses are presented as the mean prediction ± cross-validation standard error, calculated by jack-knifing [155]. Experimental and prediction uncertainties are not shown for the training data. (B-C) Closer inspection of the signaling time-course data reveals conditions with highly inaccurate predictions have outlying signaling data. (B) NEF ± cytokine mix conditions in donor #2 induced significant p-HSP27 signal attenuation at late time-points, which was not observed in the training data or the other test data. (C) MEX + cytokine mix condition in donor #2 induced significant p-Akt signal activation at the 24 hour time-point, which was not observed in the training data or the other test data. In (B) and (C), training and test data from non-outlier conditions are presented as mean values (of 1-3 biological replicates) only, test data from outlier conditions are presented as the mean ± SEM of three biological replicates, and phosphoprotein levels are plotted on a log_2-scaled axis. (D) Removal of the outlier drug/cytokine treatment conditions from donor #2 demonstrates accurate model predictions. A correlation plot relating observed and predicted LDH release responses as in (A) but omitting the outlier drug/cytokine conditions from donor #2. After removal of outlier conditions, it is evident that the model demonstrates reasonable fitness in predicting cell death responses for test data from conditions present in the training compendium (R^2 = 0.56), but is not as accurate for predictions of conditions not present in the training compendium (R^2 = -0.86). Two test conditions (chlorpromazine [CHL] ± cytokine mix) not present in the training compendium but nonetheless predicted with quantitative accuracy are noted.

data from donor #1 (R^2 = -0.62) and the ten drug/cytokine co-treatment conditions not present in the training data (R^2 = -0.26; Figure 4-7A). Further inspection of these observation-prediction relationships from donor #2 identified that a small subset of treatment conditions (nefazodone ± cytokine mix and mexiletine + cytokine mix) resulted in substantially inaccurate predictions that skewed the model prediction fitness evaluations. Inspection of individual phosphoprotein signaling time-courses for these conditions revealed signaling activities that were significantly outside of both the model training data from donor #1 and the remainder of the test data from donor #2 (Figure 4-7B-C). Specifically, the nefazodone ± cytokine mix conditions in donor #2 induced significant p-HSP27 signal attenuation at late time-points, which was not observed in the

training data or the other test data (Figure 4-7B). A reduced level of sustained p-HSP27 activation is interpreted by the model as a reduction in cell death due to late p-HSP27 metrics having highly positive (pro-death) model loadings (Figure 4-4C). Consequently, the model under-predicted cell death for the nefazodone ± cytokine mix conditions in donor #2. The mexiletine + cytokine mix condition in donor #2 induced significant p-Akt activation at the 24 hour time-point, which was not observed in the training data or the other test data (Figure 4-7C). An increased level of p-Akt activation at t = 24 hr is interpreted by the model as a reduction in cell death due to late p-Akt metrics having highly negative (pro-survival) model loadings (Figure 4-4C). Thus, the model under-predicted cell death for the mexiletine + cytokine mix conditions in donor #2.

After removal of these outlier drug/cytokine treatment conditions from donor #2, the 6-phosphoprotein OPLSR model trained on data from donor #1 demonstrated reasonably accurate predictions of cell death responses for test data from conditions present in the training compendium ($R^2 = 0.56$; Figure 4-7D). The model still generated inaccurate predictions of conditions not present in the training compendium ($R^2 = -0.86$), although two of the test conditions (chlorpromazine ± cytokine mix) not present in the training compendium were nonetheless predicted with quantitative accuracy. This demonstrated that the 6-phosphoprotein OPLSR model can accurately predict drug/cytokine responses across human hepatocyte donors, but only for non-outlier drug/cytokine treatment present in the training data. It is possible that other signaling pathways, such as JNK, play a more substantial role in integrating hepatocellular responses drug-cytokine co-stimulation for some of the drugs, such as clomipramine and riluzole, not present in the training set. Inclusion of these additional pathways in might enable more accurate cell death predictions for more varied set of drug/cytokine treatment conditions.

The model's ability to successfully predict hepatotoxicity signaling-response relationships across human hepatocyte donors for similar drug/cytokine conditions suggests that hepatocytes from multiple human donors share a "common effector" processing function [64]. In human hepatocytes from two different human donors, specific drug/cytokine treatment conditions (see clarithromycin + cytokine mix in donors #1 and 2; Figure 4-8) can elicit significantly different signaling network activation

profiles and induce different levels of cell death but the trained OPLSR model can accurately predict the cell death responses from both signaling network activity profiles by considering all the time-dependent signaling activity variables across the six measured phosphoproteins.

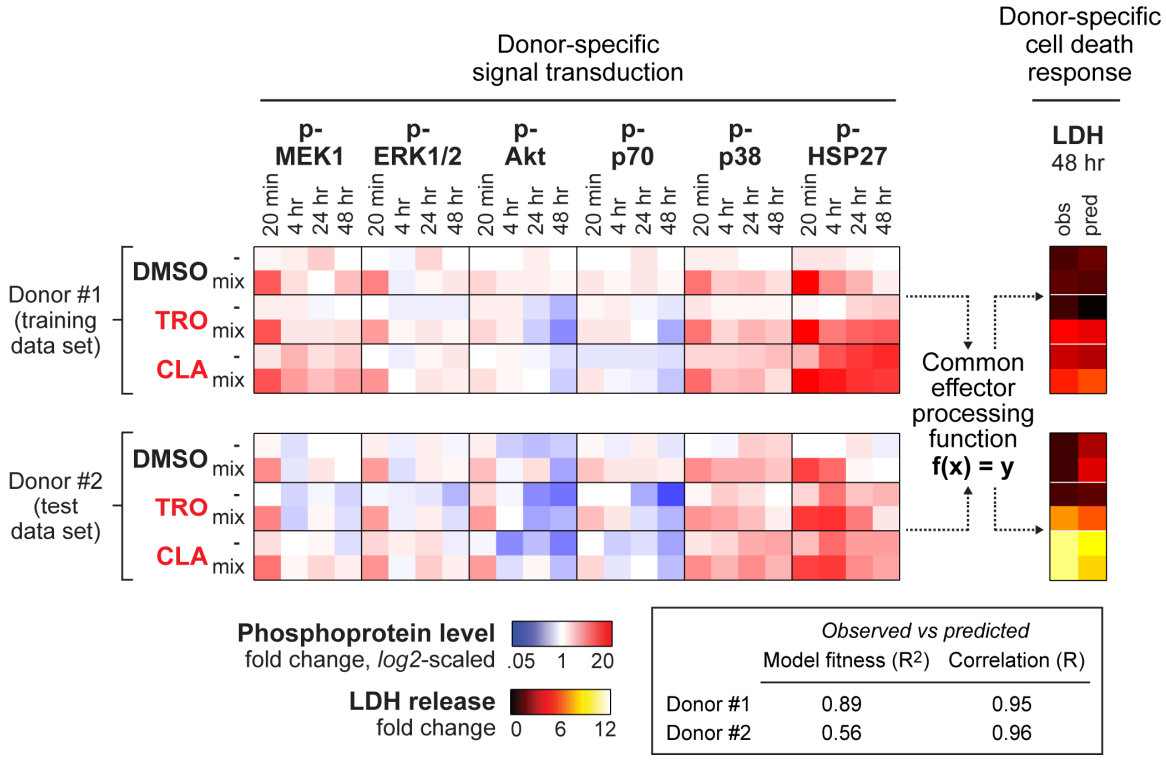

Figure 4-8. Common-effector processing mediates donor-specific responses to drug and/or cytokine stimulation. Signaling and response data from non-outlier conditions present in both human hepatocyte donors is shown as in Figures 4-2 and 4-6. An OPLSR model was trained on the 66-condition, 6-phosphoprotein CSR data compendium from donor #1, as described in Figure 4-7. This OPLSR model generated quantitatively accurate predictions of cell death responses in donor #1 (for the conditions shown here, R^2 = 0.89 and R [Pearson correlation coefficient] = 0.95) and donor #2 (for the conditions shown here, R^2 = 0.56 and R = 0.96), even though donor-specific signaling network activation profiles and cell death responses were observed under the same drug/cytokine treatments. (Compare clarithromycin [CLA] ± cytokine mix across the two donors.) The predictive accuracy of this OPLSR model suggests that a common-effector processing mechanism (f(x) = y) encompassing the integration of the survival and stress signaling network (x) yields quantitatively concerted cell death responses (y) to toxic drug/cytokine conditions exists and is shared between hepatocytes from different human donors.

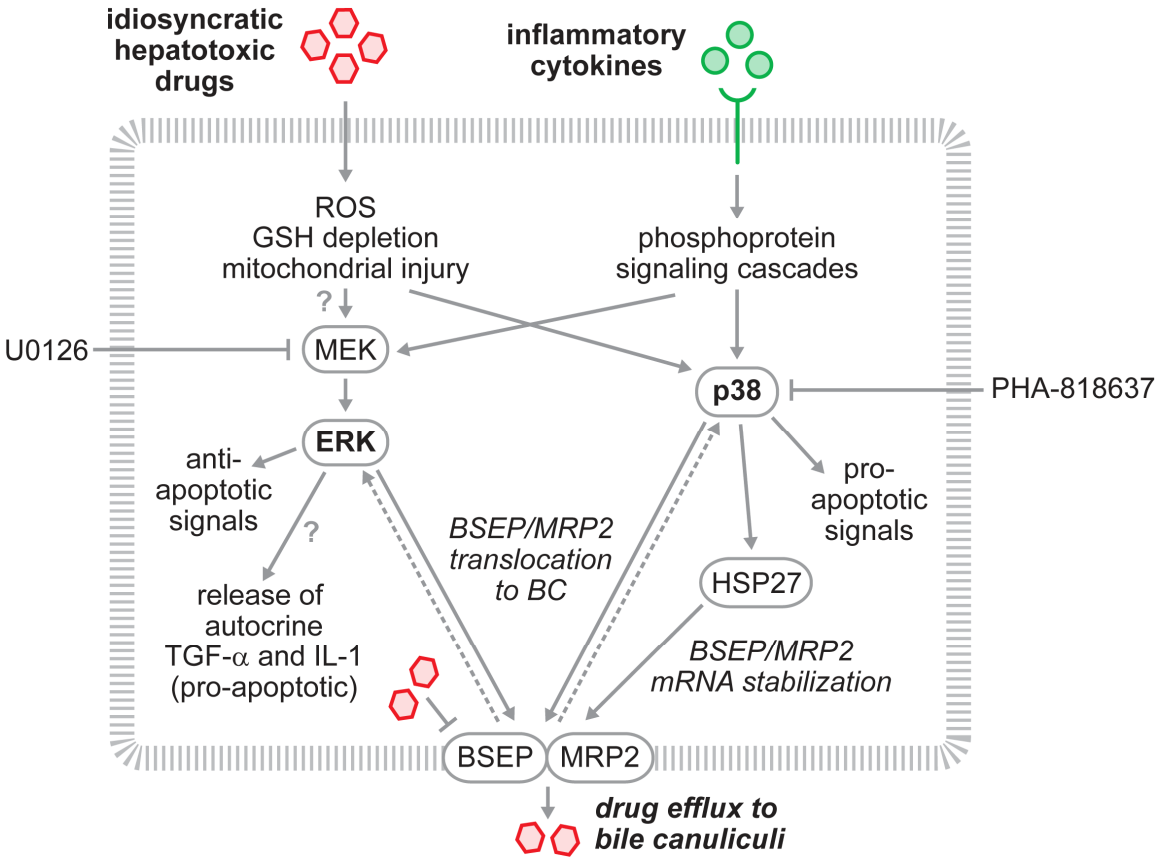

Figure 4-9. MEK–ERK and p38–HSP27 pathways at the confluence of drug/cytokine-induced signaling and drug efflux transporter regulation. Interpretations from the OPLSR model of hepatotoxicity suggest that the MEK–ERK and p38–HSP27 pathways are activated by drug- and/or cytokine treatments and positively regulate the resulting cell death response. Experimentally testing these model interpretations must be made with a complex cellular context in mind. Whereas the MEK–ERK pathway is generally considered pro-survival through its activation of anti-apoptotic effectors such as Bad [157], the p38–HSP27 pathway is generally considered pro-apoptotic due to its transcription regulation of effector caspases [17]. Both pathways have been implicated in the regulation of the translocation of hepatocyte drug efflux transporters, including the bile salt export pump (BSEP) and the conjugate export pump (MRP2), to the bile canaliculi (BC). Consequently, inhibitors of the kinase activities of MEK [158] and p38 [159, 160] decrease drug efflux transporter translocation and activity, leading to cholestasis upon prolonged administration. Possibly due to their inhibition of drug efflux transporter activities or, more likely, in the case of MEK–ERK, due to their perturbation of apoptosis regulatory mechanisms, MEK [161, 162] and p38 [163] inhibitors elicit liver toxicity some cellular and animals models and clinical investigations. Moreover, some hepatotoxic drugs (either directly or through their reactive metabolites) such as nefazodone inhibit BSEP and/or MRP2 activities [138], which can induce transient activation of ERK and p38 signaling and consequently stimulate additional transporter protein translocation to the BC to enable recovery of drug efflux capacity. Additionally, ERK signaling has been associated with controlling the release of EGFR autocrine ligands such as TGF-α [107, 164]. Following TNF stimulation, autocrine TGF-α is contributes to the subsequent release and pro-apoptotic function of autocrine IL-1 in hepatocytes (see Chapter 2 and [77, 129]). Thus, the experimental perturbation of the MEK–ERK and p38–HSP27 pathways must be made with careful consideration to their complex, and possibly counter-acting, functions in response to drug and/or cytokine stimuli.

4.3.4. Kinase inhibition reveals pro-death control of drug- and cytokine-induced hepatotoxicity by the MEK–ERK and p38–HSP27 signaling pathways

The initial 17-phosphoprotein OPLSR model suggested that sustained activation of the MEK–ERK and p38–HSP27 signaling pathways positively contributes to drug- and cytokine-induced hepatocellular death. Whereas the p38–HSP27 pathway is generally considered pro-apoptotic, agreeing with the model predictions, due to its transcription regulation of effector caspases [17], the MEK–ERK pathway is generally considered pro-survival, counter to the model predictions, in hepatocytes through its activation of anti-apoptotic effectors such as Bad [157]. Moreover, the MEK–ERK and p38–HSP27 pathways have complex functions as they are involved in not only apoptosis regulation but also are necessary signals for the proper maintenance of hepatocyte drug efflux transporters such as BSEP (see Figure 4-9 for additional details). As such, inhibition of MEK or p38 kinase activity can perturb drug efflux transporter availability and function [158-160], leading to diminished drug efflux capability and a cholestatic hepatocellular phenotype. And since some MEK [161, 162] and p38 [163] inhibitors elicit liver toxicity in cellular and animal models and clinical investigations, we selected MEK and p38 inhibitors from panel of candidate small molecular inhibitors that were examined for their ability to potently inhibit phosphoprotein signaling and to induce minimal toxicity in human hepatocytes (from donor #3; Figure 4-10). The MEK inhibitors U0126 (10 μM; Figure 4-10B) and PD325901 (1 μM; Figure 4-10D) potently inhibited TGF-α-induced p-ERK1/2 activation, elicited minimal toxicity, and were selected for additional studies. The p38 inhibitors PHA-666859 (1 μM; Figure 4-10K) and PHA-818637 (1 nM; Figure 4-10L) potently inhibited TNF-induced p-HSP27 activation, elicited minimal toxicity, and were selected for additional studies.

These selected MEK and p38 inhibitors were used to evaluate the control of MEK–ERK and p38–HSP27 signaling pathways in drug- and cytokine-induced hepatotoxicity. In human hepatocytes (from donor #4) treated with the clomipramine + cytokine mix both p38 kinase inhibitors, but neither MEK inhibitors, attenuated the observed hepatotoxicity (LDH release measured at t = 24 hr; Figure 4-11B). In human hepatocytes treated with nimesulide + cytokine mix (t = 24 hr; Figure 4-11C), cytokine mix alone (t = 48 hr; Figure 4-11D), and nortriptyline + cytokine mix (t = 48 hr; Figure 4-

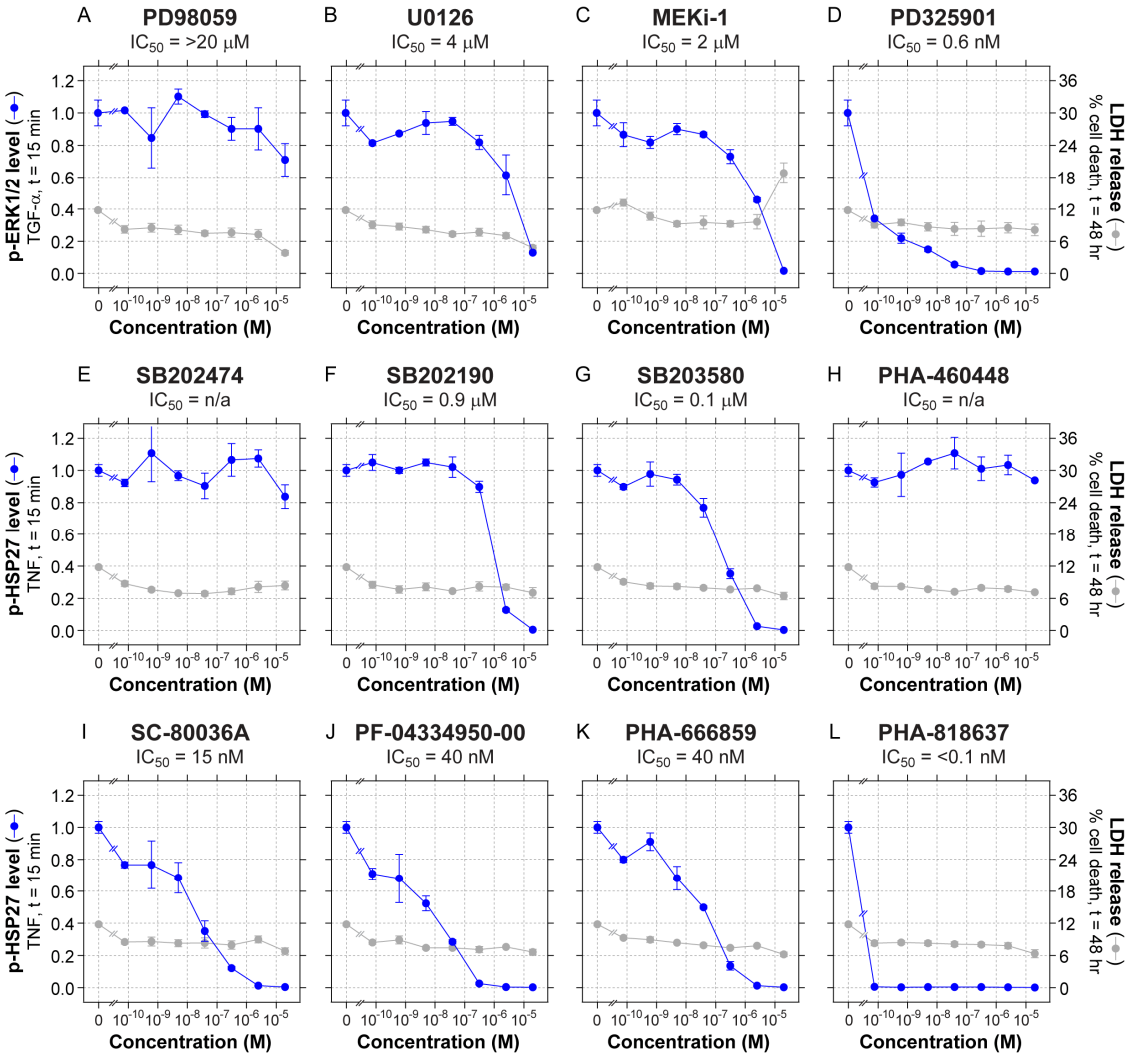

Figure 4-10. Selection of MEK and p38 kinase inhibitors based on potent signaling inhibition efficacy and minimal toxicity in human hepatocytes. MEK (A-D) and p38 (E-L) kinase inhibitors were evaluated for efficacy and toxicity in human hepatocytes (from donor #3) over a range of concentrations at seven 8× serial dilution concentrations from 20 μM (20 μM, 2.5 μM, 0.31 μM, 39 nM, 4.9 nM, 0.61 nM, 76 pM). SB202474 is an inactive control for SB202190 and SB203580. PHA-460448 is an inactive control for the p38 inhibitors in (I) to (L). (A-L) To evaluate MEK and p38 kinase inhibitor toxicity, inhibitors were added at 1× final concentrations in fresh medium for 48 hours, then medium samples were assayed for LDH release. LDH results were normalized to wells from the same culture plate lysed in 1% Triton X for 10 minutes, and values were reported as % cell death, with the lysed samples assumed to represent 100% cell death. (Note that only 20 μM MEKi-1 elicited significant toxicity.) (A-D) To evaluate MEK kinase inhibitor efficacy, human hepatocytes were pretreated with inhibitor for one hour before treatment with 100 ng/ml TGF-α for 15 minutes and then were assayed for p-ERK1/2 activation. (E-L) To evaluate p38 kinase inhibitor efficacy, human hepatocytes were pretreated with inhibitor for one hour before treatment with 100 ng/ml TNF for 15 minutes and then were assayed for p-HSP27 activation. (A-L) Signaling inhibition IC_{50} values were manually estimated from the signaling down-regulation curves by identifying the inhibitor concentrations that elicited half-maximal phosphoprotein activation. The following kinase inhibitors/ concentrations were selected for their potent signaling inhibition and minimal toxicity and were used to perturb kinase activities in drug- and cytokine co-treatment experiments: 10 μM U0126, 1 μM PD325901, 1 μM PHA-666859, and 1 nM PHA-818637. At these concentrations, these inhibitors yield the following reductions in phosphoprotein signaling: U0126, 70% reduction, and PD325901, 99%, for MEK–ERK inhibition; and PHA-666859, 93%, and PHA-818637, 99.5%, for p38–HSP27 inhibition.

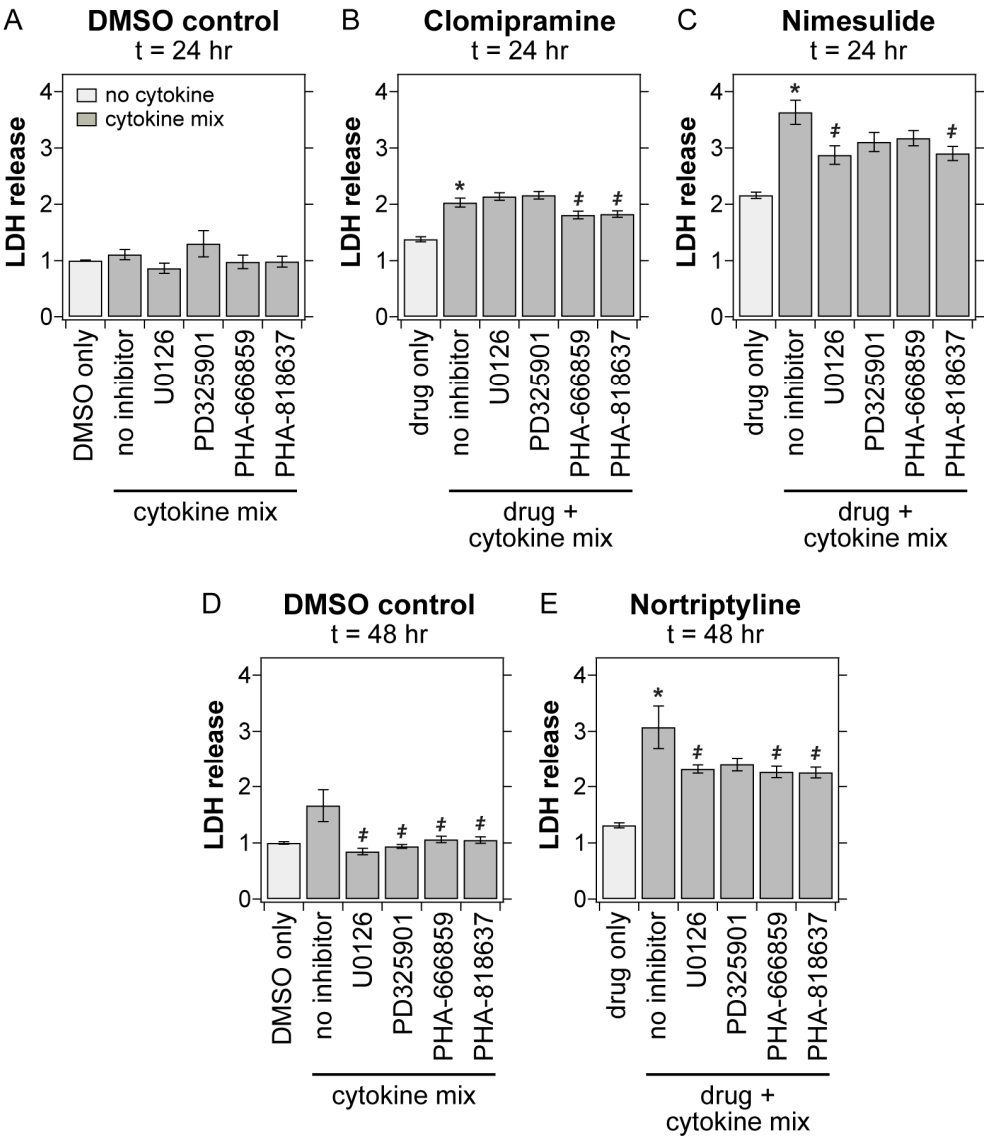

Figure 4-11. Kinase inhibitor perturbation of MEK and p38 signaling demonstrates their pro-death signaling control of drug/cytokine hepatotoxicity synergy. Human hepatocytes (from donor #4) were cultured as described in Chapter 4.2. Cells were treated with drugs (13 μM clomipramine [B], 2.1 mM nimesulide [C], 10 μM nortriptyline [E], or 0.25% DMSO control [A, D]) ± cytokine mix (20 ng/ml IL-1α, 10 μg/ml LPS, 100 ng/ml TNF, and 20 ng/ml IL-6). After 24 or 48 hours, conditioned medium samples were assayed for LDH release. To inhibit MEK kinase activity, cells were pretreated with 10 μM U0126 or 1 μM PD325901 one hour before drug/cytokine stimulation. To inhibit p38 kinase activity, cells were pretreated with 1 μM PHA-666859 or 1 nM PHA-818637 one hour before drug/cytokine stimulation. Data are presented as the mean ± SEM of eight biological replicates. Drug-cytokine mix co-treatment conditions that elicited supra-additive hepatotoxicity synergy, evaluated as described in Chapter 4.2.11, are denoted as (*). Differences between uninhibited and kinase inhibitor pretreatments are labeled as significant (ǂ) if $P < 0.05$ by a Student's *t* test. Kinase inhibitor pretreatments did not significantly perturb cell death responses in the absence of cytokine mix co-stimulation and thus are not shown.

11E), one or both of MEK and p38 kinase inhibitors attenuated the observed hepatotoxicities. These results demonstrate that MEK and p38 signaling both contribute to the induction of hepatocellular death across multiple drug/cytokine mix and cytokine mix-only treatment conditions, confirming the OPLSR model suggestions.

4.3.5. A multipathway OPLSR model predicts MEK and p38 kinase inhibition effects on drug- and cytokine-induced hepatotoxicity with qualitative accuracy

To further test the utility of the reduced 6-phosphoprotein OPLSR model, we asked if it could make accurate *a priori* predictions of kinase inhibitor perturbations of drug- and/or cytokine-induced hepatocellular death. To generate a test signaling data set, we

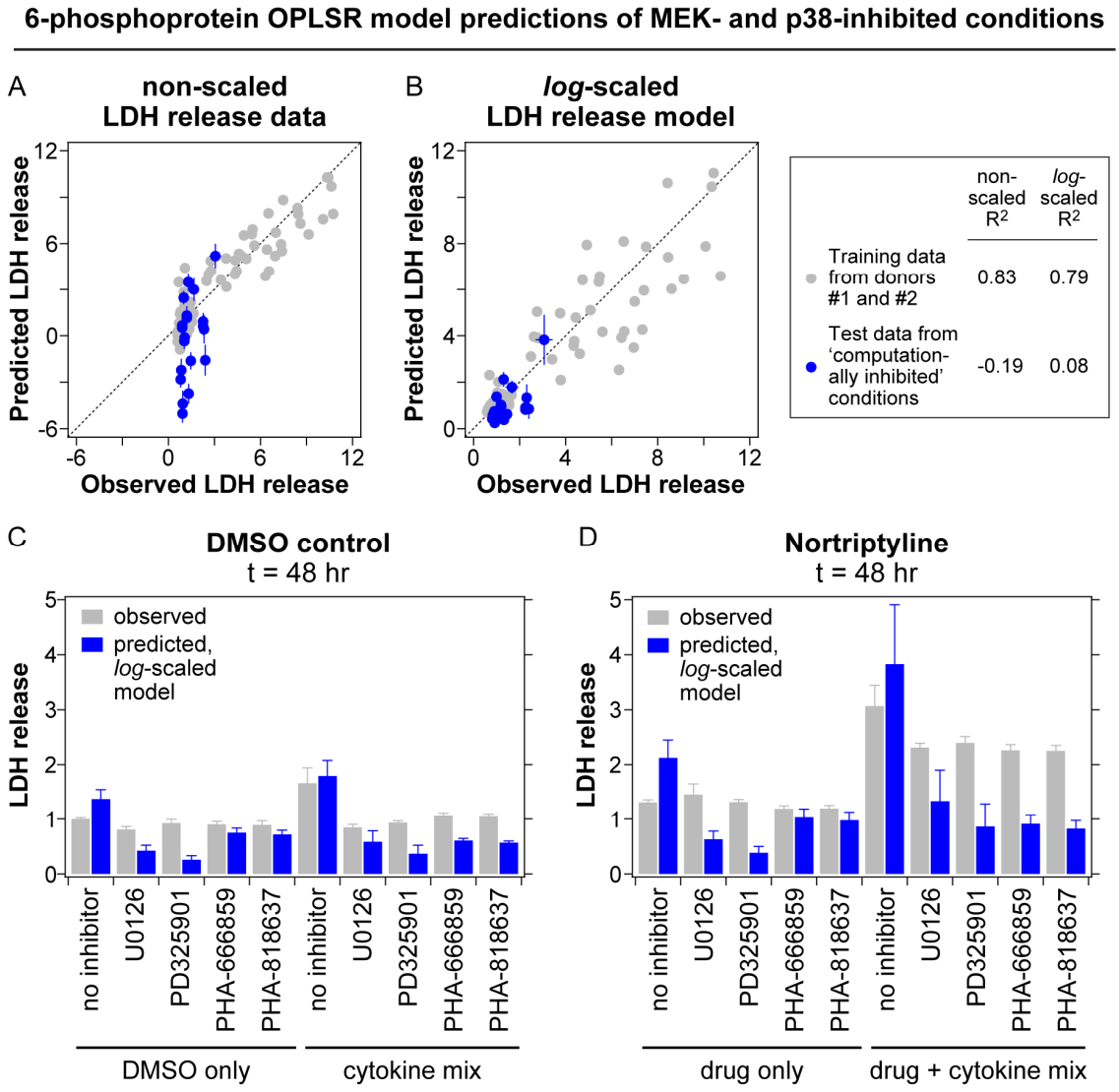

Figure 4-12. (Previous page) OPLSR model makes qualitatively accurate predictions of the effects of MEK and p38 inhibitors in perturbing drug- and cytokine-induced hepatotoxicity. To make *a priori* predictions of a kinase inhibitor perturbation to a drug- and/or cytokine-induced hepatocellular death response, "computationally inhibited" signaling time-courses (based on uninhibited signaling data from donors #1 and/or #2) were generated by reducing the activation of the specific phosphoprotein signaling molecules targeted by a kinase inhibitor by an amount based on the inhibitor's experimentally measurement signaling inhibition (in samples from donor #3; see Figure 4-10). Signaling proteins from pathways not targeted by the kinase inhibitor were left unchanged. These time courses were generated for the treatment conditions of DMSO ± cytokine mix and nortriptyline ± cytokine mix, in the presence or absence of 10 μM U0126, 1 μM PD325901, 1 μM PHA-666859, and 1 nM PHA-818637. After computationally inhibiting the time-point data, the integral and late average metrics were re-calculated, and the resultant computationally-inhibited signaling metric compendium was used to predict cell death responses from trained OPLSR models. See Chapter 4.2.10 for additional details. Model fitness of the predicted inhibitor conditions was assessed by comparing to experimental measurements collected in human hepatocytes from donor #4 (Figure 4-11). Two different 6-phosphoprotein OPLSR models were trained on a fused CSR data compendium from both donors #1 and #2. (A) One model was trained using non-scaled cell death response data. Although this OPLSR model demonstrated good model fitness for the training data (R^2 = 0.83), it poorly predicted the inhibitor test data (R^2 = -0.19) and led to significantly under-predicted cell death responses. (B-D) A second OPLSR model was generated from the fused training compendium by regressing *log*-scaled cell death response data. Logarithmic scaling of response data can provide a more accurate OPLSR model prediction of low response level observations, especially for non-uniformly distributed response data sets (B.D.C., unpublished observations). The *log*-scaled model demonstrated reasonable model fitness for the training data (R^2 = 0.79) but only qualitatively accurate predictions of the test "computationally inhibited" data (R^2 = 0.08). Using a less stringent Pearson correlation metric, the *log*-scaled model yielded correlated prediction of the training (R = 0.90) and test inhibition (R = 0.63) data sets. In (A) to (D), experimental data are presented as mean ± SEM of eight biological replicates. In (A) and (B), model-predicted responses are presented as the mean prediction ± cross-validation standard error, calculated by jack-knifing [155], and experimental and prediction uncertainties are not shown for the training data. In (A) and (B), a one-to-one correlation line demonstrating perfect model fitness (R^2 = 1) is shown for clarity.

"computationally inhibited" signaling time-courses for the DMSO ± cytokine mix and nortriptyline ± cytokine mix conditions using uninhibited signaling data from donors #1 and/or #2 and signaling inhibition data from donor #3. See Chapter 4.2.10 and Figure 4-12 for additional details. Model fitness of the predicted inhibitor conditions was assessed by comparing to experimental measurements collected in human hepatocytes from donor #4 (Figure 4-11). Two different 6-phosphoprotein OPLSR models were trained on a fused CSR data compendium from both donors #1 and #2. One model was trained using non-scaled cell death response data (Figure 4-12A). Although this OPLSR model demonstrated good model fitness for the training data (R^2 = 0.83), it poorly predicted the inhibitor test data (R^2 = -0.19) and led to significantly under-predicted cell death responses. A second OPLSR model was generated from the fused training compendium by regressing *log*-scaled cell death response data (Figure 4-12B-D). Logarithmic scaling of response data can provide a more accurate OPLSR model prediction of low response level observations, especially for non-uniformly distributed response data sets (B.D.C.,

unpublished observations). The *log*-scaled model demonstrated reasonable model fitness for the training data ($R^2 = 0.79$) but only qualitatively accurate predictions of the test inhibitor data ($R^2 = 0.08$). Using a less stringent Pearson correlation metric, the *log*-scaled model generated well-correlated predictions of the training ($R = 0.90$) and test inhibitor ($R = 0.63$) data sets. This demonstrates that the reduced 6-phosphoprotein OPLSR model is capable of qualitatively accurate predictions of kinase inhibitor perturbations to drug- and cytokine-induced hepatotoxicity.

4.4. Discussion

4.4.1. Inflammatory cytokine-associated drug hepatotoxicity is governed by the integrated behavior of multiple intracellular signaling pathways

Through a data-driven modeling approach, we demonstrated that synergistic induction of hepatocellular death by idiosyncratic hepatotoxins and physiologically-relevant inflammatory cytokine co-stimuli is governed by the integrated behaviors of multiple intracellular signaling pathways. From an initial set of 17 phosphoproteins from 8 signaling pathways (MEK–ERK, mTOR–p70 S6K, Akt, IKK–NF-κB, JNK, p38–HSP27, STAT3, and STAT6), cell cycle regulation, and DNA damage signaling, we identified a subset four key signaling pathways that were highly informative to an orthogonal least-squares regression model calibrated on a drug/cytokine-induced data compendium consisting of combinations of 10 drug and 6 cytokine treatments. This informative subset contained two pathways with model-assigned pro-survival functions -- Akt and mTOR–p70 S6K, in agreement with their well-documented survival signaling roles [149, 165] -- and two pathways with model-assigned pro-death functions -- MEK–ERK and p38–HSP27, counter to ERK's canonical role as contributing to survival signaling [157] but in agreement with p38's apoptotic signaling role [17]. Together, these four signaling pathways represent a useful "network gauge" [68] capturing the balance between survival and death signaling in drug- and cytokine-treated hepatocytes. Much effort has been focused on multivariate analyses of gene expression data to predict overt drug hepatotoxicity [166] and inflammation-associated idiosyncratic drug hepatotoxicity [167], but little attention has been focused on phosphoproteomic-based prediction models of liver toxicity. This work demonstrates that quantitatively predictive models of drug-

and cytokine-induced toxicity in human hepatocyte cultures can be generated using as few as four phosphoprotein signals. Furthermore, it shows that hepatotoxicity can be thought of in terms of a "network toxicity", in which the integrated behavior of multiple hepatocellular signaling pathways should be considered in evaluating the hepatotoxicity of a given treatment condition (see Figure 4-13).

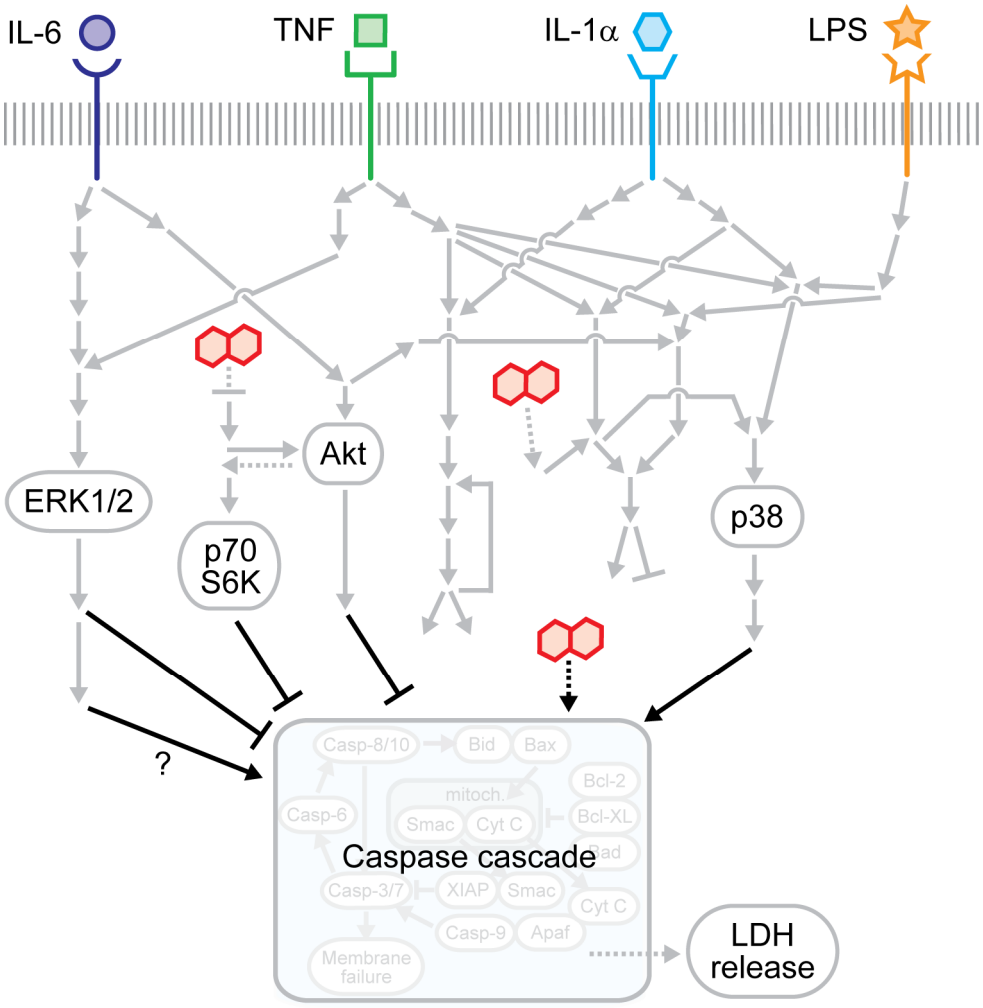

Figure 4-13. Inflammatory cytokine-associated idiosyncratic drug hepatotoxicity as a "network toxicity". The multipathway modeling approach presented here suggests that an integration of multiple intracellular signaling pathway -- namely the MEK–ERK, mTOR–p70 S6K, Akt, and p38–HSP27 pathways -- activities is necessary for hepatocytes to specify death responses to hepatotoxic drug/cytokine co-treatment conditions. This provides motivation of the network-level consideration of multiple survival, stress, and apoptosis signaling pathways in evaluating the hepatotoxicity mechanisms of context-dependent hepatotoxic drugs.

4.4.2. MEK–ERK and p38–HSP27 as pro-death signaling pathways in hepatocytes

Interpretations from the OPLSR model of hepatotoxicity suggested that the MEK–ERK and p38–HSP27 pathways are activated by drug- and/or cytokine treatments and positively regulate the resulting cell death response. In follow up experiments, the model-suggested pro-death signaling contributions were confirmed using small molecule MEK and p38 kinase inhibitors for a select set of drug/cytokine mix synergy conditions.

Both the MEK–ERK and p38–HSP27 pathways operate at the confluence of drug/cytokine-induced signaling and drug efflux transporter regulation (Figure 4-9). Both pathways have been implicated in the regulation of the translocation of hepatocyte drug efflux transporters, including the bile salt export pump (BSEP) and the conjugate export pump (MRP2), to the bile canaliculi (BC). Consequently, inhibitors of the kinase activities of MEK [158] and p38 [159, 160] decrease drug efflux transporter translocation and activity, leading to cholestasis upon prolonged administration. Possibly due to their inhibition of drug efflux transporter activities or more likely, in the case of MEK–ERK, due to their perturbation of apoptosis regulatory mechanisms, some MEK [161, 162] and p38 [163] inhibitors elicit liver toxicity some cellular and animals models and clinical investigations. Moreover, some hepatotoxic drugs (either directly or through their reactive metabolites) such as nefazodone inhibit BSEP and/or MRP2 activities [138], which can induce transient activation of ERK and p38 signaling and consequently stimulate additional transporter protein translocation to the BC to enable recovery of drug efflux capacity.

Still, it is unclear (and not demonstrated in this work), how ERK signaling might potentiate a death response to toxic drug and cytokine co-stimuli conditions. One possibility is through ERK's regulation of protein phosphatases [168] that may act to attenuate signaling in orthogonal, pro-survival pathways. Although these protein phosphatases largely act to dephosphorylate ERK itself and the pro-stress/death kinases JNK and p38 [168], they operate within complex, multi-layered feedback loops [169] that may act, in net, to serve a pro-apoptotic function. Additionally, ERK signaling has been associated with controlling the release of EGFR autocrine ligands such as TGF-α [107, 164]. Following TNF stimulation, autocrine TGF-α is contributes to the subsequent release and pro-apoptotic function of autocrine IL-1 in hepatocytes (see Chapter 2 and

[77, 129]). Thus, it is possible that drug- and/or cytokine-induced ERK activation leads to the release and pro-death activity of autocrine IL-1 ligands. We preliminarily investigated this possible mechanism (see Appendix E), but did not observe any drug-cytokine cell death synergies controlled by autocrine TGF-α or IL-1 activities. Additional investigations in the role of these autocrine ligands under a more well-selected set of drug/cytokine treatment conditions may prove fruitful.

4.4.3. Hepatotoxicity predictions across human hepatocyte donors via OPLSR modeling

An OPLSR model using data from six phosphoproteins from the four informative "network gauge" pathways demonstrated accurate predictions of hepatotoxicities induced by drug/cytokine treatments across two human donors, but only for non-outlier drug/cytokine treatments present in the training data. The model's ability to successfully predict hepatotoxicity signaling-response relationships across human hepatocyte donors for similar drug/cytokine conditions suggests that hepatocytes from multiple human donors share a "common effector" processing function [64]. This common effector processing function is captured in the model regression coefficients and allows for quantitatively accurate predictions of donor-specific cell death responses based on donor-specific signaling network activation (see Figure 4-8). To generate a model with more robust prediction accuracies in additional human hepatocyte donors, especially for hepatotoxicity conditions not present in the model training, it is likely that additional phosphoprotein signaling pathways, such as the stress- and cytokine-induced JNK pathway, will have to be included in the model and the model will have to be trained under an even more diverse set of drug/cytokine-conditions. Increased model utility could also be demonstrated by showing that this "common effector" processing function is shared across hepatocytic cell systems, such as between primary rat hepatocytes and primary human hepatocytes. If so, this would allow for robust model training in more readily available cell systems.

4.4.4. Implementation of multipathway modeling in more physiologically relevant hepatotoxicity models

As discussed in Chapter 3.4.4, *in vitro* studies of drug-cytokine hepatotoxicity relationships will likely be benefited by the use of tissue-engineered hepatocyte cell culture systems that allow for prolonged maintenance of differentiated hepatocellular function and are assessable in reasonably high-throughput manner. This work presents an example of the utility of large-scale cue-signal-response data compendia modeling to identify salient phosphoprotein signaling mechanisms governing drug- and cytokine-induced hepatotoxicities in standard Matrigel-overlay cultures of primary human hepatocytes. Considering the future directions of *in vitro* hepatotoxicity evaluations towards more physiologically relevant tissue-engineered culture systems, our work motivates additional efforts to bring the tools and techniques of "systems"-level biology to bare on the challenges of investigating physiologically-complex *in vitro* tissue models. This leads to a discussion in Chapter 5.2 how such systems biology approaches might be more fully implemented in microenvironmentally complex tissue-engineered culture systems.

CHAPTER 5

Future directions

5.1. Assaying autocrine signaling in *in vivo* biology

In Chapter 2, we demonstrated that hepatocyte responses to TNF are regulated by an inducible, coupled, and self-antagonizing TGF-α–IL-1α/β–IL-1ra autocrine cascade that contributes to multiple intracellular signaling pathways that govern both hepatocyte proliferation and apoptosis. This autocrine cascade promotes both TNF-induced apoptosis in hepatocytes infected with an adenoviral vector and TNF-induced proliferation in the absence of viral infection. These and other recent findings illustrate the integral role of autocrine factors in hepatocyte proliferation, apoptosis, survival [114], and transformation [88] responses to exogenous cytokine stimuli and implicate diverse autocrine signaling connections between cytotoxic, inflammatory, and mitogenic ligands in hepatocytes. Further development of animal models and quantitative *in vivo* signaling tools will be critical to parse the complex autocrine and paracrine signaling mechanisms regulating autocrine signaling in hepatocytes and other liver cell types *in vivo* and to validate any therapeutic interventions directed towards the autocrine control mechanisms. More generally, such tools would useful to interrogate aberrant autocrine signaling mechanisms related to human disease and cancer [170]. This section discusses the motivation for and application of non-invasive molecular imaging tools to the study of *in vivo* autocrine signal transduction.

An increasing array of molecular imaging tools are available to interrogate the *in vivo* activities of specific signaling molecules. These molecular imaging tools are useful not only for use in experimental animal models but also for improved diagnostics in human patients. Ideally, the study of *in vivo* signal transduction would focus on informative signaling molecules governing the key cellular behaviors, such as the survival–death decision process. Amongst these key signaling molecules are a series of intracellular kinases, such as Akt and ERK, that serve as signaling hubs that are activated by a variety of growth factor and matrix stimulatory cues and promote cell survival and migration (see Chapter 4). A number of molecular imaging methods have been validated

to study the activities of these kinases in living cells and animals. These include bioluminescence and fluorescence approaches requiring stably transfected constructs that are predominantly activated by the activity of a kinase enzyme of interest through its phosphorylation of a consensus peptide sequence present on the expressed peptide [171-173]. Unfortunately, these methods require either the intracellular delivery of the kinase-activated peptide sequence or transfection with a vector expressing this peptide; both having limited potential to serve as a noninvasive molecular imaging platform for imaging cellular signal transduction in human subjects. Consequently, noninvasive molecular imaging approaches to assess *in vivo* signal transduction have, to date, focused on probing cells via their expression of cell surface receptors of growth factor or adhesion ligands associated with disease or cancer. Amongst these probed receptors are those of the ErbB family of receptor tyrosine kinases, whose dysregulated signaling are implicated in various mechanisms of cancer progression [174] and whose activities are implicitly involved in the TNF–TGF-α–IL-1–IL-1ra autocrine cascade examined in Chapter 2.

The ligands for EGFR and other ErbB receptors are expressed as membrane-bound peptides that are proteolytically cleaved for release and eventual receptor binding. EGFR ligands are cleaved and released by members of the ADAM family of proteases with EGF processed by ADAM10 and TGF-α, HB-EGF, and amphiregulin (and also the inflammatory cytokine TNF) processed by ADAM17. These proteases recognize and cleave the transmembrane peptide precursors to the mature ligands at conserved ~15-20 amino acid sequences in their ectodomain regions [175]. The activity of ADAM proteases is controlled by phosphorylation of their intracellular domains, which is mediated by ERK and p38 kinase signaling [176]. Consequently, ADAM proteases act in part of a positive feedback loop between EGFR stimulation, ERK/p38 activation, and EGFR ligand release [177]. As such, ADAM10/17 proteases can serve as extracellular readouts of EGFR activity and its downstream signaling. The release and autocrine signaling of the EGFR ligands TGF-α and amphiregulin are activated by G-couple protein receptor signaling, the cytokines IL-6 and TNF, and also EGFR ligands themselves. The development of molecular imaging tools to assay autocrine ligand production (namely for EGFR and IL-1R ligands) will be an important step for providing quantitative assessment of multiple signal transduction pathways *in vivo*. Since autocrine

ligands are released into circulation in only negligible quantities and receptor expression levels do not accurately reflect their signaling activity, the most direct and tractable target of noninvasive molecular imaging probes of autocrine ligand production is the activity of the transmembrane proteases (such as ADAM17 and ICE) that regulate their release; moreover, the development of multiplexible probes will critical to investigate the complex, inter-related autocrine signaling mechanisms.

Initial efforts to develop multiplexible autocrine ligand protease-dependent optical imaging probes could focus on the proteases ADAM10 (involved in release of EGF), ADAM17 (involved in release of TGF-α, amphiregulin, etc.), and ICE (as known as caspase-1; involved in release of IL-1β). Numerous classes of extracellular proteases have been targeted for activity-based optical imaging probes including calpains [178], cathepsins [179], MMP's [180], and caspases [181], but ICE is the only autocrine ligand protease that has been previously assayed by molecular imaging [182]. To simultaneously interrogate these three autocrine ligand proteases, three multiplexible optical imaging probes could be developed: two quenched near-IR peptide-based sensors, each containing an NIR emitter (Cy5.5 or AF750), a NIR absorber, and protease-selective sequence encoding the consensus cleavage sequence for ADAM10 or ADAM17, and one bioluminescence sensor, whose luciferase activity is dependent on peptide cleavage by ICE. These three multiplexed probes could be imaged by multichannel NIRF and would have some ability to be imaged in deep tissues of small animals. The multiplexing ability of these probes would have to be validated *in vitro* using recombinant proteases and cell lines expressing each of the proteases (*e.g.* the breast cancer cell line T4-2). Additionally, the specificity of these probes would have to be examined using scrambled protease-cleavage sequences and improved specificity from consensus cleavage sequences could be obtained by sequence evolution strategies. Then, these multiplexed probes could be evaluated in xenograft models [183], in which they could be used to probe not only autocrine protease activity in various stages of cancer progression but also be used to directly assay the efficacy of proposed anti-cancer therapies such as autocrine ligand protease small molecule inhibitors (*e.g.* TAPI-2 for ADAM10/17 and Z-VAD-FMK for ICE) or siRNA. These studies could be used to parse the mechanistic

relationships between autocrine EGFR and IL-1R signaling and cancer progression in xenografts and models of liver, colon, and breast cancer.

In general, molecular imaging probes of autocrine ligand protease activities offer the opportunity to assay cell signal transduction via extracellularly accessible proteases and could be implemented in a multiplexible and noninvasive manner. In the future, these probes could provide early detection of aberrant autocrine signaling mechanisms related to cancer and thus improve disease diagnosis. More immediately, they will serve as a much-needed tool set for interrogating the role of autocrine ligand signaling in experiment animal models and generate new insights to its roles in tissue homeostasis and pathophysiology. The improvements to multiplex nature of these probes could bring systems biology approaches to noninvasive molecular imaging in whole animals through the simultaneous and repeatable quantitative assessment of multiple signal transduction pathways and its ability inform interpretive and predictive multivariate models of *in vivo* signal transduction.

5.2. Systems biology approaches for tissue engineering

As discussed in Chapters 3.4.4 and 4.4.4, *in vitro* studies of drug-cytokine hepatotoxicity relationships will likely be benefited by the use of tissue-engineered hepatocyte cell culture systems that allow for prolonged maintenance of differentiated hepatocellular function and are assessable in reasonably high-throughput manner. The findings in Chapter 4 present an example of the utility of large-scale cue-signal-response data compendia modeling to identify salient phosphoprotein signaling mechanisms governing drug- and cytokine-induced hepatotoxicities in primary human hepatocytes. Considering the future directions of *in vitro* hepatotoxicity evaluations (towards more physiologically relevant tissue-engineered culture systems), our work motivates additional efforts to bring the tools and techniques of "systems"-level biology to bare on the challenges of investigating physiologically-complex *in vitro* tissue models. This section contains a discussion how such systems biology approaches might be more fully implemented in microenvironmentally complex tissue-engineered culture systems.

5.2.1. Tissue engineering

Tissue engineering is a biotechnology centered on developing materials, scaffolds, or devices that provide biochemical and biophysical cues to facilitate cell survival, proliferation, differentiation, and organization into functional three-dimensional (3D) tissues [184]. The field of tissue engineering began decades ago with a focus on *in vivo* therapeutic constructs, but has progressed to now include a substantial emphasis on the likely greater impact of providing more effective experimental systems for studying complex human tissue physiology and pathophysiology *in vitro* [185]. This direction emerged in part because animal models fail to capture many crucial facets of human physiology, notably in the areas of tissue-specific transcriptional regulation [186], drug-induced liver toxicity [8], pathogenic infection, host immune responses, and cancer [187, 188]. Further, though human cells cultured in standard formats can be adapted to high-throughput assays, most scalable cell cultures lack physiologically relevant microenvironmental stimuli of native tissues. Engineered tissues built with human cells are thus being developed for a range of application areas, including hepatic drug metabolism and toxicity [8, 189, 190], mammary gland morphogenesis and oncogenesis [191, 192], lymphoid tissue neogenesis [193, 194], and stem cell differentiation [195], and offer promise for scaling to the data collection demands of high-throughput screening and systems biology.

In tissues, individual cells are stimulated by a diverse set of microenvironmental cues that arise from adhesion to extracellular matrix (ECM) components, mechanical forces, and soluble signaling factors from adjacent and distant cells [185]. Together, these cues activate a system of cell signaling pathways whose integrated operation regulates cell behavioral phenotypes [196]. Resultant cell behaviors are dependent not only on which microenvironmental cues are present, but also on their quantitative amounts, spatial arrangements, and temporal sequences. A central challenge in tissue engineering is to elicit and maintain desired cell behaviors through externally-applied and -induced chemical signals and mechanical forces in a predictable fashion. A tremendous diversity of tools – including biomaterials, bioreactors, and microfabricated devices – have been developed to manipulate tissue microenvironments [185, 197]. Design principles for deploying these tools are likewise emerging, but they are primarily aimed

at relating the magnitude of select external cues directly to cell phenotypic behaviors through quantitative analysis of molecular diffusion, convection, reaction, binding, and consumption [185, 198]. In increasingly complex engineered microenvironments, detailed understanding of how the multitude of cell signaling pathways process various microenvironmental cues to govern their behaviors will require application of systems-level approaches. To this end, systems biology offers a powerful new tool for the design and analysis of engineered tissues.

This discussion focuses on molecular-level models that attempt to relate microenvironment stimuli to intracellular signal transduction pathways and their regulation of cellular behavioral responses. (For discussion of systems-level modeling of transcription and metabolism, see references [45, 199].) Although some promising systems-level studies [195, 200-202] have been examined in contexts that capture some of the physiological complexity of native tissues, systems-level cell signaling-response measurements and models, to date, have been largely implemented in simple, "prototypical" experimental contexts. Consequently, we focus on how systems biology might be more fully integrated into the design and analysis of engineered tissues.

5.2.2. Fusing tissue engineering and multivariate measurement methods

Systems-level models require experimental data of activities of multiple cell signaling molecules and behavioral phenotypes across a diverse combination of treatments, perturbations, and time points. Accordingly, they require cell culture systems that are both addressable in a high-throughput manner and amenable to multivariate measurement methods. Recent advances offer promise for parallelizing the culture of microenvironmentally complex engineered tissues (in so-called "multicellular arrays" or "tissue arrays") sufficient to meet the data demands of systems biology. Culture arrays have risen out of the desire to screen phenotypes of multicellular structures in a high-throughput manner, and have been applied to drug discovery [203] and toxicology [190] and combinatorial approaches to directing and maintaining cell differentiation [202, 204-206]. Such combinatorial screens of cell differentiation have provided unexpected insights into relationships between multiple microenvironmental cues [205] (*e.g.* printed ECM ligands) or intracellular signals [65, 202] and the maintenance of differentiated

phenotypes through multiparameter analyses. (Note that we refer to culture arrays with ~10^2-10^3 cells per spot or well as "tissue microarrays" and those with ~10^5-10^6 cells per sample well as "multiwell-format tissue arrays".)

We emphasize that systems biology models to date have focused on responses to "acute", bolus administration of cytokines and growth factors and thus have inferred substantial predictive significance to the transient signals and derived time course metrics immediately following receptor activation [50]. However, in tissue engineered constructs as in physiological contexts, most cell behaviors more likely are governed by longer time-scale stimuli, under more "chronic", quasi-steady-state conditions. There might indeed be significant differences in relationships between cues, signals, and responses for chronic as opposed to acute cue treatment, as in a recent report of important pathophysiological differences in 2D mammary epithelial migration by autocrine ligands or bolus stimulation from exogenously-added ligand [107].

5.2.3. Tissue microarrays

Efforts in developing tissue microarrays have been focused on validating consistency of cellular phenotypes and assays such as drug-induced hepatocyte toxicity [190, 207], stem cell differentiation [204], and epithelial tissue organization [208, 209], and have not been used to systematically examine cue- or signal-response relationships. A tissue microarray system well-suited for systems biology approaches is that of mammary epithelial cells in microprinted Matrigel cultures [209]. Matrigel culture of mammary epithelial cells fosters the establishment of 3D multicellular structures that resemble *in vivo* mammary gland acini, with the development epithelial cell structures that resemble either normal or cancerous mammary acini depending on a well-documented variety of both microenvironmental cues (such as matrix mechanical stiffness and composition and growth factor stimulation) and oncogenic perturbations [191, 192, 210, 211]. As of yet, tissue microarrays have not been adapted to allow inclusion of ECM components with a combinatorial complexity matching that used in the 2D microprinting methods [205] which will be necessary for systematic investigation of cellular cue-signal-response relationships.

Although tissue microarrays could be scaled to be amenable to lysate-based measurements (requiring ~10^5 cells), they are nonetheless appropriate for systems biology approaches, such as Bayesian network inference, that are based on data from single cells or small populations of cells examined over a multitude of conditions. Critical will be the adaption of single-cell multivariate measurement techniques of flow and image cytometry for use in 3D engineered tissues. Multicolor flow cytometry for quantifying multiple phosphoproteins has been carefully validated [55] and implemented [56, 212] for non-adherent cells but not adherent cells. Multicolor flow cytometry in adherent cells, especially from intact 3D tissues, is a significant challenge as single-cell isolation methods can elicit stress-related signaling themselves and thus disturb signaling network states. Further, prolonged isolation requirements could restrict the ability to measure the highly-informative phosphorylation events that follow within minutes of cell stimulation. In contrast, image cytometry does not require isolation and permits for immediate cell fixation, allowing for sufficient temporal resolution to measure immediate phosphorylation events. Instead, it is currently limited in its ability to include more than ~4 simultaneous single-cell measurements due technical constraints [58]. Multicolor 3D imaging (so-called "tissue cytometry" [57]) using confocal microscopy is not yet sufficiently high-throughput to capture multivariate single-cell data across hundreds of tissue samples in an automated fashion. Improvements in 3D imaging with respect to these limitations could make it a highly attractive approach for system-level, single-cell data acquisition, especially in the context of engineered tissues, such as immunological synapse arrays [213], whose cellular behaviors are dependent on microscale patterning of stimulatory cues thus necessitate spatially-resolved single-cell data.

Immunofluorescence methods, such as in-cell westerns, which are reasonably high-throughput but not strictly multiplexible, could be used to measure phosphoprotein levels or cell phenotypes in small populations of cells (~10^2-10^3) within tissue microarrays. In-cell western measurements of arrayed tissues over a large combination of treatment conditions, assay targets, and, likely, sample replicates could yield a data set sufficient for Bayesian models. As in-cell western measurements are not multiplexible, multivariate data sets will require assembly from multiple independent samples of cells, thus obscuring the single-cell covariations of signaling activities that are particularly

informative in Bayesian models [56]. Consequently, a substantial set of microenvironmental stimuli combinations (~100) might be required for accurate Bayesian network inference. Moreover, care must be taken to insure that the biological heterogeneity, due to the small number of cells per sample, and measurement inaccuracy, which often arises due to the restrictive dynamic range of in-cell westerns, does not confound multivariate measurement fusion.

5.2.4. Multiwell-format tissue arrays

Multiwell-format tissue arrays [8, 10] are based on 12- or 24-well culture formats and can accommodate ~10^5-10^6 cells per sample well (sufficient for lysate-based measurements) and be scaled to a moderate number of sample conditions (*i.e.* treatments, time points) and thus are suitable for a greater diversity of systems-level modeling approaches than tissue microarrays. A well-developed example of these multiwell-format tissue arrays that utilizes a 3D microenvironment is a perfused liver cell microreactor [8, 10]. Perfused microreactors foster the maintenance of *in vivo*-like function of primary hepatocytes [8] and/or liver sinusoidal endothelial cells [94] over a prolonged culture duration (~14 days) in a physiologically-relevant 3D microenvironment. And, as such, have been used examine hepatic drug metabolism and enzyme induction [8] and sinusoidal morphogenesis [94] over physiologically-relevant time scales.

The larger cell numbers per sample permit lysate methods such as bead-based arrays [52] and multiplexed kinase activity assays [48] to be utilized in addition to multicolor flow and image cytometry (given the aforementioned improvements) to measure cell signaling activities and phenotypes in a multivariate manner. Bead-based phosphoprotein arrays allow for a greater number of measureable signaling molecules as they are benefited by an expansive set of validated, multiplexible reagents, while kinase activity assays have the advantage of measuring signal transduction activity directly, rather than inferred via phosphorylation state. Consequently, activity data from kinases, especially of those thought to be at nodes of signaling networks that integrate multiple pathways, are often found to be highly informative signals in PLSR cell signaling-response models trained on protein signaling data from heterogeneous assays [50, 62]. Practical limitations on cell material and knowledge of which protein signaling assays

have been informative previously [50] together suggest that PLSR models using multiwell-format tissue arrays might be best constructed using ~2-3 kinase assays and ~10 bead-based phosphoprotein measurements (all from a single lysate) of proteins distributed across multiple cell signaling pathways. A challenge in multivariate measurement of engineered liver cell co-cultures (usually containing hepatocytes and second liver cell type) is the correct attribution of signaling profiles to each of the multiple cell types present. Flow cytometry methods can simply employ one staining channel to a cell type marker, but lysate based methods require less straight-forward approaches such as those that rely on biomolecular mixture models [214] to infer cell type-specific phosphoprotein profiles.

5.2.5. Implementing systems-level modeling for the design and analysis of engineered tissues

In contrast to the fields of genomics and proteomics, a systems biology approach insists that knowledge and understanding about biology resides not in databases but instead in models – and that given the complexity of multivariate experimental measurements these models must be computational in nature. Thus, the data generated in tissue engineering contexts as discussed in the previous section will be most gainfully employed by analysis in terms of one or more of the data-driven modeling methods described earlier.

Data-driven models of dynamic, multivariate cell signaling and response data can suggest hypotheses that relate activities of signaling molecules to behavioral phenotypes and can be implemented to generate *a priori* predictions of responses to new signaling network profiles. Such models are most effectively constructed on the basis of training across a broad landscape of conditions, including conflicting or antagonizing cues, that stimulate a diversity of signaling network activities and cell responses that might be hypothesized to comprehend a range of physiological phenotypic behaviors (see Chapter 4 and [62, 64, 66, 68]). Prediction of cell behavior can then be effectively interpolative rather than extrapolative. *A priori* prediction of cell phenotypes based on signaling network states could lead to the identification nonintuitive combinations to signaling activities (through computation searches, for example) that optimally produce a desired cell phenotype in an engineered tissue. Design of novel engineered tissue micro-

environments that generate the optimal signaling network state could be furthermore governed by physicochemical models of receptor activation and downstream signaling, thus integrating mechanistic and data-driven model approaches [72] to design features for fostering desired tissue phenotypes. Moreover, models of cell behavior within a tissue engineered to mimic a particular physiology or pathophysiology could yield models capable of predictions of drug efficacy and toxicity in physiologically-relevant, tissue-specific contexts. In particular, such approaches could be used to select target pathways for interfering with 3D cell migration behaviors critical to cancer metastasis [215, 216] and matrix stiffness-induced mammary acinar oncogenesis [210]. For instance, successful *a priori* PLSR model prediction of cell phenotypic changes due to perturbation by one or more small molecular inhibitor(s) has been verified for compounds with specified kinase targets that lie upstream of protein signal(s) contained in the model and implemented by "computationally inhibiting" only the measured signals in a subset of the training data and then comparing the predicted results to new experiment observations (see [64, 66] and Chapter 4). Perturbations that affect signaling networks more globally (therefore less predictably) such as growth factor receptor overexpression [68], disruption of autocrine ligand signaling [62], and RNA interference [67] have been evaluated using complete re-collection of signaling data rather than the straightforward estimation methods successful for small molecular inhibitors. When measuring multiple diverse kinds of cell phenotypic behaviors, as is desired for understanding complex tissue physiology, constructing separate submodels for the various behaviors might allow for easier interpretation of the various respective signaling-response relationships.

Decision tree and Bayesian network models can extend predictive capabilities to causality, more strongly indicating molecular mechanisms. For example, a Bayesian network model for the signaling network regulating differentiation versus self-renewal processes of mouse embryonic stem cells permitted experimentally validated prediction of effects of Raf-1 independent of the canonical Raf–MEK–ERK pathway [217]. Analogously, one can envision developing a similar predictive capability for signals governing lineage specification of mesenchymal stem cells cultured in complex 3D microenvironments containing varying adhesion ligands, matrix rigidities, and growth factors [217]. Likewise, predicted signaling network influences could suggest

microenvironmental cue and pharmacological intervention combinations for influencing osteoblast specification for implantable bone regeneration therapies [217].

Moreover, Bayesian network inference approaches could ask fundamental questions about the perhaps subtle differences in signaling network structure and function in cells of varying lineages and disease states and how those networks diverge from canonical models [212]. Such understanding could drive clinical therapies that are motivated by context-specific cell signaling networks. Bayesian approaches could be employed in the challenging task of investigating the crosstalk between multiple cell types in healthy or diseased tissues. By engineering tissue arrays that contain multiple interacting cell types, such as the immune system cells within a lymph node [193] or the varied cells within the liver [94], and measuring both cell type-specific phosphoprotein signaling and levels of soluble or matrix-related signaling factors, Bayesian network inference models can be constructed to provide mechanistic hypotheses for complex cellular crosstalk in tissues.

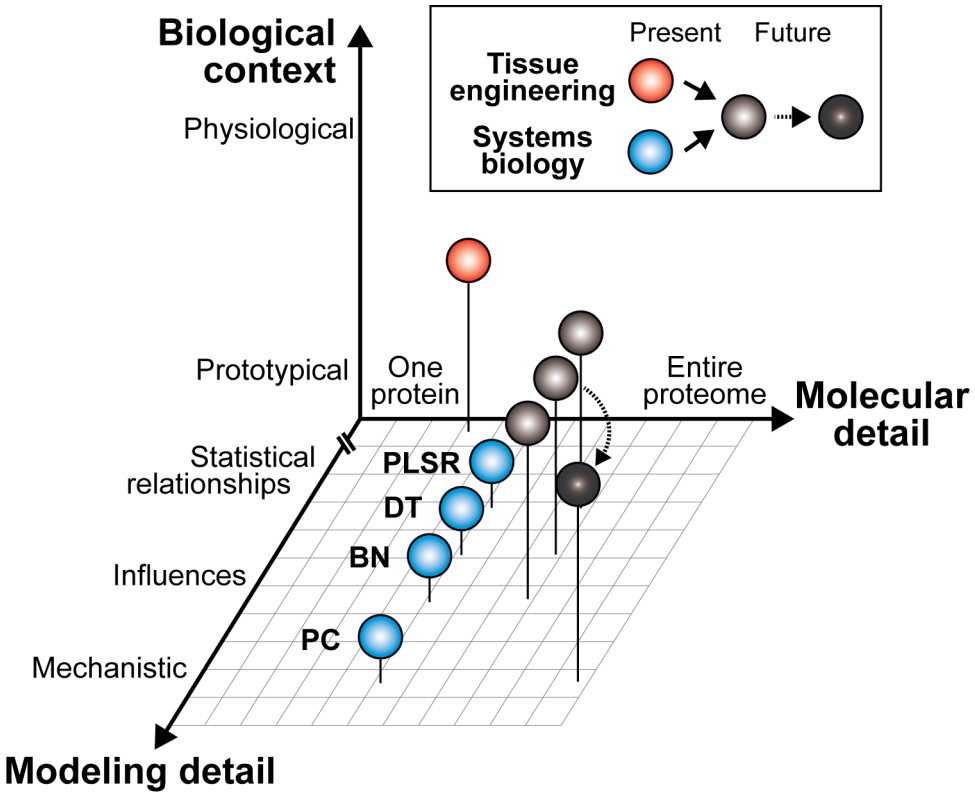

Figure 5-1. The scope of measurement and modeling in systems biology and tissue engineering. The present and future implementation of systems biology and tissue engineering are depicted with respect to: biological context (ranging from prototypical cell lines to engineered and native tissues to whole organisms); modeling detail (ranging from statistical models to influence models to mechanistic models); and molecular detail (ranging from a single protein to the entire proteome). To date, tissue engineering has been focused on the recapitulation of the physiological complexity of native tissues but has not been studied in great molecular detail nor has been fused with systems-level computational modeling efforts. In contrast, systems-level computational models, such as partial least-squares regression (PLSR), decision trees (DT), Bayesian networks (BN), and physicochemical (PC) models, can interpret a variety of molecular relationships governing cellular behavior but have been studied largely in a prototypical biological context (*e.g.* cell lines). Future fusion of tissue engineering and system biology will require adaption of tissue engineering to the measurement demands systems-level computational models. Considering these demands, PLSR, DT, and Bayesian models provide attractive candidates for analysis of cell behaviors within engineered tissues in the near future. More substantial progress in tissue engineering and multivariate measurement technologies will be required for implementation of models with more mechanistic and molecular detail.

Appendix A

Abbreviations

2D	two-dimensional
3D	three-dimensional
ADAM	a disintegrin and metalloproteinase protein
Adv	adenoviral vector
Akt	serine-threonine protein kinase B (PKB)/Akt
ANOVA	analysis of variance
AP-1	activator protein 1
APAP	acetaminophen
ASK1	apoptosis signal-regulating kinase 1
ASP	aspirin
BC	bile canaliculi
BCA	bicinchonicic assay
BID	BH3 interacting domain death agonist
BN	Bayesian network
BrdU	5-bromo-2'-deoxyuridine
BSA	bovine serum albumin
BSEP	bile salt export pump
BUS	buspirone
β-gal	β-galactosidase
C/EBP	CCAAT-enhancer-binding protein
CAR	coxsackie- and adenovirus-receptor
CHL	chlorpromazine
CIM	cimetidine
CLA	clarithromycin
CLO	clomipramine
C_{max}	average plasma maximum drug concentration

CM-H_2DCDA	5-(and-6)-chloromethyl-2’7’-dichlorodihydrofluorescein diacetate acetyl ester
CREB	cAMP response element binding
CSR	cue-signal-response
DILI	drug-induced liver injury
DMEM	Dulbecco’s Modified Eagle’s Medium
DMSO	dimethyl sulfoxide
DRAQ5	1,5-bis{[2-(di-methylamino)ethyl]amino}-4,8-dihydroxyanthracene-9,10-dione
DT	decision tree
ECM	extracellular matrix
EGF	epidermal growth factor
EGFR	epidermal growth factor receptor
ELISA	enzyme-linked immunoabsorbant assay
EMEM	Eagle’s minimum essential medium
ERK	extracellular signal-regulated kinase
FADD	Fas-associated death domain protein
FBS	fetal bovine serum
G2	HepG2 cells
gp130	glycoprotein 130
Grb-2	growth factor receptor-bound protein-2
GSH	glutathione
GSK-3α/β	glycogen synthase kinase-3α/β
HB-EGF	heparin-binding EGF-like growth factor
HBSS	Hank’s Balanced Salt Solution
HEPES	4-(2-hydroxyethyl)-1-piperazineethanesulfonic acid
HGF	hepatocyte growth factor
HGM	hepatocyte growth medium
HH	primary human hepatocytes
HNF	hepatocyte nuclear factor
HSP27	heat shock protein 27

ICE	also known as caspase 1
IFN-γ	interferon-γ
IKK	inhibitor of nuclear factor-κB (IκB) kinase
IL-10	interleukin-10
IL-1R	interleukin-1 receptor
IL-1ra	interleukin-1 receptor antagonist
IL-1α/β	interleukin-1α/β
IL-6	interleukin-6
IL-6R	interleukin-6 receptor
iNOS	inducible nitric oxide synthases
IRS-1	insulin receptor substrate-1
IκB-α	inhibitor of nuclear factor-κB-α
JAK	Janus kinase
JNK	c-Jun N-terminal kinase
LDH	lactate dehydrogenase
LEV	levofloxacin
LPS	lipopolysaccharide
mBCl	monochlorobimane
MEK	MAPK-ERK kinase
MEKK1	MAPK-ERK kinase kinase 1
MEX	mexiletine
MMP-3	matrix metalloproteinase-3
MOI	multiplicity of infection
MRP2	conjugate export pump
MtMP	mitochondrial membrane potential
mTOR	mammalian target of rapamycin
NEF	nefazodone
NF-κB	nuclear factor-κB
NIM	nimesulide
NIPALS	non-linear iterative partial least-squares
NO	nitric oxide

NOR	nortriptyline
NPC	non-parenchymal cell
NSAID	non-steroidal anti-inflammatory drug
OPLSR	orthogonal partial least-squares regression
p38	p38 mitogen-activated protein kinase (MAPK)
p70 S6K	p70 S6 protein kinase
p90 RSK	p90 ribosomal S6 kinase
PARP	poly(ADP-ribose) polymerase
PBS	phosphate buffered saline
PBS-T	PBS with 0.1% Tween-20
PBS-TB	PBS with 0.1% Tween-20 and 1% BSA
PC	principal component
PDK1	phosphoinositide-dependent kinase-1
PFA	paraformaldehyde
PH	Pleckstrin homology
PHx	partial hepatectomy
PI3K	phosphoinositide 3-kinase
PLSR	partial least-squares regression
RAN	ranitidine
RFU	relative fluorescence units
RH	primary rat hepatocytes
RIL	riluzole
ROS	reactive oxygen species
SEC	sinusoidal endothelial cell
SEM	standard error of the mean
SHP-2	SH2-domain-containing protein tyrosine phosphatase-2
SOCS3	suppressor of cytokine signaling-3
STAT3	signal transducer and activator of transcription-3
TACE	tumor necrosis factor-α-converting enzyme
TCPS	tissue culture polystyrene
TEL	telithromycin

TGF-α	transforming growth factor-α
TGF-β1	transforming growth factor-β1
TMRM	tetramethyl rhodamine ester
TNF	tumor necrosis factor-α
TNFR	tumor necrosis factor receptor
TRADD	TNFR1-associated death domain protein
TRAF-2	TNFR-associated factor-2
TRO	trovafloxacin
v.p.	viral particle
VIP	variable importance of projection
WEM	William's E medium
XIAP	X-linked inhibitor of apoptosis protein

Appendix B

Multiplexed bead-based phosphoprotein assays

B.1. Lysis of primary rat hepatocytes in single-layer collagen gel cultures

Rat hepatocytes were cultured on single-layer collagen gels and treated as described in Chapter 2.2.3. At the desired time point, cells were placed on ice and culture medium was removed and centrifuged at 1000*g* for 4 minutes at 4°C to pellet non-adherent cells. Adherent cells and pelleted non-adherent cells were lysed with Phosphoprotein Lysis Buffer (Bio-Rad, Hercules, CA) for 20 minutes at 4°C. Adherent cell lysates were collected by vigorous pipetting but without scrapping to avoid significant removal of the underlying collagen gel. Lysates were clarified by centrifugation at 16,000*g* for 15 minutes at 4°C. Clarified lysates were analyzed using a bicinchonicic assay (Pierce, Rockford, IL) to determine the total protein concentration. In each culture plate, a well without cells was maintained, lysed, and analyzed to calculate the protein contribution from the collagen gel alone and estimate the cellular protein concentration. The gel-only protein concentration accounted for ~15-25% of the total protein concentration in wells containing cells and was subtracted from the protein concentrations from wells contains cells in a plate-specific manner to estimate the cellular protein concentration in each lysate sample.

B.2. Lysis of primary human hepatocytes in Matrigel-overlay cultures

Human hepatocytes were maintained in Matrigel-overlay cultures and treated as described in Chapter 3.2.3. At the desired time point, cells were placed on ice and culture medium was removed. Matrigel overlays were partially dissolved by adding ice cold PBS for 15 minutes at 4°C. PBS was removed and cells were lysed with Phosphoprotein Lysis Buffer for 20 minutes at 4°C. Lysates were collected by scrapping and vigorous pipetting. Lysates were clarified by centrifugation at 16,000*g* for 15 minutes at 4°C. Clarified lysates were analyzed using a bicinchonicic assay to determine the total protein concentration. In each culture plate, a well without cells was maintained, lysed, and

analyzed to calculate the protein contribution from the Matrigel overlay alone and estimate the cellular protein concentration. The Matrigel-only protein concentration accounted for ~10-20% of the total protein concentration in cellular samples containing. An average of Matrigel-only protein concentrations from all plates in the same experiment was subtracted from the protein concentrations from wells contains cells to estimate the cellular protein concentration in each lysate sample. (Compared to the lysis of rat hepatocytes on single-layer collagen gels, lysis of Matrigel-only wells showed less plate-to-plate correlation so the average across multiple plate in the same experiment was used to minimize error.)

B.3. Lysis of HepG2 cells

HepG2 cells were cultured and treated as described in Chapter 3.2.3. At the desired time point, cells were placed on ice and culture medium was removed. Cells were lysed with Phosphoprotein Lysis Buffer for 20 minutes at 4°C. Lysates were collected by scrapping and vigorous pipetting. Lysates were clarified by centrifugation at 16,000*g* for 15 minutes at 4°C. Clarified lysates were analyzed using a bicinchonicic assay to determine the total cellular protein concentration. Adjustments for protein contributions from gel substrates (as in Chapters B.1 and B.2) were unnecessary.

B.4. Bead-based phosphoprotein assays

Bio-Plex bead-based assays (Bio-Rad) were used to quantify the following phosphoproteins: p-Akt (Ser^{473}), p-CREB (Ser^{133}), p-c-Jun (Ser^{63}), p-GSK-3α/β (Ser^{21}/Ser^{9}), p-IκB-α (Ser^{32}/Ser^{36}), p-IRS-1 (Ser^{636}/Ser^{639}), p-ERK1/2 (Thr^{202}/Tyr^{204}, Thr^{185}/Tyr^{187}), p-Histone H3 (Ser^{10}), p-HSP27 (Ser^{78}), p-JNK (Thr^{183}/Tyr^{185}), p-MEK1 (Ser^{217}/Ser^{221}), p-STAT3 (Ser^{727}), p-STAT6 (Tyr^{641}), p-p38 (Thr^{180}/Tyr^{182}), p-p53 (Ser^{15}), p-p70 S6 kinase (Thr^{421}/Ser^{424}), and p-p90 RSK (Thr^{359}/Ser^{363}). Bio-Plex assays were conducted per manufacturer's recommendations on a Luminex 200 instrument (Luminex, Austin, TX) with protein lysates loaded in technical duplicate. Cellular protein concentrations were adjusted by dilution of clarified protein lysates (following any necessary subtraction for estimated gel contributions to the total protein concentration) in Phosphoprotein Lysis Buffer. Each phosphoprotein assay was individually validated for

each cell type using multiple positive control treatments over a range of cellular protein loading concentrations (0-20 μg cellular protein per assay well).

Whereas some phosphoprotein assays demonstrated robust linearity across all protein loading concentrations (Figure B-1A), other assays showed problematic saturation effects. One type of saturation effect was related to saturation of the instrument's fluorescence detector, usually occurring for samples with >20,000 relative fluorescence units (RFU). This detector saturation effect was observed for p-Akt (Figure B-1B) and p-HSP27 (data not shown) assays. To avoid this saturation effect, assays were loaded at protein concentrations lower at <10 μg/well and/or under low PMT detector mode.

A second type of saturation effect was related to saturation of the capture and/or detection antibody on the bead-based assay. In this saturation effect, increasing protein loading amounts from a given sample biological resulted in a plateauing in assay fluorescence detection at fluorescence levels lower than detector saturation. This antibody saturation effect was observed for p-IκB-α (Figure B-1C) and p-ERK1/2 (data not shown) assays. To avoid this saturation effect, assays were loaded at consistent protein concentrations as relative phosphoprotein detection levels (*i.e.* fold-change versus the untreated samples) were well-maintained within a given protein loading concentration (data not shown).

A final consideration made for phosphoprotein assay validation was to select a protein loading concentration that allowed for robust fold-change consistency and maximal assay dynamic range. In considering this, we found that even for the same phosphoprotein assay, different cell types yielded distinctly different optimal loading concentrations. For example, rat hepatocytes (optimal at 5 μg/well) versus HepG2 cells (optimal at 10 μg/well) for the p-Akt assay (see Figure B-1D-E). Using these considerations to avoid assay saturation effects and to yield robust fold-change consistency and maximal assay dynamic range, we selected the following cellular protein loading concentrations: 10 μg/well for all phosphoprotein assays for rat hepatocyte, HepG2, and human hepatocyte lysates, except 5 μg/well for p-Akt, p-c-Jun, and p-ERK1/2 assays for rat hepatocyte lysates.

To fuse raw fluorescence data from multiple technical assay plates, multiple (~3-5) positive control treatments were loaded on each assay plate to scale raw fluorescence data to self-consistent relative values (Figure B-1F). Positive control lysates were used from the same cell type as the sample lysates and were selected to contain at least one control condition that elicited roughly maximal phosphoprotein activation for every multiplexed phosphoprotein assayed simultaneously.

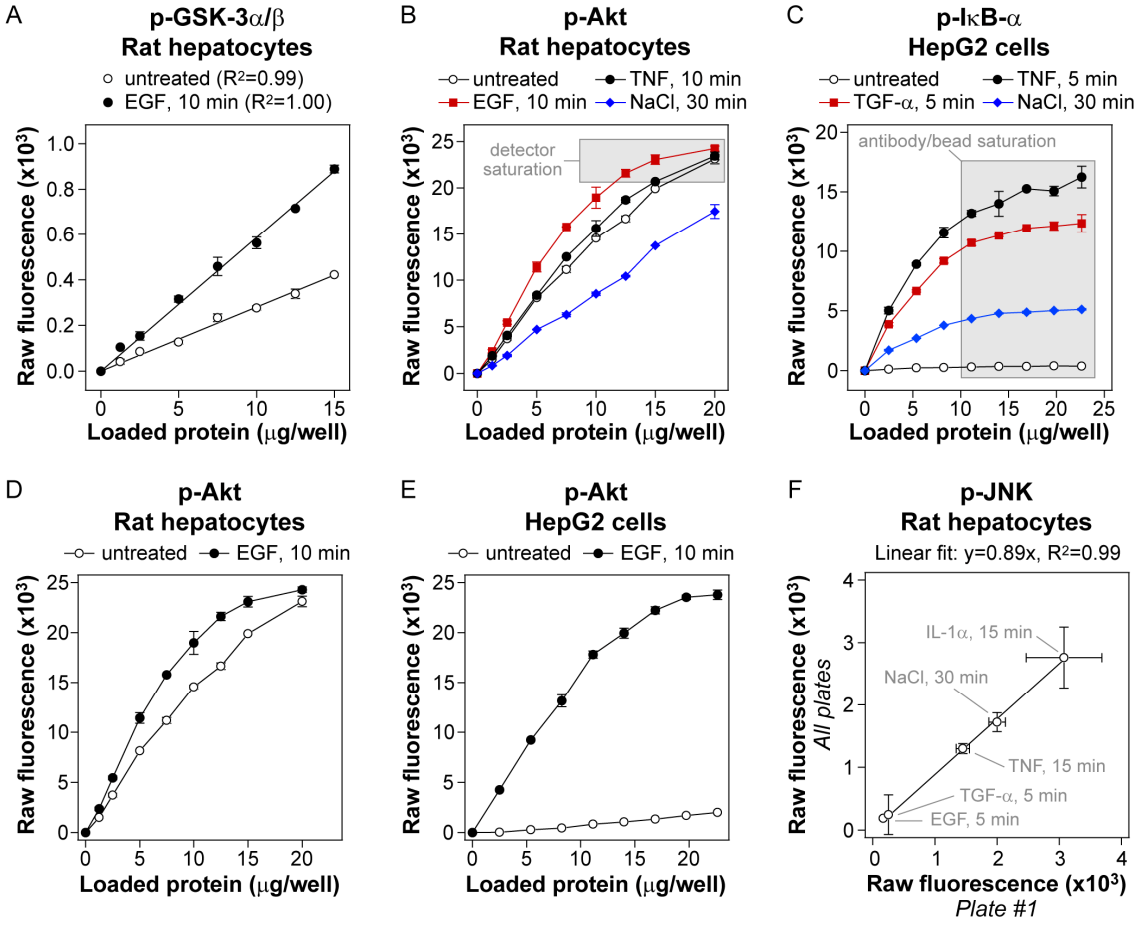

Figure B-1. Validation of multiplexed bead-based phosphoprotein assays. Cell lysates were prepared under various treatment conditions and assayed as described in Appendix B. (A) Linearity validation of bead-based p-GSK-3α/β assay using rat hepatocytes lysates loaded at 0 to 15 μg/well cellular protein. (B) Linearity validation of bead-based p-Akt assay using rat hepatocyte lysates loaded at 0 to 20 μg/well cellular protein. Note the detector saturation for samples with raw fluorescence values at >20,000 relative fluorescence units (RFU). (C) Linearity validation of bead-based p-IκB-α assay using HepG2 lysates loaded at 0 to 20 μg/well cellular protein. Note the antibody saturation for samples loaded at >10 μg/well cellular protein. (D-E) Linearity of bead-based p-Akt assay using rat hepatocyte (D) or HepG2 (E) lysates loaded at 0 to 20 μg/well cellular protein. Note discrepancy between cell types in the p-Akt level for the untreated samples and similar detector saturation effects at >15 μg/well for the EGF-treated samples. (F) Plate-to-plate normalization standards for bead-based p-JNK assay using rat hepatocyte lysates loaded at 10 μg/well. In panels (A) to (F), data is presented as the mean ± standard deviation of two technical replicates. In panel (F), the data on the y-axis represents mean ± standard deviation of four assay plates.

Appendix C

Human hepatocyte donor information

Table C-1. Human hepatocyte donor information

Donor ID	Experiment	Data in	Culture start date	Lot #[1]	Donor information and history			
					Gender, age	Obesity[2]	Smoking, drug, alcohol use	Disease, viral infection
A	Drug-cytokine compendium, sub-lethal imaging data	Figs. 3-3, 3-7	11/08/07	Hu0697	Female, 64 yrs old	Not obese, BMI 24	None known	None known[3]
B	90-drug study	Fig. 3-9	04/23/08	Hu0793	Female, 33 yrs old	Obese, BMI 37	None known	None known
1	CSR training data set	Fig. 4-2	05/20/07	Hu4000	Female, 4 yrs old	Not obese, BMI unknown	None known	None known
2	CSR test data set	Fig. 4-6	10/18/08	Hu0921	Male, 38 yrs old	Not obese, BMI 25	None known	None known
3	MEK and p38 inhibitor IC50 study	Fig. 4-10	10/17/08	Hu0920	Female, 52 yrs old	Not obese, BMI 21	None known	None known
4	Kinase and autocrine inhibitor drug-cytokine toxicity study	Figs. 4-11, E-1	11/13/08	Hu0935	Female, 54 yrs old	Not obese, BMI 20	None known	None known

[1]Lot number assigned by CellzDirect, Inc.
[2]BMI = body mass index. A BMI of 30 or greater is generally considered obese.
[3]No known history of, or exposure to, Hepatitis B, Hepatitis C, cirrhosis, biliary disease or HIV. Not serology-tested.

Appendix D

Generation of an orthogonal partial least-squares regression model

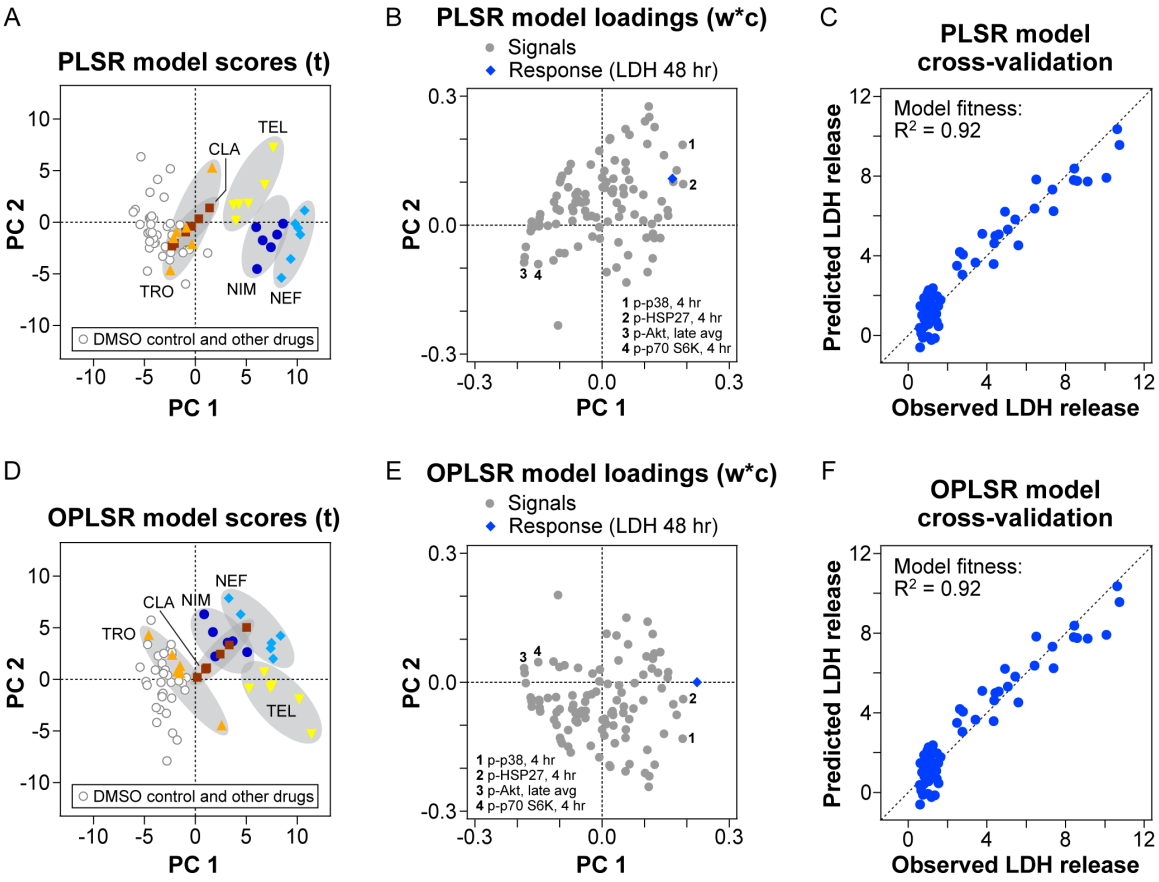

Figure D-1. Comparison of PLSR and OPLSR models. A partial least-squares regression (PLSR) model was generated from the CSR data compendium in Figure 4-2 using the NIPALS algorithm in SIMCA-P software (Umetrics, Inc., Kinnelon, NJ) following standard methods [62-64, 152, 153]. The PLSR model was generated using four principal components under standard optimization criteria [63], and its model scores (A), loadings (B), and cross-validated predictions (C) are plotted. The calibrated PLSR model was then subjected to a principal-component-space linear transformation by rotating the projection (in 4-dimensionl principal-component-space, with only the first two PC's shown in [A] and [B]) of the single cell death response variable completely into the first principal-component to allow for simplified interpretation of model loadings (E) and scores (B), thus yielding an "orthogonal" PLSR (OPLSR) model [154]. The signal (X) model loadings and model scores were similarly rotated. The OPLSR model demonstrated equivalent cross-validated model predictions and model fitness (F) as the original PLSR model (C).

Appendix E

Role of autocrine signaling in drug- and cytokine-induced hepatotoxicity

Based on the Adv/TNF-induced rat hepatocyte apoptosis findings in Chapter 2, it was speculated that autocrine TGF-α and IL-1 ligands may control drug/cytokine synergies. An initial examination in human hepatocytes (donor #4) did not show autocrine TGF-α or IL-1 ligand control of drug-cytokine hepatotoxicity synergy (Figure E-1). It is possible that autocrine signaling control of drug/cytokine-induced hepatotoxicity can be perturbed only under:

- sub-saturating TNF dosing concentrations (as in Figure 2-6J for Adv/TNF-induced hepatocyte apoptosis);
- drug/cytokine dosing conditions showing a greater synergy with TNF co-treatment (such as trovafloxacin); and/or
- other cytokine treatments such as TNF + IFN-γ (as in [77]) or TNF + LPS.

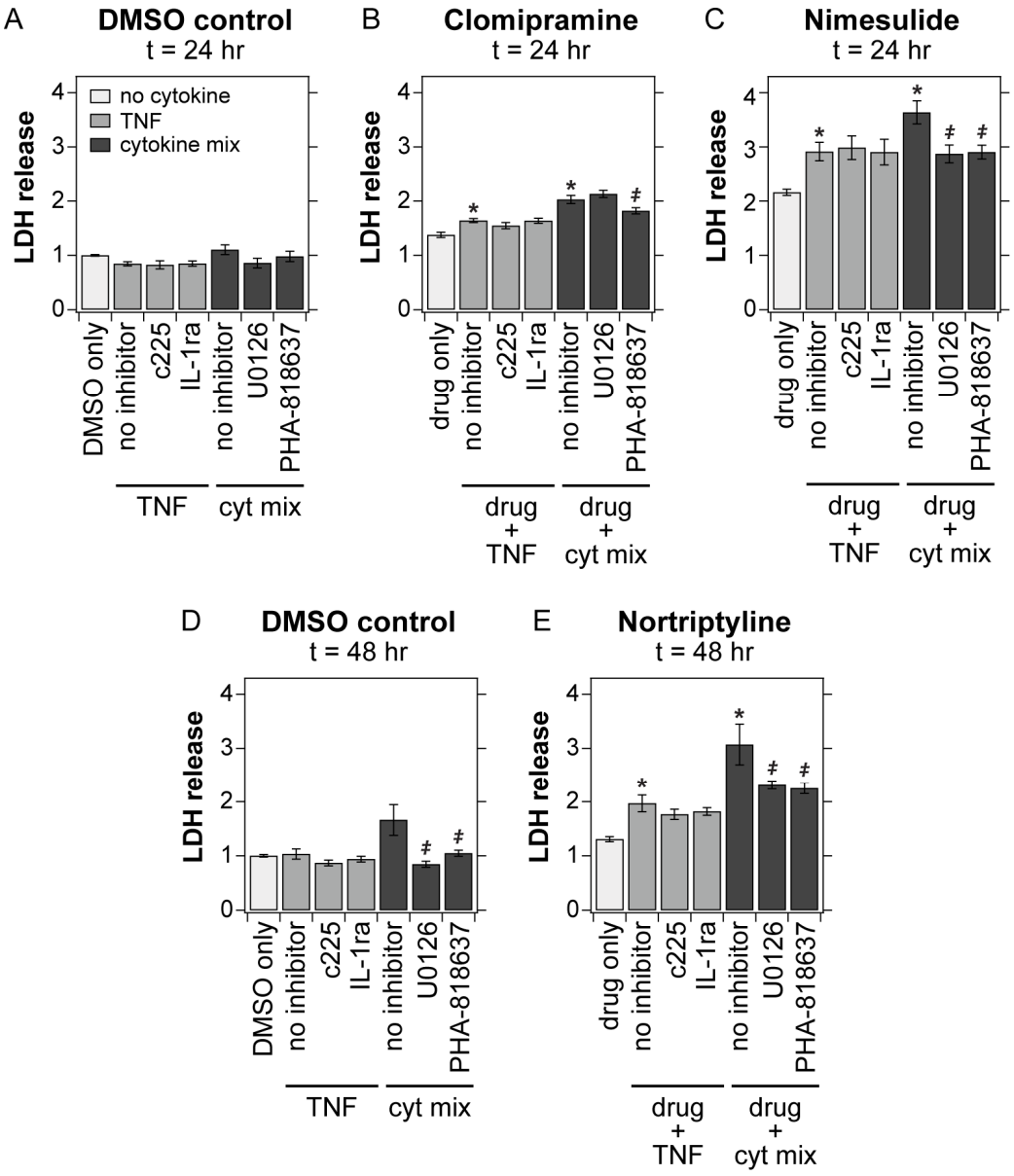

Figure E-1. Autocrine ligand and kinase inhibitor perturbations of drug/cytokine hepatotoxicity synergy. Human hepatocytes (from donor #4) were cultured as described in Chapter 4.2. Cells were treated with drugs (13 μM clomipramine [B], 2.1 mM nimesulide [C], 10 μM nortriptyline [E], or 0.25% DMSO control [A, D]) ± 100 ng/ml TNF or a cytokine mix (20 ng/ml IL-1α, 10 μg/ml LPS, 100 ng/ml TNF, and 20 ng/ml IL-6). After 24 or 48 hours, conditioned medium samples were assayed for LDH release. To inhibit MEK kinase activity, cells were pretreated with 10 μM U0126 or 1 μM PD325901 one hour before drug/cytokine stimulation. To inhibit p38 kinase activity, cells were pretreated with 1 μM PHA-666859 or 1 nM PHA-818637 one hour before drug/cytokine stimulation. To inhibit autocrine EGFR ligand activity, cells were pretreated with 5 μg/ml anti-TGF-α neutralizing antibody (data not shown) or 10 μg/ml c225 monoclonal antibody one hour before drug/cytokine stimulation. To inhibit autocrine IL-1 activity, cells were pretreated with 10 μg/ml recombinant human IL-1ra one hour before drug/cytokine stimulation. Data are presented as the mean ± SEM of eight biological replicates. Drug-cytokine co-treatment conditions that elicited supra-additive hepatotoxicity synergy, evaluated as described in Chapter 4.2.10, are denoted as (*). Differences between uninhibited and inhibitor pretreatments are labeled as significant (‡) if $P < 0.05$ by a Student's *t* test. Autocrine ligand and kinase inhibitor pretreatments did not significantly perturb cell death responses in the absence of cytokine mix co-stimulation and thus are not shown.

REFERENCES

1. LeCluyse EL, Bullock PL, Parkinson A. (1996). Strategies for restoration and maintenance of normal hepatic structure and function in long-term cultures of rat hepatocytes. *Advanced Drug Delivery Reviews* 22, 133.

2. Arias IM, ed. (2001). The liver: biology and pathobiology, 4th ed. Lippincott, Williams & Wilkins.

3. Costa RH, Kalinichenko VV, Holterman AX, Wang X. (2003). Transcription factors in liver development, differentiation, and regeneration. *Hepatology* 38, 1331-47.

4. Rana B, Mischoulon D, Xie Y, Bucher NL, Farmer SR. (1994). Cell-extracellular matrix interactions can regulate the switch between growth and differentiation in rat hepatocytes: reciprocal expression of C/EBP alpha and immediate-early growth response transcription factors. *Mol Cell Biol* 14, 5858-69.

5. Nagaki M, Shidoji Y, Yamada Y, Sugiyama A, Tanaka M, Akaike T, Ohnishi H, Moriwaki H, Muto Y. (1995). Regulation of hepatic genes and liver transcription factors in rat hepatocytes by extracellular matrix. *Biochem Biophys Res Commun* 210, 38-43.

6. Lindblad WJ, Schuetz EG, Redford KS, Guzelian PS. (1991). Hepatocellular phenotype in vitro is influenced by biophysical features of the collagenous substratum. *Hepatology* 13, 282-8.

7. Sidhu JS, Farin FM, Omiecinski CJ. (1993). Influence of extracellular matrix overlay on phenobarbital-mediated induction of CYP2B1, 2B2, and 3A1 genes in primary adult rat hepatocyte culture. *Arch Biochem Biophys* 301, 103-13.

8. Sivaraman A, Leach JK, Townsend S, Iida T, Hogan BJ, Stolz DB, Fry R, Samson LD, Tannenbaum SR, Griffith LG. (2005). A microscale in vitro physiological model of the liver: predictive screens for drug metabolism and enzyme induction. *Curr Drug Metab* 6, 569-91.

9. Powers MJ, Domansky K, Kaazempur-Mofrad MR, Kalezi A, Capitano A, Upadhyaya A, Kurzawski P, Wack KE, Stolz DB, Kamm R, Griffith LG. (2002). A microfabricated array bioreactor for perfused 3D liver culture. *Biotechnol Bioeng* 78, 257-69.

10. Domansky K, Inman W, Serdy J, Griffith L. (2005). Perfused microreactors for liver tissue engineering. *Conf Proc IEEE Eng Med Biol Soc* 7, 7490-2.

11. Plumpe J, Streetz K, Manns MP, Trautwein C. (1999). Tumour necrosis factor alpha--mediator of apoptosis and cell proliferation of hepatocytes. *Ital J Gastroenterol Hepatol* 31, 235-43.

12. Karin M, Ben-Neriah Y. (2000). Phosphorylation meets ubiquitination: the control of NF-[kappa]B activity. *Annu Rev Immunol* 18, 621-63.

13. Heinrich PC, Behrmann I, Haan S, Hermanns HM, Muller-Newen G, Schaper F. (2003). Principles of interleukin (IL)-6-type cytokine signalling and its regulation. *Biochem J* 374, 1-20.

14. Toker A, Newton AC. (2000). Cellular signaling: pivoting around PDK-1. *Cell* 103, 185-8.

15. Zauberman A, Zipori D, Krupsky M, Ben-Levy R. (1999). Stress activated protein kinase p38 is involved in IL-6 induced transcriptional activation of STAT3. *Oncogene* 18, 3886-93.

16. Galun E, Axelrod JH. (2002). The role of cytokines in liver failure and regeneration: potential new molecular therapies. *Biochim Biophys Acta* 1592, 345-58.

17. Ono K, Han J. (2000). The p38 signal transduction pathway: activation and function. *Cell Signal* 12, 1-13.

18. Canbay A, Friedman S, Gores GJ. (2004). Apoptosis: the nexus of liver injury and fibrosis. *Hepatology* 39, 273-8.

19. Leist M, Jaattela M. (2001). Four deaths and a funeral: from caspases to alternative mechanisms. *Nat Rev Mol Cell Biol* 2, 589-98.

20. Shayakhmetov DM, Li ZY, Ni S, Lieber A. (2005). Interference with the IL-1-signaling pathway improves the toxicity profile of systemically applied adenovirus vectors. *J Immunol* 174, 7310-9.

21. Lieber A, He CY, Meuse L, Schowalter D, Kirillova I, Winther B, Kay MA. (1997). The role of Kupffer cell activation and viral gene expression in early liver toxicity after infusion of recombinant adenovirus vectors. *J Virol* 71, 8798-807.

22. Miller-Jensen K, Janes KA, Wong YL, Griffith LG, Lauffenburger DA. (2006). Adenoviral vector saturates Akt pro-survival signaling and blocks insulin-mediated rescue of tumor necrosis-factor-induced apoptosis. *J Cell Sci* 119, 3788-98.

23. Zhang F, Cheng J, Hackett NR, Lam G, Shido K, Pergolizzi R, Jin DK, Crystal RG, Rafii S. (2004). Adenovirus E4 gene promotes selective endothelial cell survival and angiogenesis via activation of the vascular endothelial-cadherin/Akt signaling pathway. *J Biol Chem* 279, 11760-6.

24. Tibbles LA, Spurrell JC, Bowen GP, Liu Q, Lam M, Zaiss AK, Robbins SM, Hollenberg MD, Wickham TJ, Muruve DA. (2002). Activation of p38 and ERK

signaling during adenovirus vector cell entry lead to expression of the C-X-C chemokine IP-10. *J Virol* 76, 1559-68.

25. Wang WH, Gregori G, Hullinger RL, Andrisani OM. (2004). Sustained activation of p38 mitogen-activated protein kinase and c-Jun N-terminal kinase pathways by hepatitis B virus X protein mediates apoptosis via induction of Fas/FasL and tumor necrosis factor (TNF) receptor 1/TNF-alpha expression. *Mol Cell Biol* 24, 10352-65.

26. Ganey PE, Luyendyk JP, Maddox JF, Roth RA. (2004). Adverse hepatic drug reactions: inflammatory episodes as consequence and contributor. *Chem Biol Interact* 150, 35-51.

27. Kaplowitz N. (2005). Idiosyncratic drug hepatotoxicity. *Nat Rev Drug Discov* 4, 489-99.

28. Uetrecht J. (2007). Idiosyncratic drug reactions: current understanding. *Annu Rev Pharmacol Toxicol* 47, 513-39.

29. Uetrecht J. (2008). Idiosyncratic drug reactions: past, present, and future. *Chem Res Toxicol* 21, 84-92.

30. Obach RS, Kalgutkar AS, Soglia JR, Zhao SX. (2008). Can in vitro metabolism-dependent covalent binding data in liver microsomes distinguish hepatotoxic from nonhepatotoxic drugs? An analysis of 18 drugs with consideration of intrinsic clearance and daily dose. *Chem Res Toxicol* 21, 1814-22.

31. Peters TS. (2005). Do preclinical testing strategies help predict human hepatotoxic potentials? *Toxicol Pathol* 33, 146-54.

32. Buchweitz JP, Ganey PE, Bursian SJ, Roth RA. (2002). Underlying endotoxemia augments toxic responses to chlorpromazine: is there a relationship to drug idiosyncrasy? *J Pharmacol Exp Ther* 300, 460-7.

33. Deng X, Stachlewitz RF, Liguori MJ, Blomme EA, Waring JF, Luyendyk JP, Maddox JF, Ganey PE, Roth RA. (2006). Modest inflammation enhances diclofenac hepatotoxicity in rats: role of neutrophils and bacterial translocation. *J Pharmacol Exp Ther* 319, 1191-9.

34. Luyendyk JP, Maddox JF, Cosma GN, Ganey PE, Cockerell GL, Roth RA. (2003). Ranitidine treatment during a modest inflammatory response precipitates idiosyncrasy-like liver injury in rats. *J Pharmacol Exp Ther* 307, 9-16.

35. Shaw PJ, Hopfensperger MJ, Ganey PE, Roth RA. (2007). Lipopolysaccharide and trovafloxacin coexposure in mice causes idiosyncrasy-like liver injury dependent on tumor necrosis factor-alpha. *Toxicol Sci* 100, 259-66.

36. Bergheim I, Luyendyk JP, Steele C, Russell GK, Guo L, Roth RA, Arteel GE. (2006). Metformin prevents endotoxin-induced liver injury after partial hepatectomy. *J Pharmacol Exp Ther* 316, 1053-61.

37. Tukov FF, Luyendyk JP, Ganey PE, Roth RA. (2007). The role of tumor necrosis factor alpha in lipopolysaccharide/ranitidine-induced inflammatory liver injury. *Toxicol Sci* 100, 267-80.

38. Gilot D, Serandour AL, Ilyin GP, Lagadic-Gossmann D, Loyer P, Corlu A, Coutant A, Baffet G, Peter ME, Fardel O, Guguen-Guillouzo C. (2005). A role for caspase-8 and c-FLIPL in proliferation and cell-cycle progression of primary hepatocytes. *Carcinogenesis* 26, 2086-94.

39. Mari M, Colell A, Morales A, Caballero F, Moles A, Fernandez A, Terrones O, Basanez G, Antonsson B, Garcia-Ruiz C, Fernandez-Checa JC. (2008). Mechanism of mitochondrial glutathione-dependent hepatocellular susceptibility to TNF despite NF-kappaB activation. *Gastroenterology* 134, 1507-20.

40. Warren GW, Poloyac SM, Gary DS, Mattson MP, Blouin RA. (1999). Hepatic cytochrome P-450 expression in tumor necrosis factor-alpha receptor (p55/p75) knockout mice after endotoxin administration. *J Pharmacol Exp Ther* 288, 945-50.

41. Zolfaghari R, Cifelli CJ, Lieu SO, Chen Q, Li NQ, Ross AC. (2007). Lipopolysaccharide opposes the induction of CYP26A1 and CYP26B1 gene expression by retinoic acid in the rat liver in vivo. *Am J Physiol Gastrointest Liver Physiol* 292, G1029-36.

42. Albeck JG, MacBeath G, White FM, Sorger PK, Lauffenburger DA, Gaudet S. (2006). Collecting and organizing systematic sets of protein data. *Nat Rev Mol Cell Biol* 7, 803-12.

43. Ideker T, Winslow LR, Lauffenburger DA. (2006). Bioengineering and systems biology. *Ann Biomed Eng* 34, 1226-33.

44. Kim TH, Ren B. (2006). Genome-Wide Analysis of Protein-DNA Interactions. *Annu Rev Genomics Hum Genet* 7, 81-102.

45. Nielsen J, Oliver S. (2005). The next wave in metabolome analysis. *Trends Biotechnol* 23, 544-6.

46. Janes KA, Yaffe MB. (2006). Data-driven modelling of signal-transduction networks. *Nat Rev Mol Cell Biol* 7, 820-8.

47. Wolf-Yadlin A, Kumar N, Zhang Y, Hautaniemi S, Zaman M, Kim HD, Grantcharova V, Lauffenburger DA, White FM. (2006). Effects of HER2 overexpression on cell signaling networks governing proliferation and migration. *Mol Syst Biol* 2, 54.

48. Janes KA, Albeck JG, Peng LX, Sorger PK, Lauffenburger DA, Yaffe MB. (2003). A high-throughput quantitative multiplex kinase assay for monitoring information flow in signaling networks: application to sepsis-apoptosis. *Mol Cell Proteomics* 2, 463-73.

49. Shults MD, Janes KA, Lauffenburger DA, Imperiali B. (2005). A multiplexed homogeneous fluorescence-based assay for protein kinase activity in cell lysates. *Nat Methods* 2, 277-83.

50. Gaudet S, Janes KA, Albeck JG, Pace EA, Lauffenburger DA, Sorger PK. (2005). A compendium of signals and responses triggered by prodeath and prosurvival cytokines. *Mol Cell Proteomics* 4, 1569-90.

51. Kortum RL, Costanzo DL, Haferbier J, Schreiner SJ, Razidlo GL, Wu MH, Volle DJ, Mori T, Sakaue H, Chaika NV, Chaika OV, Lewis RE. (2005). The molecular scaffold kinase suppressor of Ras 1 (KSR1) regulates adipogenesis. *Mol Cell Biol* 25, 7592-604.

52. Morgan E, Varro R, Sepulveda H, Ember JA, Apgar J, Wilson J, Lowe L, Chen R, Shivraj L, Agadir A, Campos R, Ernst D, Gaur A. (2004). Cytometric bead array: a multiplexed assay platform with applications in various areas of biology. *Clin Immunol* 110, 252-66.

53. Knickerbocker T, Chen JR, Thadhani R, MacBeath G. (2007). An integrated approach to prognosis using protein microarrays and nonparametric methods. *Mol Syst Biol* 3, 123.

54. Sevecka M, MacBeath G. (2006). State-based discovery: a multidimensional screen for small-molecule modulators of EGF signaling. *Nat Methods* 3, 825-31.

55. Perez OD, Nolan GP. (2002). Simultaneous measurement of multiple active kinase states using polychromatic flow cytometry. *Nat Biotechnol* 20, 155-62.

56. Sachs K, Perez O, Pe'er D, Lauffenburger DA, Nolan GP. (2005). Causal protein-signaling networks derived from multiparameter single-cell data. *Science* 308, 523-9.

57. Ecker RC, Tarnok A. (2005). Cytomics goes 3D: toward tissomics. *Cytometry A* 65, 1-3.

58. Loo LH, Wu LF, Altschuler SJ. (2007). Image-based multivariate profiling of drug responses from single cells. *Nat Methods* 4, 445-53.

59. Zhang Y, Wolf-Yadlin A, White FM. (2007). Quantitative proteomic analysis of phosphotyrosine-mediated cellular signaling networks. *Methods Mol Biol* 359, 203-12.

60. Janes KA, Lauffenburger DA. (2006). A biological approach to computational models of proteomic networks. *Curr Opin Chem Biol* 10, 73-80.

61. Aldridge BB, Burke JM, Lauffenburger DA, Sorger PK. (2006). Physicochemical modelling of cell signalling pathways. *Nat Cell Biol* 8, 1195-203.

62. Janes KA, Albeck JG, Gaudet S, Sorger PK, Lauffenburger DA, Yaffe MB. (2005). A systems model of signaling identifies a molecular basis set for cytokine-induced apoptosis. *Science* 310, 1646-53.

63. Geladi P, Kowalski B. (1986). Partial least-squares regression: a tutorial. *Anal. Chim. Acta* 185, 1-17.

64. Miller-Jensen K, Janes KA, Brugge JS, Lauffenburger DA. (2007). Common effector processing mediates cell-specific responses to stimuli. *Nature* 448, 604-8.

65. Prudhomme W, Daley GQ, Zandstra P, Lauffenburger DA. (2004). Multivariate proteomic analysis of murine embryonic stem cell self-renewal versus differentiation signaling. *Proc Natl Acad Sci U S A* 101, 2900-5.

66. Kemp ML, Wille L, Lewis CL, Nicholson LB, Lauffenburger DA. (2007). Quantitative network signal combinations downstream of TCR activation can predict IL-2 production response. *J Immunol* 178, 4984-92.

67. Kumar D, Srikanth R, Ahlfors H, Lahesmaa R, Rao KV. (2007). Capturing cell-fate decisions from the molecular signatures of a receptor-dependent signaling response. *Mol Syst Biol* 3, 150.

68. Kumar N, Wolf-Yadlin A, White FM, Lauffenburger DA. (2007). Modeling HER2 effects on cell behavior from mass spectrometry phosphotyrosine data. *PLoS Comput Biol* 3, e4.

69. Breiman L, *Classification and regression trees*. Wadsworth statistics/probability series. 1984, Belmont, CA: Wadsworth Intl. Group. 358 pp.

70. Hautaniemi S, Kharait S, Iwabu A, Wells A, Lauffenburger DA. (2005). Modeling of signal-response cascades using decision tree analysis. *Bioinformatics* 21, 2027-35.

71. Kharait S, Hautaniemi S, Wu S, Iwabu A, Lauffenburger DA, Wells A. (2007). Decision tree modeling predicts effects of inhibiting contractility signaling on cell motility. *BMC Syst Biol* 1, 9.

72. Hua F, Hautaniemi S, Yokoo R, Lauffenburger DA. (2006). Integrated mechanistic and data-driven modelling for multivariate analysis of signalling pathways. *J R Soc Interface* 3, 515-26.

73. Woolf PJ, Prudhomme W, Daheron L, Daley GQ, Lauffenburger DA. (2005). Bayesian analysis of signaling networks governing embryonic stem cell fate decisions. *Bioinformatics* 21, 741-53.

74. David LA, Wiggins CH. (2007). Benchmarking of dynamic Bayesian networks inferred from stochastic time-series data. *Ann N Y Acad Sci* 1115, 90-101.

75. Taub R. (2004). Liver regeneration: from myth to mechanism. *Nat Rev Mol Cell Biol* 5, 836-47.

76. Schwabe RF, Brenner DA. (2006). Mechanisms of Liver Injury. I. TNF-alpha-induced liver injury: role of IKK, JNK, and ROS pathways. *Am J Physiol Gastrointest Liver Physiol* 290, G583-9.

77. Janes KA, Gaudet S, Albeck JG, Nielsen UB, Lauffenburger DA, Sorger PK. (2006). The response of human epithelial cells to TNF involves an inducible autocrine cascade. *Cell* 124, 1225-39.

78. Diehl AM, Yin M, Fleckenstein J, Yang SQ, Lin HZ, Brenner DA, Westwick J, Bagby G, Nelson S. (1994). Tumor necrosis factor-alpha induces c-jun during the regenerative response to liver injury. *Am J Physiol* 267, G552-61.

79. Webber EM, Bruix J, Pierce RH, Fausto N. (1998). Tumor necrosis factor primes hepatocytes for DNA replication in the rat. *Hepatology* 28, 1226-34.

80. Mead JE, Fausto N. (1989). Transforming growth factor alpha may be a physiological regulator of liver regeneration by means of an autocrine mechanism. *Proc Natl Acad Sci U S A* 86, 1558-62.

81. Berasain C, Garcia-Trevijano ER, Castillo J, Erroba E, Santamaria M, Lee DC, Prieto J, Avila MA. (2005). Novel role for amphiregulin in protection from liver injury. *J Biol Chem* 280, 19012-20.

82. Iocca HA, Isom HC. (2003). Tumor necrosis factor-alpha acts as a complete mitogen for primary rat hepatocytes. *Am J Pathol* 163, 465-76.

83. Gallucci RM, Simeonova PP, Toriumi W, Luster MI. (2000). TNF-alpha regulates transforming growth factor-alpha expression in regenerating murine liver and isolated hepatocytes. *J Immunol* 164, 872-8.

84. Argast GM, Campbell JS, Brooling JT, Fausto N. (2004). Epidermal growth factor receptor transactivation mediates tumor necrosis factor-induced hepatocyte replication. *J Biol Chem* 279, 34530-6.

85. Nakamura T, Arakaki R, Ichihara A. (1988). Interleukin-1 beta is a potent growth inhibitor of adult rat hepatocytes in primary culture. *Exp Cell Res* 179, 488-97.

86. Boulton R, Woodman A, Calnan D, Selden C, Tam F, Hodgson H. (1997). Nonparenchymal cells from regenerating rat liver generate interleukin-1alpha and -1beta: a mechanism of negative regulation of hepatocyte proliferation. *Hepatology* 26, 49-58.

87. Wang Z, Wang M, Carr BI. (1998). The inhibitory effect of interleukin 1beta on rat hepatocyte DNA synthesis is mediated by nitric oxide. *Hepatology* 28, 430-5.

88. Del Castillo G, Murillo MM, Alvarez-Barrientos A, Bertran E, Fernandez M, Sanchez A, Fabregat I. (2006). Autocrine production of TGF-beta confers resistance to apoptosis after an epithelial-mesenchymal transition process in hepatocytes: Role of EGF receptor ligands. *Exp Cell Res* 312, 2860-71.

89. Fujioka N, Mukaida N, Harada A, Akiyama M, Kasahara T, Kuno K, Ooi A, Mai M, Matsushima K. (1995). Preparation of specific antibodies against murine IL-1ra and the establishment of IL-1ra as an endogenous regulator of bacteria-induced fulminant hepatitis in mice. *J Leukoc Biol* 58, 90-8.

90. Russell WE, Kaufmann WK, Sitaric S, Luetteke NC, Lee DC. (1996). Liver regeneration and hepatocarcinogenesis in transforming growth factor-alpha-targeted mice. *Mol Carcinog* 15, 183-9.

91. Gabay C, Smith MF, Eidlen D, Arend WP. (1997). Interleukin 1 receptor antagonist (IL-1Ra) is an acute-phase protein. *J Clin Invest* 99, 2930-40.

92. Tsukui T, Kikuchi K, Mabuchi A, Sudo T, Sakamoto T, Asano G, Yokomuro K. (1994). Production of interleukin-1 by primary cultured parenchymal liver cells (hepatocytes). *Exp Cell Res* 210, 172-6.

93. Seglen PO. (1976). Preparation of isolated rat liver cells. *Methods Cell Biol* 13, 29-83.

94. Hwa AJ, Fry RC, Sivaraman A, So PT, Samson LD, Stolz DB, Griffith LG. (2007). Rat liver sinusoidal endothelial cells survive without exogenous VEGF in 3D perfused co-cultures with hepatocytes. *Faseb J* 21, 2564-79.

95. Block GD, Locker J, Bowen WC, Petersen BE, Katyal S, Strom SC, Riley T, Howard TA, Michalopoulos GK. (1996). Population expansion, clonal growth, and specific differentiation patterns in primary cultures of hepatocytes induced by HGF/SF, EGF and TGF alpha in a chemically defined (HGM) medium. *J Cell Biol* 132, 1133-49.

96. Lim YS, Kim KA, Jung JO, Yoon JH, Suh KS, Kim CY, Lee HS. (2002). Modulation of cytokeratin expression during in vitro cultivation of human hepatic stellate cells: evidence of transdifferentiation from epithelial to mesenchymal phenotype. *Histochem Cell Biol* 118, 127-36.

97. Heuff G, van der Ende MB, Boutkan H, Prevoo W, Bayon LG, Fleuren GJ, Beelen RH, Meijer S, Dijkstra CD. (1993). Macrophage populations in different stages of induced hepatic metastases in rats: an immunohistochemical analysis. *Scand J Immunol* 38, 10-6.

98. Neubauer K, Knittel T, Aurisch S, Fellmer P, Ramadori G. (1996). Glial fibrillary acidic protein--a cell type specific marker for Ito cells in vivo and in vitro. *J Hepatol* 24, 719-30.

99. Ohmura T, Enomoto K, Satoh H, Sawada N, Mori M. (1993). Establishment of a novel monoclonal antibody, SE-1, which specifically reacts with rat hepatic sinusoidal endothelial cells. *J Histochem Cytochem* 41, 1253-7.

100. Arend WP. (2002). The balance between IL-1 and IL-1Ra in disease. *Cytokine Growth Factor Rev* 13, 323-40.

101. Chaisson ML, Brooling JT, Ladiges W, Tsai S, Fausto N. (2002). Hepatocyte-specific inhibition of NF-kappaB leads to apoptosis after TNF treatment, but not after partial hepatectomy. *J Clin Invest* 110, 193-202.

102. Beyer TA, Xu W, Teupser D, auf dem Keller U, Bugnon P, Hildt E, Thiery J, Kan YW, Werner S. (2008). Impaired liver regeneration in Nrf2 knockout mice: role of ROS-mediated insulin/IGF-1 resistance. *Embo J* 27, 212-23.

103. Serandour AL, Loyer P, Garnier D, Courselaud B, Theret N, Glaise D, Guguen-Guillouzo C, Corlu A. (2005). TNFalpha-mediated extracellular matrix remodeling is required for multiple division cycles in rat hepatocytes. *Hepatology* 41, 478-86.

104. Kim JE, Tannenbaum SR. (2004). S-Nitrosation regulates the activation of endogenous procaspase-9 in HT-29 human colon carcinoma cells. *J Biol Chem* 279, 9758-64.

105. Dinarello CA. (1997). Interleukin-1. *Cytokine Growth Factor Rev* 8, 253-65.

106. Burns K, Martinon F, Tschopp J. (2003). New insights into the mechanism of IL-1beta maturation. *Curr Opin Immunol* 15, 26-30.

107. Joslin EJ, Opresko LK, Wells A, Wiley HS, Lauffenburger DA. (2007). EGF receptor-mediated mammary epithelial cell migration is driven by sustained ERK signaling from autocrine stimulation. *J Cell Sci* in press.

108. Schulze A, Lehmann K, Jefferies HB, McMahon M, Downward J. (2001). Analysis of the transcriptional program induced by Raf in epithelial cells. *Genes Dev* 15, 981-94.

109. Kiso S, Kawata S, Tamura S, Miyagawa J, Ito N, Tsushima H, Yamada A, Umeki S, Higashiyama S, Taniguchi N, Matsuzawa Y. (1999). Expression of heparin-

binding epidermal growth factor-like growth factor in the hepatocytes of fibrotic rat liver during hepatocarcinogenesis. *J Gastroenterol Hepatol* 14, 1203-9.

110. Mohammed FF, Khokha R. (2005). Thinking outside the cell: proteases regulate hepatocyte division. *Trends Cell Biol* 15, 555-63.

111. Monine MI, Berezhkovskii AM, Joslin EJ, Wiley HS, Lauffenburger DA, Shvartsman SY. (2005). Ligand accumulation in autocrine cell cultures. *Biophys J* 88, 2384-90.

112. Tschumperlin DJ, Dai G, Maly IV, Kikuchi T, Laiho LH, McVittie AK, Haley KJ, Lilly CM, So PT, Lauffenburger DA, Kamm RD, Drazen JM. (2004). Mechanotransduction through growth-factor shedding into the extracellular space. *Nature* 429, 83-6.

113. Scheving LA, Zhang L, Stevenson MC, Kwak ES, Russell WE. (2006). The emergence of ErbB2 expression in cultured rat hepatocytes correlates with enhanced and diversified EGF-mediated signaling. *Am J Physiol Gastrointest Liver Physiol* 291, G16-25.

114. Castillo J, Erroba E, Perugorria MJ, Santamaria M, Lee DC, Prieto J, Avila MA, Berasain C. (2006). Amphiregulin contributes to the transformed phenotype of human hepatocellular carcinoma cells. *Cancer Res* 66, 6129-38.

115. Stelling J, Sauer U, Szallasi Z, Doyle FJ, 3rd, Doyle J. (2004). Robustness of cellular functions. *Cell* 118, 675-85.

116. Webber EM, Wu JC, Wang L, Merlino G, Fausto N. (1994). Overexpression of transforming growth factor-alpha causes liver enlargement and increased hepatocyte proliferation in transgenic mice. *Am J Pathol* 145, 398-408.

117. Uetrecht J. (2003). Screening for the potential of a drug candidate to cause idiosyncratic drug reactions. *Drug Discov Today* 8, 832-7.

118. Kolls JK, Lei D, Nelson S, Summer WR, Greenberg S, Beutler B. (1995). Adenovirus-mediated blockade of tumor necrosis factor in mice protects against endotoxic shock yet impairs pulmonary host defense. *J Infect Dis* 171, 570-5.

119. Malhi H, Gores GJ. (2008). Cellular and molecular mechanisms of liver injury. *Gastroenterology* 134, 1641-54.

120. Tacke F, Luedde T, Trautwein C. (2008). Inflammatory Pathways in Liver Homeostasis and Liver Injury. *Clin Rev Allergy Immunol*.

121. Olson H, Betton G, Robinson D, Thomas K, Monro A, Kolaja G, Lilly P, Sanders J, Sipes G, Bracken W, Dorato M, Van Deun K, Smith P, Berger B, Heller A. (2000). Concordance of the toxicity of pharmaceuticals in humans and in animals. *Regul Toxicol Pharmacol* 32, 56-67.

122. Hewitt NJ, Lechon MJ, Houston JB, Hallifax D, Brown HS, Maurel P, Kenna JG, Gustavsson L, Lohmann C, Skonberg C, Guillouzo A, Tuschl G, Li AP, LeCluyse E, Groothuis GM, Hengstler JG. (2007). Primary hepatocytes: current understanding of the regulation of metabolic enzymes and transporter proteins, and pharmaceutical practice for the use of hepatocytes in metabolism, enzyme induction, transporter, clearance, and hepatotoxicity studies. *Drug Metab Rev* 39, 159-234.

123. LeCluyse EL, Alexandre E, Hamilton GA, Viollon-Abadie C, Coon DJ, Jolley S, Richert L. (2005). Isolation and culture of primary human hepatocytes. *Methods Mol Biol* 290, 207-29.

124. Xu JJ, Diaz D, O'Brien PJ. (2004). Applications of cytotoxicity assays and pre-lethal mechanistic assays for assessment of human hepatotoxicity potential. *Chem Biol Interact* 150, 115-28.

125. O'Brien P, Haskins JR. (2007). In vitro cytotoxicity assessment. *Methods Mol Biol* 356, 415-25.

126. Xu JJ, Henstock PV, Dunn MC, Smith AR, Chabot JR, de Graaf D. (2008). Cellular Imaging Predictions of Clinical Drug-Induced Liver Injury. *Toxicol. Sci.* 105, 97-105.

127. Tukov FF, Maddox JF, Amacher DE, Bobrowski WF, Roth RA, Ganey PE. (2006). Modeling inflammation-drug interactions in vitro: a rat Kupffer cell-hepatocyte coculture system. *Toxicol In Vitro* 20, 1488-99.

128. Box GEP, Hunter WG, Hunter JS, *Statistics for experimenters*. 1978, New York: Wiley.

129. Cosgrove BD, Cheng C, Pritchard JR, Stolz DB, Lauffenburger DA, Griffith LG. (2008). An inducible autocrine cascade regulates rat hepatocyte proliferation and apoptosis responses to tumor necrosis factor-alpha. *Hepatology* 48, 276-288.

130. Black M. (1987). Hepatotoxic and hepatoprotective potential of histamine (H2)-receptor antagonists. *Am J Med* 83, 68-75.

131. Chitturi S, George J. (2002). Hepatotoxicity of commonly used drugs: nonsteroidal anti-inflammatory drugs, antihypertensives, antidiabetic agents, anticonvulsants, lipid-lowering agents, psychotropic drugs. *Semin Liver Dis* 22, 169-83.

132. Clay KD, Hanson JS, Pope SD, Rissmiller RW, Purdum PP, 3rd, Banks PM. (2006). Brief communication: severe hepatotoxicity of telithromycin: three case reports and literature review. *Ann Intern Med* 144, 415-20.

133. Luedde T, Trautwein C. (2006). Intracellular survival pathways in the liver. *Liver Int* 26, 1163-74.

134. Alexopoulos LG, Saez-Rodriguez J, Cosgrove BD, Lauffenburger DA, Sorger PK. (submitted). Comparative pathway maps of normal and transformed human hepatocytes reveal widespread differences in inflammatory and NF-κB signaling.

135. Gomez-Lechon MJ, Donato MT, Castell JV, Jover R. (2003). Human hepatocytes as a tool for studying toxicity and drug metabolism. *Curr Drug Metab* 4, 292-312.

136. Boelsterli UA. (2002). Nimesulide and hepatic adverse effects: roles of reactive metabolites and host factors. *Int J Clin Pract Suppl* 30-6.

137. Dykens JA, Jamieson JD, Marroquin LD, Nadanaciva S, Xu JJ, Dunn MC, Smith AR, Will Y. (2008). In vitro assessment of mitochondrial dysfunction and cytotoxicity of nefazodone, trazodone, and buspirone. *Toxicol Sci* 103, 335-45.

138. Kostrubsky SE, Strom SC, Kalgutkar AS, Kulkarni S, Atherton J, Mireles R, Feng B, Kubik R, Hanson J, Urda E, Mutlib AE. (2006). Inhibition of hepatobiliary transport as a predictive method for clinical hepatotoxicity of nefazodone. *Toxicol Sci* 90, 451-9.

139. Xu Y, Bialik S, Jones BE, Iimuro Y, Kitsis RN, Srinivasan A, Brenner DA, Czaja MJ. (1998). NF-kappaB inactivation converts a hepatocyte cell line TNF-alpha response from proliferation to apoptosis. *Am J Physiol* 275, C1058-66.

140. Kaplowitz N. (2001). Drug-induced liver disorders: implications for drug development and regulation. *Drug Saf* 24, 483-90.

141. Lee WM. (2003). Drug-induced hepatotoxicity. *N Engl J Med* 349, 474-85.

142. Ostapowicz G, Fontana RJ, Schiodt FV, Larson A, Davern TJ, Han SH, McCashland TM, Shakil AO, Hay JE, Hynan L, Crippin JS, Blei AT, Samuel G, Reisch J, Lee WM. (2002). Results of a prospective study of acute liver failure at 17 tertiary care centers in the United States. *Ann Intern Med* 137, 947-54.

143. Lammert C, Einarsson S, Saha C, Niklasson A, Bjornsson E, Chalasani N. (2008). Relationship between daily dose of oral medications and idiosyncratic drug-induced liver injury: search for signals. *Hepatology* 47, 2003-9.

144. Hoek JB, Pastorino JG. (2002). Ethanol, oxidative stress, and cytokine-induced liver cell injury. *Alcohol* 27, 63-8.

145. Trusheim MR, Berndt ER, Douglas FL. (2007). Stratified medicine: strategic and economic implications of combining drugs and clinical biomarkers. *Nat Rev Drug Discov* 6, 287-93.

146. Clayton TA, Lindon JC, Cloarec O, Antti H, Charuel C, Hanton G, Provost JP, Le Net JL, Baker D, Walley RJ, Everett JR, Nicholson JK. (2006). Pharmaco-metabonomic phenotyping and personalized drug treatment. *Nature* 440, 1073-7.

147. Gunawan BK, Liu ZX, Han D, Hanawa N, Gaarde WA, Kaplowitz N. (2006). c-Jun N-terminal kinase plays a major role in murine acetaminophen hepatotoxicity. *Gastroenterology* 131, 165-78.

148. Wajant H, Pfizenmaier K, Scheurich P. (2003). Tumor necrosis factor signaling. *Cell Death Differ* 10, 45-65.

149. Sarbassov DD, Ali SM, Sabatini DM. (2005). Growing roles for the mTOR pathway. *Curr Opin Cell Biol* 17, 596-603.

150. Hotamisligil GS, Erbay E. (2008). Nutrient sensing and inflammation in metabolic diseases. *Nat Rev Immunol* 8, 923-34.

151. Yuan L, Kaplowitz N. (2008). Glutathione in liver diseases and hepatotoxicity. *Mol Aspects Med*.

152. Kumar N, Afeyan R, Kim HD, Lauffenburger DA. (2008). Multipathway model enables prediction of kinase inhibitor cross-talk effects on migration of Her2-overexpressing mammary epithelial cells. *Mol Pharmacol* 73, 1668-78.

153. Janes KA, Reinhardt HC, Yaffe MB. (2008). Cytokine-induced signaling networks prioritize dynamic range over signal strength. *Cell* 135, 343-54.

154. Bylesjö M, Rantalainen M, Cloarec O, Nicholson JK, Holmes E, Trygg J. (2006). OPLS discriminant analysis: combining the strengths of PLS-DA and SIMCA classification. *J Chemometrics* 20, 341-351.

155. Efron B, Tibshirani RJ. (1993). An introduction to the bootstrap. *Chapman and Hall, London*.

156. Wold S. (1994). Exponentially weighted moving principal components analysis and projections to latent structures. *Chemometrics and intelligent laboratory systems* 23, 149-161.

157. McCubrey JA, Milella M, Tafuri A, Martelli AM, Lunghi P, Bonati A, Cervello M, Lee JT, Steelman LS. (2008). Targeting the Raf/MEK/ERK pathway with small-molecule inhibitors. *Curr Opin Investig Drugs* 9, 614-30.

158. Schliess F, Kurz AK, vom Dahl S, Haussinger D. (1997). Mitogen-activated protein kinases mediate the stimulation of bile acid secretion by tauroursodeoxycholate in rat liver. *Gastroenterology* 113, 1306-14.

159. Kubitz R, Sutfels G, Kuhlkamp T, Kolling R, Haussinger D. (2004). Trafficking of the bile salt export pump from the Golgi to the canalicular membrane is regulated by the p38 MAP kinase. *Gastroenterology* 126, 541-53.

160. Kurz AK, Graf D, Schmitt M, Vom Dahl S, Haussinger D. (2001). Tauroursodesoxycholate-induced choleresis involves p38(MAPK) activation and translocation of the bile salt export pump in rats. *Gastroenterology* 121, 407-19.

161. Wentz SC, Wu H, Yip-Schneider MT, Hennig M, Klein PJ, Sebolt-Leopold J, Schmidt CM. (2008). Targeting MEK is effective chemoprevention of hepatocellular carcinoma in TGF-alpha-transgenic mice. *J Gastrointest Surg* 12, 30-7.

162. Brown AP, Carlson TC, Loi CM, Graziano MJ. (2007). Pharmacodynamic and toxicokinetic evaluation of the novel MEK inhibitor, PD0325901, in the rat following oral and intravenous administration. *Cancer Chemother Pharmacol* 59, 671-9.

163. Xu JJ, Hendriks BS, Zhao J, de Graaf D. (2008). Multiple effects of acetaminophen and p38 inhibitors: towards pathway toxicology. *FEBS Lett* 582, 1276-82.

164. Russell WE, Dempsey PJ, Sitaric S, Peck AJ, Coffey RJ, Jr. (1993). Transforming growth factor-alpha (TGF alpha) concentrations increase in regenerating rat liver: evidence for a delayed accumulation of mature TGF alpha. *Endocrinology* 133, 1731-8.

165. Hatano E, Brenner DA. (2001). Akt protects mouse hepatocytes from TNF-alpha- and Fas-mediated apoptosis through NK-kappa B activation. *Am J Physiol Gastrointest Liver Physiol* 281, G1357-68.

166. Fielden MR, Kolaja KL. (2006). The state-of-the-art in predictive toxicogenomics. *Curr Opin Drug Discov Devel* 9, 84-91.

167. Shaw PJ, Ditewig AC, Waring JF, Liguori MJ, Blomme EA, Ganey PE, Roth RA. Coexposure of mice to trovafloxacin and lipopolysaccharide, a model of idiosyncratic hepatotoxicity, results in a unique gene expression profile and interferon gamma-dependent liver injury. *Toxicol Sci*.

168. Owens DM, Keyse SM. (2007). Differential regulation of MAP kinase signalling by dual-specificity protein phosphatases. *Oncogene* 26, 3203-13.

169. Amit I, Citri A, Shay T, Lu Y, Katz M, Zhang F, Tarcic G, Siwak D, Lahad J, Jacob-Hirsch J, Amariglio N, Vaisman N, Segal E, Rechavi G, Alon U, Mills GB, Domany E, Yarden Y. (2007). A module of negative feedback regulators defines growth factor signaling. *Nat Genet* 39, 503-12.

170. Hanahan D, Weinberg RA. (2000). The hallmarks of cancer. *Cell* 100, 57-70.

171. Sato M, Ozawa T, Inukai K, Asano T, Umezawa Y. (2002). Fluorescent indicators for imaging protein phosphorylation in single living cells. *Nat Biotechnol* 20, 287-94.

172. Zhang L, Lee KC, Bhojani MS, Khan AP, Shilman A, Holland EC, Ross BD, Rehemtulla A. (2007). Molecular imaging of Akt kinase activity. *Nat Med* 13, 1114-9.

173. Zhang L, Bhojani MS, Ross BD, Rehemtulla A. (2008). Molecular imaging of protein kinases. *Cell Cycle* 7, 314-7.

174. Holbro T, Civenni G, Hynes NE. (2003). The ErbB receptors and their role in cancer progression. *Exp Cell Res* 284, 99-110.

175. Harris RC, Chung E, Coffey RJ. (2003). EGF receptor ligands. *Exp Cell Res* 284, 2-13.

176. Fan H, Derynck R. (1999). Ectodomain shedding of TGF-alpha and other transmembrane proteins is induced by receptor tyrosine kinase activation and MAP kinase signaling cascades. *Embo J* 18, 6962-72.

177. Seton-Rogers SE, Lu Y, Hines LM, Koundinya M, LaBaer J, Muthuswamy SK, Brugge JS. (2004). Cooperation of the ErbB2 receptor and transforming growth factor beta in induction of migration and invasion in mammary epithelial cells. *Proc Natl Acad Sci U S A* 101, 1257-62.

178. Stockholm D, Bartoli M, Sillon G, Bourg N, Davoust J, Richard I. (2005). Imaging calpain protease activity by multiphoton FRET in living mice. *J Mol Biol* 346, 215-22.

179. Grimm J, Kirsch DG, Windsor SD, Kim CF, Santiago PM, Ntziachristos V, Jacks T, Weissleder R. (2005). Use of gene expression profiling to direct in vivo molecular imaging of lung cancer. *Proc Natl Acad Sci U S A* 102, 14404-9.

180. Pham W, Choi Y, Weissleder R, Tung CH. (2004). Developing a peptide-based near-infrared molecular probe for protease sensing. *Bioconjug Chem* 15, 1403-7.

181. Korngold EC, Jaffer FA, Weissleder R, Sosnovik DE. (2008). Noninvasive imaging of apoptosis in cardiovascular disease. *Heart Fail Rev* 13, 163-73.

182. Messerli SM, Prabhakar S, Tang Y, Shah K, Cortes ML, Murthy V, Weissleder R, Breakefield XO, Tung CH. (2004). A novel method for imaging apoptosis using a caspase-1 near-infrared fluorescent probe. *Neoplasia* 6, 95-105.

183. Kenny PA, Bissell MJ. (2007). Targeting TACE-dependent EGFR ligand shedding in breast cancer. *J Clin Invest* 117, 337-45.

184. Griffith LG, Naughton G. (2002). Tissue engineering--current challenges and expanding opportunities. *Science* 295, 1009-14.

185. Griffith LG, Swartz MA. (2006). Capturing complex 3D tissue physiology in vitro. *Nat Rev Mol Cell Biol* 7, 211-24.

186. Odom DT, Dowell RD, Jacobsen ES, Gordon W, Danford TW, MacIsaac KD, Rolfe PA, Conboy CM, Gifford DK, Fraenkel E. (2007). Tissue-specific transcriptional regulation has diverged significantly between human and mouse. *Nat Genet* 39, 730-2.

187. Rangarajan A, Hong SJ, Gifford A, Weinberg RA. (2004). Species- and cell type-specific requirements for cellular transformation. *Cancer Cell* 6, 171-83.

188. Vargo-Gogola T, Rosen JM. (2007). Modelling breast cancer: one size does not fit all. *Nat Rev Cancer* 7, 659-72.

189. Khetani SR, Bhatia SN. (2008). Microscale culture of human liver cells for drug development. *Nat Biotechnol* 26, 120-6.

190. Lee MY, Kumar RA, Sukumaran SM, Hogg MG, Clark DS, Dordick JS. (2008). Three-dimensional cellular microarray for high-throughput toxicology assays. *Proc Natl Acad Sci U S A* 105, 59-63.

191. Debnath J, Mills KR, Collins NL, Reginato MJ, Muthuswamy SK, Brugge JS. (2002). The role of apoptosis in creating and maintaining luminal space within normal and oncogene-expressing mammary acini. *Cell* 111, 29-40.

192. Paszek MJ, Zahir N, Johnson KR, Lakins JN, Rozenberg GI, Gefen A, Reinhart-King CA, Margulies SS, Dembo M, Boettiger D, Hammer DA, Weaver VM. (2005). Tensional homeostasis and the malignant phenotype. *Cancer Cell* 8, 241-54.

193. Irvine DJ, Stachowiak AN, Hori Y. (2008). Lymphoid tissue engineering: invoking lymphoid tissue neogenesis in immunotherapy and models of immunity. *Semin Immunol* 20, 137-46.

194. Stachowiak AN, Irvine DJ. (2008). Inverse opal hydrogel-collagen composite scaffolds as a supportive microenvironment for immune cell migration. *J Biomed Mater Res A* 85, 815-28.

195. Engler AJ, Sen S, Sweeney HL, Discher DE. (2006). Matrix elasticity directs stem cell lineage specification. *Cell* 126, 677-89.

196. Gerhart J. (1999). 1998 Warkany lecture: signaling pathways in development. *Teratology* 60, 226-39.

197. Khetani SR, Bhatia SN. (2006). Engineering tissues for in vitro applications. *Curr Opin Biotechnol* 17, 524-31.

198. Helm CL, Fleury ME, Zisch AH, Boschetti F, Swartz MA. (2005). Synergy between interstitial flow and VEGF directs capillary morphogenesis in vitro through a gradient amplification mechanism. *Proc Natl Acad Sci U S A* 102, 15779-84.

199. Joyce AR, Palsson BO. (2006). The model organism as a system: integrating 'omics' data sets. *Nat Rev Mol Cell Biol* 7, 198-210.

200. Calvert VS, Collantes R, Elariny H, Afendy A, Baranova A, Mendoza M, Goodman Z, Liotta LA, Petricoin EF, Younossi ZM. (2007). A systems biology approach to the pathogenesis of obesity-related nonalcoholic fatty liver disease using reverse phase protein microarrays for multiplexed cell signaling analysis. *Hepatology* 46, 166-72.

201. Klingmuller U, Bauer A, Bohl S, Nickel PJ, Breitkopf K, Dooley S, Zellmer S, Kern C, Merfort I, Sparna T, Donauer J, Walz G, Geyer M, Kreutz C, Hermes M, Gotschel F, Hecht A, Walter D, Egger L, Neubert K, Borner C, Brulport M, Schormann W, Sauer C, Baumann F, Preiss R, MacNelly S, Godoy P, Wiercinska E, Ciuclan L, Edelmann J, Zeilinger K, Heinrich M, Zanger UM, Gebhardt R, Maiwald T, Heinrich R, Timmer J, von Weizsacker F, Hengstler JG. (2006). Primary mouse hepatocytes for systems biology approaches: a standardized in vitro system for modelling of signal transduction pathways. *Syst Biol (Stevenage)* 153, 433-47.

202. Soen Y, Mori A, Palmer TD, Brown PO. (2006). Exploring the regulation of human neural precursor cell differentiation using arrays of signaling microenvironments. *Mol Syst Biol* 2, 37.

203. Takikita M, Chung JY, Hewitt SM. (2007). Tissue microarrays enabling high-throughput molecular pathology. *Curr Opin Biotechnol* 18, 318-25.

204. Gomez-Sjoberg R, Leyrat AA, Pirone DM, Chen CS, Quake SR. (2007). Versatile, Fully Automated, Microfluidic Cell Culture System. *Anal. Chem.* 79, 8557-8563.

205. Flaim CJ, Chien S, Bhatia SN. (2005). An extracellular matrix microarray for probing cellular differentiation. *Nat Methods* 2, 119-25.

206. Underhill GH, Bhatia SN. (2007). High-throughput analysis of signals regulating stem cell fate and function. *Curr Opin Chem Biol* 11, 357-66.

207. Otsuka H, Hirano A, Nagasaki Y, Okano T, Horiike Y, Kataoka K. (2004). Two-Dimensional Multiarray Formation of Hepatocyte Spheroids on a Microfabricated PEG-Brush Surface. *ChemBioChem* 5, 850-855.

208. Albrecht DR, Underhill GH, Wassermann TB, Sah RL, Bhatia SN. (2006). Probing the role of multicellular organization in three-dimensional microenvironments. *Nat Methods* 3, 369-75.

209. Sodunke TR, Turner KK, Caldwell SA, McBride KW, Reginato MJ, Noh HM. (2007). Micropatterns of Matrigel for three-dimensional epithelial cultures. *Biomaterials* 28, 4006-16.

210. Debnath J, Brugge JS. (2005). Modelling glandular epithelial cancers in three-dimensional cultures. *Nat Rev Cancer* 5, 675-88.

211. Zahir N, Weaver VM. (2004). Death in the third dimension: apoptosis regulation and tissue architecture. *Curr Opin Genet Dev* 14, 71-80.

212. Krutzik PO, Crane JM, Clutter MR, Nolan GP. (2008). High-content single-cell drug screening with phosphospecific flow cytometry. *Nat Chem Biol* 4, 132-42.

213. Doh J, Irvine DJ. (2006). Immunological synapse arrays: patterned protein surfaces that modulate immunological synapse structure formation in T cells. *Proc Natl Acad Sci U S A* 103, 5700-5.

214. Ghosh D. (2004). Mixture models for assessing differential expression in complex tissues using microarray data. *Bioinformatics* 20, 1663-9.

215. Zaman MH, Trapani LM, Sieminski AL, Mackellar D, Gong H, Kamm RD, Wells A, Lauffenburger DA, Matsudaira P. (2006). Migration of tumor cells in 3D matrices is governed by matrix stiffness along with cell-matrix adhesion and proteolysis. *Proc Natl Acad Sci U S A* 103, 10889-94.

216. Kim HD, Guo TW, Wu AP, Wells A, Gertler FB, Lauffenburger DA. (2008). Epidermal growth factor-induced enhancement of glioblastoma cell migration in 3D arises from an intrinsic increase in speed but an extrinsic matrix- and proteolysis-dependent increase in persistence. *Mol Biol Cell* 19, 4249-59.

217. Muschler GF, Nakamoto C, Griffith LG. (2004). Engineering principles of clinical cell-based tissue engineering. *J Bone Joint Surg Am* 86-A, 1541-58.